DEVELOPMENT OF A NEW STATIC SYNTHETIC APPARATUS FOR PHASE EQUILIBRIUM MEASUREMENTS

Sivanna Naicker

B. Tech. (Chemical)

This dissertation is submitted in fulfilment of the academic requirements for the degree of Master in Engineering in the Department of Chemical Engineering, Durban University of Technology

Supervisor: Mr Suresh Ramsuroop

Co-supervisors: Assoc. Prof. Paramespri Naidoo

Dr Wayne Nelson

December 2016

Abstract

Phase equilibrium data plays a significant role in the design and optimization of industrial separation schemes, such as distillation and absorption units. These separation processes are utilised for the purification of valuable chemicals, which play a pivotal role in daily human life. Separation units are operated at various conditions of temperature and pressure, however it is common for most units to operate in the moderate pressure region (100-500 kPa). On the contrary, there is a lack of phase equilibrium data available in the moderate pressure region, thus prompting an interest in this area.

In this study, a new static synthetic cell was tested, and the experimental apparatus was successfully set up and commissioned. Some key features of this design include a total working cell volume of 60 cm^3 (which reduces the amount of chemicals required compared to conventional static synthetic cells) and equilibrium is achieved faster. In addition, two high-accuracy Teledyne Isco pumps were utilised for the feed loading, as it is vital that the volume of chemicals dispensed into the cell be accurately determined.

The necessary calibrations were conducted and the overall uncertainties were found to be 0.06 K, 0.36 kPa and 0.1 ml for temperature, pressure and volume respectively. The following test systems were measured to determine the reproducibility of the apparatus and to verify the experimental technique:

- water (1) + 2-butanol (2) at 323.16 K
- n-hexane (1) + 2-butanol (2) at 329.21 K
- n-pentane (1) + 1-propanol (2) at 317.18 K
- n-pentane (1) + 2-butanol (2) at 303.17 K
- n-pentane (1) + ethanol (2) at 303.11 K

The test systems measured produced a good fit with the literature data, and thus the experimental apparatus was commissioned. New systems, previously unmeasured in the open literature, were measured in this study. These systems include:

- n-hexane (1) + perfluoro-n-heptane (2) at 313.21 and 333.12 K
- n-pentane (1) + 2-propanol (2) at 313.11, 323.11 and 333.12 K

The data was modelled on Aspen Plus®. Since the method of operation is of the static synthetic type, no analysis of the vapour and liquid phases took place, and instead an algorithm was developed using the combined method (γ-ϕ) together with the method of Barker (1953), to convert the overall composition (z_i) to liquid mole fraction (x_i). The Wilson and Non-Random Two-Liquid (NRTL) activity coefficient models together with the Ideal Gas law and Hayden O'Connell second virial coefficient were utilised to regress the data. For both the fluorinated and alkane + alcohol systems, the experimental

data produced an excellent fit with the activity coefficient models. For both systems, azeotropes were observed, indicating poor separation of these binary combinations at specific mole fractions. This is due to the boiling point of both components being similar under certain conditions. The calculated pressure residuals were well within the overall combined uncertainty for pressure, whilst the calculated temperature residuals were slightly above the overall combined uncertainty for temperature.

Declaration

The work presented in this dissertation was carried out at the Thermodynamics Research Unit in the School of Chemical Engineering at the University of KwaZulu-Natal, from January 2015 to November 2016 under the supervision of Mr S. Ramsuroop, Prof. P. Naidoo and Dr W. Nelson.

This dissertation is submitted as the full requirement for the degree M. Eng. in Chemical Engineering.

I, Sivanna Naicker, therefore declare that:

(i) The research reported in this dissertation, except where otherwise indicated, is my original work.

(ii) This dissertation has not been submitted for any degree or examination at any other university.

(iii) This dissertation does not contain other persons' data, pictures, graphs or other information, unless specifically acknowledged as being sourced from other persons.

(iv) This dissertation does not contain other persons' writing, unless specifically acknowledged as being sourced from other researchers. Where other written sources have been quoted, then:

a) Their words have been re-written but the general information attributed to them has been referenced.

b) Where their exact words have been used, their writing has been placed inside quotation marks, and referenced.

(v) This dissertation does not contain text, graphics or tables copied and pasted from the Internet, unless specifically acknowledged, and the source being detailed in the dissertation and in the reference section.

_____ _____

Sivanna Naicker (20904538) Date

As the candidate's supervisor, I, Mr Suresh Ramsuroop, approve this dissertation for submission.

_____ _____

Mr Suresh Ramsuroop Date

As the candidate's co-supervisor, I, Prof. Paramespri Naidoo, approve this dissertation for submission.

_____ _____

Assoc. Prof. Paramespri Naidoo Date

As the candidate's co-supervisor, I, Dr Wayne Nelson, approve this dissertation for submission.

_____ _____

Dr Wayne Nelson Date

Acknowledgements

I would like to extend my utmost gratitude to the following people/organizations:

- My supervisors, Dr Wayne Nelson, Assoc. Prof. Paramespri Naidoo and Mr Suresh Ramsuroop for their invaluable guidance and support throughout the duration of this study.
- The workshop and technical staff in the School of Chemical Engineering (UKZN) for their contribution toward the fabrication, commissioning and maintenance of the experimental apparatus.
- The DST/NRF SARChI programme, The University of KwaZulu-Natal and The Durban University of Technology for funding this project.
- My family, for their many years of support and encouragement throughout my academic career.
- My colleagues at the Thermodynamics Research Unit, for their support and friendship.
- All my thanks to God for everything He has provided me with.

Contents

List of Figures

CHAPTER 1

CHAPTER 2

CHAPTER 3

CHAPTER 4

CHAPTER 5

APPENDIX B

APPENDIX C

List of Tables

CHAPTER 2

CHAPTER 3

CHAPTER 5

APPENDIX C

List of Photographs

CHAPTER 4

Nomenclature

Symbols

B	Second virial coefficient ($m^3.mol^{-1}$)
f_i	Fugacity of component *i* (kPa)
$\widehat{f_i}$	Fugacity of component *i* in a solution (kPa)
G	Molar Gibbs free energy ($J.mol^{-1}$)
$g_{12} - g_{11}$	NRTL model fit parameter (K)
k	Correction factor
n_i	Number of moles of component *i* (moles)
P	Pressure (kPa)
R	Universal gas constant (8.314 $J.mol^{-1}.K^{-1}$)
T	Temperature (K)
u_c	Source of uncertainty
U_c	Combined overall uncertainty
V	Volume (ml)
v_i^L	Saturated liquid molar volume of component *i* ($m^3.mol^{-1}$)
x_i	Liquid mole fraction of component *i*
y_i	Vapour mole fraction of component *i*
Z	Compressibility
z_i	Overall composition of component *i*

Greek symbols

α	Relative volatility
α_{12}	Non-randomness parameter for the NRTL model
γ	Activity coefficient
Δ	Change in
δ	Residual
ε	Tolerance
Λ	T-K Wilson model parameter
λ_{12}- λ_{11}	Wilson model parameter (K)
μ	Chemical potential
ρ	Density
τ	NRTL model parameter
Φ	Vapour correction factor

ϕ	Fugacity coefficient
ω	Acentric factor

Subscripts

1	Component 1
2	Component 2
AVG	Average
c	Critical property
calib	Calibration property
exp	Experimental property
i,j	Component *i*,*j*
rep	Repeatability property
std	Standard property
T	Total property

Superscripts

0	Reference state
calc	Calculated property
E	Excess property
exp	Experimental property
l	Liquid
L	Liquid
lit	Literature
model	Property determined by a model
residual	The remainder of a subtraction of two variables
sat	Saturated
v	Vapour
V	Vapour

Abbreviations

EoS	Equation of state
GC	Gas Chromatograph
HOC	Hayden O'Connell
HPVLE	High pressure vapour-liquid equilibrium
LLE	Liquid-liquid equilibrium
LPVLE	Low pressure vapour-liquid equilibrium

MOC	Material of construction
MPVLE	Moderate pressure vapour-liquid equilibrium
NIST	National Institute of Standards and Technology
NRTL	Non-Random Two-Liquid
OF	Objective function
PFC	Perfluorocarbon
P&ID	Piping and instrumentation diagram
SLE	Solid-liquid equilibrium
SRK	Soave Redlich-Kwong
SS	Stainless steel
T-K Wilson	Tsuboka-Katayama Wilson
UNIQUAC	Universal quasi-chemical
VEoS	Virial equation of state
VLE	Vapour-liquid equilibrium

CHAPTER 1 : Introduction

The contemporary human lifestyle requires a broad spectrum of chemicals in almost every aspect of life. From powering households to electronics and detergents, chemicals are required in the manufacture of countless products and services as well as in the synthesis and production of new chemicals, thus making it a significant contributor to the world economy. In order to accommodate for the high demand of consumers, it is pivotal that more efficient separation schemes are designed or that existing separation processes are optimized in order to recover chemicals of high purities.

According to Bosch and de Haan (2013), separation processes such as distillation and absorption are of great economic importance as they account for 40-90% of capital and operating costs. Separation processes have several functions, namely, the purification of raw materials, the recovery of by-products, the recycling of solvents and unrecovered reactants, and the removal of contaminants from effluents.

In order for the successful and efficient design and optimization of industrial separation schemes, the measurement of accurate phase equilibrium data is imperative. Experimental thermodynamic phase equilibrium data is dependent on the measurement of several variables, i.e. pressure, temperature and phase composition. Depending on the nature of the chemicals being measured and the conditions of temperature and pressure, experimentation can yield various types of phase equilibrium data such as vapour-liquid equilibrium (VLE), liquid-liquid equilibrium (LLE) or solid-liquid equilibrium (SLE) just to name a few. The apparatus used for phase equilibrium measurements are also dependant on the variables being measured, which is discussed in greater detail in Chapter 3.

Although a large amount of phase equilibrium data exists for low and high pressure systems, there is a shortage of data available in the moderate pressure region (100-500 kPa). This region is of particular importance as many unit operations are operated at moderate temperatures and pressures (Reddy, 2006).

There is a vast array of apparatus available for the measurement of moderate pressure phase equilibrium data, which is discussed in Chapter 3. This work focuses on the static synthetic apparatus. This type of apparatus usually comprises of a cell, an agitation device and a mechanism to create an isothermal environment for experimentation. The static synthetic apparatus measures pressure, temperature and the volume dispensed to determine overall composition (z_i). No analysis of the vapour and liquid phases are conducted and instead, the method of Barker (1953) is employed to determine the liquid phase mole fraction (x_i) using the overall composition.

In 2006 a static synthetic total pressure apparatus, used to measure P-x data, was designed by J. D. Raal and commissioned by A. M. Motchelaho in the Thermodynamics Research Unit at the University of KwaZulu-Natal (Raal et al., 2011). The apparatus consisted of a 190 cm^3 stainless steel cell and two

hand-rotated piston injectors for loading the pure components into the cell. The apparatus was designed for low pressure measurements (0-100 kPa) but was rated for 2000 kPa. The apparatus proved to yield accurate data (Raal et al., 2011) and was later automated (Moodley, 2012) to reduce the number of man hours spent on experimentation, as well as to gain better control over the volume of chemicals dispensed into the cell. In this study, a new static synthetic apparatus was commissioned as a part of this project, to avoid problems associated with many of the mechanical aspects of the aforementioned apparatus. Such aspects include issues associated with the pumps, solenoid valves, mixer, and fittings.

The static synthetic apparatus available for P-x measurements published in literature, along with the apparatus of Raal et al. (2011) are discussed extensively in Chapter 3.

A new apparatus was designed within the Thermodynamics Research Unit by Dr Wayne Nelson; it was a part of this study to commission the total pressure apparatus and to develop the experimental technique for measurement of phase equilibrium data at moderate pressures. The basis of the design was to minimize the total cell volume and to eliminate dead volume by charging components directly into the liquid phase. The new design consists of a cell, 60 cm^3 in volume. This reduced volume results in a smaller amount of chemicals required for measurements, compared to the apparatus of Raal et al. (2011). The apparatus also incorporates two high accuracy syringe pumps, supplied by Teledyne Isco. Each of the pumps include a thermal jacket used to control the pump temperature, which aids in avoiding any fluctuations in volume within the pumps. There is also an improvement of sealing under vacuum, as sealing is achieved via O-rings, gaskets and compression fittings, and no threaded fittings are utilised. Dead volume in the loading lines are eliminated as the ball valves utilised for feed loading are situated at the base of the cell and components are introduced directly into the liquid phase. A WIKA P-10 pressure transmitter is used in the experimental setup as it has a pressure range of 0-500 kPa, capable of measurements in the desired moderate pressure range. Neodymium magnets and ball bearings are also employed to improve the efficiency of the mixer.

The objectives of this study are:

- To set up and commission the new static synthetic apparatus
- To develop an experimental technique for the apparatus
- To conduct measurements of the following test systems:
    - water (1) + 2-butanol (2) at 323.16 K
    - n-hexane (1) + 2-butanol (2) at 329.21 K
    - n-pentane (1) + 1-propanol (2) at 317.18 K
    - n-pentane (1) + 2-butanol (2) at 303.17 K
    - n-pentane (1) + ethanol (2) at 303.11 K

- To conduct measurements of the following new systems:
    - n-hexane (1) + perfluoro-n-heptane (2) at 313.21 and 333.12 K
    - n-pentane (1) + 2-propanol (2) at 313.11, 323.11 and 333.12 K
- To correlate the experimental data to suitable phase equilibrium models via the method of Barker (1953) as well as regression procedures

1.1 n-Hexane (1) + Perfluoro-n-heptane (2)

In the downstream beneficiation of fluorspar, various perfluorocarbon (PFC) chemicals are produced. PFC's are widely used as solvents, surfactants and fluoroelastomers, just to name a few uses. Binary mixtures of alkanes and perfluoroalkanes are of great interest in the chemical industry. Although alkanes and perfluoroalkanes have similar molecular structures (refer to Figure 1-1), their mixture properties are highly non-ideal, with some mixture combinations exhibiting regions of liquid-liquid immiscibility, large positive deviations from Raoult's law and large positive excess enthalpies and volumes. The immiscibility and weak interactions between alkanes and perfluoroalkanes have promoted an interest in their study. In addition, perfluoroalkanes on their own have numerous industrial as well as medical applications (Morgado et al., 2005). Phase equilibrium data for n-hexane (1) + perfluoro-n-heptane (2) at 313.21 and 333.12 K does not exist in open literature, promoting a further interest in their study.

Enthalpies of interactions between PFC's and hydrocarbons are smaller than the interaction enthalpies between hydrocarbons. Fluorine's low polarizability results in low Van Der Waals interactions between F-chains and low cohesive energy densities in liquid PFC's. Therefore, these low intermolecular interactions result in some of the desirable properties of PFC's, such as low surface tensions, excellent spreading properties, high fluidity, low dielectric constants, and high vapour pressures, thus, PFC's have a low affinity for the analogous hydrocarbon group with high cohesive energy densities (Gladysz et al., 2005).

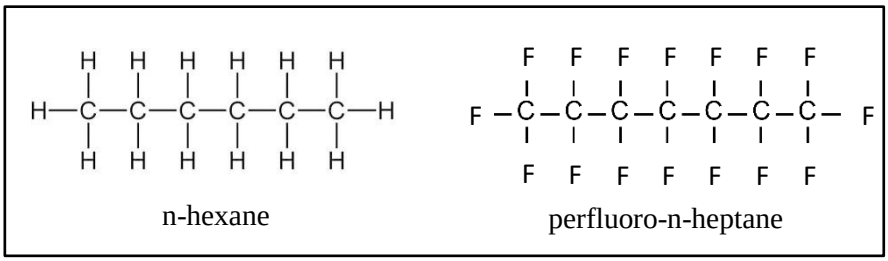

Figure 1-1: Chemical structure of n-hexane and perfluoro-n-heptane (Wikimedia, 2014).

1.2 n-Pentane (1) + 2-Propanol (2)

The second new system under investigation (n-pentane (1) + 2-propanol (2) at 313.11, 323.11 and 333.12 K) will contribute new data to the open literature as it has not previously been measured. The reason for choosing this system is due to the need for phase equilibrium data for the separation of alkanes from alcohols. Alkanes and alcohols usually form as by-products in various petrochemical processes and their recovery is of high importance (Nala, 2012). n-Pentane is used as a blending component of high octane gasoline and in the processing of isoprene (Brown and Brown, 2014). 2-Propanol is commonly used as a solvent, as it dissolves a wide range of non-polar compounds, it also serves as a chemical intermediate and is frequently used in the medical and automotive industries (Patnaik, 2007).

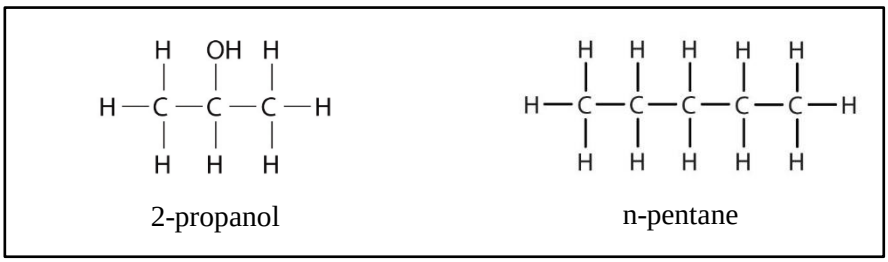

Figure 1-2: Chemical structure of 2-propanol and n-pentane (Statemaster, 2005).

P-x data for the system n-pentane (1) + 2-propanol (2) were measured, in order to better understand the phase separation behaviour of these two components at various moderate pressures and temperatures, thus the importance of their study. It is predicted using UNIFAC that 2-propanol will form an azeotrope with n-pentane as seen in Figure 1-3. This is due to the boiling points of n-pentane and 2-propanol being equal under these specific conditions, resulting in a negative deviation from Raoult's law.

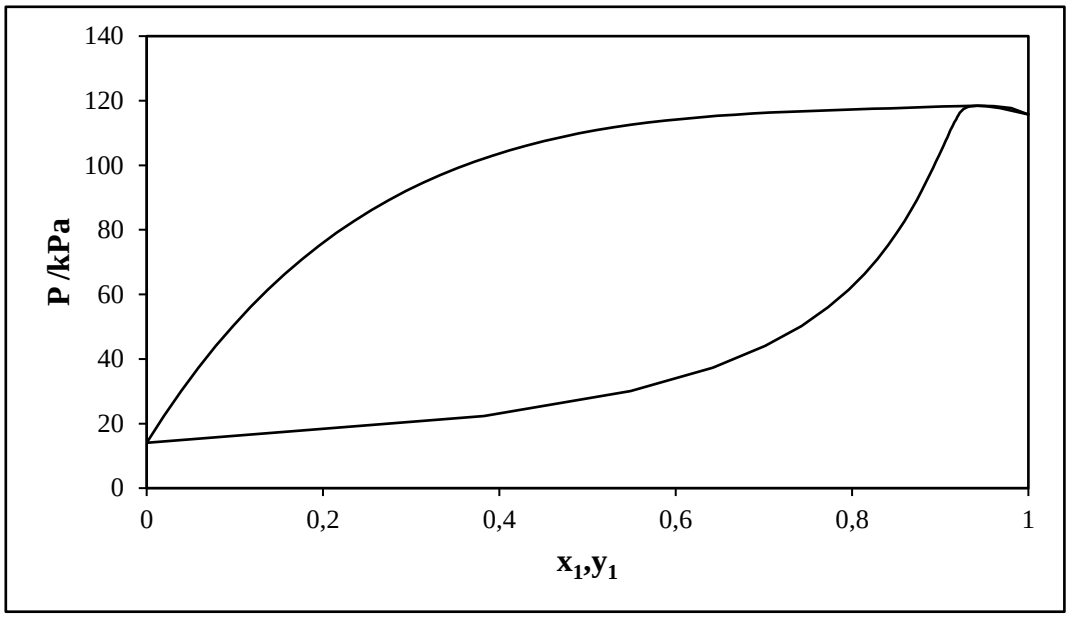

Figure 1-3: Prediction of n-pentane (1) + 2-propanol (2) at 313.15 K using the UNIFAC model.

1.3 Modelling

There are numerous simulation software packages available for the prediction of phase equilibrium data, however they are merely predictions. When it comes to the design of industrial separation schemes, processes of such a large magnitude need to be verified by experimental data, as predictions are just a guideline and are not 100% accurate.

Regression models such as activity coefficient models and equations of state (EoS) are used to regress the data and produce a model representation of the experimental data measured, as well as to extrapolate data at different conditions using the parameters obtained. For this work, the method of Barker (1953) is used to calculate the liquid mole fraction (x_i) and the Aspen Plus® simulation software package is used to regress the data. Data regression is undertaken via the combined (γ-ϕ) method using reliable models to describe the vapour and liquid phase non-idealities, which are further discussed in Chapter 2.

In this dissertation the reader will be guided through a literature review of the numerous types of apparatus used for phase equilibrium measurements, a description of the new apparatus designed and commissioned, as well as the experimental procedure developed for measurements. Thereafter the experimental data and modelling will be presented and discussed. Chapter 2 presents a review of the thermodynamic models employed to regress the experimental data.

CHAPTER 2 : Thermodynamic Principles

The feasibility and efficiency of the design of separation processes, rely upon the accuracy of experimental thermodynamic data. However, as a result of limited experimental data, such information is not always available for the design of industrial separation processes at the desired operating conditions of pressure and temperature. Therefore, reliable thermodynamic models are employed to extrapolate data over a broad spectrum, using experimental data.

Experimental phase equilibrium data consists of a number of measured variables, viz. pressure, temperature, vapour and liquid mole fractions. The different types of experimental apparatus yield a combination of these variables, for e.g. the recirculating VLE still typically yields pressure (P), temperature (T) and vapour and liquid mole fractions (y_i, x_i), whilst the static synthetic cell (such as the one utilised in this study) yields pressure, temperature and overall composition (z_i). This chapter focuses on the various thermodynamic formulae used to accurately model experimental data, as well as computational methods used to calculate unmeasured variables, such as the liquid mole fraction in the case of the static synthetic cell.

2.1 Criterion for phase equilibrium

According to Smith et al. (2005), a system at equilibrium exists such that no change in state can occur. Thus, a system is considered to be in thermodynamic equilibrium when it is in chemical, thermal and mechanical equilibrium. In order for thermodynamic equilibrium to occur, the following criteria need to be satisfied for a transfer of moles in a mixture between two phases (Smith et al., 2005):

- Uniform temperature and pressure between phases
- Minimum global Gibbs free energy
- Equivalent chemical potential (μ_i) for a specific component between each phase

Consider a closed system at equilibrium, consisting of two phases, α and β. Each of the individual species within the closed system can freely transfer mass from one phase to the other. Assuming that the temperature and pressure are constant throughout the system at equilibrium, the equilibrium conditions (equations (2-1) to (2-3)) indicate that phase equilibrium between a vapour and liquid phase at the same temperature and pressure yield

$$T^{\alpha} = T^{\beta} = \cdots T^{\pi} \qquad \text{Thermal equilibrium} \qquad (2\text{-}1)$$

$$P^{\alpha} = P^{\beta} = \cdots P^{\pi} \qquad \text{Mechanical equilibrium} \qquad (2\text{-}2)$$

$$\mu_i{}^{\alpha} = \mu_i{}^{\beta} = \cdots \mu_i{}^{\pi} \qquad \text{Chemical equilibrium} \quad (i = 1,2,\dots,N) \qquad (2\text{-}3)$$

For a detailed derivation of equation (2-3), the reader is referred to Appendix A.

2.2 Pure species fugacity and fugacity coefficient

Chemical potential (μ) is a derived thermodynamic property, unlike temperature and pressure which are measured variables, making it an abstract concept. In application, chemical potential has some inconvenient mathematical behaviours (Koretsky, 2004) and it is therefore convenient to define chemical potential in terms of an alternate derived thermodynamic property that is mathematically better behaved i.e. fugacity. In 1908 the concept of fugacity was introduced by Gilbert N. Lewis as a quantity which can directly relate to measured properties such as pressure and temperature.

The thermodynamic property of fugacity ($\hat{f}_i$) is defined as

$$\mu_i - \mu_i{}^0 \equiv RTln\left[\frac{\hat{f}_i}{\hat{f}_i{}^0}\right] \tag{2-4}$$

and accordingly has units of pressure. According to Koretsky (2004), *"fugacity plays the same role in real gases that partial pressure plays in ideal gases"*, therefore, in this sense fugacity can be thought of as a "corrected pressure".

The above definition is however not complete as the reference state is arbitrary. Considering a limiting condition to complete the definition, as the pressure tends to zero and all gases are considered ideal, consequently

$$\lim_{P\to 0}\left(\frac{\hat{f}_i}{P_i}\right) \equiv 1 \tag{2-5}$$

The term $\left(\frac{\hat{f}_i}{P_i}\right)$ is called the fugacity coefficient ($\hat{\phi}_i$) and is used to quantify the non-ideality and the extent of the deviation from unity to which a molecule (*i*) interacts with the surrounding molecules. Using equations of state and fugacity, fugacity coefficients can be applied to both the vapour and liquid phases, however only the fugacity coefficient for the vapour phase non-ideality is considered. The fugacity in the vapour phase ($\hat{f}_i^{\,V}$) of component *i*, relates to the mole fraction in the vapour phase (y_i) as well as the total pressure by the fugacity coefficient

$$\hat{\phi}_i \equiv \frac{\hat{f}_i}{p_i} = \frac{\hat{f}_i}{y_i P} \tag{2-6}$$

At low pressures (0-100 kPa) it can be assumed that behaviour in the gaseous state is ideal and therefore $\hat{\phi}_i = 1$. However, at pressures above 100 kPa, $\hat{\phi}_i$ may deviate from ideality, especially if the components in the mixture are polar (Prausnitz et al., 1967).

Since fugacity coefficients can be applied to both the vapour and liquid phases, the fugacity of any phases that co-exist, for e.g. vapour and liquid, can be equated as follows

$$\hat{f}_i^{\,L} = \hat{f}_i^{\,V} \tag{2-7}$$

For a complete derivation of equation (2-7) the reader is referred to Appendix A.

2.3 Fugacity and fugacity coefficient of a species in a gaseous mixture

The fugacity of species *i*, in addition to temperature and pressure, depends upon any additional species that are present in a mixture as the fugacity and fugacity composition are functions of the composition of the mixture. Equation (2-7) can be re-written to indicate such dependence as follows

$$\hat{f}_i^{\,V}(T, P, n_1, n_2 \ldots n_m) = y_i \hat{\phi}_i^{\,V}(T, P, n_1, n_2 \ldots n_m) P \tag{2-8}$$

In order to calculate fugacity when using an equation of state that is explicit in pressure, the following equation is used

$$RTln\left[\frac{\hat{f}_i^{\,V}}{y_i P_{low}}\right] = -\int_{\left(\frac{n_T RT}{P_{low}}\right)}^{V} \left(\frac{\partial P}{\partial n_i}\right)_{T,V,n_{j\neq 1}} dV \tag{2-9}$$

For species *i* in a mixture of *i* and *j*, equation (2-9) can be written as

$$RTln\left[\frac{\hat{f}_i^{\,V}}{y_i P_{low}}\right] = -\int_{\left(\frac{n_T RT}{P_{low}}\right)}^{V} \left(\frac{\partial P}{\partial n_i}\right)_{T,V,n_j} dV \tag{2-10}$$

The Van der Waals equation for a binary mixture can be written as follows

$$P = \frac{RT(n_i+n_j)}{V-(n_i j_i+n_j j)} - \frac{{n_i}^2 i_i + 2n_i n_j\sqrt{i_i i_j} + {n_j}^2 i_j}{V^2} \tag{2-11}$$

Where

$$i_{mix} = {y_i}^2 i_i + 2y_i y_j\sqrt{i_i i_j} + {y_j}^2 i_j \tag{2-12}$$

$$j_{mix} = n_i j_i + n_j j \tag{2-13}$$

$$n_T = n_i + n_j \tag{2-14}$$

The derivative of equation (2-11) gives

$$\left(\frac{\partial P}{\partial n_i}\right)_{T,V,n_j} = \frac{RT}{V-(n_i j_i+n_j j)} + \frac{j_i RT(n_i+n_j)}{[V-(n_i j_i+n_j j)]^2} - \frac{2(n_i i_i+n_j\sqrt{i_i i_j})}{V^2} \tag{2-15}$$

Substituting equation (2-15) into (2-9) and integrating yields

$$ln\left[\frac{\hat{f}_i^{\,V}}{y_i P_{low}}\right] = -ln\left[\frac{V-n_T j_{mix}}{\left(\frac{n_T RT}{P_{low}}\right)-n_T j_{mix}}\right] + \frac{j_i(n_i+n_j)}{V-n_T j_{mix}} - \frac{j_i(n_i+n_j)}{\left(\frac{n_T RT}{P_{low}}\right)-n_T j_{mix}} - \frac{2(n_i i_i+n_j\sqrt{i_i i_j})}{RTV} + \frac{2(n_i i_i+n_j\sqrt{i_i i_j})}{RT\left(\frac{n_T RT}{P_{low}}\right)} \quad (2\text{-}16)$$

However $\left(\frac{RT}{P_{low}}\right)$ >> j_{mix} therefore the denominators in the two terms above can be simplified. Adding lnP_{low} to each side, simplifying and then letting $P_{low} \to 0$ yields

$$ln\left[\frac{\hat{f}_i^{\,V}}{y_i}\right] = -ln\left[\frac{V-n_T j_{mix}}{n_T RT}\right] + \frac{j_i(n_i+n_j)}{V-n_T j_{mix}} - \frac{2(n_i i_i+n_j\sqrt{i_i i_j})}{RTV} \quad (2\text{-}17)$$

Subtracting lnP from both sides gives

$$ln\left[\frac{\hat{f}_i^{\,V}}{y_i P}\right] = \ln\left[\hat{\phi}_i^{\,V}\right] = -ln\left[\frac{P(v-j_{mix})}{RT}\right] + \frac{j_i}{v-j_{mix}} - \frac{2(y_i i_i+y_j\sqrt{i_i i_j})}{RTv} \quad (2\text{-}18)$$

2.4 Fugacity in the liquid phase and activity coefficient

The activity coefficient (γ) of a real solution quantifies the deviation in behaviour from a solution which is considered to be ideal. The activity coefficient can be completely defined only if the standard state fugacity ($\hat{f}_i$) is clearly specified (Prausnitz et al., 1980). The vapour phase in an ideal mixture is characterized by the fact that there are no potential intermolecular interactions. The ideal liquid phase however, is characterized by uniform intermolecular interactions between all molecules in the phase.

The activity coefficient relates the fugacity of species *i* in the liquid phase to the fugacity of an ideal solution mixture as follows

$$\gamma_i = \frac{\hat{f}_i^{\,L}}{\hat{f}_i^{\,ideal}} \quad (2\text{-}19)$$

The fugacity of species *i* in the liquid phase and the fugacity of the pure species at the reference state can be related via the activity (*a*) of species *i* as follows

$$a_i = \frac{\hat{f}_i^{\,L}}{\hat{f}_i^{\,0}} \quad (2\text{-}20)$$

The liquid phase mole fraction relates the activity to the activity coefficient as follows

$$a_i = x_i \gamma_i \quad (2\text{-}21)$$

Chemical potential for component *i* in an ideal mixture is given by

$$\mu_i = \mu_i^{\,0} + RTln(x_i) \quad (2\text{-}22)$$

Where μ_i is the chemical potential in the standard state.

In the case of a non-ideal system, the deviation from ideality can be accounted for by the chemical potential, and activity is given by

$$\mu_i = {\mu_i}^0 + RTln(a_i) \tag{2-23}$$

It is assumed that $\gamma_i \rightarrow 1$ as $x_i \rightarrow 1$ and the mixture obeys Raoult's law at this point. A positive deviation from Raoult's law is observed when the activity coefficient is > 1. Similarly, the converse is true when the activity coefficient is < 1. In the case of an ideal mixture, $\gamma_i = 1$ for all compositions (x_i), therefore $a_i = x_i$.

As $x_i \rightarrow 0$ then the activity coefficient approaches a finite limit ($\gamma_i \rightarrow {\gamma_i}^{\infty}$) which is referred to as "*the activity coefficient at infinite dilution*". Activity coefficients at infinite dilution play an integral role in the design of high purity separation schemes.

Identifying the non-idealities in the vapour and liquid phases using fugacity coefficients and activity coefficients respectively, is known as the gamma-phi (γ-ϕ) method or the combined method. This is discussed in greater detail in section 2.7.

At equilibrium

$$\hat{f}_i^{\,L} = x_i \gamma_i {P_i}^{sat} \tag{2-24}$$

$$\hat{f}_i^{\,V} = \gamma_i \Phi_i P \tag{2-25}$$

$$\text{Where } \Phi_i = \frac{\hat{\phi}_i}{{\phi_i}^{sat}} \exp\left[\frac{-{V_i}^L (P - {P_i}^{sat})}{RT}\right] \tag{2-26}$$

Φ_i is known as the Poynting correction factor, which allows for the correction of the liquid phase fugacity from the vapour pressure (${P_i}^{sat}$) to the system pressure (P).

${\phi_i}^{sat}$ is the vapour phase fugacity coefficient for the pure vapour of component *i* at the saturated pressure.

${V_i}^L$ is the saturated liquid molar volume of component *i*, and can be calculated from the Rackett equation (1970)

$$V_i^{\,L} = V_{ci} {Z_{ci}}^{(1-T_r)^{0.2857}} \tag{2-27}$$

Where V_{ci} is the critical volume and Z_{ci} the compressibility of each component, whilst $T_r = \frac{T}{T_c}$ gives the reduced temperature.

Based on the relation in equation (2-7), combining equations (2-24) and (2-25) yields

$$\gamma_i \Phi_i P = x_i \gamma_i {P_i}^{sat} \tag{2-28}$$

Equation (2-28) is known as the modified Raoult's law, specifically used when deviations from the ideal gas law occur.

2.4.1 Evaluation of activity coefficients via Gibbs excess energy models

The activity coefficient of a system is a function of composition and temperature. The following form of the Gibbs-Duhem equation is true at a constant temperature and pressure

$$\sum_i x_i \left(\frac{\partial ln\gamma_i}{\partial x_i}\right)_{T,P} = 0 \tag{2-29}$$

It can be shown that

$$ln\gamma_i = \left[\frac{\partial\left(\frac{nG^E}{RT}\right)}{\partial n_i}\right]_{T,P,nj} \tag{2-30}$$

Because $ln\gamma_i$ is a partial property with respect to the excess Gibbs energy $\left(G_i^E\right)$, the Gibbs-Duhem equation then becomes

$$G_i^E = \sum_i x_i d(ln\gamma_i) = 0 \tag{2-31}$$

The activity coefficient can be related to Gibbs excess energy, therefore at a particular pressure, temperature and composition, the activity coefficient can be determined if there is an appropriate model describing the Gibbs excess energy.

Numerous models have been developed to account for liquid phase non-idealities from Gibbs excess energy models. Table 2-1 provides a list of some of the more commonly used activity coefficient models via Gibbs excess energy. The reader is referred to the work of Raal and Mühlbauer (1998) for a more in depth review of the various activity coefficient models.

Table 2-1: Gibbs excess energy models to calculate activity coefficients.

Name	Equation	Equation Number	Reference
Van Laar	$\frac{G^E}{RT} = \frac{A_{ij}A_{ji}x_ix_j}{x_iA_{ij}+x_jA_{ji}}$	(2-32)	Van Laar (1910)
Wilson	$\frac{G^E}{RT} = \sum_{i=1}^{m} x_i ln\left(\sum_{j=1}^{m} x_j\Lambda_{ij}\right)$	(2-33)	Wilson (1964)
Tsuboka-Katayama-Wilson (T-K-Wilson)	$\frac{G^E}{RT} = x_i ln\left[\frac{x_i+V_{ij}x_j}{x_i+\Lambda_{ij}x_j}\right] + x_j ln\left[\frac{x_j+V_{ji}x_i}{x_j+\Lambda_{ji}x_i}\right]$	(2-34)	Tsuboka and Katayama (1975)
Universal Quasi-Chemical (UNIQUAC)	$\frac{G^E}{RT} = \left[\sum_{i=1}^{m} x_i\, ln\frac{\phi_i^*}{x_i} + \frac{\zeta}{2}\sum_{i=1}^{m} q_ix_i ln\frac{\theta_i}{\phi_i^*}\right] + \left[\sum_{i=1}^{m} q_ix_i ln\left(\sum_{j=1}^{m}\theta_j'\tau_{ji}\right)\right]$	(2-35)	Abrams and Prausnitz (1975)
Non-Random Two-Liquid (NRTL)	$\frac{G^E}{RT} = \sum_{i=1}^{m} x_i \frac{\sum_{j=1}^{m}\tau_{ji}G_{ji}x_j}{\sum_{l=1}^{m} G_{li}x_l}$	(2-36)	Renon and Prausnitz (1986)

2.5 Virial equation of state

Due to the relation existing between the fugacity of a component (*i*) in the vapour phase and the volumetric properties of the vapour phase, the fugacity coefficient and therefore the fugacity can be calculated from an equation of state.

The virial equation of state (VEoS) accounts for the intermolecular interactions between molecules in the vapour phase and more accurately describes the behaviour of real gases compared to the ideal gas assumption.

The VEoS can be defined by first principles, and the preferred truncated form is

$$z = \frac{PV}{RT} = 1 + \frac{BP}{RT} \tag{2-37}$$

Where Z is the compressibility factor and its unity represents an ideal gas, B is the second virial coefficient and is a function of temperature only for pure components. In the case of a mixture, it is a function of temperature as given by

$$B_{mixture} = \sum_i^N \sum_j^N y_i y_j B_{ij} \tag{2-38}$$

Where y_i and y_j are the mole fractions of components i and j in the vapour phase respectively. The second virial coefficient for a binary mixture can be expressed as follows

$$B_{mixture} = y_i B_{ii} + y_j B_{jj} + y_i y_j \delta_{ij} \tag{2-39}$$

Where $$\delta_{ij} \equiv 2B_{ij} - B_{ii} - B_{jj} \quad (2\text{-}40)$$

Accurate values for the second virial coefficient B_{ii} and B_{jj} are obtained from accurate volumetric data for pure gases *i* and *j*. For values of B_{ij} it is essential to have accurate volumetric data for gaseous mixtures of *i* and *j* (Prausnitz et al., 1967).

However, data of such nature is not usually available and it is therefore necessary to estimate the desired second virial coefficients from correlations such as Pitzer-Curl (1957), Black (1958), O'Connell and Prausnitz (1967), Kreglewski (1968), Tsonopolous (1974) and Hayden O'Connell (1975) to name a few.

Tables 2-2 and 2-3 provide a list of some of the most commonly used equations of state, and correlations used to estimate second virial coefficients respectively.

Table 2-2: Equations of state.

Name	Equation	Equation Number	Reference
Redlich-Kwong	$P = \frac{RT}{V-b} - \frac{a}{T^{0.5}V(V+b)}$	(2-41)	Redlich and Kwong (1949)
Soave-Redlich-Kwong (SRK)	$P = \frac{RT}{V-b} - \frac{aT}{V(V+b)}$	(2-42)	Redlich and Kwong (1949)
Peng-Robinson	$P = \frac{RT}{V-b} - \frac{aT}{V(V+b)+b(V-b)}$	(2-43)	Peng and Robinson (1976)

Table 2-3: Correlations used to estimate second virial coefficients.

Name	Equation	Equation Number	Reference
Pitzer- Curl	$\frac{BP_c}{RT_c} = B^0 + \omega B^1$	(2-44)	Pitzer and Curl (1957)
Tsonopolous	$\frac{BP_c}{RT_c} = f^0(T_r) + \omega f^1(T_r)$	(2-45)	Tsonopolous (1974)
Hayden-O'Connell	$B_{total} = B_{free} + B_{metastable} + B_{bound} + B_{chem}$	(2-46)	Hayden and O'Connell (1975)

2.5.1 Mixing rules

An EoS is usually accompanied by a mixing rule when representing the phase equilibrium of a mixture. Mixing rules are used in order to characterize the interaction of molecules in a mixture. Some of the most common mixing rules include that of Van der Waal (1873), Wong and Sandler (1992) and Twu and Coon (1996). Various mixing rules have been developed over the years. For this work, no mixing rules were utilised as equations of state such as Peng Robinson and Soave-Redlich Kwong, which are usually accompanied by a mixing rule, were not employed. The reader is referred to the work of Raal and Mühlbauer (1998) for a more detailed review on mixing rules.

Table 2-4: Mixing rules.

Name	Equation	Equation Number	Reference
Van der Waal	$a = \sum_i^n \sum_j^n x_i x_j a_{ij}$	(2-47)	Van der Waal
	$b = \sum_i^n \sum_j^n x_i x_j b_{ij}$	(2-48)	(1873)

2.6 Direct method $(\boldsymbol{\phi - \phi})$

Data reduction via the direct method uses fugacity coefficients from equations of state to describe the vapour and liquid phase non-idealities. Equations of state along with suitable mixing rules are used in order to describe the system in consideration. The reader is referred to the work of Mühlbauer and Raal (1995) which provides an in depth review of the direct method.

2.7 Combined method $(\boldsymbol{\gamma - \phi})$ using Barkers algorithm

The combined method utilises an activity coefficient model to describe the non-idealities in the liquid phase and fugacity coefficients from equations of state to describe the non-idealities in the vapour phase. As stated earlier, for the measurement of phase equilibrium data in a static synthetic apparatus such as the one used in this project, the measured variables are the temperature, pressure and overall composition. Overall composition (z_i) is calculated using the known volume displaced by the pump and a simple mass balance. In order to determine the liquid mole fraction (x_i) of the measured data, the combined method (γ-ϕ) is utilised in conjunction with the method of Barker (1953). The advantage of using the method of Barker (1953) is that the liquid phase mole fraction (x_i) can be calculated without any physical phase sampling, however a disadvantage is that the vapour phase mole fraction (y_i) cannot be calculated and a model representation is presented instead.

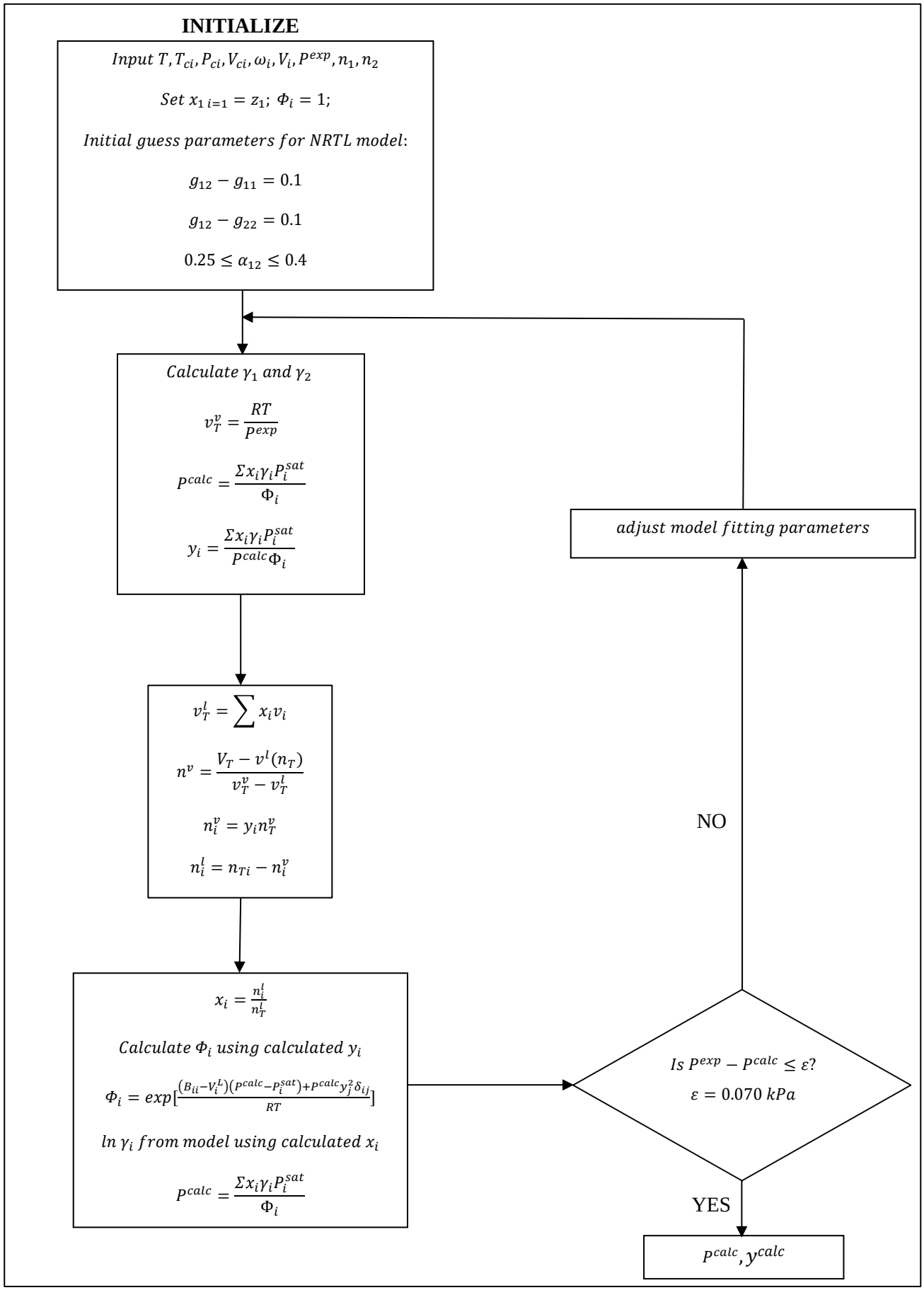

Figure 2-1: Algorithm of Moodley (2012) for phase equilibrium data reduction using the combined method of Barker (1953) with the NRTL model.

Figure 2-1 presents the algorithm used by Moodley (2012) for phase equilibrium data reduction using the combined method of Barker (1953) and the NRTL activity coefficient model. According to Moodley (2012) the method of Barker (1953) is used to minimize the pressure residual ($\delta P^{residual}$), in order to fit the measured total pressure and overall composition data to an excess Gibbs energy model. Where

$$\delta P^{residual} = P^{exp} - P^{calc} \tag{2-49}$$

An appropriate G^E model is selected and the activity coefficients of each component are determined, using the excess Gibbs Energy model. The total pressure in the system is calculated by the summation of the modified Raoult's Law i.e. equation (2-28), with the initial assumption that the vapour phase is ideal. Using this information, and the individual total phase volumes, the moles of each component in each phase is determined via a mass balance. "*The phase compositions are calculated, the activity coefficients and vapour phase correction factors are re-estimated and a new calculated pressure is yielded*" (Moodley, 2012). This process is repeated until the difference between the experimental and calculated pressure is within a specified tolerance (≤ 0.07 kPa). In order to achieve this, the objective function is minimized.

$$objective\ function = \sum \delta P^{residual^2} \tag{2-50}$$

Other work, including that of Raal (2011) and Uusi-Kyyny (2002), utilised similar algorithms in order to regress the experimental data, however, in these two cases the tolerance factor utilised to determine the final liquid mole fraction is dependent on the change in moles of the vapour and liquid phases. In the work of Uusi-Kyyny (2002), the tolerance is required to be: $x_i < 1 \times 10^{-7}$.

For this project, data regression for the attainment of model parameters was conducted using the Aspen Plus® simulation software package. The "*maximum likelihood*" objective function in Aspen Plus® was utilised during data regression as it provides a global optimum in parameter estimation (Nala, 2012), resulting in the objective function (OF) of the algorithm being the sum of both the temperature and pressure residuals. In addition the tolerance factor is dependent on the difference between the calculated x_i and the x_i value from the previous iteration. i.e. x_{i-1}. The algorithm and data regression procedure utilised in this project is discussed in greater detail in Chapter 5.

2.8 Thermodynamic consistency testing

A binary system can be described by any three measured variables i.e. pressure, temperature, liquid composition or vapour composition. The fourth variable can be determined using the Gibbs-Duhem correlation, and by comparing the particular measured variable (pressure, temperature, composition) to the calculated value of the same parameter (determined using the remaining three variables and the Gibbs-Duhem equation), the thermodynamic consistency can be determined.

In this work, Barkers method was used to determine the vapour phase composition. The computational procedure utilizes the Gibbs-Duhem equation, making it impossible to test thermodynamic consistency, as it will be redundant. According to Van Ness et al. (1973), unless a consistency test is considered essential, it is not necessary.

CHAPTER 3 : Experimental Methods and Equipment Review

The accurate measurement of phase equilibrium data enables a good understanding of the phase separation behaviour of a broad spectrum of chemicals. However, the complexity of measuring phase equilibrium data due to different operating conditions, and the significant differences in mixing behaviour, has resulted in the development of a wide variety of VLE apparatus.

The focus of this chapter is to provide a literature review of select experimental techniques that are focused around this research project. Literary work such as Fonseca et. al (2011) provides a comprehensive review on the numerous techniques and apparatus available for phase equilibrium measurements.

3.1 Experimental techniques

According to Reddy (2006), the numerous types of VLE equipment available is as a result of no single phase equilibrium apparatus being suitable for all pressure and temperature ranges, chemical systems and types of data required. Thus, general methods for determining phase equilibrium data can be classified as follows (Seker and Somer, 1993):

- Dynamic techniques
- Static techniques
- Dew/bubble point techniques

The dynamic and static techniques are the most common methods used in phase equilibrium measurements. The dynamic technique involves the circulation of components throughout a still, usually comprised of glass and stainless steel for low and high pressure stills respectively. The static method involves the agitation of the vapour and liquid phases with no circulation occurring. The dew and bubble point method is usually utilised for high pressure phase equilibrium measurements.

3.1.1 The dynamic method

The recirculating method, also known as the dynamic method can be used for the study of various types of mixtures from binary to quaternary. Figure 3-1 provides a schematic diagram of the VLE glass recirculating still used in the Thermodynamics Research Unit. Once a mixture is injected into the reboiler (M), heating is induced and the mixture is then brought to a boil. Continuous separation of the

vapour and liquid phases occur in the equilibrium chamber (N). The vapour phase is condensed in a receiver (S2) and thereafter returns as condensate to the boiling mixture. The necessary pressure and temperature sensors are appropriately situated and once a steady state of equilibrium has been reached, the desired variables are recorded. Samples are withdrawn from the vapour and liquid sampling points (S2 and S1 respectively), and analysed using a gas chromatograph in order to determine the composition of the vapour and liquid phases.

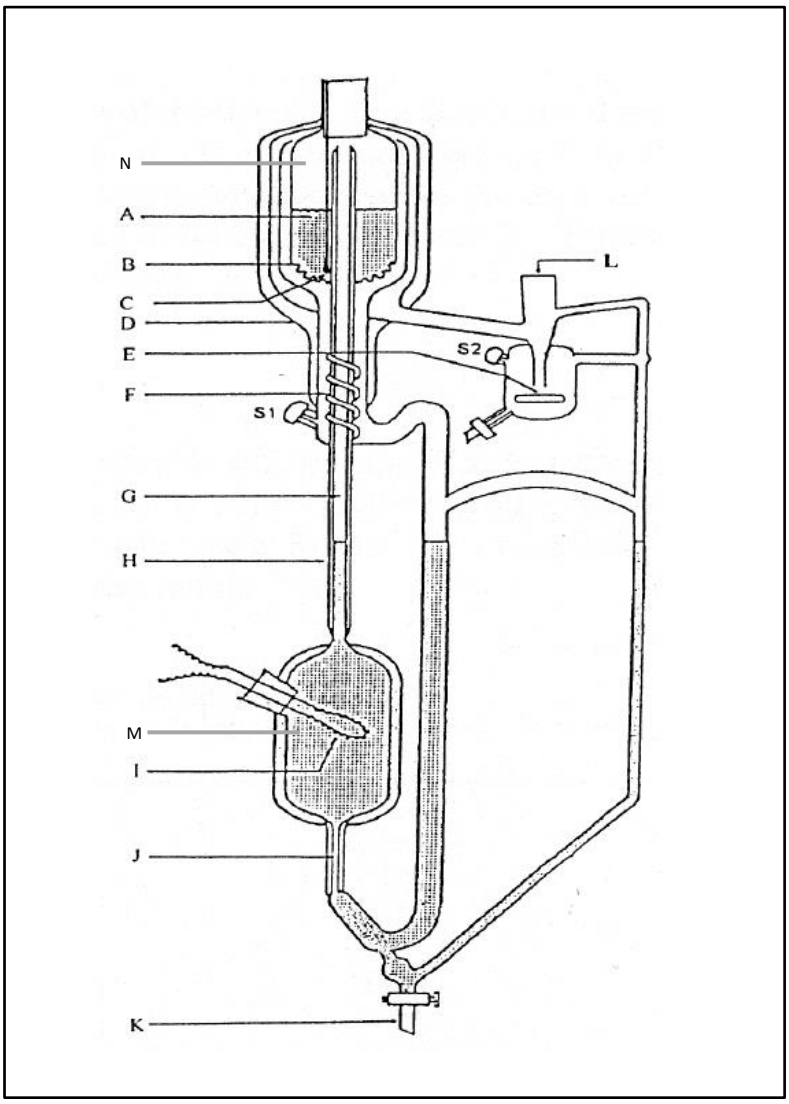

Figure 3-1: A schematic diagram of a low pressure VLE apparatus (Clifford, 2004).

A: Stainless steel wire mesh packing; B: Drainage holes; C: Pt-100 sensor; D: Vacuum jacket; E: Magnetic stirrer; F: Stainless steel mixing spiral; G: Insulated Cottrell pump; H: Vacuum jacket; I: Internal heater; J: Capillary leg; K: Drainage valve; L: Condenser attachment; M: Reboiler; N: Equilibrium chamber; S1: Liquid sampling septum; S2: Vapour sampling septum.

The dynamic method can be operated under both isobaric and isothermal conditions and there are various equipment designs available that cover a broad range of temperatures and pressures. Some examples of this are listed in Table 3-1. The work of Dohrn et al. (2010) provides a comprehensive review of the dynamic VLE technique.

Table 3-1: Some examples of recirculating apparatus.

Apparatus Type	T (K)	P (kPa)	*MOC	Reference
LPVLE	283-453	0-100	glass	Raal and Mühlbauer (1998)
LPVLE	283-453	0-100	glass	Joseph (2001)
LPVLE	283-453	0-100	glass	Ndlovu (2005)
MPVLE	283-453	0-500	glass	Lilwanth (2014)
HPVLE	383	46 000	-	Lee and Tan (1998)
HPVLE	100-300	10 000	copper	Raabe et al. (2001)

*MOC = material of construction

3.1.2 The static method

In recent times, the static technique has become more commonly employed for VLE measurements as opposed to the dynamic method. This is due to the increased durability of static cells, which are usually constructed from stainless steel, as well as the ability to perform phase equilibrium measurements over a higher temperature and pressure range.

The static apparatus usually consists of an equilibrium cell, a vacuum system and a temperature controlled bath. For the operation of a static apparatus, an equilibrium cell is evacuated and submerged in an isothermal bath of either oil or water. A liquid mixture is then charged into the cell and agitated via a mechanical stirrer, until equilibrium between the vapour and liquid phases is established. One of the key aspects in static synthetic measurements is degassing of the liquid feed to remove any dissolved gasses. It is therefore imperative to ensure that thorough degassing of the components occur in order to achieve accurate data. Degassing can be conducted via vacuum distillation, *in-situ* or external to the equilibrium cell, as described by Van Ness and Abbott (1978).

The static technique can be sub-categorised into the static analytical and static synthetic techniques. These two methods are similar however the static analytical method incorporates an additional facility for the sampling of the vapour and liquid phases. The static synthetic method requires no phase sampling and instead relies upon correlations to determine the liquid and vapour compositions.

The static analytical method

The static analytical apparatus features, along with the equilibrium cell, a thermal bath, measuring devices (temperature and pressure transmitter) and sampling and analytical devices for the measurement of the vapour and liquid phase compositions. Figure 3-2 illustrates the general setup for the static analytical technique.

The key feature of the static analytical technique is the sampling of the vapour and liquid phases. Over the years the static analytical technique has been employed in a vast amount of phase equilibrium equipment design, with some of the most significant works being Ng and Robinson (1978), Guillevic et al. (1983), Zimmerman and Keller (1989), Mühlbauer and Raal (1991), Laursen et al. (2002), Valtz et al. (2002), Naidoo et al. (2008) and Narasigadu et al. (2013), to name a few. The key variations between these studies include:

- The design of the equilibrium cell and materials of construction
- The methods of ensuring isothermal conditions in and around the cell
- The methods of agitation of the cell contents
- The methods of homogenizing the vapour and liquid phases
- The methods of sampling and composition analysis
- The methods of degassing of components prior to experimentation

One of the challenges posed by this technique is the possibility of partial condensation of the vapour phase as well as partial evaporation of the liquid phase during the sampling and analysis procedure. Dohrn et al. (2010) states that "*withdrawing a large sample from an autoclave causes a considerable pressure drop, which disturbs the phase equilibrium significantly*." Some techniques for reducing the pressure drop caused by the sampling process include withdrawing minute (μL) samples for analysis, or utilising a variable-volume cell such as that of Coquelet et al. (2003). The variable volume cell consists of a cell body and is sealed at the top by a moveable piston, which is used to compensate for the pressure loss during phase sampling. Alternatively, the pressure drop can be decreased by blocking off the sampling volume from the remaining contents of the equilibrium cell before pressure reduction (Sue et al., 2004).

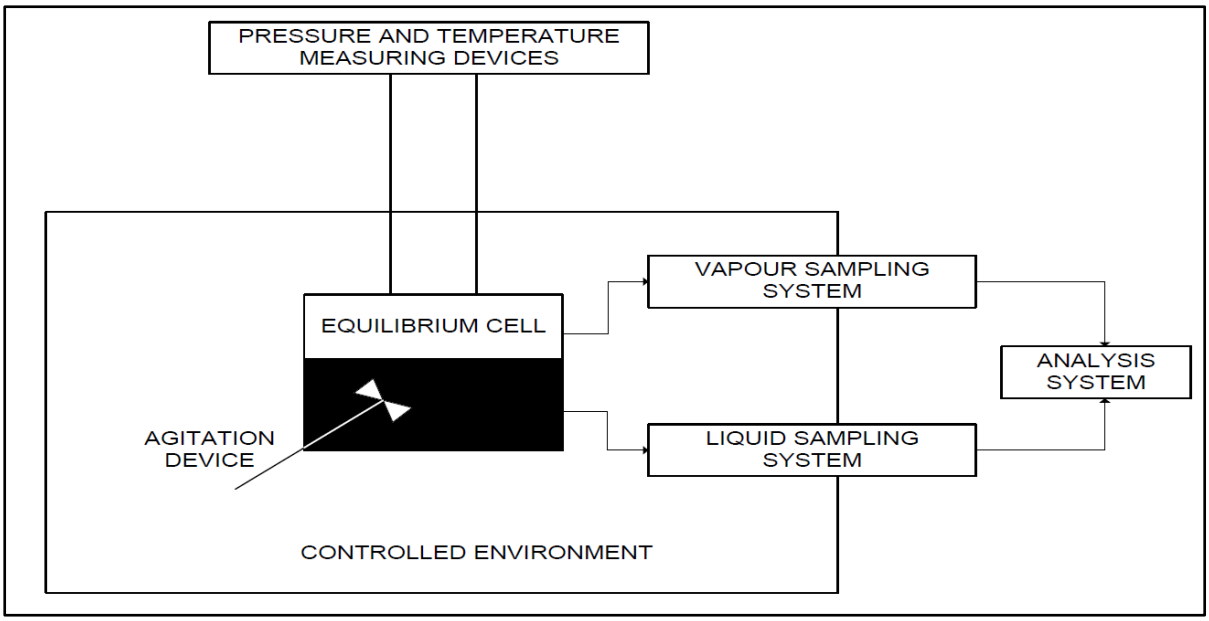

Figure 3-2: A schematic diagram of the static analytical method (Raal and Mühlbauer, 1998).

The static synthetic method

Removing samples and analysing mixture compositions can be very difficult in certain cases, however, synthesizing mixtures of known composition is easier. Generally, synthetic methods are more reliable than analytic methods and for this research project, the static synthetic technique was utilised. Thus, the focus of this section is based on the various types of static synthetic apparatus and designs, and its progression throughout the years. For the static synthetic technique, temperature, total pressure and overall composition are measured. The composition, along with correlations such as that of Barker (1953) can be used to determine the mole fraction (x_i) of the components in the cell.

This technique is well suited for systems below the critical temperature region, and incorporates a simple experimental procedure as there is no phase sampling involved. However, a disadvantage of this method is that limited information for ternary mixtures or higher can be obtained. Also, thermodynamic consistency cannot be tested as the Gibbs-Duhem equation is used both in calculating the liquid composition and in thermodynamic consistency calculations, thus rendering it redundant.

Various authors have utilised this technique in their research dating back to the 1950's. Table 3-2 displays a summary of some of the significant work regarding the static synthetic apparatus. A detailed literature review of some of the equipment is provided in this chapter.

Table 3-2: A summary of static synthetic apparatus.

Authors	Equilibrium Cell		Operating Range		Method of Degassing	Agitation	Automated
	*MOC	Vol. /cm^3	T/ K	P/ kPa			
Gibbs and Van Ness (1972)	glass	100	ambient to 348.15	-	*in-situ* refluxing	magnetic stirrer	no
Maher and Smith (1979)	glass	15 x 25	ambient to 393.15	0-100	freezing, evacuation, thaw cycle	none	no
Kolbe and Gmehling (1985)	glass	180	ambient to 423.15	10-100	independent rectification in glass column	magnetic stirrer	no
Rarey and Gmehling (1993)	glass	100	ambient to 373.15	0-100	*in-situ* refluxing	magnetic stirrer	yes
Fischer and Gmehling (1994)	steel	180	ambient to 423.15	0-12000	independent rectification in glass column	rotating magnetic field	no
Uusi-Kyyny et al. (2002)	SS 316	96	ambient to 368.15	0-690	independent vacuum distillation	magnetic stirrer	yes
Raal et al. (2011)	SS 316	190	ambient to 373.15	0-100	*in-situ* refluxing	magnetic stirrer	no
†**Moodley (2012)**	SS 316	190	ambient to 393.15	0-1600	independent vacuum distillation	magnetic stirrer	yes

*MOC- Material of construction. †Automation and change of pressure transmitter made to the apparatus of Raal et al. (2011).

3.2. A review of static synthetic apparatus

The apparatus of Gibbs and Van Ness (1972)

The apparatus of Gibbs and Van Ness (1972) is an early example of a static total pressure apparatus. Figure 3-3 provides a schematic diagram of the apparatus. The apparatus was an improvement of the design of Ljunglin and Van Ness (1962) and Van Ness et al. (1967 a, b). Although the original design yielded sufficiently accurate data (Raal and Mühlbauer, 1998), the data gathering procedure was slow. This was due to the pure liquids being degassed in the equilibrium cell and required the cell being emptied and evacuated after each degassing procedure. The new design, which consisted of a 100 cm^3 glass cell, incorporated volumetric metering of the degassed components via piston injectors.

Successful operation of the experimental setup commenced by introducing the pure components into the respective degassing units where dissolved gases are removed via *in-situ* refluxing, cooling and evacuation in a vacuum flask. Once the system was completely evacuated, the degassed liquids were loaded into the piston injectors, where they were stored for subsequent injection into the equilibrium cell. The cell was magnetically stirred and immersed into a temperature controlled oil bath. A metered amount of component 1 was loaded into the cell and the vapour pressure was observed. A further small metered amount of component 1 was added, and any change in the vapour pressure reading indicates that the component was poorly degassed. If the feed was successfully degassed, then a small metered amount of the second component was added. The system pressure was allowed to equilibrate and was thereafter recorded. A second metered amount of component 2 was added and the process was repeated until a particular volume of the second component was loaded into the cell.

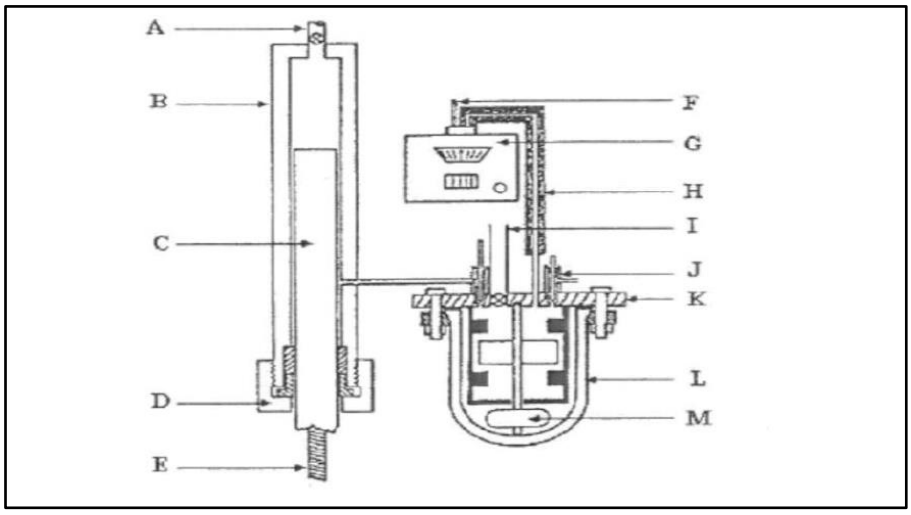

Figure 3-3: The apparatus of Gibbs and Van Ness (1972) (extracted from Motchelaho, 2006).

A: Line to degassing vessel; B: Piston-injector body; C: Piston; D: Packing nut; E: Lead screw; F: Line to reference vacuum; G: Pressure gauge; H: Heated line; I: Port to vacuum system; J: Needle valves; K: Cell cover; L: Glass cup; M: Teflon coated magnet.

Should the liquids be properly degassed, the main limitation of this method is the accuracy with which overall compositions from metered liquid volumes can be established.

The apparatus of Rarey and Gmehling (1993)

This apparatus (refer to Figure 3-4), as described by Rarey and Gmehling (1993), follows a similar operating procedure to the apparatus of Gibbs and Van Ness (1972). However, the complete automation of this apparatus is what gave it its originality. The purpose of automating the apparatus was to determine if an automated setup would produce reliable phase equilibrium data via the static synthetic method.

The apparatus was used for various types of measurements including pure component vapour pressures, binary and ternary phase equilibrium measurements, gas solubilities, isothermal compressibilities of liquids and activity coefficients at infinite dilution (Moodley, 2012). The apparatus, which consisted of a 100 cm^3 glass cell, had an operating range of 0-100 kPa and 273-373 K for pressure and temperature respectively. Pressure and temperature measurement, as well as the injection procedure were fully automated. The piston pumps were controlled by stepper motors. According to Rarey and Gmehling (1993), the accuracy of the injected volumes were reported to be within 1 mm^3. The piston design was based on the high precision design of Karrer and Gaube (1988) and had a maximum injection capacity of 32 cm^3.

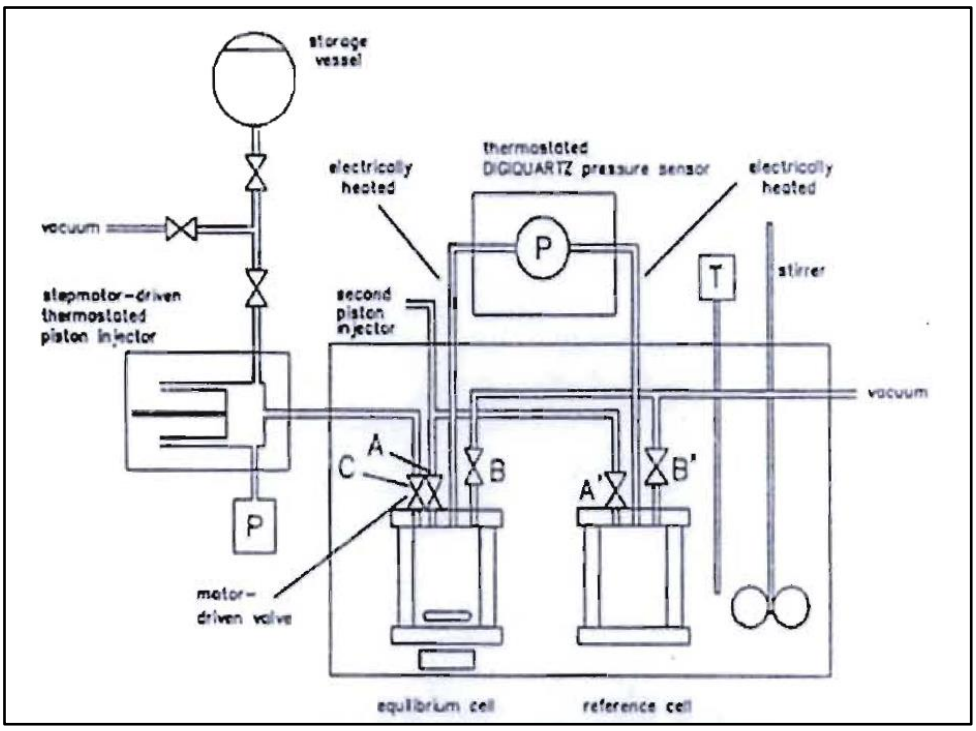

Figure 3-4: The apparatus of Rarey and Gmehling (1993) (extracted from Motchelaho, 2006).

The apparatus of Uusi-Kyyny et al. (2002)

A static total pressure apparatus was developed by Uusi-Kyyny et al. (2002) for moderate pressure phase equilibrium measurements. The apparatus (shown in Figure 3-5) was initially operated manually to ensure the setup was functioning correctly, and was thereafter automated. Degassing of the liquid components were conducted in a round bottom flask, which contained packing to enhance the boiling. The round bottom flask was attached to a water cooled condenser and placed in an ultrasonic bath, which was used as a boiler. The equipment consisted of an equilibrium cell, approximately 95.65 cm^3 in volume. The cell included small baffles to reduce equilibrium time as well as two high accuracy syringe pumps (Isco 260 D and Isco 10 0DM, operated at 900 kPa) which was used to displace the components into the cell. The contents of the cell were agitated using a magnetic stirrer. Pressure was measured using a Digiquartz 2100A-101-CE pressure transmitter with a range of 0-690 kPa. Temperature was measured using Pt-100 probes. According to Uussi-Kyyny et al. (2002), the design of Rarey and Gmehling (1993) was used as a paragon.

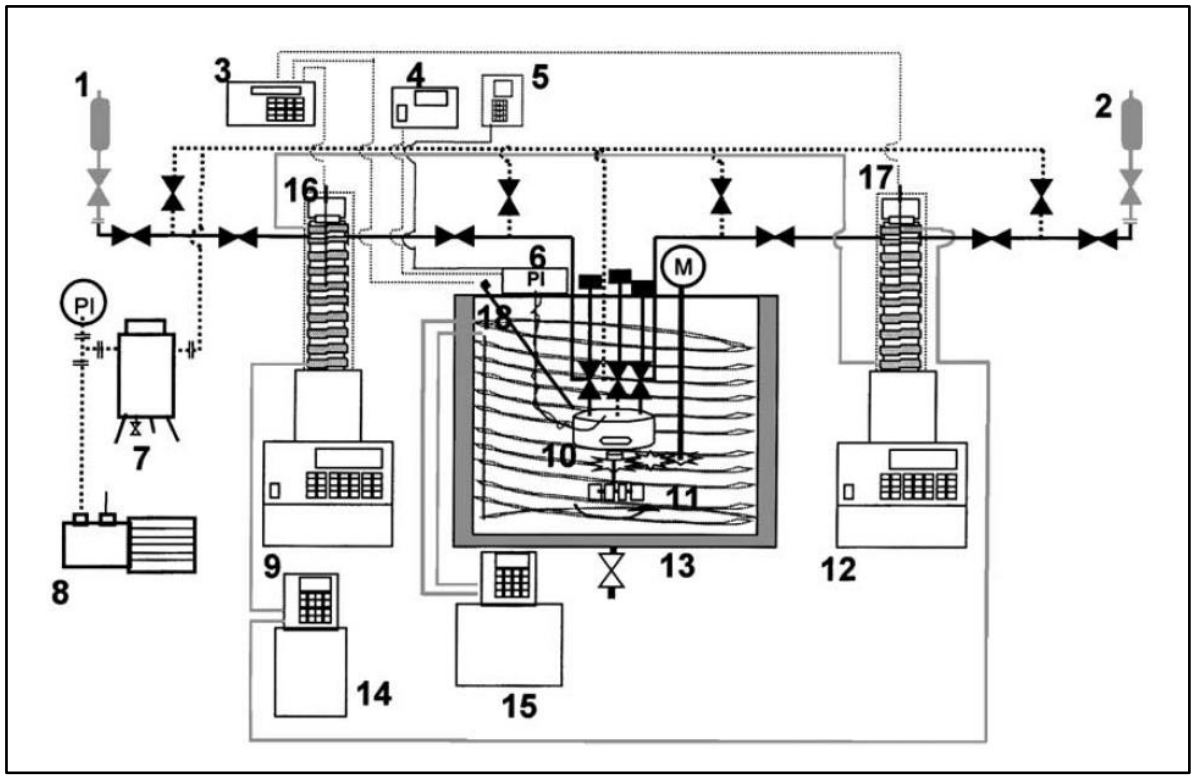

Figure 3-5: The apparatus of Uussi-Kyyny et al. (2002).

1 and 2: Feed cylinders; 3: Temperature meter; 4: Pressure display; 5: Temperature controller for transducer heating line; 6: Pressure transducer; 7: Liquid nitrogen; 8: Vacuum pump; 9: 260 cm^3 syringe pump; 10: Equilibrium cell; 11: Bath liquid mixer; 12: 100 cm3 syringe pump; 13: Thermostated water bath; 14: Circular bath for syringe pump temperature control; 15: Circular bath for water bath temperature control; 16,17 and 18: Temperature probes.

The apparatus of Raal et al. (2011)

A static synthetic, total pressure apparatus was designed by Raal and commissioned by Motchelaho (Raal et al., 2011) for phase equilibrium measurements at moderate pressures. The apparatus, shown in Figure 3-6, consisted of a stainless steel cell with an interior volume of approximately 190 cm^3. The apparatus was designed for operation at pressures up to 2000 kPa and incorporated hand-rotated dual mode piston pumps, which could dispense microliter volumes repeatedly in the micro-mode.

Pressure inside the cell was measured using a WIKA D-10 (0-100 kPa) pressure transmitter, whilst temperature was measured using a Pt-100 sensor. A magnetic stirrer was employed to ensure sufficient mixing of the cell contents. The apparatus used for the degassing of pure liquids was similar to that of Gibbs and Van Ness (1972). Over the years the piston injectors and solenoid valves posed some issues such leaks and required maintenance. The overall design of this apparatus was similar to that of Rarey and Gmehling (1993), but differed in that the patented dual mode piston pumps were capable of operation in either the macro or micro-modes, and the apparatus was not automated. This apparatus was the first low to moderate pressure, static synthetic phase equilibrium apparatus, commissioned within the Thermodynamics Research Unit at the University of KwaZulu-Natal.

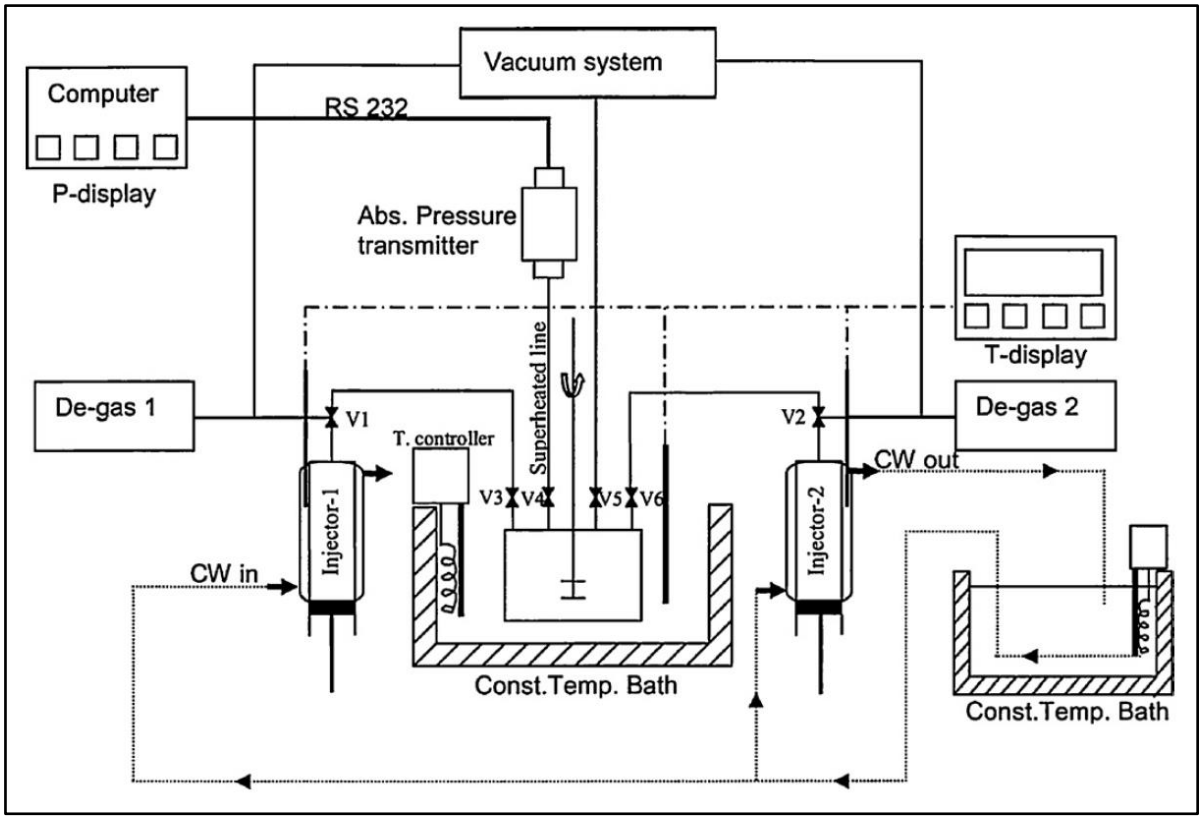

Figure 3-6: The apparatus of Raal et al. (2011).

The apparatus of Moodley (2012)

The apparatus designed and commissioned by Raal et al. (2011) was thereafter fully automated by Moodley (2012). A control scheme was developed and implemented in order to fully automate the original static total pressure apparatus of Raal et al. (2011). The scheme incorporated various pressure feedback closed loops in order to execute process step re-initialisation, valve positioning and motion control in a step wise manner. Two high resolution stepper motors were used to engage the dispensers, as they provided an accurate method for regulating precise volumes of components into the cell. The control scheme required approximately two days to produce a single forty data point isotherm (P-x), and minimized human intervention to 2-3 hours. The apparatus was modified to perform moderate pressure measurements up to 1600 kPa by replacing the original pressure transmitter with a WIKA P-10 (0-1600 kPa) transmitter.

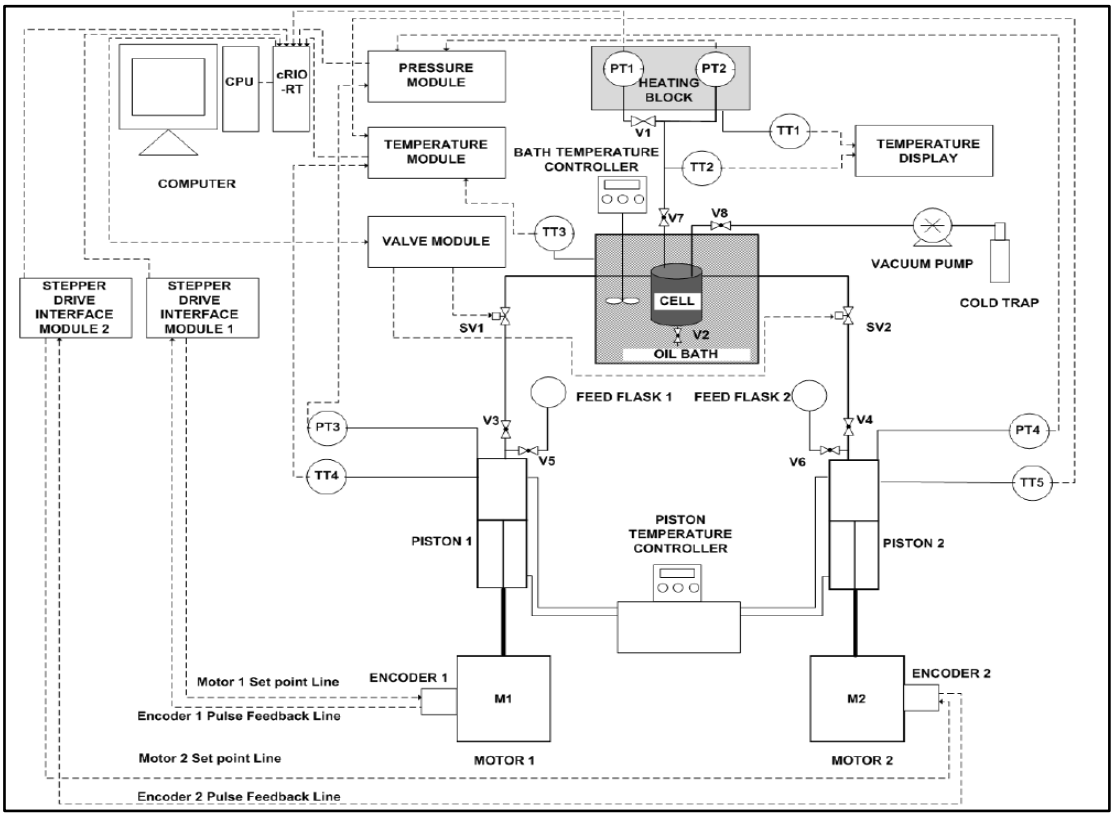

Figure 3-7: A piping and instrumentation diagram (P&ID) of the automation scheme of the apparatus of Moodley (2012).

M1-2: stepper motor 1-2; PT1: equilibrium cell pressure transducer (0-100 kPa) with isolation valve; PT2: equilibrium cell pressure transducer (0-1.6 MPa); PT3: pressure transducer (0-2.5 MPa) of piston injector 1; PT4: pressure transducer (0-2.5 MPa) of piston injector 2; SV1-2: solenoid valves; TT1: Pt-100 for the cell pressure transducer heating block; TT2: Pt-100 for the pressure transducer line; TT3: Pt-100 for the cell bath temperature; TT4: Pt-100 for the water jacket of piston 1 water jacket; TT5: Pt-100 for the water jacket of piston 2; V1-V8: manual valves.

Figure 3-7 is a P&ID of the automation scheme of the apparatus. Some key features of the automation aspect include an eight slot cRIO-9073 chassis which was used as the real time controller and housed all the modules used for measurement and feedback of the variables, two stepper motors interfaced via two single access stepper motor drives and two solenoid valves to control the flow of the feed to the cell.

From the literature reviews mentioned in section 3.2, it was observed that all of the degassing procedures follow a similar concept. The majority of degassing procedures discussed involved the distillation of feed components, either *in-situ* or independently. All of the degassing methods utilised, successfully degassed the pure components and thus a similar degassing technique was employed in this work.

The cell volume of the majority of equipment reviewed was approximately between 100 – 200 cm^3. For this work, a stainless steel cell of 60 cm^3 in volume was designed and constructed. This reduced cell volume is expected to result in equilibrium being achieved sooner, compared to a cell of larger volume, due to the smaller amount of chemicals utilised.

All of the automated apparatus yielded accurate results. The volume of components dispensed into the cell is of great importance, as it is used to determine the overall composition (z_i) in the cell. By comparing the results from the automated mode to that of the manual mode, the works of Rarey and Gmehling (1993), Uusi-Kyyny (2002) and Moodley (2012) were able to deem the automatic procedures for the respective apparatus successful.

Apart from the control valves used in an automated set up for the dispensing of the pure components into the cell, another factor that plays a major role in the accuracy of volume dispensed is the feed injection procedure. Most apparatus employ piston injectors, however there are numerous types of injectors available such as that used by Raal (2011) which were hand-rotated piston injectors, controlled by a stepper motor. However, over the years of usage it was observed that these pumps often incurred leaks and frequently required maintenance. For this work, two Teledyne Isco syringe pumps, such as those used by Uusi-Kyyny (2002) were employed. These pumps have a flow accuracy of 0.5% of the set point and can operate up to pressures of 695 000 kPa.

All of the apparatus reviewed were designed to operate isothermally and pressure was only measured and not controlled. The pressure was usually measured via a pressure transmitter device that could relay a signal to a display. The type of pressure transmitter used is dependent on the pressure rating of the cell, as well as the pressure range of interest for measurements. For this work a WIKA P-10 pressure transmitter with a range of 0-500 kPa was utilised for measurements in the moderate pressure region.

The literature review above describes some of the most successful and commonly used apparatus for phase equilibrium measurements. There are numerous other designs that have been successful in producing accurate data, which are not discussed in detail above. These include the work of Maher and Smith (1979), Kolbe and Gmehling (1985), and Fischer and Gmehling (1994) to name a few.

Chapter 4 provides a detailed description of the new apparatus designed in this this project as well as the operating procedure developed for successful utilisation of the apparatus.

CHAPTER 4 : Experimental Apparatus and Procedure

The aim of this project was to set up and commission a new static synthetic apparatus, as well as to develop an operating procedure for the measurement of P-T-z data in the low to moderate pressure range. Chapter 3 provides a historical review of the development of static synthetic apparatus over the past few decades. This chapter will highlight the unique features and advantages of the newly designed apparatus.

The focus of this chapter is based on the following aspects:

- The design of the new static synthetic equilibrium cell
- The equipment setup
- The experimental procedure utilized in this study

4.1 Experimental apparatus

The newly developed static synthetic apparatus commissioned in this project consists of the following components:

- A stainless steel equilibrium cell (60 cm^3)
- 2 x Teledyne Isco pumps (100 DX and 100 DM models with controller)
- A WIKA P-10 pressure transmitter (0-500 kPa)
- 2 x REB 1/10 DIN temperature sensors (73.15-873.15 K) for cell temperature measurement
- An Edwards RV3 vacuum pump
- 3 x stainless steel liquid baths used as follows:
    - To submerge the equilibrium cell (30 cm x 30 cm x 19 cm)
    - For the degassing unit (22.5 cm x 30.5 x 19 cm)
    - To maintain the temperature of the Isco pump thermal jackets (30 cm x 30 cm x 19 cm)
- 3 x temperature controllers used as follows:
    - A Grant TFX 200 temperature controller for the equilibrium cell bath
    - A Polyscience temperature controller used to maintain the temperature of the Isco pump thermal jackets
    - A Polyscience temperature controller used for the degassing setup
- A Heidolph RZR 2041 overhead stirrer
- An Agilent 34972A data acquisition unit

- A computer
- An electric jack
- 3 x AC DC Dynamics variacs
- 4 x additional Pt-100 sensors, situated as follows:
    - In the housing of the pressure transmitter
    - Against the nut, below the pressure transmitter
    - Against the lines between the Isco pumps and cell
    - In the heat transfer fluid bath of the Isco pumps
- A Polyscience chilling unit

Figure 4-1 is a schematic diagram of the experimental setup located in the laboratory of the Thermodynamics Research Unit. Similarly, photograph 4-1 shows the actual experimental setup in the laboratory.

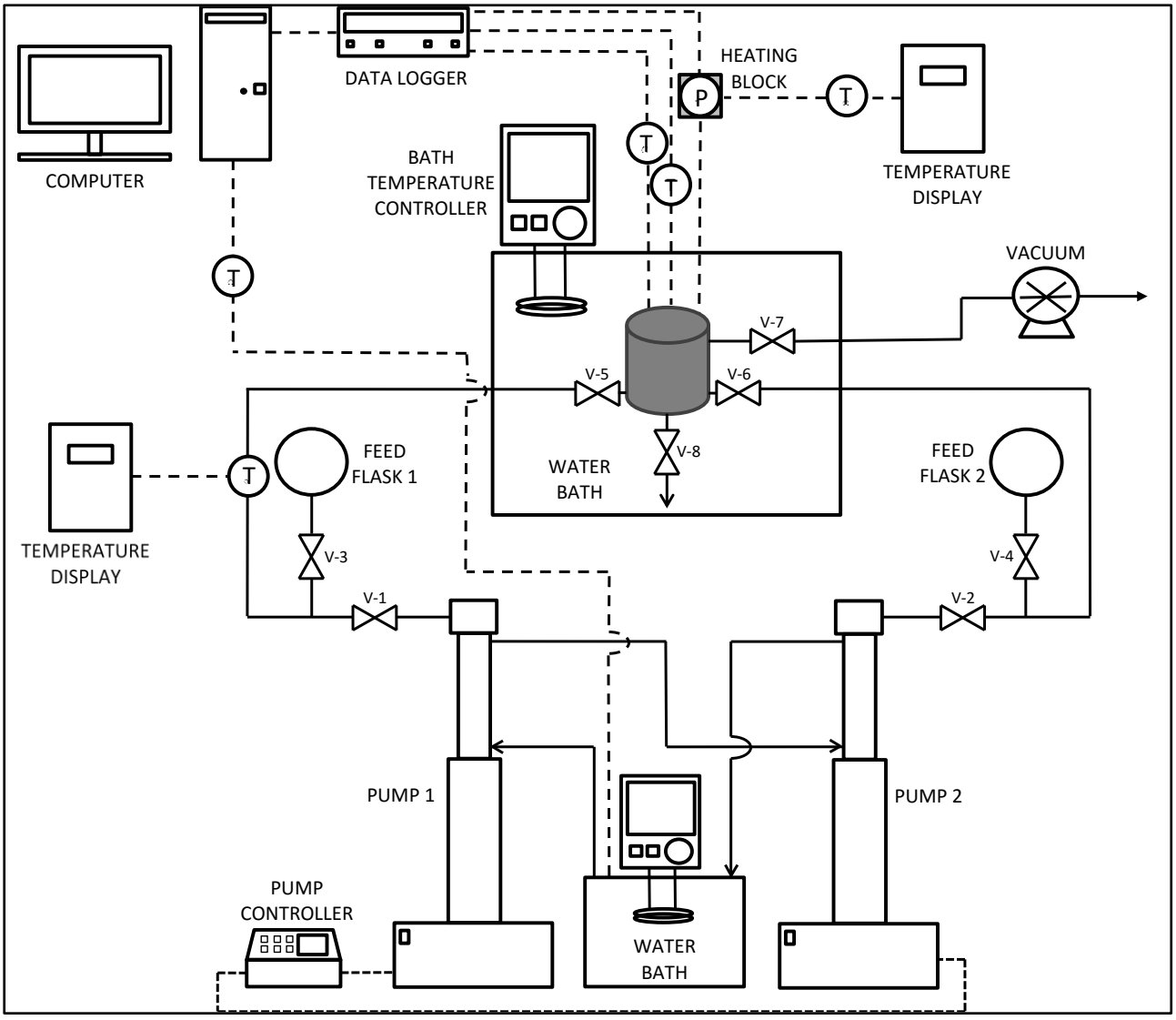

Figure 4-1: Schematic diagram of apparatus.

Photograph 4-1: The experimental setup.

4.1.1 Static synthetic equilibrium cell

The equilibrium cell incorporated in this apparatus was designed by Dr W. Nelson and constructed in the workshop at the discipline of Chemical Engineering in the University of KwaZulu-Natal. The reader is referred to Figure 4-2 for a complete set of dimensions of the cell. For the construction of the equilibrium cell, stainless steel 316 (SS 316) was the material of choice due to its durability, high resistance to corrosion, and excellent conductivity of heat. The cell is cylindrical in shape and therefore avoids the occurrence of dead-zones during mixing. A magnetic stirrer was incorporated to ensure sufficient mixing of the components in the cell. The total working volume of the cell is 60 cm^3 (excluding the volume displaced by the stirrer). The reduced volume of the cell designed in this project, in comparison to the 190 cm^3 cell used in the work of Raal et al. (2011), results in a smaller amount of chemicals required for measurements. Although the reduced cell volume will result in a smaller amount of chemicals being required, the volume of components need to be dispensed accurately into the cell, hence the use of high accuracy Isco syringe pumps for the feed.

A Viton O-ring was compressed into a groove between the cylindrical body of the cell and the flange. This particular O-ring was chosen as it has a broad chemical compatibility range. It was also expected to see an improvement of sealing under vacuum, due to the use of O-ring gasket and compression fittings, as no threaded fittings were utilised. The cell body and flange were fastened together using 6 x 4 mm SS bolts. Two holes of 6 mm in diameter were drilled through the top, outer edge of the flange in order to slot in two copper casings that house the temperature sensors.

All valves used on the experimental setup were $^{1}/_{8}$ inch SS 316 ball valves, supplied by Swagelok. The valves have a maximum temperature and pressure range of 423.15 K and 17 200 kPa respectively. At the base of the cell, a drain valve is attached to a $^{1}/_{8}$ inch SS line approximately 50 mm in length. The line is silver soldered to a hole 1,5 mm in diameter, drilled at the base. Two additional holes of approximately $^{1}/_{8}$ inch in diameter were drilled on opposite ends near the bottom of the cell body. These are the feed loading points and contain 20 threads per inch, in order to fit a ball valve at either end. The ball valves are attached directly to the cell body via a copper gasket, which was used to seal the face of each ball valve to the cell body. Attaching the valves directly to the cell body eliminates any dead volume in the line and the pure components are loaded directly into the liquid phase. However, the dead volume in the ball of the valve needs to be accounted for, thus an initial 10 ml of each component is flushed through the cell before commencing with measurements to fill up the ball chamber with liquid and eliminate dead volume. This is discussed in greater detail section 5.6. This is a key feature of the new design as all previous designs have loaded the feed through a line running through the flange at the top of the cell. This may cause liquid to get trapped in the line and result in a dead volume. Two additional holes, approximately 2 mm in diameter, are drilled through the flange. These holes are for the vacuum line and the line to the pressure transmitter.

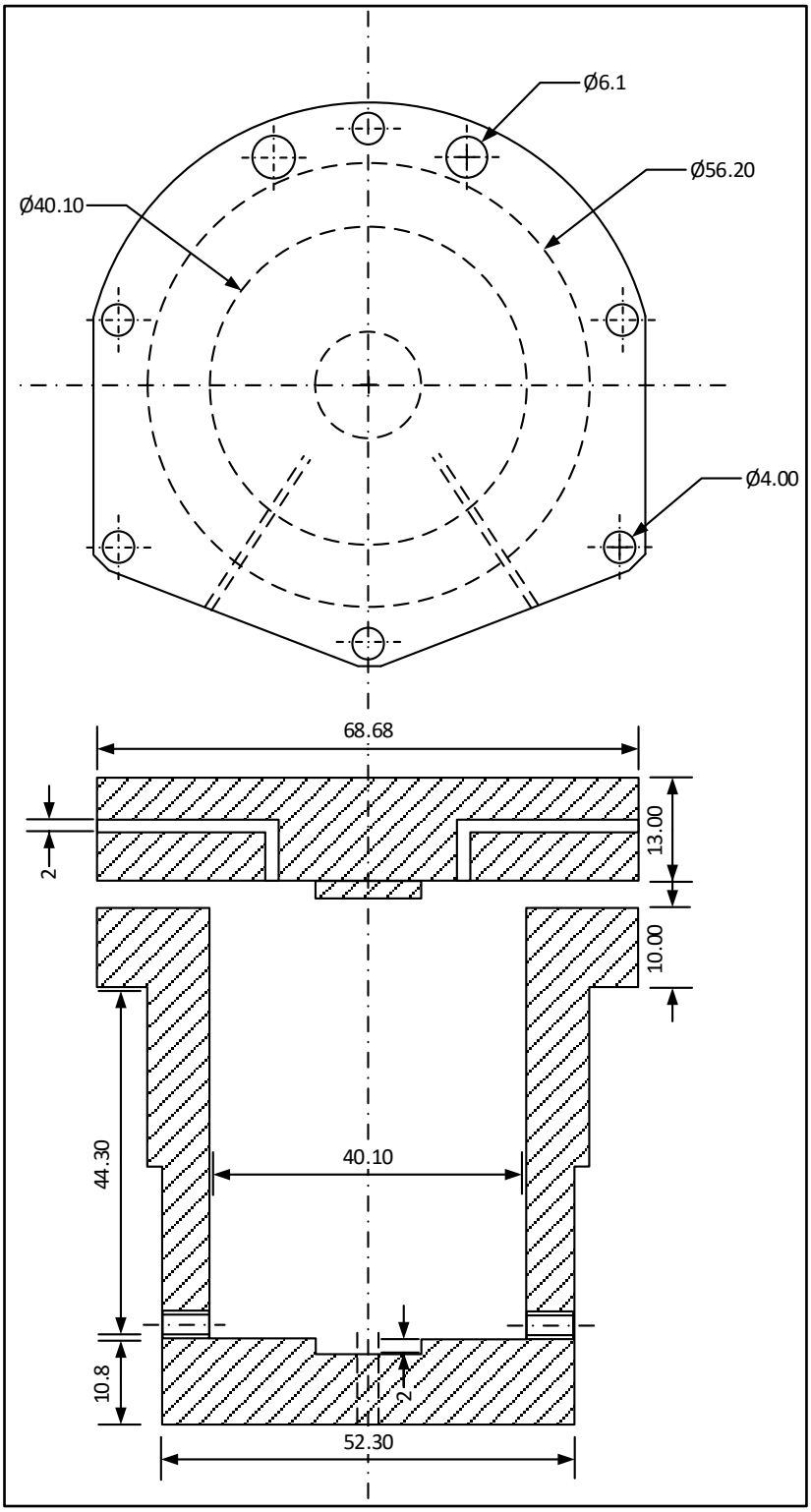

Figure 4-2: Dimensioned drawing of the cell (top and cross-sectional side view; dimensions in mm).

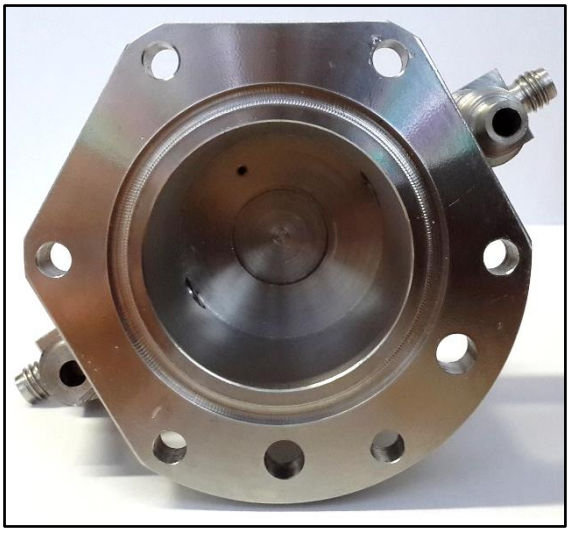

Photograph 4-2: Top view cell without magnetic stirrer.

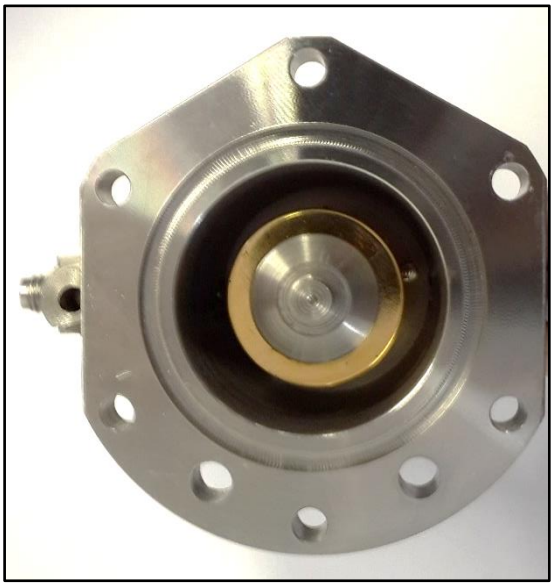

Photograph 4-3: Top view of cell with magnetic stirrer.

4.1.2 Agitation device

Adequate stirring is necessary to yield accurate P-x data, therefore it is imperative that the cell incorporate an effective agitation device to ensure even distribution of components in the cell. For this cell, a magnetic stirring device was employed. The stirring device consists of a gold and copper plated neodymium super magnet, on a small SS 316 rod (refer to photograph 4-4). This particular magnet was

chosen as it is durable and chip resistant compared to its nickel plated counterpart. The magnet consists of the following properties/dimensions (Nelson 2016, personal communication):

- Material: NdFeB
- Shape: Ring
- Outer diameter: 28 mm
- Inner diameter: 18 mm
- Height: 10 mm
- Tolerance in size: ± 0,1 mm
- Direction of magnetisation: diametral (parallel to diameter)
- Working temperature: max 393 K
- Strength of magnetisation: 40H
- Type of coating: Gold-plated nickel (Ni-Cu-Ni-Au)

A Heidolph overhead stirrer with a magnetic rod was situated directly above the cell. The overhead stirrer operates at two different speed modes, i.e. I (33 – 361 rpm) and II (170 – 1807 rpm). When switched on, the magnetic force between the magnets drive the internal stirrer. The stirrer runs smoothly due to the ball bearings fitted on the bottom of the stirrer as well as the flange (refer to Photograph 4-5). The ball bearings are made of SS 316 and the lubricants were removed with acetone.

Photograph 4-4: Magnetic stirring device.

Photograph 4-5: Magnetic stirrer fitted to the flange.

In order to determine if the stirrer is working correctly the following procedure is followed:

- Allow the pressure in the cell to stabilize at any given mixture composition
- Once stable, introduce a small amount of any of the two components into the cell
- The pressure should increase or decrease (depending on the volatility of the second component) extremely slowly, if not at all
- Switch on the mixer
- The pressure should immediately increase or decrease depending on the component added

Figure 4-3 is an example of the behaviour of the pressure in the cell when the mixer is switched on.

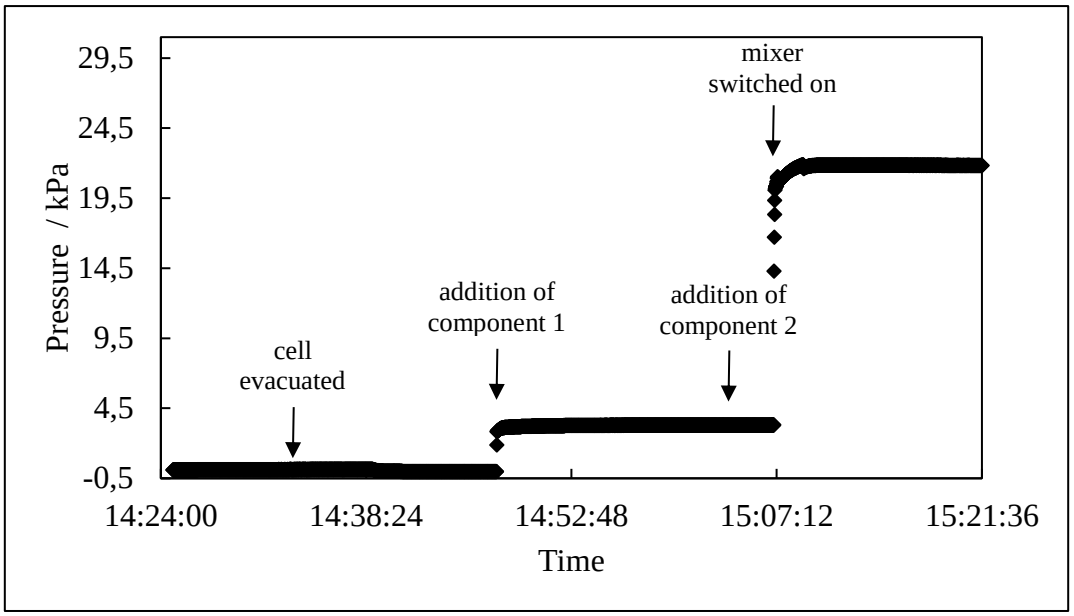

Figure 4-3: Pressure readings in the cell with the addition of components and use of stirring.

4.1.3 Feed pumps

The apparatus consists of two high accuracy syringe pumps, supplied by Teledyne Isco. The pumps used are the 100 DX and 100 DM models. In this project, the 100 DM model pump is referred to as pump 1 and the 100 DX model is referred to as pump 2. The function of the syringe pumps are to house and dispense the chemicals into the cell as accurately as possible. Each pump has two loading/dispensing points and was fitted with a secure, high pressure $^{1}/_{8}$ inch Valco fitting on one end and a SS line on the other. The SS line runs from the syringe pump to the equilibrium cell with three ball valves in between (refer to Figure 4-1). To calculate the volume loaded into the cell, the volume in the pump after loading the pure component in the cell is subtracted from the volume before loading.

The pumps are capable of operation in both constant pressure and constant flow modes. For this project, operation was carried out in the constant pressure mode, and were controlled using a "smart-key" control device. Once the components are loaded into the cell (refer to section 4.2.3 on loading), the pumps are set to the "run" mode which in this case was 2000 kPa (gauge). The piston therefore compresses the fluid to the set pressure. After conducting numerous trial runs, 2000 kPa (gauge) was selected as the pump operating pressure as it gave the most accurate results when compared to literature data. When the feed valves (V-5 and V-6) are opened to dispense the fluid into the cell, the piston then moves to compensate for the pressure loss. When the feed valve is closed, the piston then stops at the set pressure. Therefore, the difference between the volume before and after opening the feed valve, indicates the amount of the component dispensed into the cell. When dispensing fluid into the cell, the valves should be opened slowly, as the high pressure may result in back flushing in the pump if opened rapidly.

The pumps are fitted with temperature controlled, cylindrical thermal jackets to ensure that the fluid in the pumps are kept at a constant temperature. Maintaining a constant temperature throughout the feed pumps is an extremely important step, as an increase or decrease in temperature will result in the expansion or contraction of the molecules in the fluid and therefore cause a change in the density. The density of the fluid in the pump plays a significant role in the calculation of the overall composition (z_i) and ultimately the liquid phase mole fraction (x_i), thus keeping the fluid at a constant temperature is vital.

The density of the components in the pump increase with an increase in pressure and it is therefore preferable to use the density of the component at the pressure and temperature of the pump when converting from the overall composition (z_i) to the liquid phase mole fraction (x_i), and to keep these variables constant.

A SS bath (30 cm x 30 cm x 19 cm), fitted with a Polyscience temperature controller was used to circulate water at 313.15 K through the temperature jackets, and a Pt-100 temperature sensor was used to monitor the temperature of the fluid. Majority of the lines (79 cm) between the pumps and the cell were wrapped in nichrome wire and connected to a variac. This was done in order to maintain the temperature of the lines at 313.15 K and minimize any room for error in the volume calculations. The remainder of the lines (28 cm) were submerged into the isothermal cell bath along with the cell.

Both Isco pumps are fitted with high pressure transducers (0.1% linear accuracy) that can operate within a temperature and pressure range of 273.15-313.15 K ambient and 0-69500 kPa respectively. The pumps have a flow control accuracy of 0.5% of the set point. The 100 DX model has an operating flowrate range of 0-60 ml/min, whilst the 100 DM model operates between 0-30 ml/min. Both pumps have a capacity of 103 ml (Teledyne Isco, 2013).

4.1.4 Temperature

For this apparatus a total of 6 temperature sensors were employed. Two REB 1/10 DIN sensors were housed in copper casings to provide extra protection for the probe against bumping and bending, which can alter temperature measurements. These copper casings slot through the lip of the flange and cell. The sensors were used for the measurement of the temperature of the cell contents and isothermal bath. In addition there are four Pt-100 sensors used to monitor the following:

- Temperature of the heating block housing the pressure transmitter
- Temperature of the nut below the pressure transducer
- Temperature of the heating fluid in the bath for the Isco pump thermal jackets
- Temperature of the insulated SS $^1/_8$ inch line between the pumps and cell

The REB 1/10 DIN sensors used to measure the temperature of the cell contents have a manufacturer stated uncertainty of ± 0.03 K and are capable of sensing temperatures between 73.15 K and 873.15 K. The sensors were situated at different heights in order to monitor the temperature gradient within the cell, which was within ± 0.03 K. Both probes were connected to an Agilent 34972A data acquisition unit which displays and logs the temperature on a PC, along with other variables such as pressure and time.

4.1.5 Pressure

Pressure was measured using a WIKA P-10 pressure transmitter with an operating range of 0-500 kPa (absolute). The transmitter was housed in a SS block which was heated via a variac and kept at a constant temperature of 323.15 K. This was done in order to avoid pressure fluctuations due to changes in ambient temperature. The transmitter consists of a built in temperature compensation from 273.15 to 313.15 K. If the temperature of the transmitter rises above 313 K, the pressure signal will change slightly. The nut at the bottom of the transmitter was wrapped in nichrome wire and heated to the temperature of the isotherm being measured, via a variac. The pressure transmitter is connected to the equilibrium cell via a SS line. The line is $^{1}/_{16}$ inch in diameter and 13.5 cm in length. A thin line was chosen as a smaller number of moles would occupy the line, creating minimal disturbance to the equilibrium of the system. Two pieces of $^{1}/_{8}$ inch SS line approximately 2 cm in length, were silver soldered to either end of the $^{1}/_{16}$ inch line. This was done to allow for easy connection of the line. The line was silver soldered to connect to the pressure transmitter at one end, whilst the other end was connected to a Valco compression fitting, which fits into the cell via a male nut and ferrule. Valco fittings offer the best stability and reliability for high pressure applications (Valco Instruments Co. Inc., 2016), compared to fittings previously used, for e.g. the NTP fittings employed by Raal et al. (2011). The Valco compression fittings are highly favourable as it does not require components such as thread tape. It is important to note that during operation, the line between the pressure transmitter and equilibrium cell was completely submerged into the isothermal bath therefore every component of the apparatus that the chemical was in contact with was temperature controlled.

4.1.6 Data logger

The pressure transmitter, two REB 1/10 DIN temperature sensors used to measure temperature of the cell contents and the Pt-100 used to measure temperature of the Isco pump thermal jackets, were connected to an Agilent 34972A data acquisition unit. The unit was connected to a PC running Agilent Benchlink Data Logger software. The software enabled the above mentioned pressure and temperatures to be displayed and recorded on the PC. Some features of the software include selecting the specific variable to be displayed/recorded, selecting the time interval in which the data is logged and the specific

period of time which the user may require data for, just to name a few. This eliminates the time consuming task in which data is manually recorded. For all data points, the final value was determined by taking an average of the recordings over the final 10 minutes.

4.1.7 Isothermal baths

For this experimental setup, three liquid baths constructed of stainless steel were used. The first bath, 30 cm x 30 cm x 19 cm, was used to completely submerge the equilibrium cell in water and was raised using an electric jack. This was done in order to create an isothermal environment for measurements.

The second bath, 22.5 cm x 30.5 cm x 19 cm in dimensions, consisted of a 1:1 mixture of anti-freeze and water. This bath contained the coolant for the degassing setup, discussed in greater detail in section 4.2.2.

The third bath, 30 cm x 30 cm x 19 cm, was used to circulate water at a constant temperature (313.15 K) through the temperature jackets of the syringe pumps. The fluid in the pump was therefore maintained at a constant temperature.

4.1.8 Temperature controllers

Similar to the isothermal baths in section 4.1.7, three temperature controllers were employed in the experimental setup. The temperature of the cell bath was controlled using a Grant TFX 200 temperature controller. The controller can operate within a range of 226.15 to 473.15 K and has a rated bath stability of ± 0.01 K. The unit incorporates a high powered variable speed pump for fluid circulation and a programmable controller that cools or heats the fluid in the bath to the desired temperature (Grant, n.d.). Two Polyscience controllers were utilised: one in the degassing setup with a temperature range of 222.15 to 425.15 K and the other, used to maintain the temperature of the fluid in the pump jackets at 313.15 K and has a temperature range of 223.15 to 475.15 K.

4.2 Experimental procedure

For the static synthetic method, experiments were conducted isothermally. Pressure, temperature and composition are the variables of importance in order to determine accurate P-x data for this type of apparatus. No visual observation or complicated calculations are necessary for the determination of the data.

Considering the apparatus is a new setup, after commissioning and calibrations, numerous experimental runs were conducted in order to determine the most accurate and efficient operating procedure. This is discussed in greater detail in section 5.6

4.2.1 Determining the total cell working volume

As discussed in Chapter 2, the total working volume of the cell is required in order to convert the overall composition (z_i) to the mole fraction of the liquid phase (x_i), using the method of Barker (1953). The method used to determine the total working cell volume was conducted as follows:

- Pump 1 was filled with approximately 65 ml of distilled water and set to run in the constant pressure mode, at 500 kPa (absolute).
- The pump and stainless steel lines leading to the cell were maintained at 313.15 K.
- The isothermal bath was controlled to 313.15 K.
- The cell was evacuated to 0.1 kPa.
- The volume in the pump was recorded (0 at the start).
- Approximately 40 ml of fluid was dispensed into the cell and the pressure was allowed to stabilize.
- Thereafter small increments of fluid (1-2 ml) were added, and the increments decreased in volume with an increase in pressure.
- This procedure continued until the pressure in the cell and pump balanced out at 500 kPa.

The total working volume of the cell was established as 60.008 ml.

4.2.2 Calibrations

Temperature

Both REB 1/10 DIN temperature sensors were calibrated against a WIKA CTH 6500 standard, over a temperature range of 303.15 to 403.15 K. The standard had a manufacturer stated uncertainty of ± 0.03 K. Both sensors and the standard were evenly aligned and wrapped together using a thin piece of wire. This was done in order to create an even temperature profile among the probes and to avoid discrepancies if gradients existed within the bath or along the probes. The probes were thereafter submerged in a WIKA CTB 9100 bath filled with silicone oil. The bath was first set to 303.15 K. Once the temperature of the bath had stabilized at the set point temperature (which takes approximately half an hour), the temperature of each probe was recorded for approximately two minutes and the average value was taken. The temperature of the bath was then increased by an increment of 10 K and the same procedure was followed. This process was repeated until a set point of 403.15 K was reached. In order to account for the effect of hysteresis, the calibration procedure was repeated in descending order of temperature increments and then again in ascending order of temperature increments. In this study, the temperature sensors used to measure the cell temperature are referred to as temperature sensor 1 and 2 respectively, where temperature sensor 1 was situated near the top end of the cell and temperature sensor two was situated near the bottom.

Pressure

A WIKA P-10 pressure transmitter was utilized in this study for pressure measurement. The transmitter has a pressure range of 0-500 kPa. Housed in a stainless steel block which is heated by a variac, the transmitter was kept at a constant temperature of 323.15 K. This ensures no fluctuations in pressure readings occur due to ambient temperature changes. The transmitter was calibrated against a Mensor CPC 8000 pressure standard, between the range of 10-500 kPa. A $^{1}/_{8}$ inch SS line was used to connect a cylinder of nitrogen gas to the pressure transmitter in order to conduct calibrations at above-atmospheric pressure. The regulator on the gas cylinder was fixed to 500 kPa and the set point on the Mensor unit, which incorporated a precision needle valve regulator, was manually adjusted. A second $^{1}/_{8}$ inch SS line was connected from the standard to the pressure transmitter. Once the necessary lines were connected and the transmitter block temperature was stable at 323.15 K, the set point pressure on the standard was set to 100 kPa and stabilized within 1-2 minutes. Once stable, the reading on the standard was recorded for approximately 2 minutes and the average value was taken. The same was done for the pressure transmitter reading. Thereafter the set point was increased by an increment of 50 kPa and the process continued until a set point of 500 kPa was reached. The process was then repeated in order of descending pressure increments, then again in ascending order to account for the effect of

hysteresis, as mentioned above. In order to calibrate the pressure transducer over the sub-atmospheric range, the same procedure utilised for the above atmospheric pressure range was followed, however an Edwards RV3 vacuum pump was connected to the Mensor unit in place of the nitrogen cylinder.

Isco pumps

Once the apparatus was set up and the pressure and temperature sensors were calibrated, the measurement of binary systems commenced to determine an optimal experimental procedure. Initially, 2 Isco 100 DM model pumps were employed. However, during this stage of the project, it was determined that the second 100 DM pump was not functioning accurately. The phase envelope did not produce a good fit as the equilibrium data points from both the dilute and concentrated regions of component 1 did not coincide smoothly in the equimolar region. A decision was thereafter taken to replace the pump with an alternative pump available in the Thermodynamic Research Unit laboratories i.e. the Isco 100 DX model. The necessary steps taken to determine the cause of the problem and find an appropriate solution is discussed in extensive detail in section 5.6. After the replacement of the second 100 DM model with the 100 DX model, a calibration of the Isco pumps were undertaken. For the calibration procedure, a Mettler Toledo AB204-S scale with a ± 0.2 mg linearity was employed as the standard. A 120 ml glass beaker was centred on the scale and a $^{1}/_{8}$ inch SS line was connected from the pump to the airspace in the beaker. The beaker was initially filled with distilled water and the pump was set to the "refill" mode. The pump was set to refill until approximately 100 ml of distilled water was loaded into the pump, and approximately 20 ml of water remained in the beaker which submerged the SS line. Thereafter approximately 5 ml of water was dispensed by the pump into the beaker and then refilled back into the pump. This was repeated approximately three times and was done in order to remove any air bubbles that may be trapped in the pump or line. The end of the SS line remained submerged in the remaining water and a further 20 ml of distilled water was added to the beaker. The pump was operated in the constant flow mode. The scale was zeroed and calibrations could thereafter commence. Approximately 10 ml of water was dispensed into the beaker and the mass recorded by the scale, as well as the volume in the pump before and after dispensing the liquid were recorded. The difference in volume before and after dispensing, results in the total volume dispensed by the pump. Using the density of water at ambient conditions and the mass recorded by the scale, the volume dispensed by the pump as determined by the standard, could be calculated. A further 10 ml was loaded into the beaker and the necessary variables recorded. This process was repeated until the beaker was almost full. At this stage in the calibration procedure approximately 60 ml was dispensed by the pump. A syringe was used to withdraw 60 ml of distilled water from the beaker, and any contact between the syringe and beaker/line was avoided. The withdrawal from the beaker was conducted due to the constraint of the beaker size as well as the maximum mass that could be withstood by the scale (210 g).

The remaining 40 ml of water submerged the end of line. The scale was zeroed and the calibration procedure continued until the pump was almost empty. The difference in volume calculated by the pump was plotted against the volume calculated by the scale (via a mass balance) to produce the calibration curve. This process was conducted twice to ensure repeatability in results.

4.2.3 Preparation of the equilibrium cell for measurements

Cleaning

Prior to experimental measurements, the equilibrium cell was cleaned in order to remove impurities that could cause discrepancies in the measured data. Approximately 30 ml of n-hexane was charged into the cell and agitated for an hour at approximately 313.15 K. The cell was thereafter flushed with nitrogen at 200 kPa to remove any remaining liquid and was thereafter evacuated for 1-2 hours using a vacuum pump. This ensures the removal of all impurities, including air.

Leak testing

In order to reduce the risk of errors, it is imperative that the equilibrium cell be tested for leaks. The initial leak test was conducted by pressurizing the cell with nitrogen at approximately 10 000 kPa and submerging it in a water bath. The cell was not connected to the pressure transmitter at this point and instead a Valco fitting was used to seal the cell at the pressure transmitter end. The cell was monitored under water for half an hour and no air bubbles were observed. The second leak test involved the cell again being pressurized to 10 000 kPa and a leak detection fluid (Snoop®) was applied over all the joints and fittings on the cell. Leaks can be detected by the presence of foam or bubbles from the fluid, however none had formed. A third method used to eliminate leaks in the cell involved evacuating the cell to approximately 0.1 kPa and shutting off all valves. For this test, the pressure transmitter was connected to the cell. The cell was thereafter submerged in an isothermal bath at a temperature of 303.15 K. The pressure was monitored over a period of 24 hours and if no significant pressure increase was observed, the cell is deemed ready for equilibrium measurements. It is easier to pressure test at above atmospheric pressures than under vacuum, as it can be difficult to observe leaks visually under sub-atmospheric conditions. The cell was also pressure tested at 500 kPa when attached to the pressure transmitter in order to test the pressure transmitter line and gaskets.

Degassing

For the dynamic method, no degassing of the pure components prior to experimentation is required, as the chemicals are degassed during experimentation. For the static method, external degassing of the chemicals is a pivotal step in the experimental procedure, as it removes the air and any dissolved gases from the components for accurate P-x measurements. For this project, degassing was accomplished via vacuum distillation as described by Van Ness and Abbott (1978).

Three different degassing procedures were attempted in this work in order to find the most efficient degassing method. The methods outlined make reference to Figure 4-1. For the first method degassing was initially conducted directly in the Isco pumps. Both pumps were loaded with approximately 80 ml of component 1 and 2 respectively. Once the liquid filled into the pumps, the feed flasks were disconnected and the vacuum line was attached to V-3. At this stage all valves in the system are closed. After waiting approximately 5 minutes for the vapour space to fill up with the component in the pump as well as any air and undissolved gases (as the pump was merely stopped and not yet set to the "run" mode to compress the fluid), the vacuum pump was switched on and V-3 was opened for approximately 1-2 seconds. This process continued 5-10 times, depending on the volatility of the chemical. Once completed, the pump was set to the "run" mode to compress the fluid to the desired pressure, and the vacuum line was disconnected and attached to V-4, to degas the component in pump 2. This method was deemed inadequate as degassing was not always successful (the measured vapour pressure readings did not correspond well with literature) and resulted in the cell being drained, cleaned and degassing being conducted for a second time. In addition, a notable amount of chemical was also lost in the process as ± 20 ml of would be withdrawn by the vacuum in the case of volatile components and ± 5 ml in the case of heavy boiling components.

The second attempted method of degassing, involved loading approximately 80 ml of the desired component into a 250 ml round bottom flask and connecting the flask to a vacuum line using glass adapters and SS fittings. The round bottom flask was then submerged into an ultrasonic bath which was kept at a constant temperature of 303.15 K. The ultrasonic bath and the vacuum pump was switched on. The Teflon valve on the round bottom flask was opened slightly and the component was left to degas. Degassing usually occurred for 5-15 minutes, depending on the chemical volatility. Although this method proved successful as the measured vapour pressures corresponded well with literature, there were problems experienced whereby the glassware would implode during degassing. It is suspected that this was caused by the rapid vaporisation of the components.

The third method attempted was found to be the most optimal method overall and was the chosen degassing procedure for the measurements conducted in this work. The degassing procedure is conducted as follows (refer to Figure 4-4 below):

Approximately 80 ml of the chemical under investigation was filled into a 250 ml round bottom flask and sealed via the Teflon valve. It was thereafter fitted to the bottom of a glass condenser, and a vacuum was drawn through the top of the condenser to remove any gases in the condenser airspace. A SS bath, 22,5 cm x 30,5 cm x 19 cm in dimensions, was filled with a water and anti-freeze mixture in a 1:1 ratio. A Polyscience chilling unit was used to chill the mixture in the bath. The coolant temperature was controlled to 268.15 K for all chemicals, except water which was controlled to 276.15 K to prevent freezing. The coolant temperature was controlled using a Polyscience temperature controller and was circulated through the glass condenser. Once the set point temperature of the coolant had been reached and the condenser was evacuated, the Teflon valve was opened to allow the degassing procedure to occur. The air and other gases in the flask were drawn out, whilst the component vapourized and condensed in the condenser, and thereafter returned to the round bottom flask via gravity. Considering the round bottom flask is attached to a condenser only, the procedure is similar to a single stage distillation process and degassing was only required for approximately 15 minutes for most of the components and approximately 5-10 minutes for n-pentane as it has a very low boiling point (309.15 K). Many authors using the static synthetic method report long degassing times, for e.g. in the work Raal (2011) degassing was conducted for as long as 8 hours.

In order to determine if the components were properly degassed, the vapour pressure of each component was measured and compared to literature before any binary measurements could commence. Although this method accurately degasses the chemicals under investigation, it does result in a 5-15 ml loss of sample during the degassing procedure. However, this is an improvement compared to the previous two methods. A staged column with internal reflux is the ideal method for degassing in this work, as it uses a glass Vigreux® column which will allow for a longer degassing time without losing large volumes of sample. This is discussed in greater detail in Chapter 7.

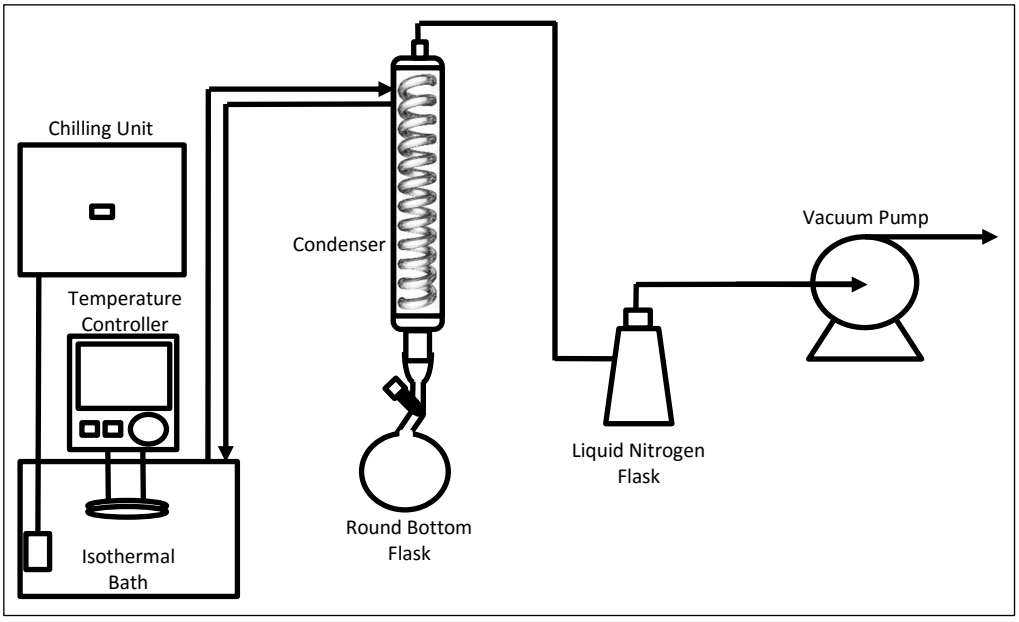

Figure 4-4: Schematic diagram of the degassing setup.

4.2.4 Experimental measurements

Start-up / loading procedure

Once the cell has been sufficiently cleaned, the vacuum pump was used to evacuate the cell to 0.1 kPa. The nichrome heating wire around the lines between the pumps and cell were switched off and the jackets were kept at a constant temperature of 288.15 K in order to ensure a smooth loading procedure, and that no vaporisation of components occurred in the pump. Glass adapters that fit onto the top of the round bottom flask were fastened to V-3 and V-4. After degassing the pure components, the round bottom flasks were rotated 180^0 vertically and slotted over the glass fittings attached to V-3 and V-4. All valves were kept in the "open" position, apart from V-8 (the drain valve) and the Teflon valves on the round bottom flasks which were kept closed. A vacuum was thereafter drawn throughout the system to remove any remaining air from the glass fittings. Once the system has reached 0.1 kPa, valves V-3 and V-4 were closed. The Teflon valves in the round bottom flask were then opened and the degassed liquid was allowed to fill the chamber between the fittings. Valves V-5, V-6 and V-7 were closed and the vacuum pump was switched off. Both feed pumps were set to the "refill" mode and valves V-3 and V-4 were opened. Usually, the more volatile component was filled into pump 1, and the component with the higher boiling point was filled into pump 2. This was done merely for convenience. Refill rates were set to approximately 5 ml/min for volatile components and 20 ml/min for components with high boiling points. Ice packs were placed around the fittings of valves V-3 and V-4 to prevent vaporisation of the components in the flask during the loading procedure. Once the glass chambers were almost empty, valves V-3 and V-4 were closed, and the pumps were stopped and set to the "run" mode in constant pressure at 2000 kPa (gauge). The purpose of closing the valves and leaving behind approximately 2 ml of sample was to prevent any gases from entering the system. The pumps were selected to run at 2000 kPa (gauge) as after many trial runs, this pressure was found to be the most efficient operating pressure for this system.

P-x data measurements

In order to conduct accurate isothermal P-x measurements, the followings procedure was carried out:

STEP 1: Once the pure components are loaded into the pumps, the jackets are controlled to a temperature of 313.15 K. The nichrome wire around the pump lines are heated via a variac and maintained at a temperature of 313.15 K as well. The cell is submerged in the isothermal bath and controlled to the desired temperature. The nut around the bottom of the pressure transmitter is also heated with nichrome wire and maintained at the temperature of the isotherm being measured. The pressure transmitter itself is housed in a stainless steel block and heated via a variac to 323.15 K (which is the same temperature at which the transmitter was calibrated). This is done to ensure accuracy in the

data logged off the pressure transmitter, as a constant temperature will eliminate fluctuations in the pressure readings due to the surroundings.

STEP 2: The cell is again evacuated via V-7 to 0.1 kPa. Once all the desired temperatures have been established, V-7 is closed and approximately 10-15 ml of component 1 is loaded into the cell via opening and closing V-5. The stirrer is not switched on as it is a pure component and thus no mixing is required. This is to confirm that the component has been accurately degassed as well as to displace the initial pump volume. The reason for displacing an initial volume is discussed in greater detail in section 5.6.

STEP 3: Once the pressure is stable, the data logger is stopped and the average pressure and temperature readings over the last 10 minutes are taken. The pressure is then compared to literature values to ensure that the component is accurately degassed.

STEP 4: The temperature controller for the bath is switched off and the bath is lowered using an electric jack. The cell is flushed with nitrogen gas, cleaned and evacuated for an hour. The cell is re-submerged into the bath and STEPS 1 to 3 are repeated in order to determine if component 2 is sufficiently degassed. After it is established that both components are sufficiently degassed, isothermal P-x measurements can then commence.

STEP 5: The cell is cleaned and STEP 1 is repeated. A pre-determined amount of component 2 is loaded into the cell. The necessary variables (pressure, temperature and volume) are logged on the PC once equilibrium has been established.

STEP 6: A small pre-determined amount of component 1 is introduced into the cell. The mixer is switched on to approximately 750 rpm. Mixing can take between 6-20 minutes, depending on the system being measured.

STEP 7: Once the pressure is stable, the mixer is switched off. This is to allow accurate temperature measurements as the vibrations from the mixer create a slight scatter (0.01 K) in the temperature data due to the rotating magnetic field when the mixer is on. Pressure stays stable and the system is allowed to run for a further 10-15 minutes, before the data logger is stopped and the variables are recorded.

STEP 8: A small amount of component 1 was introduced into the cell again and STEPS 6 to 7 are repeated until just over half the phase diagram is complete.

STEP 9: The cell is allowed to cool and is thereafter drained, cleaned and evacuated. The entire process is repeated beginning with component 1 and adding 2 so that the entire phase diagram is completed. It is also important to ensure good overlapping of the measured data points which displays successful degassing and correct method of operation of the equipment.

After numerous trial and error runs, the above mentioned procedure was deemed the most accurate for measuring P-T-z data, and was employed when measuring all data discussed in Chapter 5.

4.3 Uncertainty analysis for P-x equilibrium data

Experimental uncertainty plays an integral role in the description of measured variables, as they provide an indication of the accuracy of the variables being measured. According to Soo (2012), *"uncertainty results from doubts that originate from the measurement, and is quantified as an interval within which the true value of measurement has a high probability of residing".*

When there are multiple sources of uncertainty present, the combined standard uncertainty of the measurement result y, designated by $u_c(y)$, and taken to represent the estimated standard deviation of the result, is the positive square root of the estimated variance ${u_c}^2(y)$ obtained from

$$ {u_c}^2(y) = \sum_{i=1}^{N} \left(\frac{\partial f}{\partial x_i}\right)^2 u^2(x_i) + 2\sum_{i=1}^{N-1}\sum_{j=i+1}^{N} \left(\frac{\partial f}{\partial x_i}\right)\left(\frac{\partial f}{\partial x_j}\right) u(x_i, x_j) \quad (4\text{-}1) $$

Equation (4-1) is based on a first-order Taylor series approximation of the measurement equation $Y = f(X_1, X_2, \ldots, X_N)$ and is referred to as the law of propagation of uncertainty. The partial derivatives of f with respect to the X_i (also referred to as sensitivity coefficients) are equal to the partial derivatives of f with respect to the X_i, evaluated at $X_i = x_i$. In addition, $u(x_i)$ is the standard uncertainty associated with the input estimate x_i; and $u(x_i, x_j)$ is the estimated covariance associated with x_i and x_j (Physical Measurement Laboratory, 2016). Equation (4-1) can be simplified to the following

$$ u_c(\theta) = \pm\sqrt{\sum_i u_i(\theta)^2} \quad (4\text{-}2) $$

Where $u_c(\theta)$is any source of uncertainty, for example, errors resulting from a calibration polynomial. The possible sources of error for the measurements conducted in this project are discussed below. The uncertainties stated in this dissertation were represented in accordance with the National Institute of Standards and Technology (NIST) guidelines for reporting uncertainty.

Temperature and Pressure

Sources of error for temperature and pressure include calibration imperfections, repeated readings of a single transmitter and the manufacturer specified uncertainty of the instruments. Therefore the uncertainty for pressure and temperature can be calculated via equations (4-3) and (4-4) respectively.

$$ u_c(P) = \pm\sqrt{u_{std}(P)^2 + u_{cal}(P)^2 + u_{rep}(P)^2} \quad (4\text{-}3) $$

Where $u_{std}(P)$ is the uncertainty of the pressure standard utilised for calibrations, $u_{cal}(P)$ is the uncertainty as a result of the pressure calibration and $u_{rep}(P)$ is the transmitter uncertainty due to measurement repeatability.

$$u_c(T) = \pm\sqrt{u_{std}(T)^2 + u_{cal}(T)^2 + u_{rep}(T)^2} \tag{4-4}$$

Where $u_{std}(T)$ is the uncertainty of the temperature standard utilised for calibrations, $u_{cal}(T)$ is the uncertainty as a result of the temperature calibration and $u_{rep}(T)$ is the temperature probe uncertainty due to measurement repeatability.

Uncertainty calculations consist of several components which can be grouped into two categories, namely:

Type A – Uncertainties evaluated by statistical means

Type B – Uncertainties evaluated by other means

Type A uncertainties for variables such as temperature and pressure arise from various data readings of a stable system, whilst type B uncertainties are as a result of polynomials fitted to calibrations as well as manufacturer specifications.

In this work, all uncertainties measured were determined to be type B. For variables such as pressure, temperature, and volume, the upper and lower limit of uncertainty is obtained from the calibration plots (refer to Figures 5-1 to 5-12), where the deviation from the set point can clearly be observed. When calculating uncertainty, it is assumed that the value will always fall within the estimated range.

Equation (4-5) is an indication of the shape distribution in the scatter for Figure 5-2, for example, which is rectangular.

$$u_{cal}(T) = \frac{b}{\sqrt{3}} \tag{4-5}$$

Where *b* is the maximum deviation from the calibration plot. Depending on the shape distribution, the equation used to calculate the uncertainty of each factor for a particular variable will vary. For this work, the shape distribution in all calibration plots were determined to be rectangular, and therefore equation (4-5) was employed. The reader is referred to the work of Taylor et al. (1994) for a more detailed review on shape distribution and uncertainty.

Once the combined standard uncertainty is determined, it is necessary to apply a coverage factor (k), to the combined standard uncertainty. The combined expanded uncertainty is thus defined as

$$U_c(\theta) = ku_c(\theta) \tag{4-6}$$

The purpose of the coverage factor is to create an interval within which it is confidently believed that θ will lie i.e. $\theta_{measured} - Uc(\theta) \leq \theta_{final} \leq \theta_{measured} + Uc(\theta)$. Typically, a coverage factor of 2 is used to define an interval having a level of confidence of approximately 95%.

Volume

Another measured variable in which uncertainty needs to be taken into consideration is the volume dispensed by the Isco pumps. For this variable, two factors need to be taken into consideration, i.e. the uncertainty as a result of the volume calibration $u_{cal}(V)$ and the uncertainty in the density of the fluid in the Isco pump $u_\rho(V)$. This can be represented as follows

$$u_c(V) = \pm\sqrt{u_{cal}(V)^2 + u_\rho(V)^2} \tag{4-7}$$

Assuming that an approximate 2% error results from the density in the Isco pump, the uncertainty of the pump density can be expressed as

$$u_\rho(V) = \frac{0.02\rho}{\sqrt{3}} = 0.012\rho \tag{4-8}$$

Similarly, the percentage error for the Isco pump volume calibration was determined to be 0.58% and can therefore be expressed as

$$u_{cal}(V) = \frac{0.0058V}{\sqrt{3}} = 0.0033V \tag{4-9}$$

Number of moles

Another variable in which uncertainty needs to be accounted for is the number of moles of each component. This takes into account the uncertainty of the volume dispensed by the Isco pump as well as the density in the Isco pump, and can be described by equation (4-10)

$$u(n_1) = n_1\sqrt{\left(\frac{u(V)}{V}\right)^2 + \left(\frac{u(\rho)}{\rho}\right)^2} \tag{4-10}$$

For a single point with pressure 100 kPa and temperature 323.15 K, the following is true

$$u(n_1) = n_1\sqrt{\left(\frac{0.0033(V)}{V}\right)^2 + \left(\frac{0.012(\rho)}{\rho}\right)^2}$$

$$= 0.012n_1$$

Overall composition

The final variable for which uncertainty needs to be accounted for is the overall composition (z_i) of each component. Uncertainty of the overall composition takes into consideration the number of moles of each component for a given data point, as well as the uncertainty in the number of moles and is represented by equation (4-11)

$$u(z_i) = \sqrt{\left[\frac{n_2}{(n_1+n_2)^2}u(n_1)\right]^2 + \left[\frac{n_1}{(n_1+n_2)^2}u(n_2)\right]^2} \quad (4\text{-}11)$$

In Chapter 5, all results including calibrations, purity checks, vapour pressures and binary measurements as well as the modelling conducted for this project are presented and discussed.

CHAPTER 5 : Results and Discussion

The focus of this project was to set up and commission a new static synthetic apparatus, develop an appropriate operating procedure, conduct measurements of test systems as well as previously unmeasured systems, and finally, to model the experimental data using the appropriate thermodynamic models.

The experimental setup was successfully assembled. The operating procedure for the apparatus was determined by conducting numerous experimental runs and making the necessary adjustments until a successful operating procedure was achieved. Thereafter the measurement of test systems commenced and further adjustments were made to the setup. Once the test systems were successfully measured, measurement of the new systems commenced. Pressure, temperature and overall composition (z_i) were the measured variables recorded during experimentation. The volume dispensed by the pumps together with a basic mass balance are used to determine the overall composition (z_i). z_i was converted to x_i using the method of Barker (1953) to yield P-T-x data. In this chapter, modifications to the setup and the experimental results and modelling are presented, with a discussion thereof. Sensitivity analyses were also conducted to display the effect an error on certain variables yield on the final result.

The motivation for conducting the measurement of n-hexane + perfluoro-n-heptane, despite the discernible similarities between the two components, are due to the large positive deviations from Raoult's law and large positive excess enthalpies and volumes which they exhibit (Morgado et al., 2005). Due to their chemical inertness, biocompatibility and peculiar physical properties, perfluoroalkanes have become crucial in a broad range of fields. Perfluoroalkanes can be used in medical, technological and chemical applications, resulting in a considerable amount of work being conducted on the theoretical and computational modelling of n-alkane + perfluoroalkane mixtures.

Alkane-alcohol mixtures occur as by-products in various petrochemical processes and the separation/purification of these components are of great value due to the various uses of alkanes and alcohols. The n-pentane + 2-propanol system is of particular interest as this system has not been previously measured.

5.1 Calibrations

Temperature

The two REB 1/10 DIN temperature sensors were calibrated against a WIKA CTH 6500 standard, which had a manufacturer stated uncertainty of ± 0.03 K. The sensors were calibrated over a temperature range of 303.15 - 403.15 K, using the method outlined in section 4.2.2. Figures 5-1 and 5-3 display a first order relationship between the temperature of the standard and the temperature sensor for sensors 1 and 2 respectively, whilst the plot of the temperature deviation from the standard is displayed in Figures 5-2 and 5-4. The maximum calibration uncertainty for each temperature sensor used to measure the cell temperature was found to be 0.03 K and 0.02 K for sensor 1 and sensor 2 respectively and an overall temperature uncertainty of 0.06 K was established. The additional Pt-100 sensors employed to monitor the temperature of the Isco pump heating fluid, the temperature of the nut below the pressure transmitter and the lines joining the Isco pump to the cell, were also calibrated in the same manner. These results are reported in Appendix B.

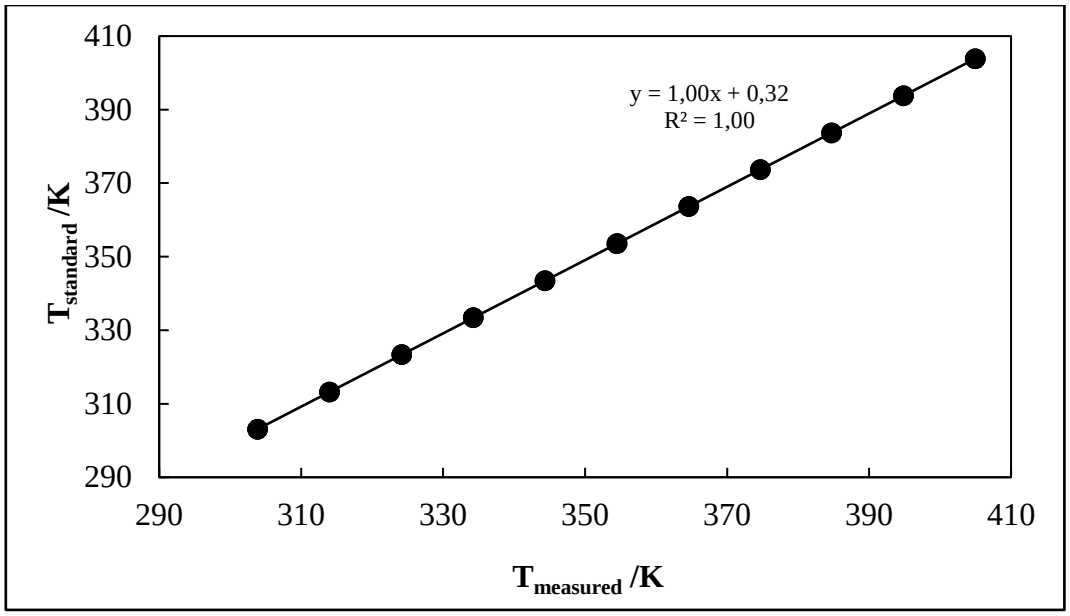

Figure 5-1: Calibration curve for temperature sensor 1. First order relation between standard and temperature sensor.

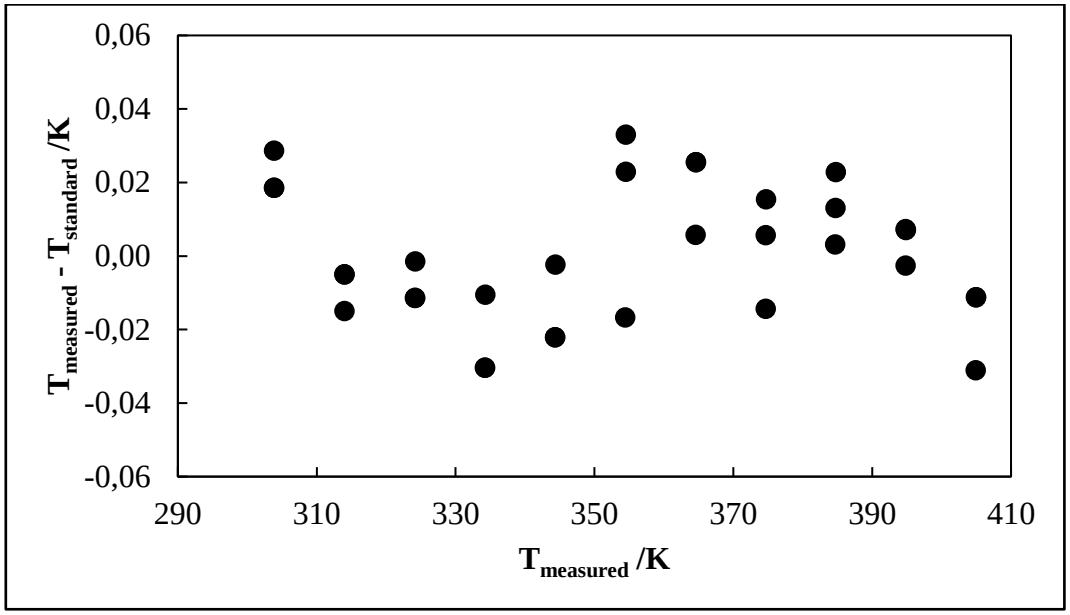

Figure 5-2: Deviations from standard temperature for temperature sensor 1.

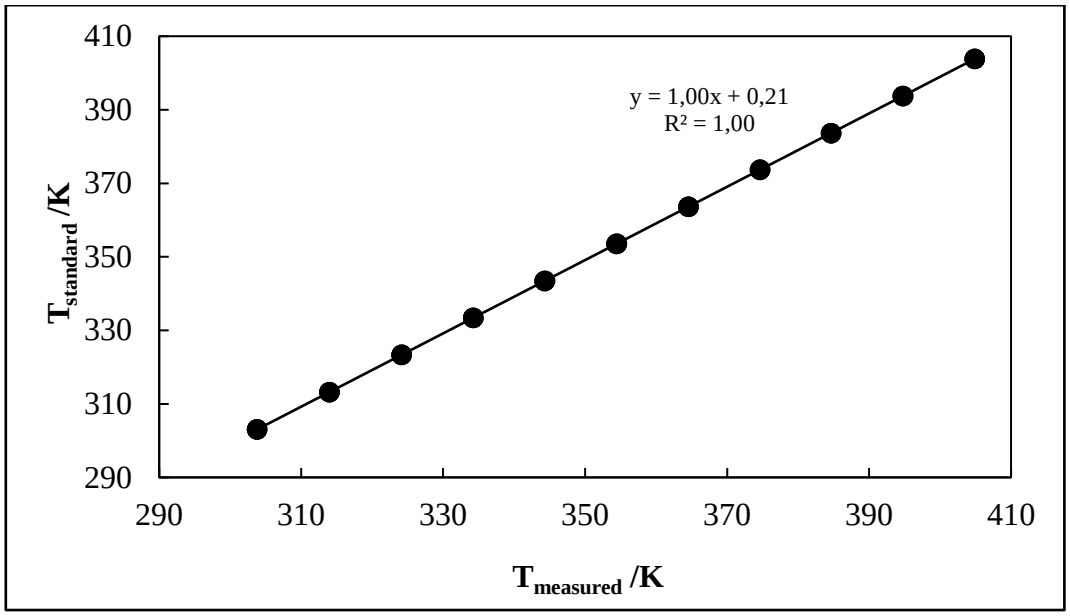

Figure 5-3: Calibration curve for temperature sensor 2. First order relation between standard and REB 1/10 DIN sensor.

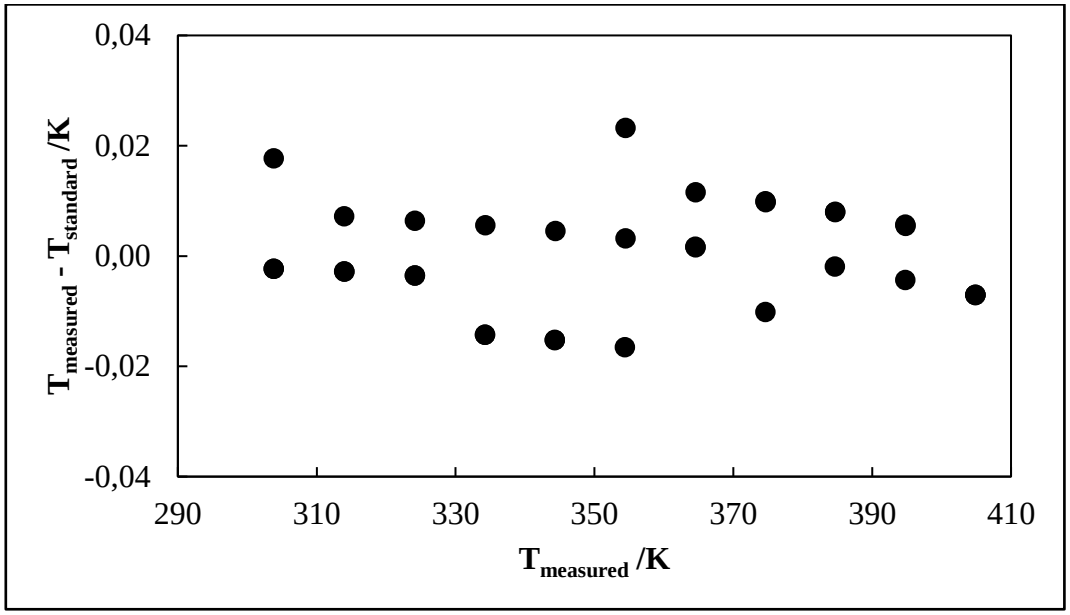

Figure 5-4: Deviations from standard temperature for temperature sensor 2.

Pressure

In this study a WIKA P-10 pressure transmitter was used to measure the pressure in the cell. The transmitter has a pressure range of 0-500 kPa and was housed in a stainless steel block which was heated by a variac. The transmitter was heated and kept at a constant temperature of 323.15 K to ensure no fluctuations in pressure readings occur, due to a change in the ambient temperature. The transmitter was calibrated against a Mensor CPC 8000 pressure standard, between the ranges of 10-500 kPa. Figures 5-5 and 5-7 show the first order relationship between the pressure of the standard and the WIKA P-10 pressure transmitter at above atmospheric and sub atmospheric conditions respectively. Figures 5-6 and 5-8, display the pressure deviation from the standard. The maximum calibration uncertainty for the above atmospheric and below atmospheric calibrations were found to be 0.046 kPa and 0.069 kPa respectively, whilst the overall pressure uncertainty was established as 0.36 kPa.

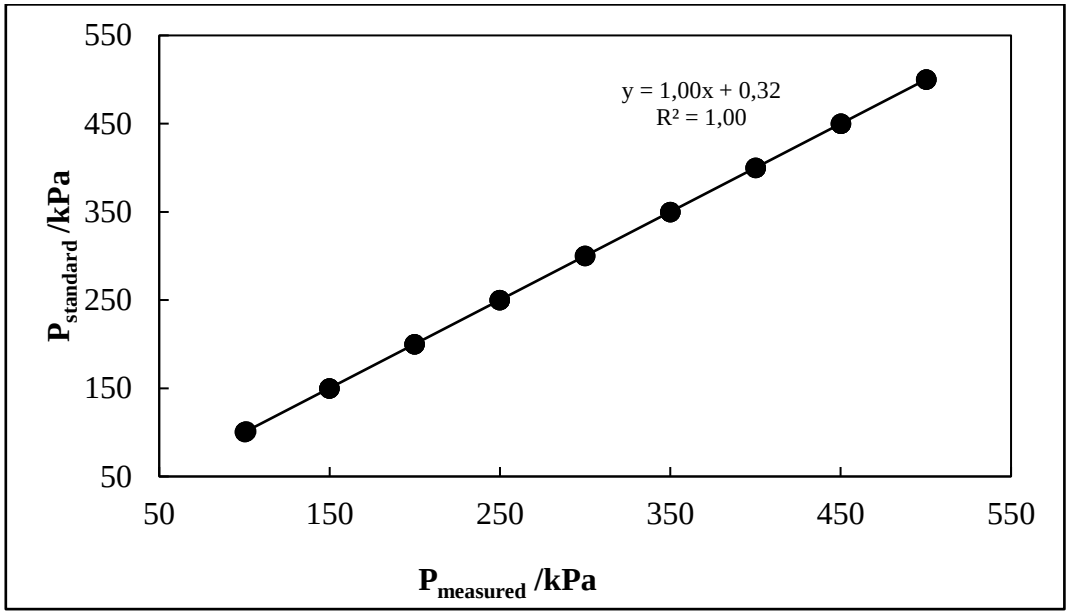

Figure 5-5: Calibration plot for the pressure transmitter at above-atmospheric conditions. First order relation between standard and WIKA P-10 transmitter.

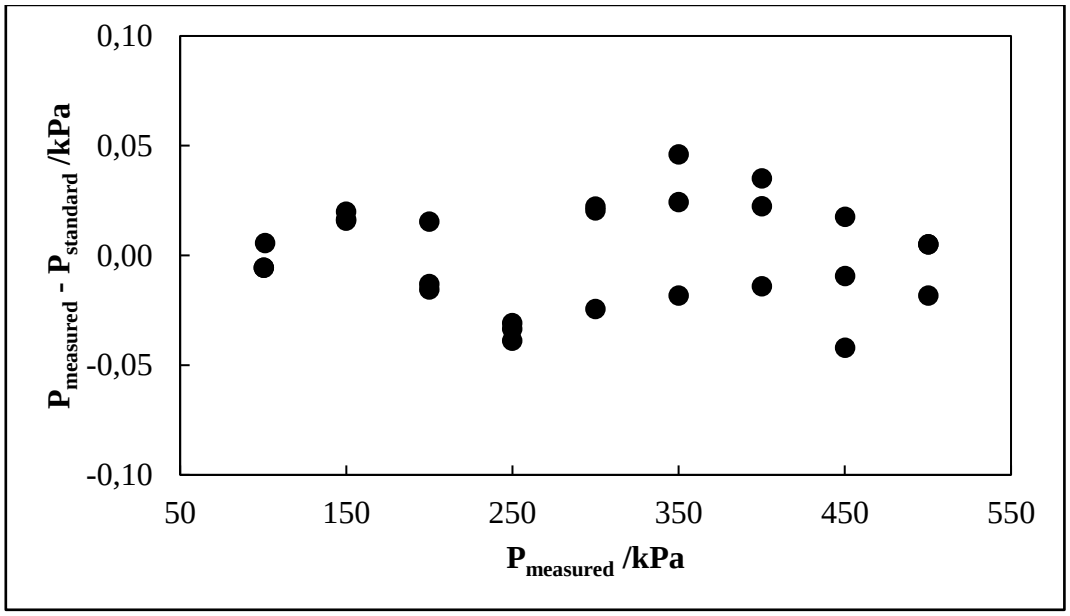

Figure 5-6: Deviations from standard pressure at above-atmospheric conditions.

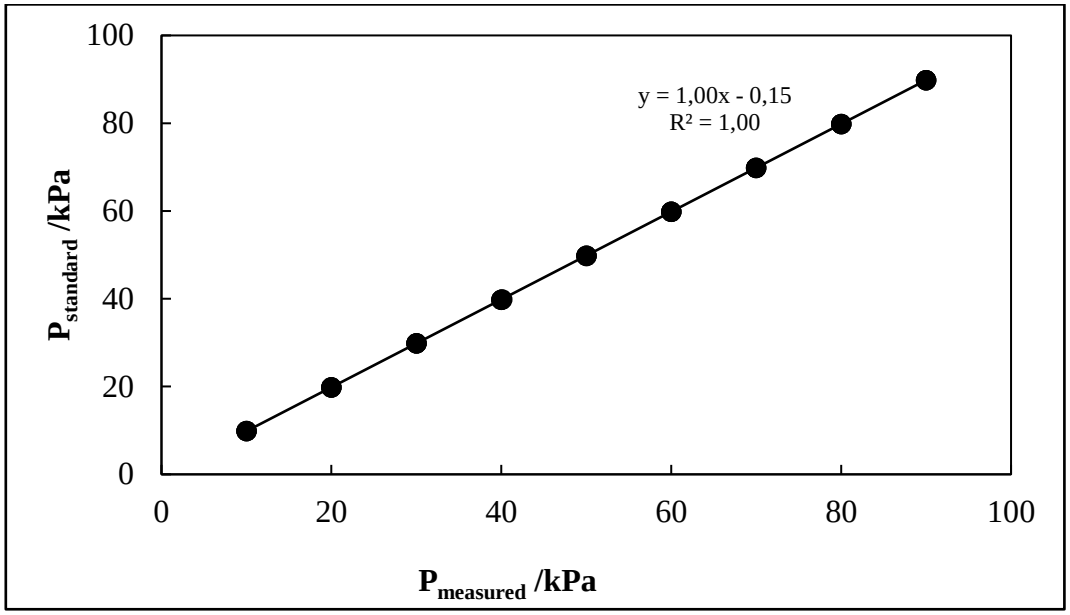

Figure 5-7: Calibration plot for the pressure transmitter at sub-atmospheric conditions. First order relation between standard and WIKA P-10 transmitter.

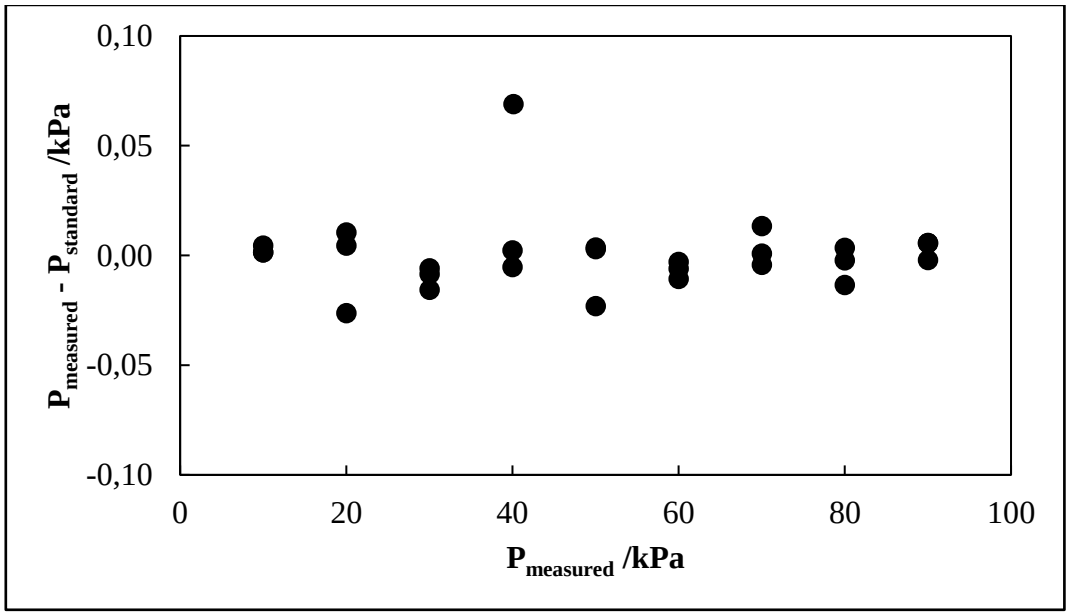

Figure 5-8: Deviations from standard pressure at sub-atmospheric conditions.

Isco pumps

Figures 5-9 and 5-11 depict the graphs of the standard volume versus the measured volume, where the volume calculated via the Mettler Toledo AB204-S scale is the standard and the volume calculated via the feed pumps is the measured volume. The scale has manufacturer stated uncertainty of ± 0.03 g. The uncertainties for pumps 1 and 2 were established as 0.04 and 0.09 ml respectively, and the overall uncertainty of the pumps were established to be 0.1 ml. Overall, the pumps were fairly accurate prior to calibrations and was adjusted by 0.58 % after the calibration. The effect of the pump calibration on the experimental data is discussed in greater detail in section 5.7.4.

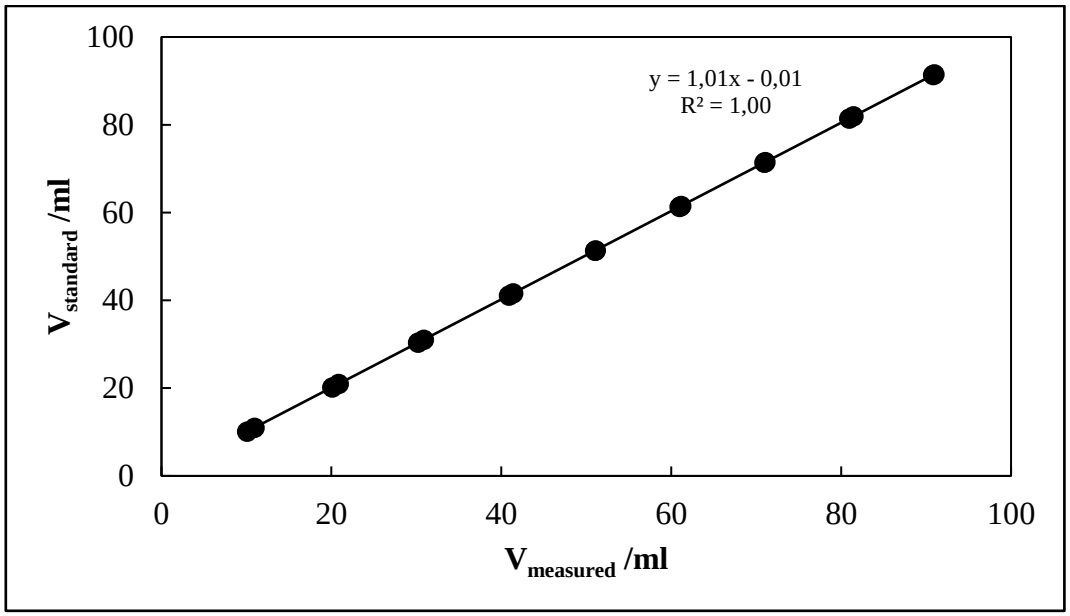

Figure 5-9: Calibration plot for pump 1. First order relation between standard and pump 1.

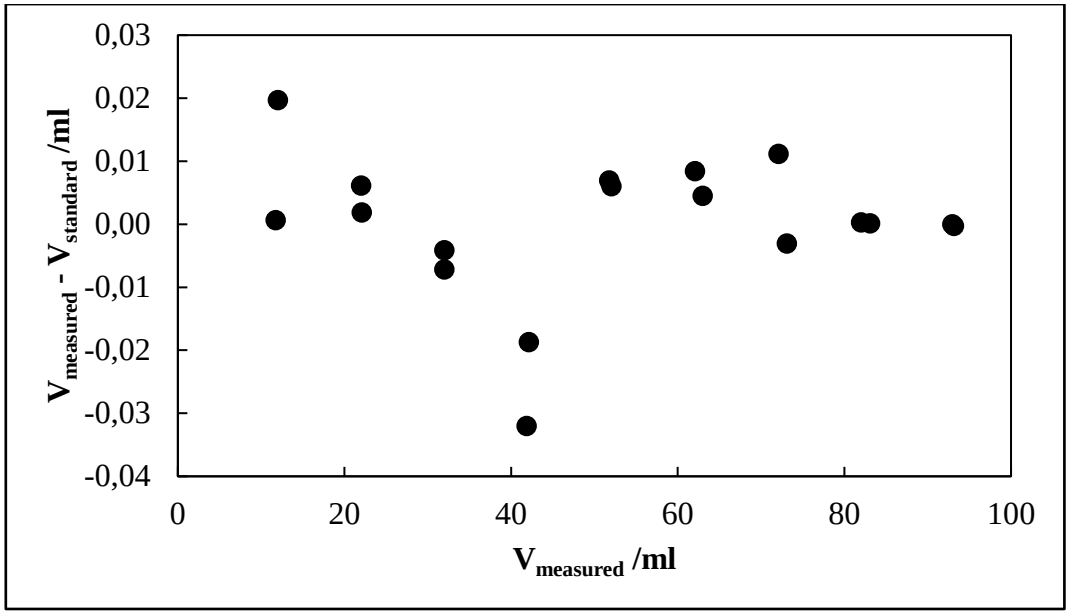

Figure 5-10: Deviations from standard volume for pump 1.

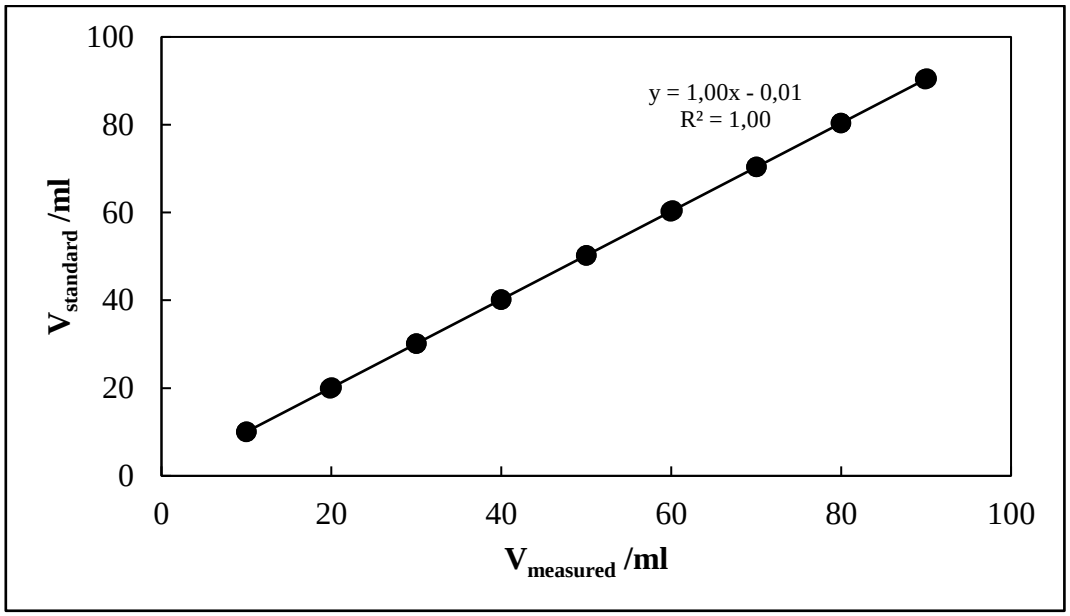

Figure 5-11: Calibration plot for pump 2. First order relation between standard and 100 DX pump.

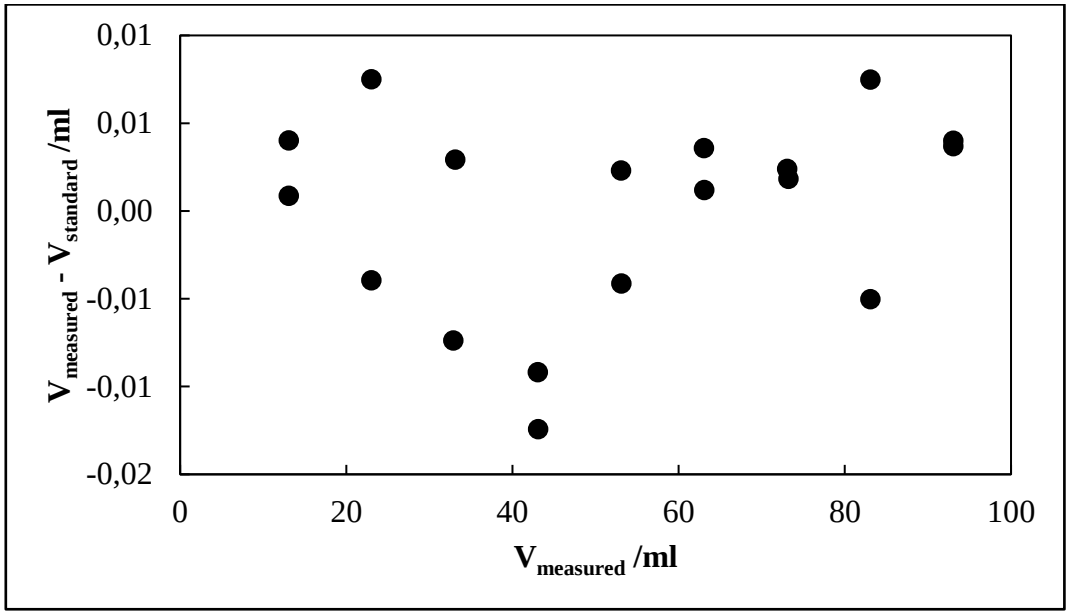

Figure 5-12: Deviations from standard volume for pump 2.

5.2 Chemical purities

The chemicals used in this study, along with the suppliers, and stated as well as measured purities, are presented in Table 5-1. The chemical purity was determined using a Shimadzu 2014 gas chromatograph (GC) with a thermal conductivity detector (TCD). The column used was a Porapak Q, stainless steel packed column with an internal diameter of 2.2 mm and a length of 2 m. Injection of samples into the GC were conducted with an SGE 1 µL analytical syringe. The density of each component was measured using an Anton Paar DSA 5000 M densitometer. The densitometer is temperature controlled and has a reported temperature uncertainty of 0.01 K with the estimated uncertainty of the measured densities at 5×10^{-6} g.cm^{-3}. Refractive indices of the chemicals used were measured using an Atago RX-7000 digital automatic refractometer, which is temperature controlled to within an uncertainty of 0.01 K and the estimated uncertainty in refractive index is 1×10^{-4}. The water used in this study was distilled, de-ionised water, obtained from the Analytical Chemistry laboratory in the School of Engineering at the University of KwaZulu Natal. The water was purified using a PURELAB Option Q water purification system. The perfluoro-n-heptane used in this study was purchased from Apollo Scientific and consisted of a mixture of isomers.

Table 5-1: Chemical purities.

Component	Supplier	Density at 293.15 K ($kg.m^{-3}$)		Refractive Index at 293.15 K		Minimum Claimed Purity wt. %*	GC Analysis % Peak Area
		Experimental	Literature[1]	Experimental	Literature[2]		
n-pentane	Sigma Aldrich	626.83	626	1.357	1.358	≥ 99	99.99
n-hexane	Merck	660.06	659	1.375	1.375	≥ 99	99.21
perfluoro-n-heptane	Apollo Scientific	1742.69	1733	1.261	1.250	-	99.36
ethanol	Merck	789.86	789	1.361	1.361	≥ 99.5	99.90
1-propanol	Merck	803.49	804	1.385	1.386	≥ 99.5	99.48
2-propanol	Sigma Aldrich	790.00	786	1.377	1.377	99.5	99.99
2-butanol	Sigma Aldrich	806.60	807	1.395	1.395[3]	≥ 99	99.21
water	PURELAB Option Q water purification system	998.22	998	1.333	1.333	-	99.71

[1]Literature: Coulson and Richardson (2005) at 293.15 K. [2]Literature: Dean (1998) at 293.15 K. [3]Literature: Dean (1998) at 298.15 K. *As stated by the supplier.

5.3 Vapour pressure measurements

Vapour pressure measurements are a critical step in determining if the chemicals are thoroughly degassed. Vapour pressures are measured according to the steps outlined in section 4.2.3, and Table 5-2 displays a comparison of the measured vapour pressures and literature. A graphical representation of the measured data is presented in Figure 5-13, in the form of ln P vs 1/T, to produce a straight line.

Table 5-2: Measured and literature vapour pressure data.

Component	T /K	Vapour Pressure /kPa			Deviation /kPa*	
		Experimental	Literature[1]	Literature[2]	Literature[1]	Literature[2]
n-Pentane	308.10	97.15	97.55	97.70	0.39	0.55
	313.10	115.07	115.49	115.67	0.43	0.61
	323.11	158.52	159.03	159.27	0.51	0.75
	328.11	184.19	185.07	185.15	0.87	0.96
	333.12	213.29	214.24	214.39	0.95	1.10
n-Hexane	308.11	30.42	30.58	30.58	0.16	0.15
	313.11	37.03	37.23	37.23	0.20	0.20
	318.10	44.76	44.98	44.98	0.22	0.22
	323.11	54.56	54.01	54.01	0.55	0.55
	333.13	76.48	76.36	76.38	0.11	0.09
2-Propanol	313.10	13.84	14.19	13.93	0.35	0.09
	318.11	18.10	18.50	18.24	0.41	0.15
	323.11	23.38	23.88	23.65	0.51	0.27
	328.11	29.96	30.54	30.36	0.58	0.39
	333.11	38.04	38.71	38.60	0.67	0.56
2-Butanol	303.16	3.36	3.40	3.25	0.04	0.11
	323.16	10.44	11.07	10.75	0.63	0.31
	329.17	14.87	15.20	14.84	0.33	0.04
Water	313.18	7.26	7.42	7.39	0.15	0.13
	318.18	9.66	9.63	9.60	0.03	0.06
	323.16	12.02	12.38	12.35	0.35	0.32

Literature[1]: Poling et al. (2001). Literature[2]: NIST ThermoData Engine of Aspen Plus® V8.6.

*$Deviation = \left|P^{exp} - P^{model}\right|$

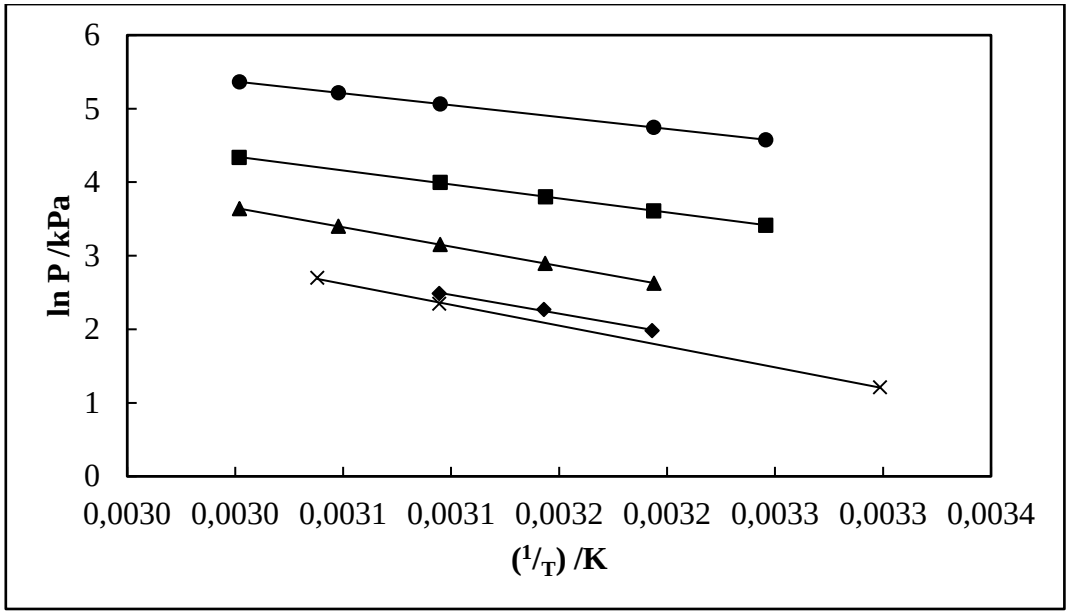

Figure 5-13: Plot of ln P vs 1/T for pure component vapour pressures.

Where n-pentane; ●, n-hexane; ■, 2-propanol; ▲, 2-butanol; ˣ , water; ♦, line of best fit; —.

5.4 Data regression and computational procedure

As discussed in Chapter 2, thermodynamic models play an integral role in the design and optimization of separation processes as they are used to extrapolate data over a broad spectrum where experimental data are unavailable.

In this work, the combined method $(\gamma - \phi)$ along with Barker's algorithm was employed, which uses activity coefficients to account for the non-idealities in the liquid phase as well as fugacity coefficients from equations of state to describe the non-idealities in the vapour phase. For the experimental data measured in this project, three activity coefficient models were utilised. These are the Non-Random Two-Liquid (NRTL), Wilson and Universal Quasi-Chemical (UNIQUAC) models. The Wilson activity coefficient model is advantageous as it produces an accurate representation of phase equilibrium data using only two adjustable parameters, as well as accurately predicting multi-component properties from binary data. Another reason for choosing the Wilson activity coefficient model was due to the fact that it provides a superior fit to alcohol + hydrocarbon mixtures, which are otherwise poorly represented by algebraic expressions (Palmer, 1987). The NRTL model, similar to the Wilson, can accurately represent phase equilibrium data using just a few parameters (in this case, three) and effectively represents partially miscible as well as completely miscible systems. The UNIQUAC model, although slightly complex mathematically, also employs only two adjustable parameters. Abrams and Prausnitz (1975), state that the UNIQUAC model represents vapour-liquid and liquid-liquid equilibrium data well for binary and multi-component systems. These systems are inclusive of polar and non-polar compounds such as hydrocarbons, alcohols, ketones, amines, esters, nitriles and water. These models are well known, widely used and available in Aspen Plus®, which was used to regress the model parameters in this work. The vapour phase non-idealities were described using the Hayden-O'Connell correlation as it is a well-defined, non-complex model. Equations of state, such as Peng Robinson and Soave-Redlich Kwong for example, were not utilised as they are better suited for higher pressures.

Figure 5-14 displays the algorithm for P-x data reduction via the combined method and the method of Barker (1953), which was utilised in this work. The method of Barker (1953) is used to minimize the liquid phase composition residual $(\delta x_i^{residual})$, in order to fit the overall composition (z_i) and total pressure (P) to an excess Gibbs Energy model. The algorithm in Figure 5-14 involves the following steps:

STEP 1: Select an appropriate G^E model in Aspen Plus® in order to minimize the objective functions, in this case pressure and temperature, using the "*maximum likelihood*" regression algorithm. This regression algorithm was chosen as it provides a global optimum in parameter estimation (Nala, 2012). It is assumed that $x_i = z_i$ and $\Phi_i = 1$. This yields the calculated temperatures (T), pressures (P), activity coefficients (γ), calculated vapour mole fraction (y_i) and the model parameters for the activity coefficient model used.

STEP 2: The method of Barker (1953) requires the calculated vapour mole fraction (y_i) as well as conducting a mass balance to determine the number of moles of each component in the vapour and liquid phases, i.e. n_i^V and n_i^L.

STEP 3: Thereafter, calculate the liquid phase molefraction via $x_i = \frac{n_i^l}{n_T^l}$.

STEP 4: Calculate the liquid phase composition residual via $\delta x_i^{residual} = |x_i - x_{i-1}|$. If $|x_i - x_{i-1}| < 1x10^{-7}$, then stop. If $|x_i - x_{i-1}| > 1x10^{-7}$, then update z_i with the calculated x_i and repeat the process.

STEP 5: All systems measured in this project were modelled on Aspen Plus® using an activity coefficient model with Ideal Gas and Hayden O'Connell second virial coefficient. In Aspen Plus®, the "*maximum likelihood*" objective function was utilised during the data regression procedure. This objective function regresses for all measured variables, i.e. pressure, temperature and mole fraction, resulting in residuals obtained for both pressure and temperature where

$$\Delta P = \Delta P_{AVG} = \frac{1}{n}\sum_1^n \left|P^{exp} - P^{model}\right| \quad (5\text{-}1)$$

and

$$\Delta T = \Delta T_{AVG} = \frac{1}{n}\sum_1^n \left|T^{exp} - T^{model}\right| \quad (5\text{-}2)$$

STEP 6: In addition the difference between the experimental and model values for the pressure and temperature of each data point was calculated as follows

$$\Delta P = \left|P^{exp} - P^{model}\right| \quad (5\text{-}3)$$

$$\Delta T = \left|T^{exp} - T^{model}\right| \quad (5\text{-}3)$$

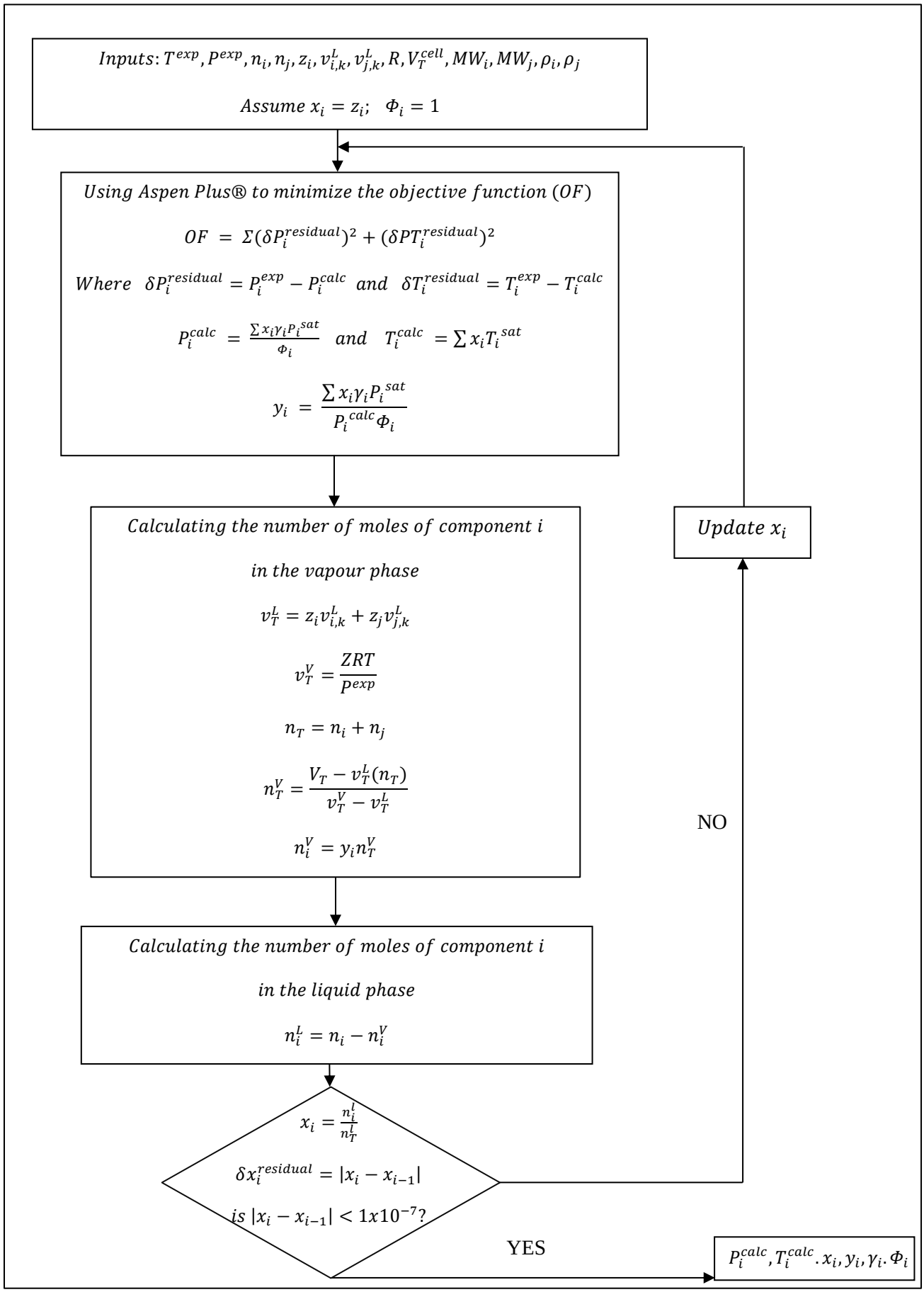

Figure 5-14: Algorithm for P-x data reduction using the combined method of Barker (1953).

5.5 Regressed parameters from vapour pressure measurements

The measured vapour pressure data was regressed on Aspen Plus® in order to determine the model parameters for the Antoine equation, given by

$$\ln P = A + \frac{B}{T+C} + DT + E \ln T + F\, T^{G} \qquad (5\text{-}1)$$

Where $H \leq T \leq I$, P is the pressure in bar and T is the temperature in Kelvin. For this work, the parameters A, B, E, F and G were taken into consideration as parameters C and D = 0 and H and I are temperature bounds. Table 5-3 presents the regressed parameters for the Antoine equation.

Table 5-3: Regressed Antoine parameters for measured vapour pressure data.

Component	Antoine Equation Parameters					ΔP/kPa*	T Range/K
	A	B	E	F	G		
n-Pentane	101.61	-6366.90	-12.29	$1.6\text{x}10^{-6}$	2.32	0.048	308.10 – 333.12
n-Hexane	97.64	-7173.75	-11.24	$2.9\text{x}10^{-5}$	1.66	0.167	308.11 – 333.13
2-Propanol	104.72	-8578.04	-11.92	$3.5\text{x}10^{-6}$	2.13	0.005	313.10 – 333.11
2-Butanol	111.23	-6831.66	-14.32	$2.5\text{x}10^{-16}$	6.33	0.000	303.16 – 329.17
Water	70.97	-8639.96	-5.58	$-7.9\text{x}10^{-6}$	2.20	0.086	313.18 – 323.16

$*\Delta P = \frac{1}{n}\sum_{1}^{n}\left|P^{exp} - P^{model}\right|$

The model fits the measured vapour pressures well, and the ΔP values are well within the overall combined pressure uncertainty.

5.6 Experimental troubleshooting

Once the apparatus was completely set up and the necessary temperature and pressure sensors were calibrated, the system n-hexane (1) + n-heptane (2) at 323.15 K was selected for measurement to test the functionality and accuracy of the apparatus. At this stage in the project, degassing was conducted in the Isco pumps, as discussed in section 4.2.3. The pumps were loaded and degassing commenced. Thereafter binary experimental measurements were conducted according to the procedures outlined in section 4.2.4. It is important to note that in this stage of the project, the nut below the pressure transmitter was not heated and insulated, and two 100 DM Isco pumps were employed. The temperature of the heating fluid circulated in the temperature jackets of the Isco pumps were not monitored but merely controlled via a Polyscience temperature controller, and the stainless steel heating block around the pressure transmitter was kept at a constant temperature of 313.15 K. The P-z diagram of the experimental points obtained is displayed in Figure 5-15 for the system n-hexane (1) + n-heptane (2) at 323.15 K. From Figure 5-15 it can be seen that the n-heptane vapour pressure point corresponds well with literature, however this is not the case for n-hexane vapour pressure. Both the n-hexane rich and n-hexane dilute regions converge in the middle of the phase envelope, forming a smooth line and resulting in no outer-lying points. This was the initial indication that the apparatus was functioning correctly, apart from the degassing procedure.

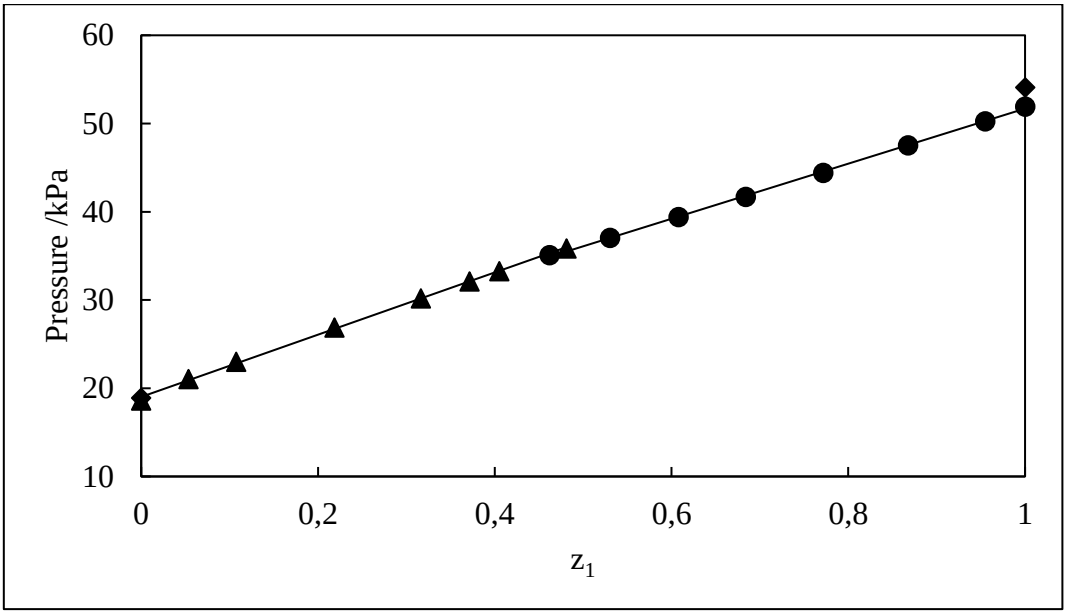

Figure 5-15: P-z diagram of the system n-hexane (1) + n-heptane at (2) 323.15 K. n-hexane rich (experimental); ●, n-hexane dilute (experimental); ▲, NIST ThermoData Engine of Aspen Plus® V8.6; ♦, line of best fit; —.

Approximately a week later, the system n-hexane (1) + n-heptane (2) at 323.15 K was remeasured to verify the experimental technique used initially. The same procedure as mentioned above was utilised and the result obtained is displayed in Figure 5-16. In Figure 5-16 it can be seen that the vapour pressure points of each component correspond well with literature, indicating the degassing process was successful. However, the n-hexane rich and n-hexane dilute regions do not converge to form a smooth line and instead deviate from convergence, as seen in the equimolar region.

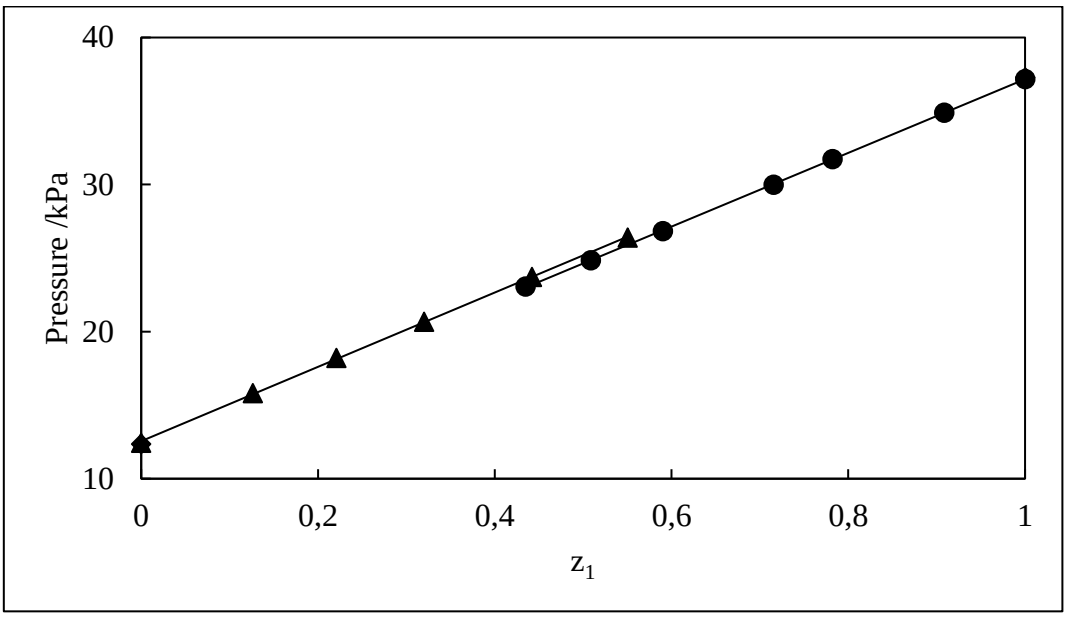

Figure 5-16: P-z diagram of the system n-hexane (1) + n-heptane (2) at 313.15 K. n-hexane rich (experimental); ●, n-hexane dilute (experimental); ▲, NIST ThermoData Engine of Aspen Plus® V8.6; ♦ line of best fit; —.

The exact cause of the problem was unknown at the time, however some possible causes speculated were:

- A leak in the cell
- Incorrect pressure readings signalled by the transmitter
- Impurities in the chemicals
- An unintentional variation in experimental technique
- Incorrect volume readings displayed by the Isco pumps

Insufficient degassing was ruled out as a possible cause as the vapour pressure points matched well with literature. The cell was then leak tested under vacuum overnight. The cell was completely evacuated, isolated via V-5, V-6, V-7, V-8, submerged in the SS bath and controlled to a temperature of 298.15 K. A leak rate of 0.004 kPa/hr was established, ruling out leakage of the cell as the problem, as the leak rate was minute. The pressure transmitter underwent a calibration check to determine if the transmitter

readings were accurate and after a successful calibration check, this was also ruled out as the cause. The system of n-hexane (1) + n-heptane (2) at 313.15 K was remeasured in the event that there were deviations from the experimental measurement technique. The result yielded is displayed in Figure 5-17. From the resulting equilibrium curve it can be observed that the problem still persists, as a similar result as that presented in Figure 5-16 was obtained. The vapour pressure points of each component correspond well with literature however, the n-hexane rich and n-hexane dilute regions do not converge to form a smooth line, ruling out the experimental technique as a possible cause.

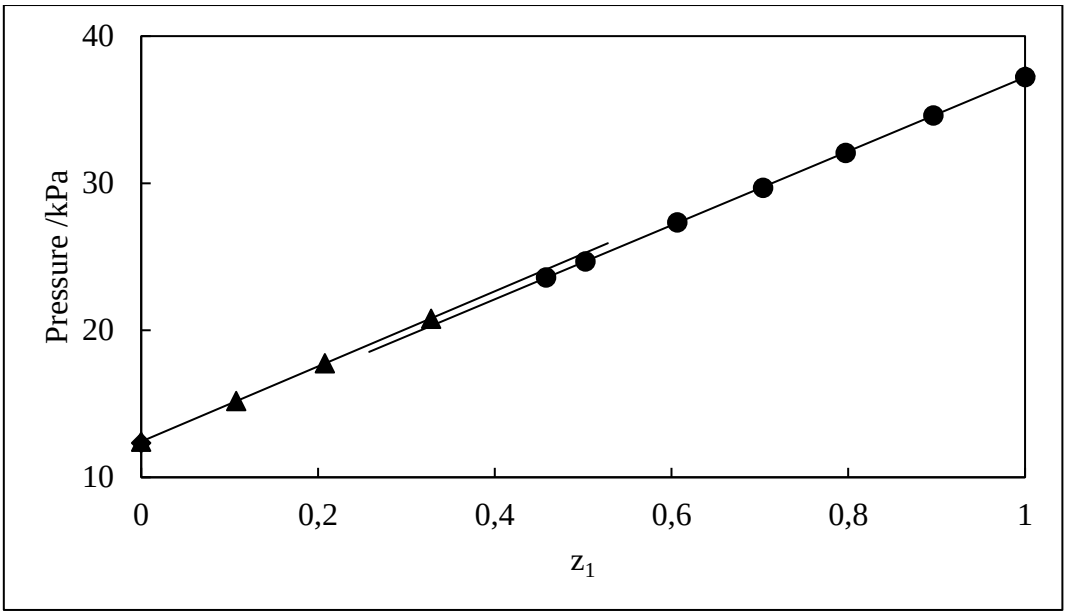

Figure 5-17: P-z diagram of the system n-hexane (1) + n-heptane (2) at 313.15 K. n-hexane rich (experimental); ●, n-hexane dilute (experimental); ▲, NIST ThermoData Engine of Aspen Plus® V8.6; ♦ line of best fit; —.

The refractive index and density of the chemicals were remeasured and the GC trace was reanalysed to eliminate any impurities existing in the chemicals. When the analytical tests produced satisfactory results, the system n-hexane (1) + 2-butanol (2) at 329.15 K was measured. The resulting phase equilibrium diagram is presented in Figure 5-18. It can be seen that degassing was successful as the vapour pressure of both the n-hexane and 2-butanol correspond well with literature. Although this system is quite different from the n-hexane + n-heptane system, as it has a greater positive deviation from Raoult's law, there is still no improvement with the change in system as the phase equilibrium curve does not converge smoothly.

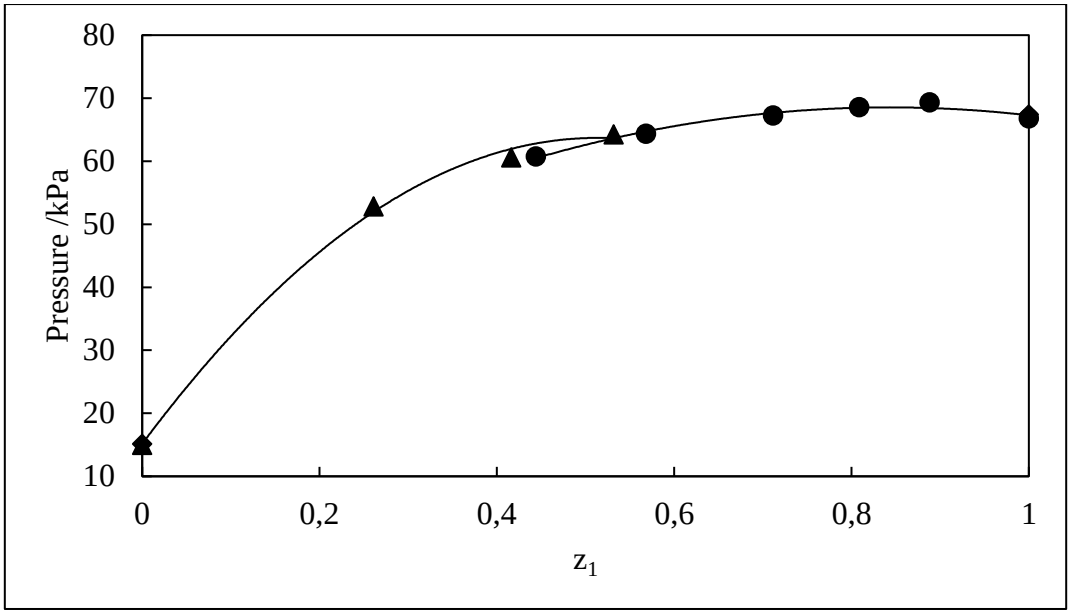

Figure 5-18: P-z diagram of the system n-hexane + 2-butanol at 329.15 K. n-hexane rich (experimental); ●, n-hexane dilute (experimental); ▲, NIST ThermoData Engine of Aspen Plus® V8.6; ♦ line of best fit; —.

A final system was measured before an investigation was conducted on the Isco pumps. n-Hexane (1) + 1-hexene (2) was measured at 328.15 K, and the resulting phase diagram is displayed in Figure 5-19. Similar to the n-hexane + n-heptane system, where the equilibrium curve has a smaller deviation from Raoult's law compared to the n-hexane + 2-butanol system, the resulting phase equilibrium curve does not converge smoothly, although the vapour pressure points correspond well with literature. After measuring three different systems and ruling out a leak in the cell, an inaccuracy in the pressure transmitter, any variation in experimental technique and impurities in the chemicals, an investigation on the Isco pumps could then commence.

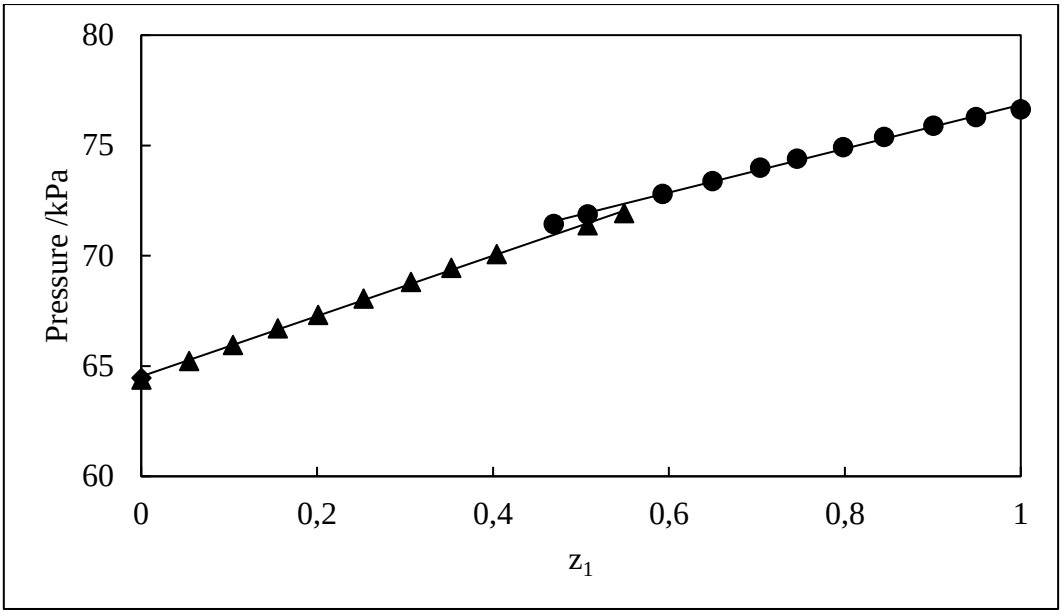

Figure 5-19: P-z diagram of the system n-hexane (1) + 1-hexene (2) at 328.15 K. n-hexane rich (experimental); ●, n-hexane dilute (experimental); ▲, NIST ThermoData Engine of Aspen Plus® V8.6; ♦ line of best fit; —.

Both 100 DM Isco pumps were disconnected from the apparatus and a stainless steel line was connected to pump 1, which was thereafter calibrated according to the procedure outlined in section 4.2.2. The same procedure was conducted for pump 2 (100 DM model at the time). The following was observed:

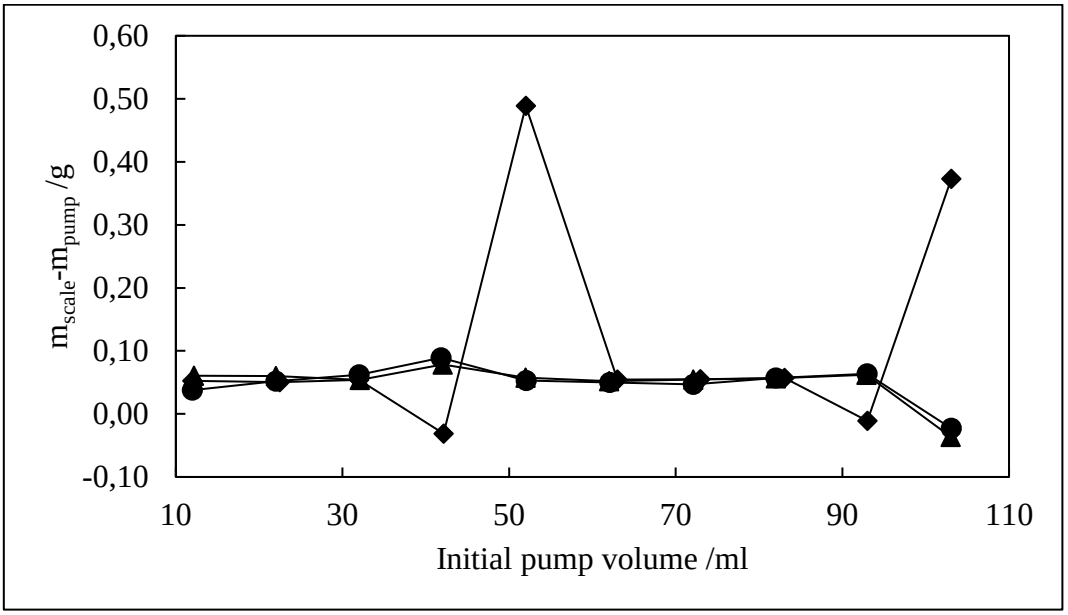

Figure 5-20: Plot of initial pump volume vs Δm at 25 ml/min. Pump 1, ●; Pump 2 (100 DM), ♦; Pump 2 (100 DX), ▲.

The difference in mass calculated between the standard (the scale) and the Isco pump (via a mass balance) for pump 1, showed a significant deviation of Δm (g) for the first point, i.e. Δm = -0.02 g, from the remainder of the points which were consistent at approximately 0.06 g (refer to Figure 5-20). For pump 2 (100 DM) however, the trend displayed was not the same as that of pump 1. For pump 2 (100 DM) the Δm value was not consistent throughout the calibration and ranged from Δm = -0.03 to 0.49 as seen in Figure 5-20. For pump 1, the excess water was extracted from the beaker when there was approximately 40 ml remaining in the pump whilst for pump 2 (100 DM) it was extracted with 50 ml remaining. From Figure 5-20 it is evident that the extraction of excess water from the beaker caused minimal disturbance in the case of pump 1, however in the case of pump 2 (100 DM) the disturbance was significant. It was thereafter decided to attempt the calibration on another Isco pump that was available in the Thermodynamics Research Unit laboratories. This pump, which was a 100 DX model, yielded similar results to pump 1, as can be seen in Figure 5-20. This suggests that there is a great deal of instability in pump 2 (100 DM). From Figure 5-20 it is evident that pump 1 and the 100 DX model behave similarly, where the first 10 ml dispensed has a Δm value which deviates from the remaining points. For pump 2 (100 DM) this procedure was repeated seven times and yielded a similar result each time, as seen in Figure 5-21.

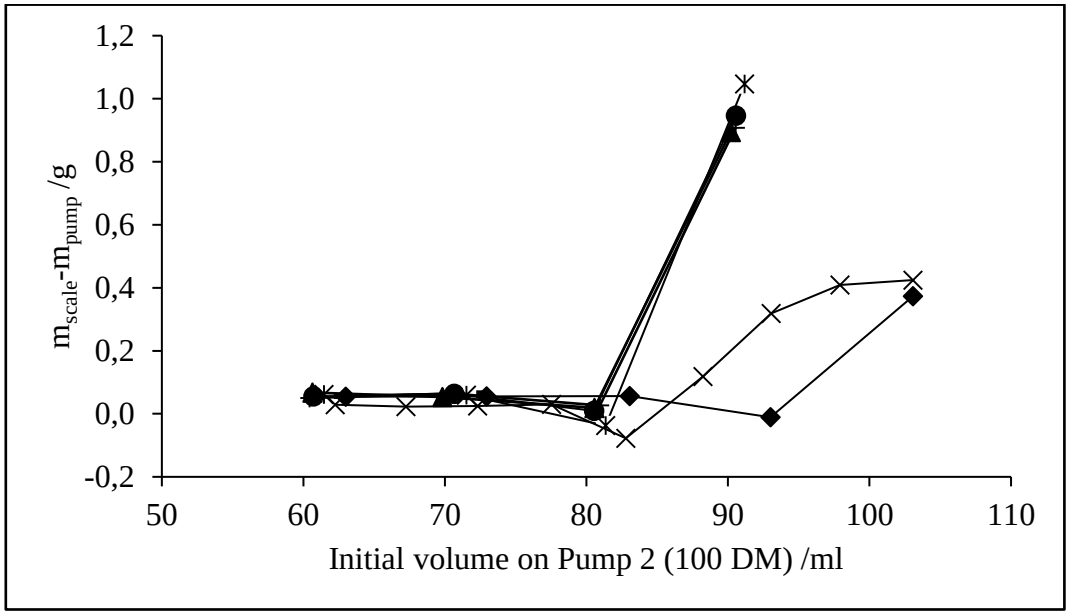

Figure 5-21: Pump 2 (100 DM) trial runs in constant flow mode.

Where run 1, ● (5 ml/min); run 2, ♦; run 3, ▲; run 4, run 5, ×; run 6, ─ ; run 7, * (runs 2-7 at 25 ml/min).

From Figure 5-21 it can be seen that pump 2 (100 DM) produces a large Δm value of approximately 0.95 g for point 1, in most cases. This is significantly larger than the initial Δm value produced by the pump 1 and the 100 DX model. In addition, after dispensing the first 10 ml of water from pump 1 and the 100 DX model, the remaining Δm values tend to stabilize whilst this is not the case for pump 2 (100 DM) which may require initially dispensing up to 20 ml of fluid. It was also observed that after extracting water from the beaker and zeroing the scale during the calibration procedure, minimal disturbance is caused to pump 1 and the 100 DX model whereas this is not the case for pump 2 (100 DM) as seen in Figure 5-20.

A decision was thereafter taken to replace pump 2 (100 DM) with the 100 DX model. A final calibration was conducted on both pumps and the results are displayed in Figures 5-9 to 5-12. It is unknown as to what was the cause of the inconsistent behaviour of pump 2 (100 DM), and it will need to be sent to Teledyne Isco for further testing. It was further concluded that before binary measurements can commence, an initial 10 ml of each component will be dispensed into the cell to counteract the discrepancy of the first point. The 10 ml of component 1 will be dispensed into the cell first and the vapour pressure checked, thereafter the cell will be flushed, cleaned and the same will be done for component 2. This has the benefit of ensuring that components are thoroughly degassed before commencing with P-z measurements as well as eliminating the dead volume in the feed ball valves.

5.7 Experimental results and data regression

After the replacement of the second Isco pump, now resulting in the 100 DX pump as pump 2, and the calibration of both feed pumps were undertaken, the measurement of test systems could thereafter commence. Five test systems were measured in total:

- water (1) + 2-butanol (2) at 323.16 K
- n-hexane (1) + 2-butanol (2) at 329.21 K
- n-pentane (1) + 1-propanol (2) at 317.18 K
- n-pentane (1) + 2-butanol (2) at 303.17 K
- n-pentane (1) + ethanol (2) at 303.11 K

The reason for measuring five test systems were due to the adjustments that were made to the apparatus during experimentation, and is discussed in greater detail in this section.

At this stage in the project the nut below the pressure transmitter was not heated and insulated, the temperature of the heating fluid for the temperature jackets in the pump were not monitored but merely controlled via a Polyscience temperature controller and the stainless steel heating block around the pressure transmitter was kept at a constant temperature of 313.15 K. In addition, prior to the measurements presented below, degassing was conducted in the feed pumps and degassing in an ultrasonic bath was also attempted.

The first test system measured was water (1) + 2-butanol (2) at 323.16 K, and the results yielded are presented below. All tables and figures of the raw experimental data measured, is presented in Appendix C.

5.7.1 Phase equilibria and modelling results for test systems

Table 5-4: Model parameters and pressure and temperature residuals for test systems.

Model and Model Parameters	A 323.16 K	B 329.21 K	C 317.18 K	D 303.17 K	E 303.11 K
Wilson – Ideal Gas					
$(\lambda_{12} - \lambda_{11})/K$	-196.58	-199.26	-255.75	-174.14	-371.98
$(\lambda_{12} - \lambda_{22})/K$	-1236.94	-563.12	-813.23	-646.67	-905.09
$\Delta P_{AVG}/kPa$	0.01	0.02	0.03	0.03	0.25
$\Delta T_{AVG}/K$	0.28	0.14	0.10	0.23	0.06
Wilson – HOC					
$(\lambda_{12} - \lambda_{11})/K$	-191.88	-211.36	-270.78	-183.92	-382.84
$(\lambda_{12} - \lambda_{22})/K$	-1237.46	-547.21	-801.41	-649.78	-874.51
$\Delta P_{AVG}/kPa$	0.01	0.02	0.03	0.03	0.25
$\Delta T_{AVG}/K$	0.28	0.14	0.1	0.24	0.06

A = water (1) + 2-butanol (2), B = n-hexane (1) + 2-butanol (2), C = n-pentane (1) + 1-propanol (2), D = n-pentane (1) + 2-butanol (2), E = n-pentane (1) + ethanol (2).

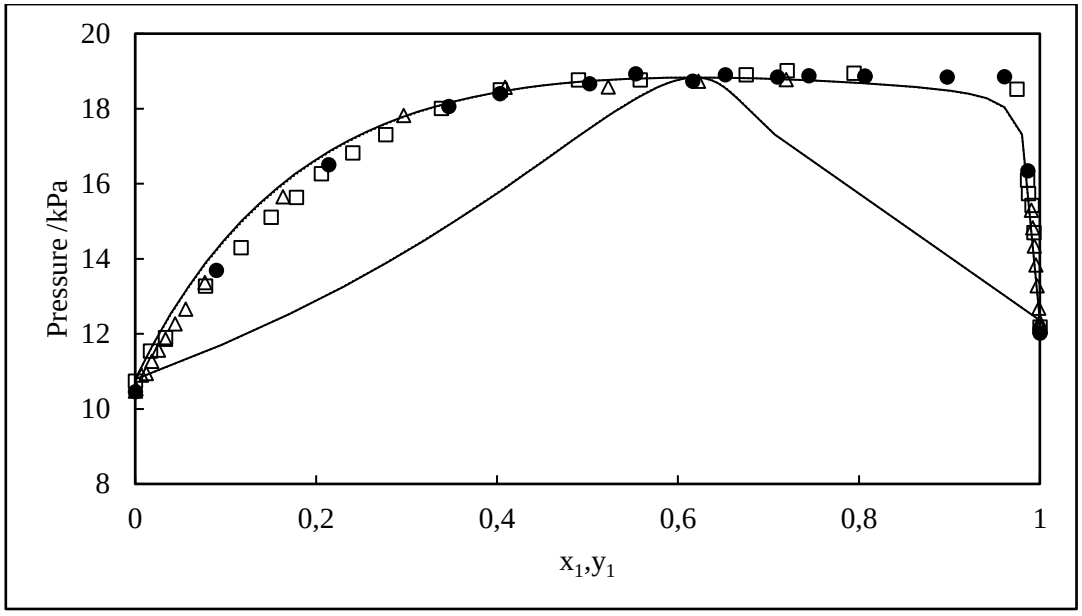

Figure 5-22: P-x plot for the water (1) + 2-butanol (2) system at 323.16 K.

●, P-x Experimental; ——, Wilson + Ideal Gas model; ·····, Wilson + HOC model; Δ, Gmehling et al. (1994); □, Motchelaho (2006).

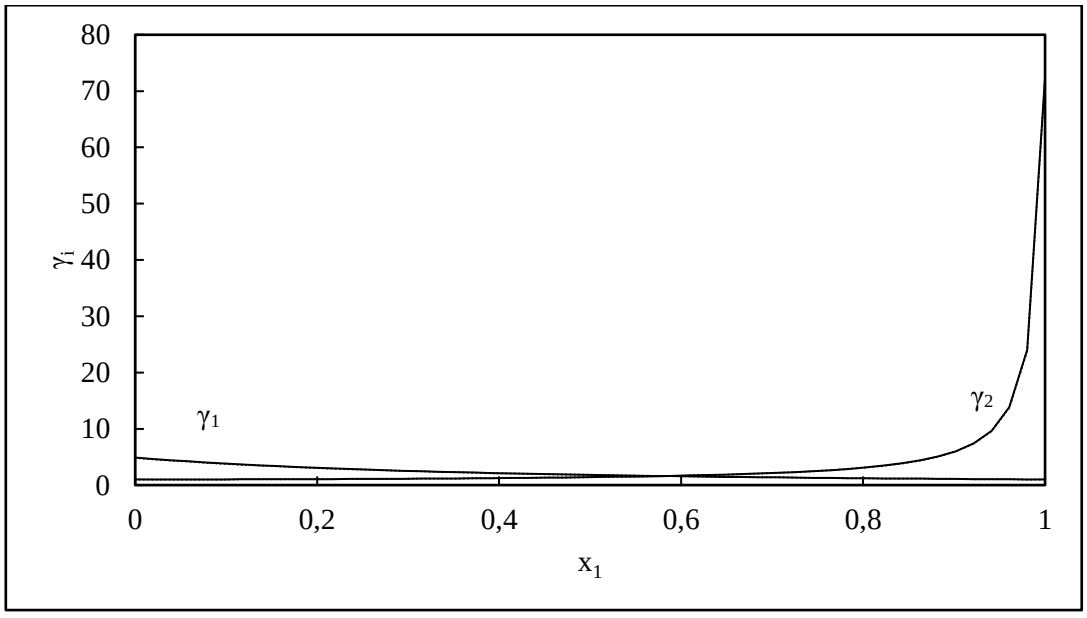

Figure 5-23: γ_i-x plot for the water (1) + 2-butanol (2) system at 323.16 K.

——, Wilson + Ideal Gas model; ·····, Wilson + HOC model.

Table 5-5: Regressed data for the water (1) + 2-butanol (2) system at 323.16 K using the Wilson + Ideal Gas models.

Experimental			Wilson + Ideal Gas								
z_1	P/kPa	T/K	P_{calc}/kPa	T_{calc}/K	x_1	y_1	ΔP	ΔT	γ_1	γ_2	α
1.000	12.02	323.16	12.03	322.62	1.000	1.000	0.000	0.538	-	-	-
0.986	16.34	323.16	16.35	322.73	0.987	0.733	0.000	0.433	1,004	35,158	0.04
0.961	18.85	323.16	18.82	324.01	0.960	0.675	0.000	0.846	1,026	13,721	0.08
0.898	18.84	323.16	18.83	323.53	0.897	0.655	0.000	0.365	1,092	5,755	0.22
0.807	18.86	323.17	18.85	323.36	0.806	0.644	0.000	0.186	1,207	3,179	0.43
0.806	18.87	323.16	18.86	323.37	0.806	0.644	0.000	0.206	1,207	3,178	0.43
0.745	18.88	323.17	18.88	323.30	0.744	0.637	0.000	0.125	1,298	2,469	0.60
0.710	18.84	323.16	18.84	323.22	0.710	0.632	0.000	0.062	1,354	2,205	0.70
0.652	18.90	323.16	18.90	323.25	0.652	0.624	0.000	0.087	1,457	1,884	0.89
0.617	18.73	323.16	18.73	323.07	0.616	0.619	0.000	0.089	1,529	1,734	1.01
0.553	18.93	323.16	18.92	323.30	0.554	0.607	0.000	0.138	1,668	1,533	1.25
0.502	18.66	323.17	18.66	323.09	0.502	0.596	0.000	0.076	1,888	1,346	1.46
0.404	18.40	323.17	18.40	323.12	0.403	0.567	0.000	0.051	2,135	1,226	1.94
0.348	18.06	323.16	18.06	323.07	0.346	0.546	0.000	0.086	2,368	1,156	2.26
0.215	16.51	323.16	16.52	322.83	0.211	0.464	0.000	0.333	3,108	1,049	3.19
0.091	13.69	323.16	13.71	322.52	0.088	0.300	0.000	0.644	4,070	1,007	4.36
0.000	10.46	323.16	10.47	322.62	0.000	0.000	0.000	0.537	-	-	-

Table 5-6: Regressed data for the water (1) + 2-butanol (2) system at 323.16 K using the Wilson + HOC models.

Experimental			Wilson + HOC								
z_1	P/kPa	T/K	P_{calc}/kPa	T_{calc}/K	x_1	y_1	ΔP	ΔT	γ_1	γ_2	α
1.000	12.02	323.16	12.03	322.62	1.000	1.000	0.000	0.538	-	-	-
0.986	16.34	323.16	16.35	322.73	0.987	0.735	0.000	0.426	1.004	34.836	0.04
0.961	18.85	323.16	18.82	324.01	0.960	0.676	0.000	0.846	1.026	13.700	0.08
0.898	18.84	323.16	18.83	323.52	0.897	0.656	0.000	0.361	1.092	5.721	0.22
0.807	18.86	323.17	18.85	323.35	0.806	0.645	0.000	0.177	1.207	3.160	0.43
0.806	18.87	323.16	18.86	323.36	0.806	0.645	0.000	0.197	1.207	3.160	0.43
0.745	18.88	323.17	18.88	323.28	0.744	0.637	0.000	0.114	1.297	2.456	0.60
0.710	18.84	323.16	18.84	323.21	0.710	0.633	0.000	0.050	1.354	2.193	0.70
0.652	18.90	323.16	18.90	323.23	0.652	0.624	0.000	0.074	1.456	1.875	0.89
0.617	18.73	323.16	18.73	323.06	0.616	0.619	0.000	0.102	1.805	1.398	1.01
0.553	18.93	323.16	18.93	323.29	0.554	0.607	0.000	0.125	1.666	1.527	1.25
0.502	18.66	323.17	18.66	323.08	0.502	0.595	0.000	0.086	1.895	1.336	1.46
0.404	18.40	323.17	18.40	323.11	0.403	0.566	0.000	0.055	2.131	1.222	1.94
0.348	18.06	323.16	18.06	323.08	0.346	0.544	0.000	0.085	2.357	1.154	2.26
0.215	16.51	323.16	16.52	322.85	0.211	0.462	0.000	0.313	3.078	1.049	3.19
0.091	13.69	323.16	13.71	322.55	0.088	0.297	0.000	0.613	4.047	1.006	4.36
0.000	10.46	323.16	10.47	322.62	0.000	0.000	0.000	0.537	-	-	-

For the first test system, water (1) + 2-butanol (2) at 323.16 K, degassing was conducted externally by circulating coolant and drawing a vacuum through a glass condenser, as discussed in section 4.2.3. From Figure 5-22 it can be seen that the vapour pressure points correspond well with literature, indicating that the degassing procedure was successful. From Figure 5-22 it can also be seen that in the water dilute and concentrated regions, the measured data corresponds well with both literature sources of Gmehling et al. (1994) and Motchelaho (2006). However, between the mole fraction range of x = 0.5 to x = 0.7, a variation between the literature sources can be seen. The experimental data however, lies between both literature sources. In terms of the modelling, it is evident that both model combinations produced a similar result and did not match the experimental and literature data perfectly. It is possible that due to the low pressure of this system, it could not be measured as accurately using a 0-500 kPa pressure transmitter and perhaps a 0-100 kPa transmitter would be better suited. The ΔP_{AVG} values were within the calculated pressure uncertainty, whilst the ΔT_{AVG} values were slightly above the temperature uncertainty, as seen in Table 5-4. Both models yielded similar activity coefficients as shown in Figure 5-23. An azeotrope was observed at the mole fraction x = 0.62, suggesting poor separation of the two components in that particular region. Figure 5-23 indicates a deviation from ideality in the concentrated region for each component, especially γ_2 at x = 1, where γ_2 = 72. It was decided to increase the temperature of the block housing the pressure transmitter, from 313.15 K to 323.15 K, as 323.15 K is closer to the temperature of most of the isotherms being measured.

The second test system measured was n-hexane (1) + 2-butanol (2) at 329.15 K. From figure 5-24 it can be seen that the experimental data, including the vapour pressure, points, correspond well with literature.

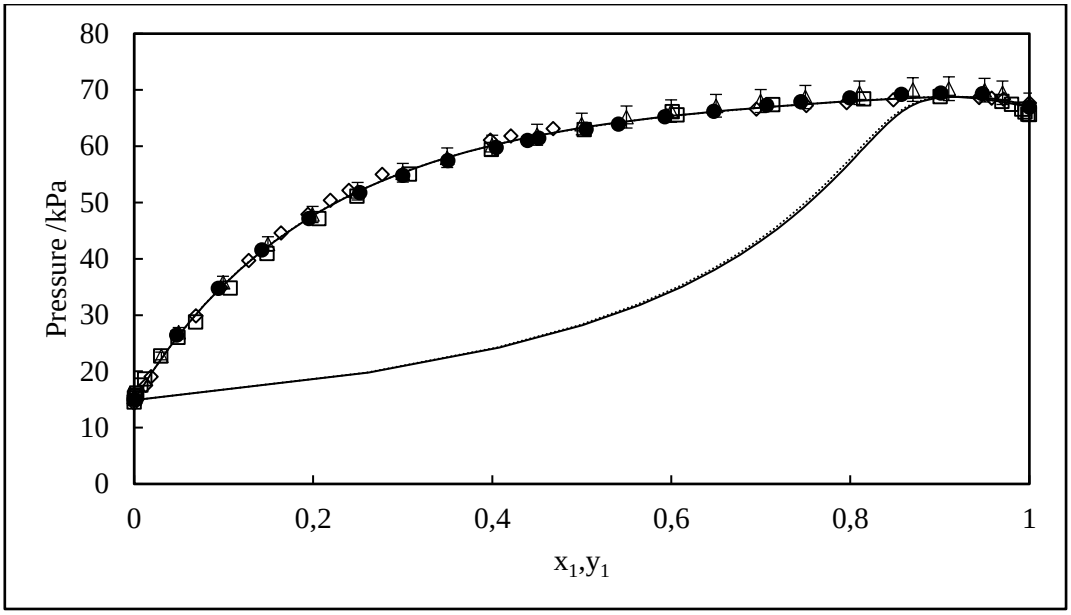

Figure 5-24: P-x plot for the n-hexane (1) + 2-butanol (2) system at 329.21 K.

●, P-x Experimental; —, Wilson + Ideal Gas model; ·····, Wilson + HOC model; Δ, Uusi-Kyyny et al. (2002); ◊, Moodley (2012); □, Raal et al. (2011).

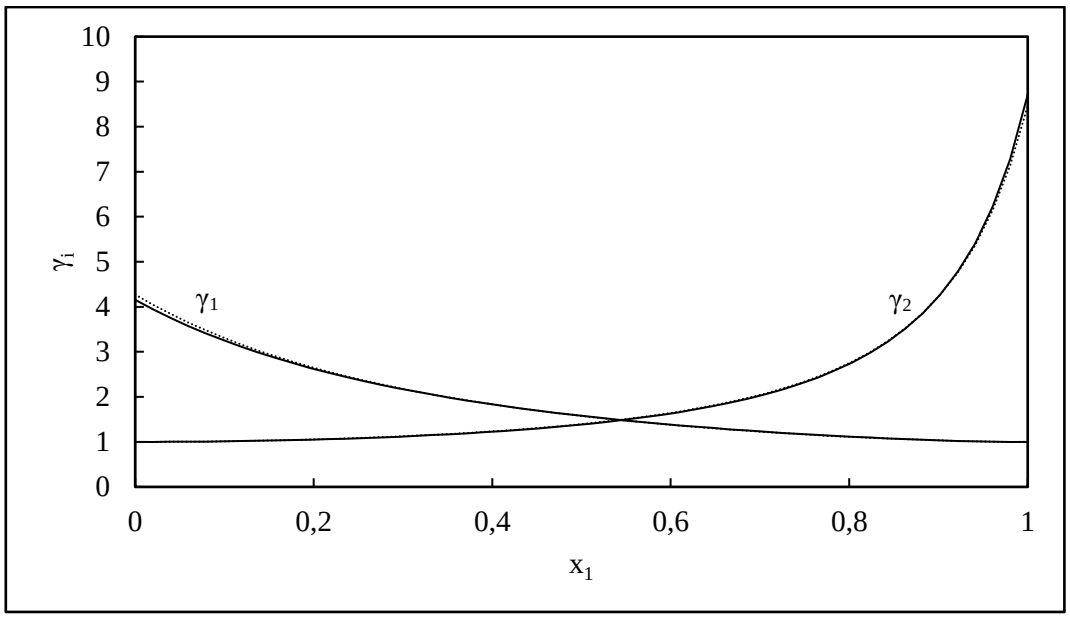

Figure 5-25: γ_i-x plot for the n-hexane (1) + 2-butanol (2) system at 329.21 K.

—, Wilson + Ideal Gas model; ·····, Wilson + HOC model.

Table 5-7: Regressed data for the n-hexane (1) + 2-butanol (2) system at 329.21 K using the Wilson + Ideal Gas models.

Experimental			Wilson + Ideal Gas								
z_1	P/kPa	T/K	P_{calc}/kPa	T_{calc}/K	x_1	y_1	ΔP	ΔT	γ_1	γ_2	α
1.000	66.93	329.21	66.93	329.17	1.000	1.000	0.000	0.042	-	-	-
0.948	69.33	329.21	69.33	329.48	0.948	0.935	0.001	0.267	1.035	4.247	0.80
0.901	69.46	329.21	69.46	329.47	0.901	0.908	0.001	0.261	1.035	4.247	1.09
0.857	69.20	329.21	69.20	329.47	0.857	0.893	0.001	0.254	1.066	3.425	1.40
0.800	68.62	329.21	68.62	329.44	0.800	0.880	0.000	0.229	1.117	2.724	1.84
0.745	67.90	329.21	67.90	329.39	0.745	0.871	0.000	0.179	1.176	2.287	2.31
0.707	67.29	329.20	67.29	329.33	0.707	0.865	0.000	0.130	1.224	2.061	2.67
0.648	66.22	329.20	66.22	329.23	0.648	0.858	0.000	0.030	1.307	1.794	3.28
0.593	65.23	329.20	65.23	329.20	0.593	0.850	0.000	0.003	1.397	1.609	3.90
0.542	63.95	329.21	63.95	329.11	0.538	0.843	0.000	0.091	1.519	1.446	4.55
0.505	63.03	329.20	63.03	329.09	0.502	0.837	0.000	0.114	1.601	1.369	5.05
0.453	61.41	329.20	61.41	329.04	0.447	0.828	0.000	0.155	1.736	1.277	5.84
0.440	61.03	329.21	61.03	329.05	0.435	0.826	0.000	0.158	1.766	1.260	6.04
0.405	59.76	329.20	59.76	329.04	0.400	0.818	0.000	0.160	1.863	1.215	6.62
0.352	57.44	329.20	57.44	329.04	0.346	0.804	0.000	0.152	2.029	1.157	7.62
0.302	54.83	329.20	54.83	329.07	0.297	0.788	0.000	0.126	2.201	1.114	8.67
0.254	51.76	329.20	51.76	329.12	0.250	0.768	0.000	0.081	2.390	1.081	9.80
0.197	47.17	329.20	47.17	329.18	0.195	0.734	0.000	0.015	2.651	1.049	11.34
0.145	41.56	329.20	41.56	329.25	0.144	0.684	0.000	0.050	2.956	1.026	13.01
0.096	34.77	329.20	34.77	329.32	0.095	0.605	0.000	0.120	3.297	1.011	14.80
0.049	26.43	329.20	26.43	329.42	0.049	0.456	0.000	0.217	3.681	1.003	16.74
0.000	15.00	329.20	15.00	329.33	0.000	0.000	0.000	0.136	-	-	-

Table 5-8: Regressed data for the n-hexane (1) + 2-butanol (2) system at 329.21 K using the Wilson + HOC models.

Experimental			Wilson + HOC								
z_1	P/kPa	T/K	P_{calc}/kPa	T_{calc}/K	x_1	y_1	ΔP	ΔT	γ_1	γ_2	α
1.000	66.93	329.21	66.94	329.17	1.000	1.000	0.000	0.042	-	-	-
0.948	69.33	329.21	69.28	329.47	0.948	0.935	0.001	0.259	1.034	4.241	0.80
0.901	69.46	329.21	69.41	329.46	0.901	0.908	0.000	0.245	1.034	4.241	1.08
0.857	69.20	329.21	69.15	329.45	0.857	0.891	0.000	0.238	1.064	3.436	1.37
0.800	68.62	329.21	68.58	329.43	0.800	0.877	0.000	0.218	1.115	2.742	1.80
0.745	67.90	329.21	67.87	329.39	0.745	0.868	0.000	0.176	1.173	2.306	2.25
0.707	67.29	329.20	67.26	329.33	0.707	0.862	0.000	0.133	1.220	2.079	2.59
0.648	66.22	329.20	66.21	329.24	0.648	0.854	0.000	0.039	1.303	1.810	3.18
0.593	65.23	329.20	65.23	329.21	0.593	0.847	0.000	0.007	1.392	1.624	3.79
0.542	63.95	329.21	63.96	329.13	0.539	0.839	0.000	0.080	1.512	1.460	4.43
0.505	63.03	329.20	63.05	329.10	0.502	0.834	0.000	0.103	1.595	1.381	4.91
0.453	61.41	329.20	61.44	329.05	0.448	0.824	0.000	0.148	1.733	1.285	5.68
0.440	61.03	329.21	61.06	329.06	0.435	0.822	0.000	0.151	1.764	1.268	5.88
0.405	59.76	329.20	59.79	329.04	0.400	0.814	0.000	0.155	1.863	1.221	6.46
0.352	57.44	329.20	57.46	329.04	0.346	0.800	0.000	0.152	2.034	1.162	7.44
0.302	54.83	329.20	54.85	329.07	0.296	0.784	0.000	0.128	2.212	1.118	8.48
0.254	51.76	329.20	51.77	329.11	0.250	0.764	0.000	0.086	2.407	1.083	9.60
0.197	47.17	329.20	47.17	329.18	0.195	0.730	0.000	0.019	2.679	1.051	11.12
0.145	41.56	329.20	41.56	329.24	0.143	0.680	0.000	0.044	2.995	1.027	12.79
0.096	34.77	329.20	34.76	329.32	0.095	0.601	0.000	0.117	3.354	1.012	14.58
0.049	26.43	329.20	26.42	329.41	0.049	0.452	0.000	0.216	3.763	1.003	16.53
0.000	15.00	329.20	15.00	329.33	0.000	0.000	0.000	0.136	-	-	-

Although the experimental data corresponds well with literature, it can be observed that there is some variation between the literature sources, predominantly between the region of x = 0.3 to x = 0.5. Although the experimental data lies between the literature sources, the error bars suggest that there is a maximum of 3% error among the literature sources. Both model combinations produced a similar result and produced a good fit to the experimental data. In the work of Uusi-Kyyny et al. (2002), the Wilson activity coefficient model was also utilised, whilst the work of Raal et al. (2011) and Moodley (2012) utilised models such as NRTL and T-K Wilson. The ΔP_{AVG} for both models utilised in this work were well within the pressure uncertainty of 0.36 kPa, whilst the ΔT_{AVG} values were slightly above the temperature uncertainty of 0.06 K, as seen in Table 5-4. Azeotropic points were observed between the points x = 0.90 to x = 0.92, indicating poor separation between the n-hexane and 2-butanol and a positive deviation from Raoult's Law in this region. Figure 5-25, the plot of γ_i vs x_i shows a strong similarity in the activity coefficients between the two models utilised in this work, and the deviation from ideality was not as large compared to the first test system.

It was further decided to wrap the nut below the pressure transmitter with nichrome wire and insulate it. The nut would be kept at the temperature of the isotherm being measured and monitored using a Pt-100 temperature sensor. This was done in order to prevent the condensation of any vapour below the pressure transmitter, which may cause discrepancies in the pressure readings. An additional Pt-100 was inserted in the heating fluid bath of the feed pumps to monitor the temperature. This sensor along with the Pt-100 used to monitor the transmitter nut temperature, were calibrated.

The third test system measured was n-pentane (1) + 1-propanol (2) at 317.18 K. From Figure 5-26 it is seen that the vapour pressure points correspond well with the literature data, indicating that both components were successfully degassed. However, the experimental data and literature data did not yield an excellent fit. The experimental data has a slightly negative deviation from the literature data, however both the n-pentane dilute and concentrated regions converge smoothly.

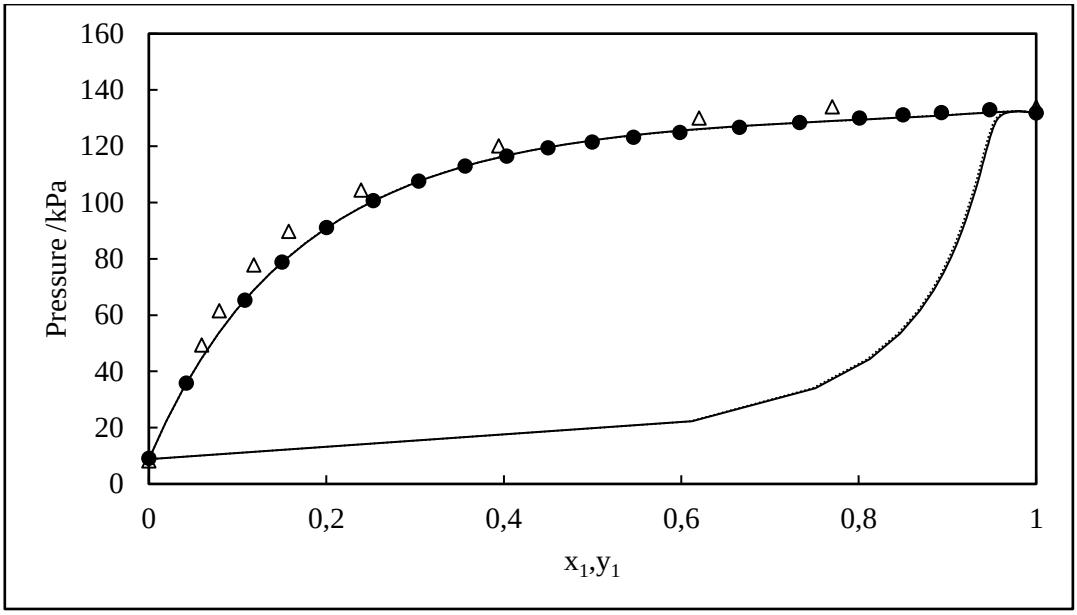

Figure 5-26: P-x plot for the n-pentane (1) + 1-propanol (2) system at 317.18 K. ●, P-x Experimental; ——, Wilson + Ideal Gas model; ·····, Wilson + HOC model; Δ, Rice et al. (1990).

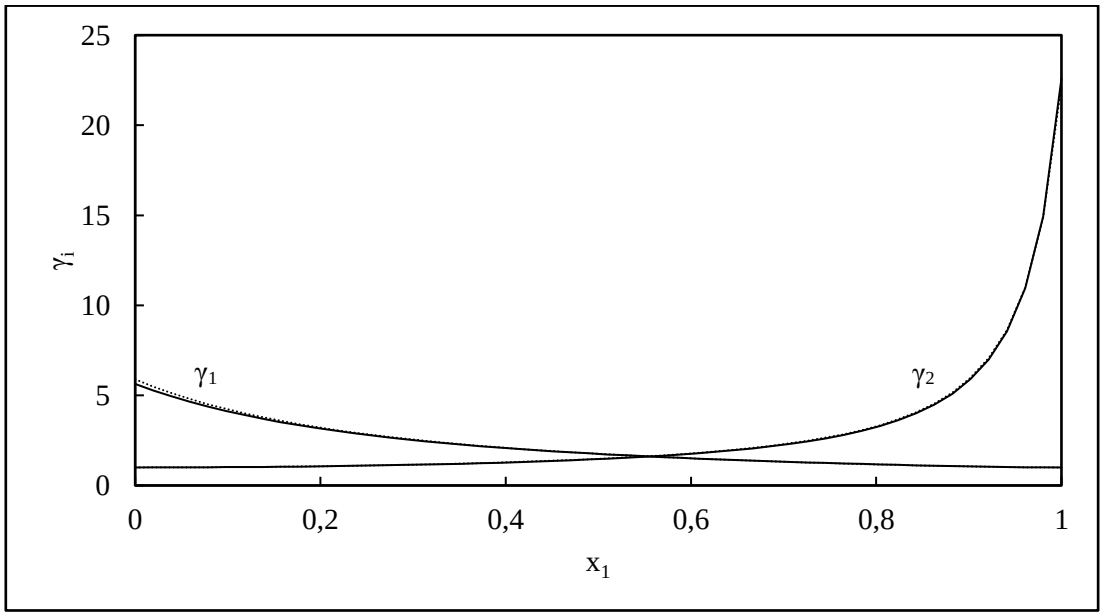

Figure 5-27: γ_i-x plot for the n-pentane (1) + 1-propanol (2) system at 317.18 K. ——, Wilson + Ideal Gas model; ·····, Wilson + HOC model.

Table 5-9: Regressed data for the n-pentane (1) +1- propanol (2) system at 317.18 K using the Wilson + Ideal Gas models.

Experimental			Wilson + Ideal Gas								
z_1	P/kPa	T/K	P_{calc}/kPa	T_{calc}/K	x_1	y_1	ΔP	ΔT	γ_1	γ_2	α
1.000	131.85	317.18	131.86	317.15	1.000	1.000	0.000	0.030	-	-	-
0.948	133.00	317.18	132.92	317.38	0.948	0.968	0.001	0.206	1.021	9.267	1.64
0.894	131.97	317.18	131.88	317.39	0.893	0.960	0.001	0.216	1.067	5.520	2.88
0.851	131.10	317.18	131.03	317.36	0.850	0.958	0.001	0.188	1.112	4.158	3.99
0.802	130.06	317.17	130.01	317.30	0.801	0.956	0.001	0.128	1.171	3.250	5.38
0.735	128.38	317.17	128.38	317.17	0.734	0.954	0.000	0.007	1.266	2.508	7.55
0.668	126.77	317.17	126.80	317.09	0.665	0.952	0.000	0.083	1.410	1.971	10.06
0.601	124.91	317.17	124.96	317.05	0.596	0.951	0.000	0.125	1.558	1.682	12.89
0.548	123.24	317.18	123.29	317.05	0.543	0.949	0.001	0.127	1.676	1.536	15.42
0.501	121.46	317.18	121.50	317.06	0.496	0.947	0.000	0.111	1.792	1.434	17.95
0.451	119.46	317.17	119.47	317.15	0.449	0.945	0.000	0.027	1.911	1.355	20.98
0.405	116.48	317.18	116.49	317.14	0.402	0.942	0.000	0.031	2.074	1.276	24.16
0.358	112.90	317.17	112.90	317.17	0.356	0.939	0.000	0.000	2.254	1.213	27.86
0.307	107.64	317.17	107.63	317.19	0.305	0.934	0.000	0.019	2.503	1.152	32.59
0.256	100.68	317.17	100.67	317.19	0.254	0.928	0.000	0.021	2.794	1.104	37.97
0.204	91.17	317.18	91.16	317.20	0.201	0.918	0.000	0.024	3.156	1.065	44.45
0.153	78.86	317.17	78.86	317.18	0.150	0.902	0.000	0.010	3.583	1.037	51.88
0.111	65.34	317.17	65.34	317.17	0.108	0.878	0.000	0.006	4.017	1.019	59.05
0.044	35.87	317.18	35.87	317.18	0.042	0.764	0.000	0.005	4.895	1.003	73.12
0.000	9.14	317.18	9.13	317.82	0.000	0.000	0.000	0.641	-	-	-

Table 5-10: Regressed data for the n-pentane (1) + 1-propanol (2) system at 317.18 K using the Wilson + HOC models.

Experimental			Wilson + HOC								
z_1	P/kPa	T/K	P_{calc}/kPa	T_{calc}/K	x_1	y_1	ΔP	ΔT	γ_1	γ_2	α
1.000	131.85	317.18	131.86	317.15	1.000	1.000	0.000	0.030	-	-	-
0.948	133.00	317.18	132.93	317.36	0.948	0.966	0.001	0.183	1.021	9.330	1.58
0.894	131.97	317.18	131.89	317.38	0.893	0.958	0.001	0.204	1.066	5.591	2.75
0.851	131.10	317.18	131.03	317.36	0.850	0.956	0.001	0.186	1.111	4.217	3.80
0.802	130.06	317.17	130.01	317.31	0.801	0.954	0.001	0.134	1.170	3.298	5.12
0.735	128.38	317.17	128.38	317.18	0.734	0.952	0.000	0.006	1.264	2.549	7.18
0.668	126.77	317.17	126.79	317.11	0.665	0.950	0.000	0.067	1.403	2.012	9.58
0.601	124.91	317.17	124.95	317.06	0.596	0.948	0.000	0.113	1.554	1.707	12.31
0.548	123.24	317.18	123.29	317.06	0.543	0.947	0.000	0.118	1.676	1.554	14.74
0.501	121.46	317.18	121.50	317.07	0.497	0.945	0.000	0.107	1.795	1.448	17.19
0.451	119.46	317.17	119.47	317.15	0.449	0.943	0.000	0.027	1.918	1.367	20.13
0.405	116.48	317.18	116.49	317.14	0.402	0.940	0.000	0.035	2.086	1.284	23.23
0.358	112.90	317.17	112.90	317.16	0.356	0.937	0.000	0.007	2.272	1.220	26.84
0.307	107.64	317.17	107.64	317.18	0.304	0.932	0.000	0.008	2.525	1.158	31.47
0.256	100.68	317.17	100.68	317.18	0.253	0.926	0.000	0.010	2.828	1.108	36.78
0.204	91.17	317.18	91.17	317.19	0.201	0.915	0.000	0.016	3.208	1.068	43.20
0.153	78.86	317.17	78.86	317.18	0.150	0.899	0.000	0.009	3.660	1.038	50.60
0.111	65.34	317.17	65.34	317.17	0.108	0.875	0.000	0.005	4.123	1.020	57.82
0.044	35.87	317.18	35.87	317.20	0.043	0.761	0.000	0.018	5.075	1.003	72.11
0.000	9.14	317.18	9.13	317.82	0.000	0.000	0.000	0.641	-	-	-

Both model combinations yielded similar results and fit the experimental data well. Both models yielded similar activity coefficients (refer to Figure 5-27) and an azeotrope can be observed at x = 0.97. The ΔP_{AVG} was 0.03 kPa, which was within the calculated pressure uncertainty, whilst the ΔT_{AVG} was slightly above the calculated uncertainty for temperature at 0.1 K. From Table 5-1 it can be seen that the chemicals used in this study are of high purity and it is therefore possible that discrepancies in the literature data may exist. Figure 5-27 suggests a deviation from ideality at the extreme ends, however the deviation is relatively lower than the first test system.

Due to the fit between the experimental and literature data for the system n-pentane (1) + 1-propanol (2) at 317.18 K being unsatisfactory, a fourth test system was measured. The system n-pentane (1) + 2-butanol (2) was measured at 303.17 K, and the resulting P-x diagram is presented in Figure 5-28. From Figure 5-28 it can be seen that the experimental points, including the vapour pressures, produce a good fit with the literature data of Thomas et al. (1991).

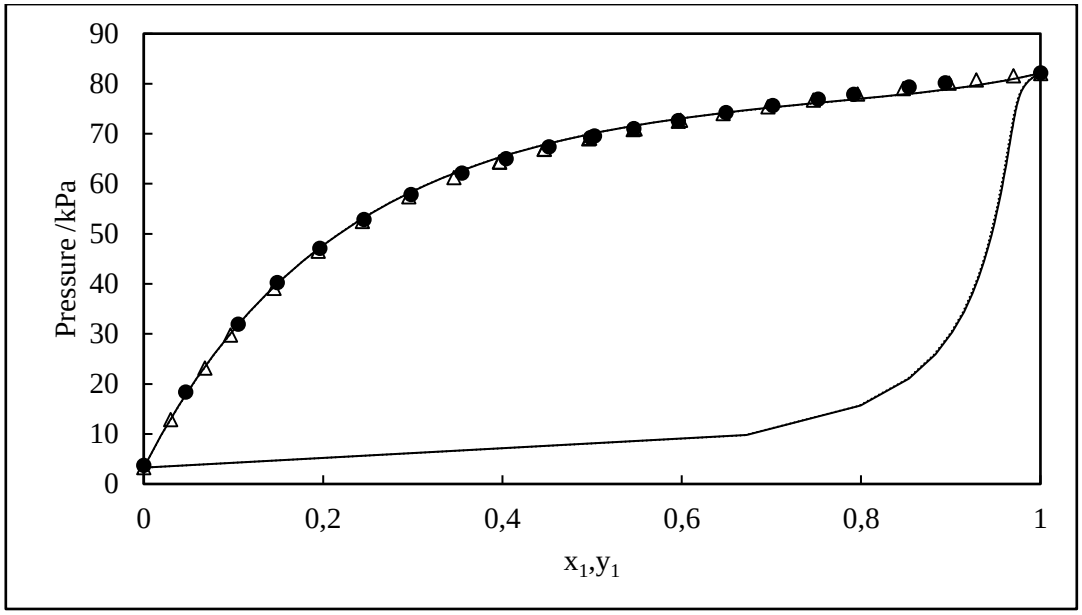

Figure 5-28: P-x plot for the n-pentane (1) + 2-butanol (2) system at 303.17 K. ●, P-x Experimental; ——, Wilson + Ideal Gas model; ·····, Wilson + HOC model; Δ, Thomas et al. (1991).

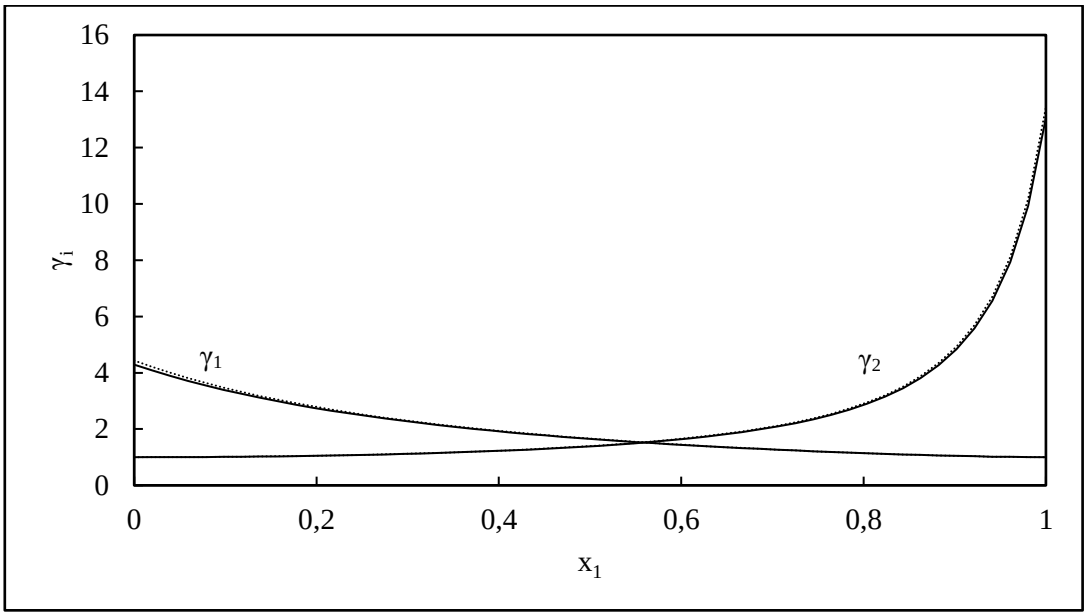

Figure 5-29: γ_i-x plot for the n-pentane (1) + 2-butanol (2) system at 303.17 K. ——, Wilson + Ideal Gas model; ·····, Wilson + HOC model.

Table 5-11: Regressed data for the n-pentane (1) + 2-butanol (2) system at 303.17 K using the Wilson + Ideal Gas models.

Experimental			Wilson + Ideal Gas								
z_1	P/kPa	T/K	P_{calc}/kPa	T_{calc}/K	x_1	y_1	ΔP	ΔT	γ_1	γ_2	α
1.000	82.15	303.17	82.15	303.18	1.000	1.000	0.000	0.010	-	-	-
0.894	80.15	303.17	80.05	303.60	0.894	0.980	0.001	0.429	1.052	4.583	5.72
0.854	79.31	303.17	79.21	303.60	0.854	0.977	0.001	0.431	1.088	3.636	7.45
0.793	77.89	303.17	77.82	303.51	0.793	0.975	0.001	0.336	1.154	2.764	10.41
0.753	76.91	303.17	76.86	303.41	0.753	0.974	0.001	0.240	1.202	2.403	12.51
0.703	75.66	303.17	75.63	303.30	0.702	0.973	0.000	0.128	1.272	2.068	15.43
0.650	74.22	303.17	74.22	303.17	0.649	0.972	0.000	0.002	1.353	1.818	18.73
0.597	72.63	303.17	72.65	303.08	0.593	0.971	0.000	0.093	1.472	1.588	22.37
0.547	71.01	303.17	71.04	303.03	0.541	0.969	0.000	0.148	1.584	1.448	26.09
0.503	69.54	303.16	69.57	303.03	0.498	0.968	0.000	0.132	1.680	1.363	29.67
0.499	69.25	303.17	69.28	303.00	0.492	0.968	0.000	0.171	1.698	1.349	30.04
0.453	67.39	303.17	67.42	303.02	0.446	0.966	0.000	0.153	1.810	1.278	34.16
0.405	65.01	303.16	65.03	303.02	0.399	0.963	0.000	0.139	1.943	1.215	38.86
0.356	62.11	303.16	62.13	303.05	0.351	0.960	0.000	0.108	2.095	1.163	44.21
0.299	57.86	303.16	57.87	303.08	0.295	0.956	0.000	0.079	2.300	1.113	51.16
0.247	52.87	303.16	52.88	303.11	0.243	0.950	0.000	0.056	2.524	1.076	58.37
0.198	47.10	303.16	47.10	303.14	0.196	0.942	0.000	0.019	2.764	1.048	66.08
0.151	40.24	303.16	40.23	303.21	0.150	0.929	0.000	0.044	3.042	1.028	74.87
0.107	31.93	303.16	31.93	303.19	0.106	0.907	0.000	0.025	3.342	1.014	83.22
0.048	18.35	303.16	18.34	303.35	0.048	0.828	0.000	0.188	3.824	1.003	98.58
0.000	3.71	303.16	3.70	305.11	0.000	0.000	0.000	1.946	-	-	-

Table 5-12: Regressed data for the n-pentane (1) + 2-butanol (2) system at 303.17 K using the Wilson + HOC models.

Experimental			Wilson + HOC								
z_1	P/kPa	T/K	P_{calc}/kPa	T_{calc}/K	x_1	y_1	ΔP	ΔT	γ_1	γ_2	α
1.000	82.15	303.17	82.15	303.18	1.000	1.000	0.000	0.010	-	-	-
0.894	80.15	303.17	80.05	303.61	0.894	0.979	0.001	0.435	0.979	1.053	5.44
0.854	79.31	303.17	79.21	303.61	0.854	0.976	0.001	0.440	0.976	1.089	7.09
0.793	77.89	303.17	77.81	303.52	0.793	0.974	0.001	0.346	0.974	1.155	9.93
0.753	76.91	303.17	76.86	303.42	0.753	0.973	0.001	0.251	0.973	1.204	11.95
0.703	75.66	303.17	75.63	303.31	0.702	0.972	0.000	0.137	0.972	1.274	14.76
0.650	74.22	303.17	74.22	303.18	0.649	0.971	0.000	0.004	0.971	1.356	17.95
0.597	72.63	303.17	72.65	303.08	0.593	0.969	0.000	0.092	0.969	1.476	21.49
0.547	71.01	303.17	71.04	303.02	0.541	0.968	0.000	0.149	0.968	1.592	25.10
0.503	69.54	303.16	69.57	303.02	0.497	0.967	0.000	0.136	0.967	1.690	28.60
0.499	69.25	303.17	69.28	303.00	0.492	0.966	0.000	0.174	0.966	1.709	28.95
0.453	67.39	303.17	67.42	303.01	0.446	0.965	0.000	0.159	0.965	1.824	32.99
0.405	65.01	303.16	65.04	303.01	0.398	0.962	0.000	0.147	0.962	1.961	37.60
0.356	62.11	303.16	62.13	303.04	0.350	0.959	0.000	0.117	0.959	2.117	42.86
0.299	57.86	303.16	57.87	303.08	0.295	0.955	0.000	0.086	0.955	2.330	49.72
0.247	52.87	303.16	52.88	303.10	0.243	0.949	0.000	0.061	0.949	2.561	56.88
0.198	47.10	303.16	47.10	303.14	0.196	0.940	0.000	0.022	0.940	2.812	64.58
0.151	40.24	303.16	40.23	303.21	0.150	0.928	0.000	0.045	0.928	3.103	73.40
0.107	31.93	303.16	31.93	303.19	0.106	0.906	0.000	0.027	0.906	3.420	81.88
0.048	18.35	303.16	18.34	303.36	0.048	0.826	0.000	0.196	0.826	3.934	97.52
0.000	3.71	303.16	3.70	305.11	0.000	0.000	0.000	1.945	-	-	-

Both model combinations yielded a similar result and correspond well with both the literature and experimental data. Both model combinations also produced similar activity coefficients (Figure 5-29) and in terms of uncertainties, the results were similar to that of the systems discussed above where the ΔP_{AVG} is well within the calculated uncertainty, however ΔT_{AVG} is slightly above as seen in Table 5-4. In addition, no azeotropes were observed in the data, indicating excellent separation between n-pentane and 2-butanol at 303.17 K. Figure 5-29 indicates a slight deviation from ideality due to the increase in the activity coefficients at the extreme ends. This test system yielded superior results, indicating that there may possibly be discrepancies in the literature data of Rice et al. (1990), which was utilised in the third test system. It was therefore evident that the equipment was functioning accurately, and thus a fifth and final test system was measured to confirm this.

The final test system measured was n-pentane (1) + ethanol (2) at 303.11 K. From Figure 5-30 it is seen that the experimental data produced an excellent fit with the literature data of Reimers et al. (1992). In addition, both model combinations also produced and excellent fit with the experimental and literature data.

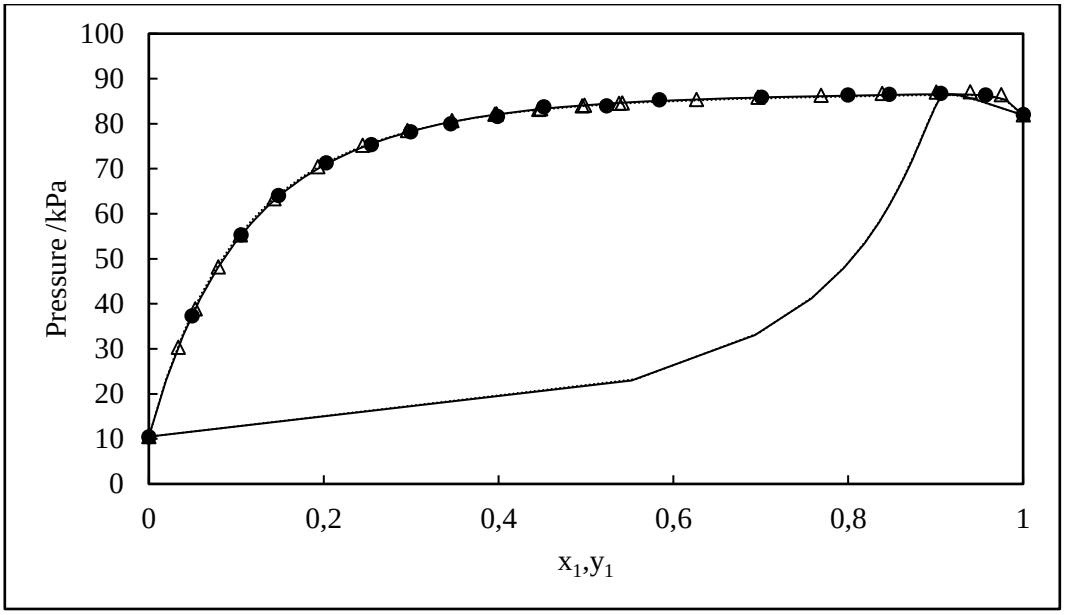

Figure 5-30: P-x plot for the n-pentane (1) + ethanol (2) system at 303.11 K. ●, P-x Experimental; —, Wilson + Ideal Gas model; ·····, Wilson + HOC model; Δ, Reimers et al. (1992).

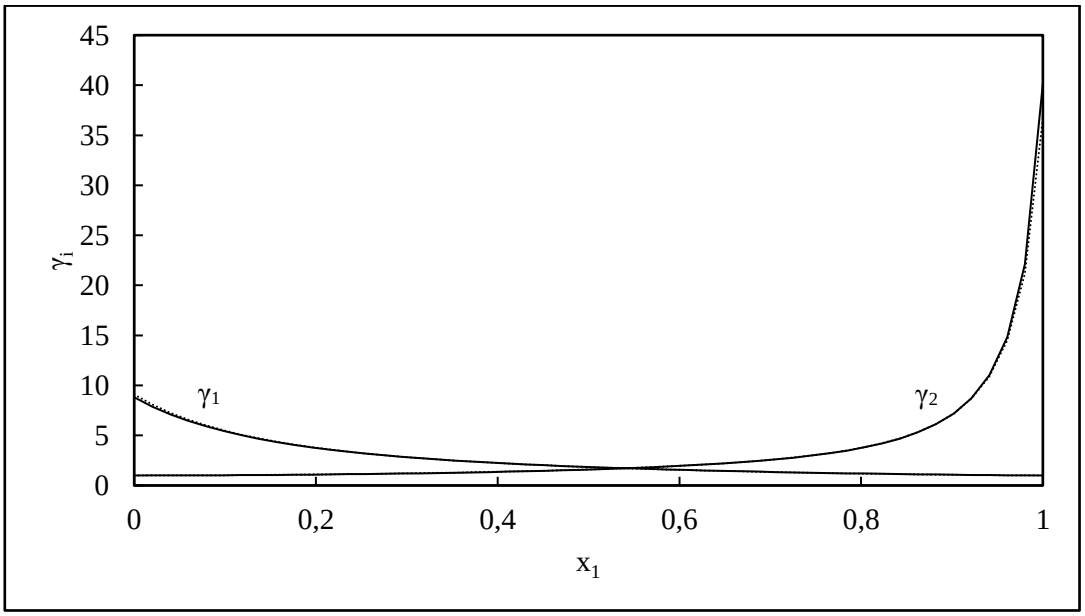

Figure 5-31: γ_i-x plot for the n-pentane (1) + ethanol (2) system at 303.11 K. —, Wilson + Ideal Gas model; ·····, Wilson + HOC model.

Table 5-13: Regressed data for the n-pentane (1) + ethanol (2) system at 303.11 K using the Wilson + Ideal Gas models.

Experimental			Wilson + Ideal Gas								
z_1	P/kPa	T/K	P_{calc}/kPa	T_{calc}/K	x_1	y_1	ΔP	ΔT	γ_1	γ_2	α
1.000	82.02	303.11	82.01	303.14	1.000	1.000	0.044	0.029	-	-	-
0.957	86.39	303.11	86.38	303.14	0.957	0.927	0.000	0.031	1.020	13.896	0.57
0.906	86.74	303.11	86.73	303.17	0.905	0.915	0.000	0.062	1.067	7.435	1.12
0.847	86.55	303.12	86.54	303.16	0.847	0.910	0.000	0.042	1.134	4.802	1.84
0.800	86.40	303.11	86.39	303.16	0.800	0.909	0.000	0.049	1.337	2.642	2.49
0.701	85.88	303.11	85.88	303.12	0.701	0.906	0.000	0.009	1.545	1.993	4.13
0.584	85.28	303.11	85.27	303.17	0.584	0.903	0.000	0.057	1.607	1.881	6.66
0.524	83.95	303.11	83.98	302.97	0.522	0.902	0.000	0.135	1.886	1.562	8.35
0.452	83.77	303.11	83.74	303.24	0.453	0.898	0.000	0.126	2.022	1.468	10.73
0.399	81.59	303.11	81.62	302.98	0.396	0.896	0.000	0.134	2.336	1.325	12.98
0.346	79.96	303.11	79.98	303.01	0.343	0.892	0.000	0.102	2.594	1.249	15.65
0.301	78.21	303.11	78.22	303.08	0.299	0.887	0.000	0.023	2.846	1.197	18.42
0.256	75.36	303.11	75.37	303.07	0.254	0.881	0.000	0.041	3.216	1.143	21.77
0.205	71.30	303.11	71.29	303.17	0.204	0.871	0.000	0.057	3.723	1.095	26.56
0.150	64.07	303.11	64.06	303.17	0.149	0.853	0.000	0.054	4.478	1.053	33.26
0.107	55.31	303.12	55.31	303.14	0.105	0.825	0.000	0.025	5.286	1.028	40.17
0.051	37.36	303.11	37.36	303.08	0.049	0.731	0.000	0.028	6.788	1.006	52.42
0.000	10.45	303.12	10.45	303.02	0.000	0.000	0.000	0.094	-	-	-

Table 5-14: Regressed data for the n-pentane (1) + ethanol (2) system at 303.11 K using the Wilson + HOC models.

Experimental			Wilson + HOC								
z_1	P/kPa	T/K	P_{calc}/kPa	T_{calc}/K	x_1	y_1	ΔP	ΔT	γ_1	γ_2	α
1.000	82.02	303.11	82.01	303.14	1.000	1.000	0.044	0.028	-	-	-
0.957	86.39	303.11	86.38	303.14	0.957	0.928	0.000	0.031	1.019	13.628	0.58
0.906	86.74	303.11	86.73	303.16	0.906	0.914	0.000	0.050	1.064	7.422	1.11
0.847	86.55	303.12	86.54	303.15	0.847	0.909	0.000	0.035	1.130	4.822	1.81
0.800	86.40	303.11	86.39	303.16	0.800	0.907	0.000	0.048	1.192	3.760	2.44
0.701	85.88	303.11	85.88	303.13	0.701	0.904	0.000	0.017	1.527	2.032	4.04
0.584	85.28	303.11	85.26	303.18	0.584	0.901	0.000	0.068	1.601	1.894	6.51
0.524	83.95	303.11	83.98	302.98	0.522	0.900	0.000	0.124	1.873	1.577	8.17
0.452	83.77	303.11	83.74	303.25	0.454	0.896	0.000	0.133	2.017	1.476	10.50
0.399	81.59	303.11	81.62	302.98	0.397	0.894	0.000	0.130	2.331	1.331	12.72
0.346	79.96	303.11	79.98	303.01	0.343	0.890	0.000	0.103	2.594	1.254	15.35
0.301	78.21	303.11	78.22	303.08	0.299	0.885	0.000	0.027	2.851	1.201	18.09
0.256	75.36	303.11	75.37	303.06	0.253	0.879	0.000	0.048	3.229	1.145	21.40
0.205	71.30	303.11	71.29	303.16	0.204	0.869	0.000	0.048	3.741	1.097	26.14
0.150	64.07	303.11	64.06	303.16	0.149	0.851	0.000	0.047	4.517	1.054	32.78
0.107	55.31	303.12	55.31	303.14	0.105	0.823	0.000	0.022	5.354	1.028	39.64
0.051	37.36	303.11	37.36	303.09	0.049	0.729	0.000	0.016	6.927	1.007	51.82
0.000	10.45	303.12	10.45	303.02	0.000	0.000	0.000	0.094	-	-	-

A slight positive deviation in Raoult's law yielded an azeotrope at approximately x = 0.92. For this test system both ΔT_{AVG} and ΔP_{AVG} are within the estimated uncertainties (refer to Table 5-4). Both equations also yielded similar activity coefficients with a slight deviation from ideality, as seen in Figure 5-31. The results from this test system indicated that the apparatus, the experimental technique and degassing procedure were functioning as desired and no further measurements of test systems were required.

Table 5-4, presents the model parameters as well as the temperature and pressure residuals for the test systems measured. It can be seen that the model combinations yielded similar results, in terms of the model parameters. For the n-hexane (1) + 2-butanol (2) system at 329.21 K, the parameters yielded differ slightly from those produced by Moodley (2012) and Uusi-Kyyny (2002). Although of similar magnitude, the parameters yielded by the literature sources were positive whilst the experimental parameters were negative. The same was observed for the system water (1) + 2-butanol (2) at 323.16 K with the literature data of Moodley (2012). In most cases it can be seen that the ΔP_{AVG} falls within the total combined uncertainty for pressure, whereas the ΔT_{AVG} is slightly out of range, except for the system n-pentane (1) + ethanol (2) at 303.11 K, which falls within the overall combined uncertainty for temperature of 0.06 K. In addition, by examining the tables of the regressed data for the test systems, it can be seen that the ΔP values for the individual pressures are quite small (usually between 3-4 decimal places), whilst the ΔT values are higher. This is caused due to the *"maximum likelihood"* objective function used in Aspen Plus®, where the estimated error in the experimental data is forced on to one variable (in this case temperature), whilst the residual of the second variable is kept to a minimum.

5.7.2 Phase equilibria and modelling results for new systems (fluorinated)

The fluorinated system measured in this project was n-hexane (1) + perfluoro-n-heptane (2) at 313.21 and 333.12 K. This system has not been previously measured at these particular isotherms and therefore contribute new data to the open literature. This system was modelled using the Wilson and NRTL activity coefficient models together with the Ideal Gas equation and the resulting parameters along with the temperature and pressure residuals are presented in Table 5-15. Figures 5-32 to 5-35 present the experimental data and models as well as the activity coefficient plots. The tables of regressed data are also presented (Tables 5-16 to 5-19) with a discussion thereof.

Table 5-15: Model parameters and pressure and temperature residuals for new systems (fluorinated).

Model and Model Parameters	A 313.21 K	B 333.12 K
Wilson – Ideal Gas		
$(\lambda_{12} - \lambda_{11})/K$	-357.12	-296.47
$(\lambda_{12} - \lambda_{22})/K$	-889.09	-780.06
$\Delta P_{AVG}/kPa$	0.03	0.06
$\Delta T_{AVG}/K$	0.24	0.23
NRTL – Ideal Gas		
$(g_{12} - g_{11})/K$	664.01	660.69
$(g_{12} - g_{22})/K$	237.94	187.22
α	0.3	0.3
$\Delta P_{AVG}/kPa$	0.02	0.04
$\Delta T_{AVG}/K$	0.22	0.15

A and B = n-heptane (1) + perfluoro-n-heptane (2).

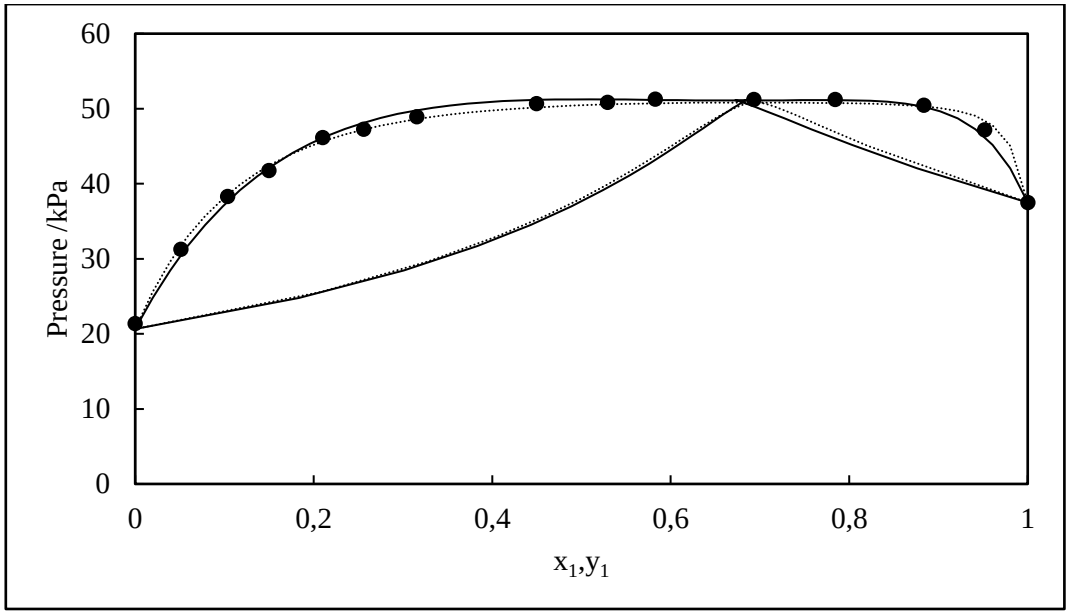

Figure 5-32: P-x plot for the n-heptane (1) + perfluoro-n-heptane (2) system at 313.21 K. ●, P-x Experimental; ——, NRTL + Ideal Gas model; ·····, Wilson + Ideal Gas model.

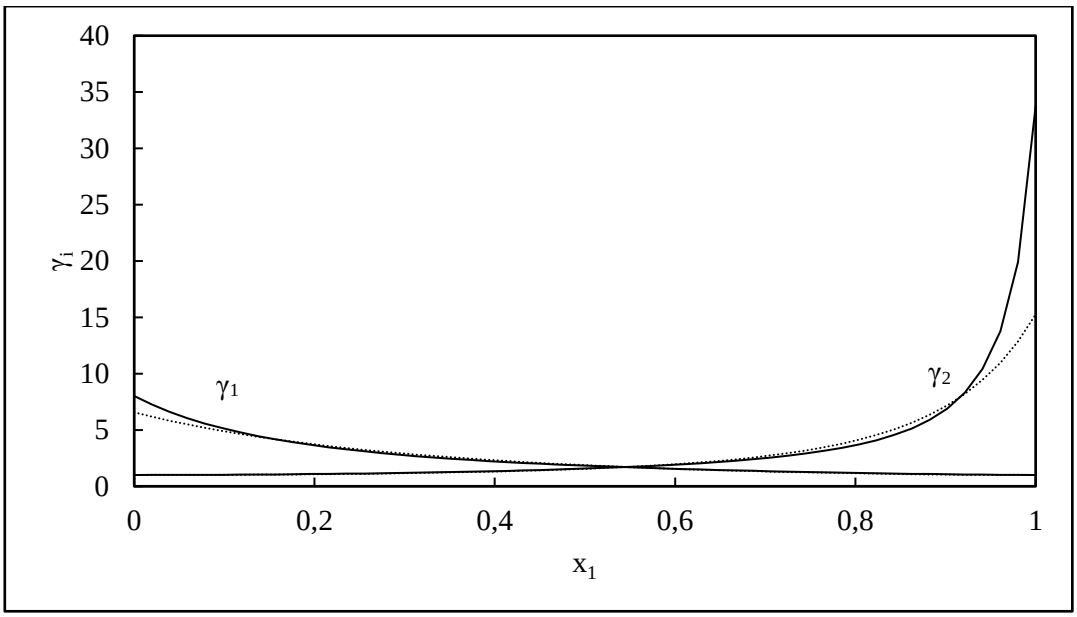

Figure 5-33: γ_i-x plot for the n-heptane (1) + perfluoro-n-heptane (2) system at 313.21 K. ——, Wilson + Ideal Gas model; ·····, NRTL + Ideal Gas model.

Table 5-16: Regressed data for the n-heptane (1) + perfluoro-n-heptane (2) system at 313.21 K using the Wilson + Ideal Gas models.

Experimental			Wilson + Ideal Gas								
z_1	P/kPa	T/K	P_{calc}/kPa	T_{calc}/K	x_1	y_1	ΔP*	ΔT†	γ_1	γ_2	α
1.000	37.48	313.21	37.48	313.18	1.000	1.000	0.000	0.029	-	-	-
0.951	47.17	313.21	47.25	312.56	0.952	0.754	0.001	0.641	1.012	15.239	0.15
0.883	50.48	313.21	50.47	313.28	0.883	0.715	0.000	0.075	1.086	5.949	0.33
0.784	51.21	313.20	51.18	313.41	0.784	0.702	0.000	0.210	1.211	3.396	0.65
0.693	51.24	313.21	51.22	313.40	0.693	0.695	0.000	0.191	1.358	2.445	1.01
0.583	51.27	313.21	51.24	313.46	0.583	0.687	0.000	0.249	1.594	1.842	1.57
0.529	50.83	313.21	50.82	313.32	0.530	0.682	0.000	0.114	1.738	1.653	1.91
0.450	50.68	313.21	50.65	313.43	0.451	0.673	0.000	0.226	2.002	1.443	2.52
0.316	48.92	313.21	48.90	313.34	0.317	0.649	0.000	0.133	2.662	1.209	4.00
0.257	47.28	313.21	47.28	313.23	0.256	0.630	0.000	0.020	3.094	1.139	4.94
0.211	46.14	313.21	46.11	313.43	0.212	0.609	0.000	0.220	3.524	1.095	5.87
0.151	41.77	313.21	41.80	312.94	0.147	0.563	0.000	0.267	4.399	1.044	7.33
0.104	38.33	313.21	38.34	313.11	0.103	0.507	0.000	0.095	5.084	1.024	8.91
0.052	31.28	313.21	31.30	312.97	0.050	0.376	0.000	0.240	6.338	1.006	11.19
0.000	21.36	313.20	21.32	313.93	0.000	0.000	0.000	0.730	-	-	-

Table 5-17: Regressed data for the n-heptane (1) + perfluoro-n-heptane (2) system at 313.21 K using the NRTL + Ideal Gas models.

Experimental			NRTL + Ideal Gas								
z_1	P/kPa	T/K	P_{calc}/kPa	T_{calc}/K	x_1	y_1	ΔP*	ΔT†	γ_1	γ_2	α
1.000	37.48	313.21	37.48	313.18	1.000	1.000	0.000	0.029	-	-	-
0.951	47.17	313.21	47.25	312.56	0.952	0.754	0.001	0.641	1.012	15.239	0.15
0.883	50.48	313.21	50.47	313.28	0.883	0.715	0.000	0.075	1.086	5.949	0.33
0.784	51.21	313.20	51.18	313.41	0.784	0.702	0.000	0.210	1.211	3.396	0.65
0.693	51.24	313.21	51.22	313.40	0.693	0.695	0.000	0.191	1.358	2.445	1.01
0.583	51.27	313.21	51.24	313.46	0.583	0.687	0.000	0.249	1.594	1.842	1.57
0.529	50.83	313.21	50.82	313.32	0.530	0.682	0.000	0.114	1.738	1.653	1.91
0.450	50.68	313.21	50.65	313.43	0.451	0.673	0.000	0.226	2.002	1.443	2.52
0.316	48.92	313.21	48.90	313.34	0.317	0.649	0.000	0.133	2.662	1.209	4.00
0.257	47.28	313.21	47.28	313.23	0.256	0.630	0.000	0.020	3.094	1.139	4.94
0.211	46.14	313.21	46.11	313.43	0.212	0.609	0.000	0.220	3.524	1.095	5.87
0.151	41.77	313.21	41.80	312.94	0.147	0.563	0.000	0.267	4.399	1.044	7.33
0.104	38.33	313.21	38.34	313.11	0.103	0.507	0.000	0.095	5.084	1.024	8.91
0.052	31.28	313.21	31.30	312.97	0.050	0.376	0.000	0.240	6.338	1.006	11.19
0.000	21.36	313.20	21.32	313.93	0.000	0.000	0.000	0.730	-	-	-

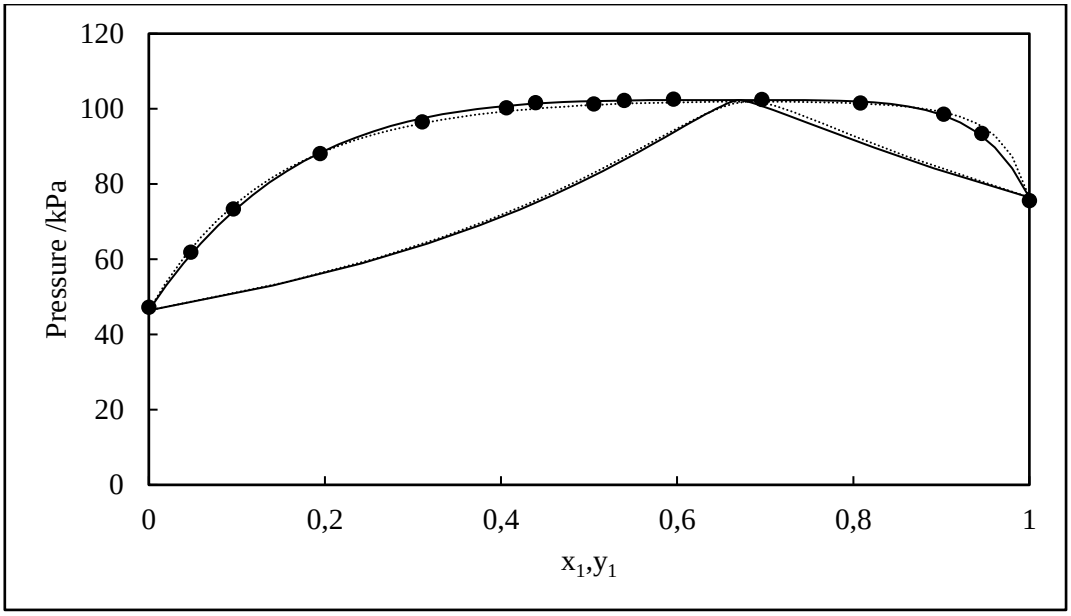

Figure 5-34: P-x plot for the n-heptane (1) + perfluoro-n-heptane (2) system at 333.12 K. ●, P-x Experimental; ——, NRTL + Ideal Gas model; ·····, Wilson + Ideal Gas model.

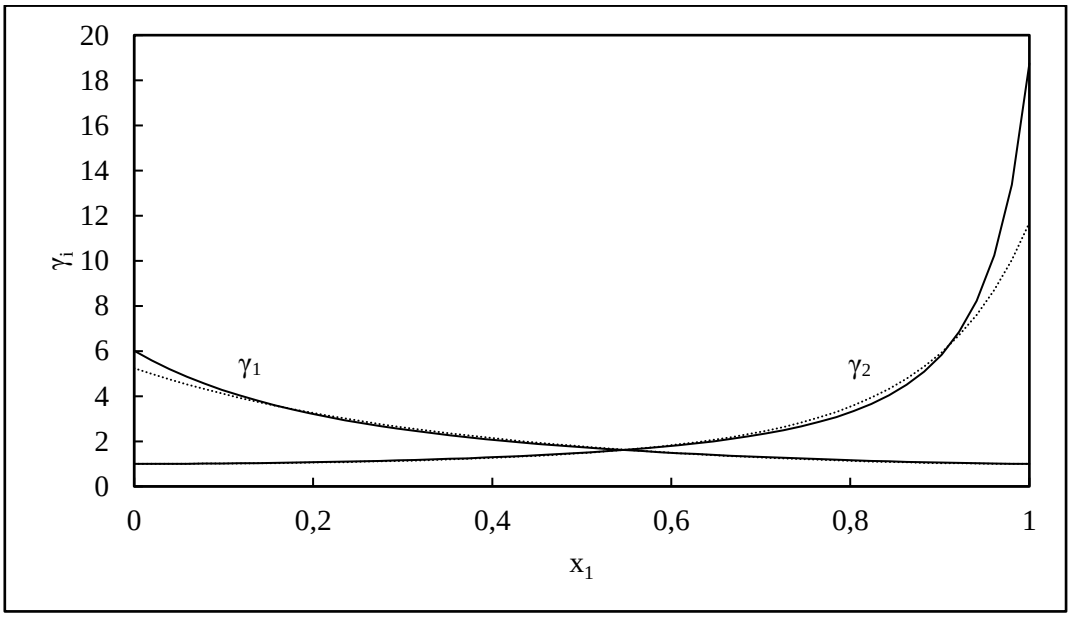

Figure 5-35: γ_i-x plot for the n-heptane (1) + perfluoro-n-heptane (2) system at 333.12 K. ——, Wilson + Ideal Gas model; ·····, NRTL + Ideal Gas model.

Table 5-18: Regressed data for the n-heptane (1) + perfluoro-n-heptane (2) system at 333.12 K using the Wilson + Ideal Gas models.

Experimental			Wilson + Ideal Gas								
z_1	P/kPa	T/K	P_{calc}/kPa	T_{calc}/K	x_1	y_1	ΔP*	ΔT†	γ_1	γ_2	α
1.000	75.56	333.12	75.63	332.80	1.000	1.000	0.001	0.325	-	-	-
0.944	93.52	333.12	93.67	332.60	0.947	0.774	0.001	0.519	1.013	9.865	0.19
0.901	98.56	333.11	98.60	332.97	0.903	0.733	0.000	0.142	1.044	6.346	0.30
0.807	101.58	333.12	101.57	333.17	0.808	0.701	0.000	0.048	1.151	3.407	0.56
0.696	102.51	333.11	102.46	333.28	0.696	0.684	0.001	0.164	1.311	2.281	0.95
0.596	102.60	333.12	102.53	333.35	0.597	0.672	0.001	0.231	1.501	1.779	1.39
0.540	102.26	333.12	102.19	333.36	0.541	0.664	0.001	0.238	1.631	1.594	1.68
0.506	101.27	333.12	101.25	333.18	0.506	0.659	0.000	0.066	1.722	1.502	1.89
0.439	101.63	333.12	101.51	333.52	0.443	0.647	0.001	0.405	1.927	1.358	2.34
0.407	100.28	333.12	100.21	333.35	0.409	0.640	0.001	0.235	2.046	1.300	2.60
0.312	96.58	333.12	96.55	333.22	0.312	0.611	0.000	0.103	2.476	1.169	3.49
0.197	88.14	333.13	88.15	333.10	0.194	0.548	0.000	0.025	3.260	1.066	5.02
0.098	73.34	333.13	73.39	332.91	0.094	0.423	0.000	0.224	4.370	1.015	6.90
0.049	61.89	333.13	61.94	332.84	0.047	0.290	0.001	0.294	5.106	1.004	8.17
0.000	47.27	333.13	47.21	333.57	0.000	0.000	0.001	0.445	-	-	-

Table 5-19: Regressed data for the n-heptane (1) + perfluoro-n-heptane (2) system at 333.12 K using the NRTL + Ideal Gas models.

Experimental			NRTL + Ideal Gas								
z_1	P/kPa	T/K	P_{calc}/kPa	T_{calc}/K	x_1	y_1	ΔP*	ΔT†	γ_1	γ_2	α
1.000	75.56	333.12	75.63	332.80	1.000	1.000	0.001	0.325	-	-	-
0.944	93.52	333.12	93.46	333.32	0.946	0.787	0.001	0.205	1.011	7.858	0.21
0.901	98.56	333.11	98.54	333.19	0.903	0.726	0.000	0.081	1.034	5.970	0.28
0.807	101.58	333.12	101.61	333.03	0.808	0.680	0.000	0.091	1.097	4.058	0.50
0.696	102.51	333.11	102.49	333.16	0.696	0.671	0.000	0.050	1.289	2.391	0.89
0.596	102.60	333.12	102.58	333.19	0.596	0.669	0.000	0.073	1.503	1.805	1.37
0.540	102.26	333.12	102.26	333.13	0.540	0.667	0.000	0.014	1.652	1.594	1.71
0.506	101.27	333.12	101.33	332.91	0.504	0.665	0.001	0.208	2.014	1.321	1.94
0.439	101.63	333.12	101.61	333.18	0.440	0.657	0.000	0.063	1.984	1.337	2.44
0.407	100.28	333.12	100.32	332.99	0.405	0.651	0.000	0.132	2.205	1.241	2.73
0.312	96.58	333.12	96.64	332.91	0.307	0.623	0.001	0.209	2.655	1.128	3.67
0.197	88.14	333.13	88.15	333.09	0.194	0.554	0.000	0.037	3.304	1.051	5.14
0.098	73.34	333.13	73.31	333.25	0.097	0.418	0.000	0.119	4.137	1.012	6.78
0.049	61.89	333.13	61.86	333.31	0.048	0.279	0.000	0.174	4.648	1.003	7.70
0.000	47.27	333.13	47.21	333.57	0.000	0.000	0.001	0.445	-	-	-

For the new fluorinated systems measured, i.e. n-heptane (1) + perfluoro-n-heptane (2) at 313.21 and 333.12 K, the perfluoro-n-heptane used consisted of a mixture of isomers and was purchased from Apollo Scientific. The NRTL and Wilson models, together with the ideal gas equations were utilised to model the data, as these models provided the best fit and are suitable for fluorinated compounds. For the NRTL model, the non-randomness parameter (α) was set to a value of 0.3 for both isotherms. According to Walas (1985), the activity coefficients are relatively insensitive to values of α_{12} between values of 0.1 and 0.5. Walas (1985) recommends a value of 0.3 for non-aqueous mixtures and 0.4 for aqueous mixtures.

For the isotherm n-heptane (1) + perfluoro-n-heptane (2) at 313.21 K, both models yield a good comparison to the experimental data, as seen in Figure 5-34. Between the 0.5 to 0.8 mole fraction range, both models yield a similar fit, however in the n-heptane rich region (0.9 – 1 mole fraction) and in the n-heptane dilute region (0 – 0.4 mole fraction) the models produce a slight deviation from one another, with the Wilson model demonstrating a superior fit. An azeotrope was observed at approximately x = 0.69 indicating poor separation between the n-heptane and perfluoro-n-heptane at these conditions. Figure 5-33 depicts the activity coefficient plot for each model. Both models produced a similar result, however the curves tend to deviate from one another in the dilute region for each component. The ΔP_{AVG} for both models are within the calculated uncertainty for pressure, whilst the ΔT_{AVG} was slightly above the temperature uncertainty (refer to Table 5-15).

For the isotherm n-heptane (1) + perfluoro-n-heptane (2) at 333.12 K, similar results to the 313.21 K isotherm were observed. Both models provided a suitable fit to the experimental data as seen in Figure 5-34, and again the Wilson model appears to produce a slightly better visual fit. An azeotrope can be observed at approximately x = 0.7, similar to the 313.21 K isotherm. The activity coefficient plots also produced similar behaviour. The models yielded similar results but deviate from one another toward the dilute region for each component. In terms of uncertainty, similar results to the 313.21 K isotherm was observed as seen in Table 5-15.

5.7.3 Phase equilibria and modelling results for new systems (alkane + alcohol)

As previously mentioned, the alkane + alcohol system measured in this project is n-pentane (1) + 2-propanol (2) at 313.11, 323.11 and 333.12 K. This system has not been measured previously as there is no existing phase equilibrium data available in the open literature in relation to this system. This system was modelled using the Wilson – Ideal Gas and Wilson – HOC model combinations, and the resulting parameters along with the temperature and pressure residuals are presented in Table 5-20. Figures 5-36 to 5-41 present the experimental data and models as well as the activity coefficient plots. The tables of regressed data are presented in Tables 5-21 to 5-26, with a discussion thereof.

Table 5-20: Model parameters and pressure and temperature residuals for new systems (alkane + alcohol).

Model and Model Parameters	A 313.11 K	B 323.11 K	C 333.12 K
Wilson – Ideal Gas			
$(\lambda_{12} - \lambda_{11})/K$	-242.36	-235.68	-228.63
$(\lambda_{12} - \lambda_{22})/K$	-700.10	-685.37	-661.25
$\Delta P_{AVG}/kPa$	0.04	0.05	0.08
$\Delta T_{AVG}/K$	0.13	0.13	0.15
Wilson – HOC			
$(\lambda_{12} - \lambda_{11})/K$	-256.48	-254.24	-228.63
$(\lambda_{12} - \lambda_{22})/K$	-682.53	-658.75	-661.25
$\Delta P_{AVG}/kPa$	0.04	0.05	0.08
$\Delta T_{AVG}/K$	0.13	0.12	0.15

A, B and C = n-pentane (1) + 2-propanol (2).

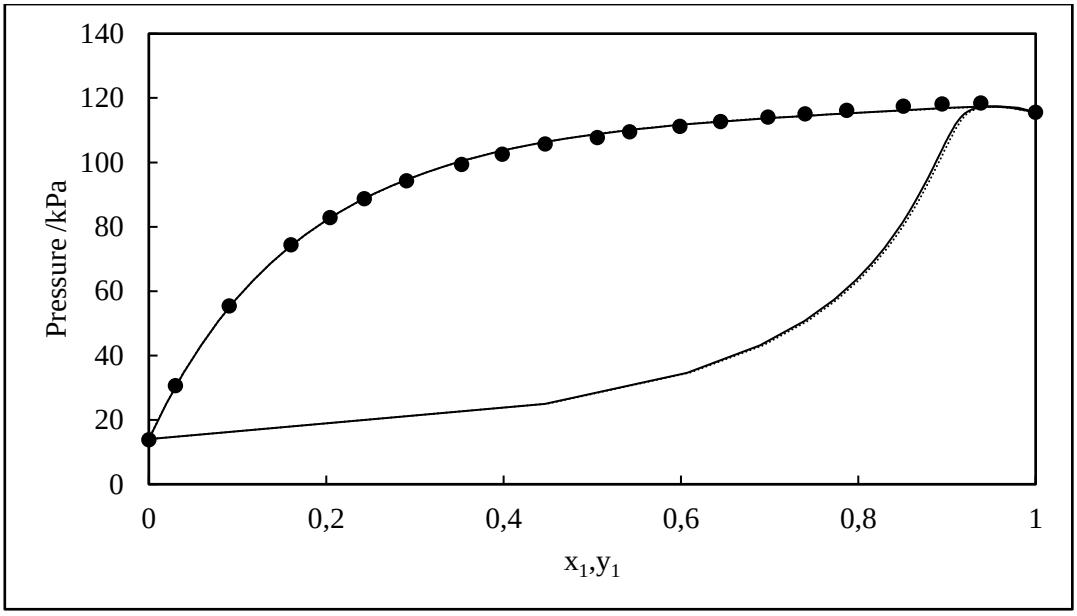

Figure 5-36: P-x plot for the n-pentane (1) + 2-propanol (2) system at 313.11 K. ●, P-x Experimental; ——, Wilson + HOC model; ·····, Wilson + Ideal Gas model.

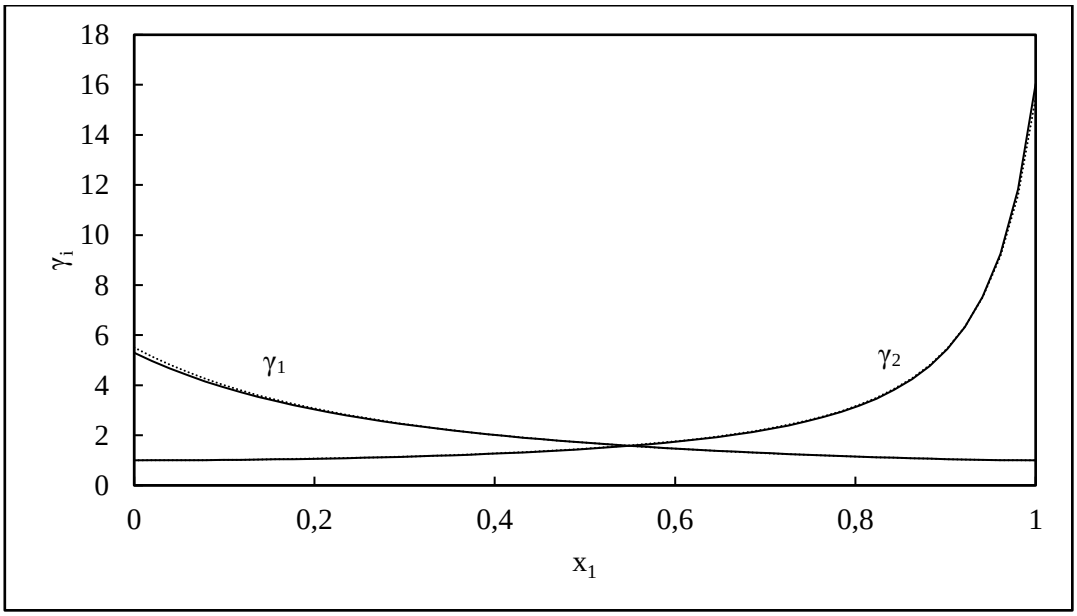

Figure 5-37: γ_i-x plot for the n-pentane (1) + 2-propanol (2) system at 313.11 K. ——, Wilson + Ideal Gas model; ·····, Wilson + HOC model.

Table 5-21: Regressed data for the n-pentane (1) + 2-propanol (2) system at 313.11 K using the Wilson + Ideal Gas models.

Experimental			Wilson + Ideal Gas								
z_1	P/kPa	T/K	P_{calc}/kPa	T_{calc}/K	x_1	y_1	ΔP	ΔT	γ_1	γ_2	α
1.000	115.57	313.12	115.57	313.11	1.000	1.000	0.000	0.007	-	-	-
0.938	118.46	313.11	118.36	313.39	0.938	0.946	0.001	0.275	1.023	7.335	1.14
0.895	118.15	313.11	118.04	313.43	0.895	0.934	0.001	0.317	1.056	5.165	1.68
0.851	117.47	313.11	117.36	313.42	0.851	0.928	0.001	0.306	1.097	3.967	2.27
0.788	116.16	313.11	116.08	313.34	0.787	0.923	0.001	0.224	1.169	2.963	3.24
0.741	115.08	313.11	115.03	313.25	0.740	0.920	0.000	0.141	1.232	2.503	4.05
0.699	114.06	313.11	114.04	313.18	0.699	0.918	0.000	0.066	1.294	2.206	4.83
0.645	112.66	313.11	112.67	313.09	0.644	0.915	0.000	0.021	1.392	1.902	5.95
0.599	111.19	313.11	111.23	313.00	0.596	0.913	0.000	0.110	1.514	1.667	7.00
0.543	109.54	313.11	109.58	312.99	0.539	0.909	0.000	0.119	1.640	1.511	8.47
0.507	107.76	313.11	107.83	312.89	0.500	0.907	0.001	0.219	1.763	1.405	9.51
0.447	105.73	313.11	105.76	313.00	0.444	0.902	0.000	0.114	1.893	1.323	11.39
0.400	102.55	313.11	102.61	312.92	0.393	0.897	0.001	0.190	2.078	1.240	13.13
0.355	99.38	313.11	99.43	312.94	0.348	0.891	0.000	0.169	2.247	1.187	15.02
0.293	94.29	313.11	94.30	313.06	0.289	0.881	0.000	0.050	2.497	1.131	18.01
0.246	88.67	313.12	88.67	313.11	0.243	0.869	0.000	0.007	2.749	1.092	20.72
0.208	82.87	313.11	82.87	313.13	0.205	0.857	0.000	0.016	2.998	1.065	23.22
0.164	74.42	313.11	74.41	313.15	0.161	0.835	0.000	0.046	3.335	1.040	26.51
0.094	55.42	313.11	55.41	313.17	0.092	0.766	0.000	0.065	4.014	1.013	32.87
0.031	30.59	313.11	30.58	313.21	0.030	0.552	0.000	0.096	4.808	1.001	39.86
0.000	13.83	313.11	13.84	312.88	0.000	0.000	0.000	0.239	-	-	-

Table 5-22: Regressed data for the n-pentane (1) + 2-propanol (2) system at 313.11 K using the Wilson + HOC models.

Experimental			Wilson + HOC								
z_1	P/kPa	T/K	P_{calc}/kPa	T_{calc}/K	x_1	y_1	ΔP	ΔT	γ_1	γ_2	α
1.000	115.57	313.12	115.57	313.11	1.000	1.000	0.000	0.007	-	-	-
0.938	118.46	313.11	118.37	313.36	0.938	0.945	0.001	0.248	1.022	7.315	1.12
0.895	118.15	313.11	118.05	313.41	0.895	0.932	0.001	0.292	1.054	5.193	1.62
0.851	117.47	313.11	117.37	313.40	0.851	0.926	0.001	0.289	1.094	4.004	2.18
0.788	116.16	313.11	116.08	313.33	0.787	0.920	0.001	0.221	1.166	2.998	3.11
0.741	115.08	313.11	115.03	313.26	0.740	0.917	0.001	0.146	1.229	2.533	3.88
0.699	114.06	313.11	114.03	313.19	0.699	0.915	0.000	0.077	1.291	2.232	4.63
0.645	112.66	313.11	112.66	313.11	0.645	0.912	0.000	0.006	1.383	1.938	5.70
0.599	111.19	313.11	111.22	313.02	0.597	0.909	0.000	0.094	1.506	1.694	6.72
0.543	109.54	313.11	109.57	313.01	0.540	0.906	0.000	0.105	1.633	1.531	8.13
0.507	107.76	313.11	107.82	312.90	0.500	0.903	0.001	0.208	1.759	1.419	9.14
0.447	105.73	313.11	105.76	313.01	0.444	0.899	0.000	0.107	1.893	1.335	10.97
0.400	102.55	313.11	102.61	312.92	0.393	0.894	0.001	0.189	2.083	1.249	12.68
0.355	99.38	313.11	99.43	312.94	0.348	0.888	0.000	0.170	2.258	1.193	14.52
0.293	94.29	313.11	94.31	313.05	0.289	0.877	0.000	0.057	2.516	1.136	17.46
0.246	88.67	313.12	88.67	313.10	0.242	0.866	0.000	0.014	2.778	1.096	20.12
0.208	82.87	313.11	82.87	313.12	0.205	0.853	0.000	0.009	3.036	1.068	22.60
0.164	74.42	313.11	74.41	313.15	0.161	0.832	0.000	0.041	3.390	1.042	25.87
0.094	55.42	313.11	55.41	313.17	0.092	0.763	0.000	0.062	4.112	1.014	32.24
0.031	30.59	313.11	30.58	313.22	0.030	0.549	0.000	0.104	4.971	1.002	39.29
0.000	13.83	313.11	13.84	312.87	0.000	0.000	0.000	0.240	-	-	-

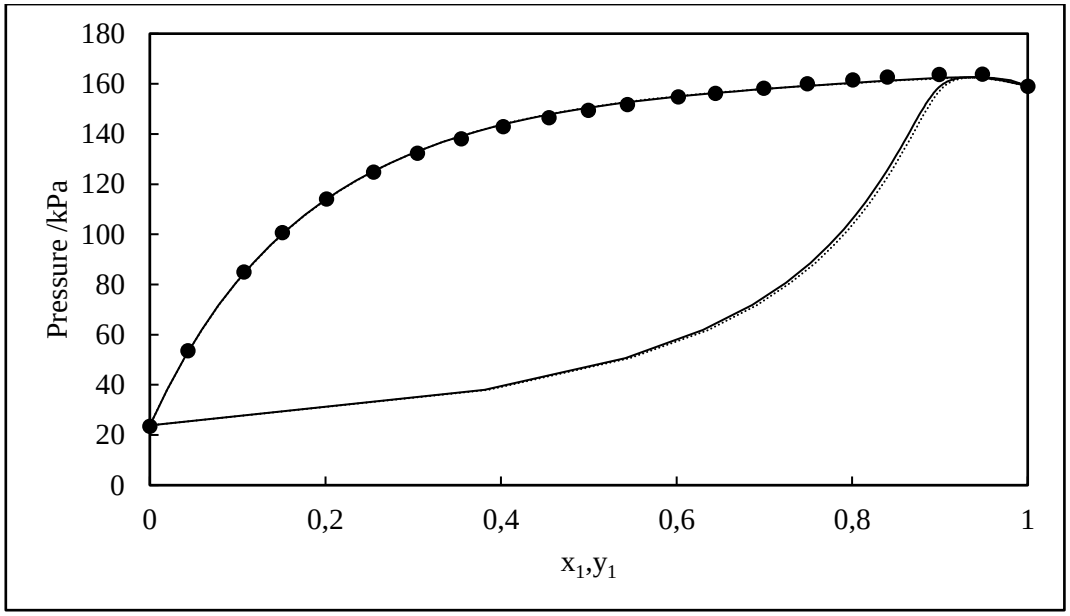

Figure 5-38: P-x plot for the n-pentane (1) + 2-propanol (2) system at 323.11 K.

●, P-x Experimental; ──, Wilson + HOC model; ·····, Wilson + Ideal Gas model.

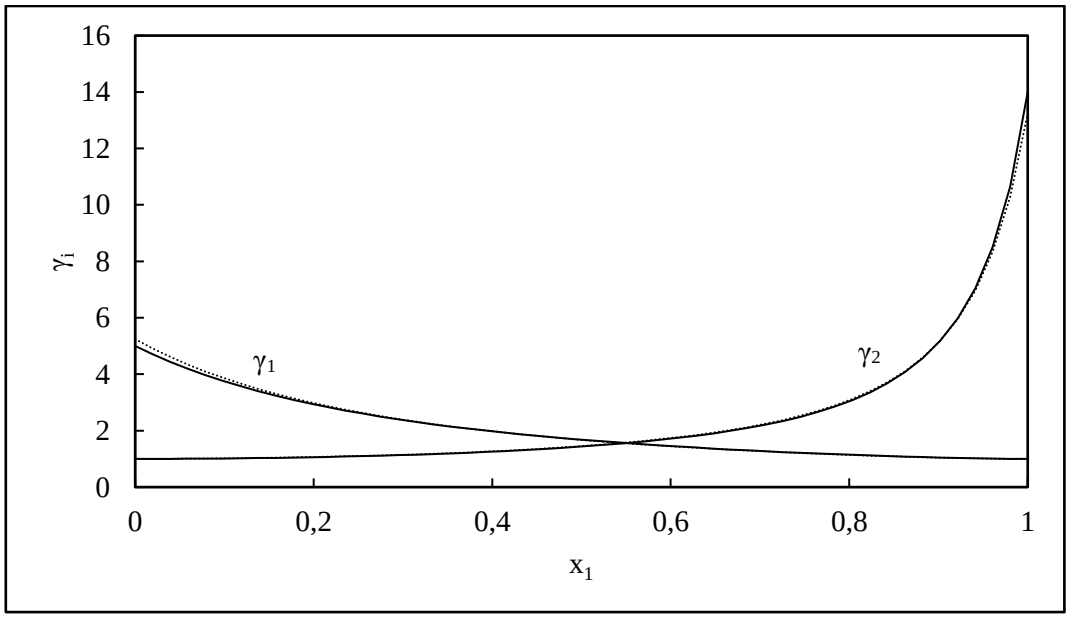

Figure 5-39: γ_i-x plot for the n-pentane (1) + 2-propanol (2) system at 323.11 K

──, Wilson + Ideal Gas model; ·····, Wilson + HOC model.

Table 5-23: Regressed data for the n-pentane (1) + 2-propanol (2) system at 323.11 K using the Wilson + Ideal Gas models.

Experimental			Wilson + Ideal Gas								
z_1	P/kPa	T/K	P_{calc}/kPa	T_{calc}/K	x_1	y_1	ΔP	ΔT	γ_1	γ_2	α
1.000	158.94	323.10	158.95	323.08	1.000	1.000	0.000	0.012	-	-	-
0.948	163.80	323.10	163.67	323.35	0.948	0.943	0.001	0.247	1.015	7.516	0.90
0.899	163.68	323.11	163.54	323.38	0.899	0.924	0.001	0.275	1.048	5.090	1.37
0.840	162.73	323.11	162.58	323.40	0.840	0.914	0.001	0.294	1.102	3.629	2.02
0.801	161.60	323.10	161.48	323.34	0.801	0.909	0.001	0.244	1.145	3.049	2.50
0.750	160.02	323.11	159.94	323.26	0.749	0.905	0.001	0.154	1.209	2.521	3.19
0.700	158.29	323.10	158.26	323.16	0.699	0.902	0.000	0.062	1.281	2.169	3.94
0.645	156.25	323.11	156.27	323.07	0.644	0.898	0.000	0.034	1.383	1.856	4.86
0.602	154.75	323.11	154.78	323.05	0.601	0.895	0.000	0.059	1.468	1.688	5.63
0.545	151.78	323.11	151.85	322.96	0.540	0.890	0.001	0.149	1.622	1.488	6.80
0.501	149.38	323.11	149.46	322.94	0.495	0.886	0.001	0.174	1.735	1.391	7.81
0.456	146.52	323.11	146.60	322.93	0.449	0.882	0.001	0.178	1.859	1.312	8.93
0.403	142.92	323.11	142.97	322.99	0.399	0.875	0.001	0.121	2.003	1.245	10.40
0.357	138.08	323.11	138.14	322.97	0.350	0.867	0.001	0.132	2.182	1.184	11.92
0.308	132.28	323.11	132.31	323.03	0.302	0.858	0.000	0.080	2.379	1.137	13.73
0.258	124.75	323.11	124.76	323.08	0.254	0.844	0.000	0.032	2.615	1.096	15.83
0.205	114.06	323.11	114.05	323.13	0.202	0.823	0.000	0.018	2.928	1.061	18.45
0.155	100.66	323.11	100.64	323.17	0.152	0.792	0.000	0.069	3.296	1.034	21.41
0.111	84.99	323.11	84.97	323.18	0.108	0.745	0.000	0.073	3.682	1.017	24.35
0.046	53.53	323.11	53.52	323.19	0.044	0.571	0.000	0.083	4.388	1.003	29.43
0.000	23.40	323.11	23.42	322.77	0.000	0.000	0.000	0.333	-	-	-

Table 5-24: Regressed data for the n-pentane (1) + 2-propanol (2) system at 323.11 K using the Wilson + HOC models.

Experimental			Wilson + HOC								
z_1	P/kPa	T/K	P_{calc}/kPa	T_{calc}/K	x_1	y_1	ΔP	ΔT	γ_1	γ_2	α
1.000	158.94	323.10	158.95	323.08	1.000	1.000	0.000	0.012	-	-	-
0.948	163.80	323.10	163.69	323.32	0.948	0.942	0.001	0.215	1.014	7.409	0.89
0.899	163.68	323.11	163.56	323.34	0.899	0.922	0.001	0.236	1.046	5.097	1.32
0.840	162.73	323.11	162.60	323.37	0.840	0.910	0.001	0.268	1.098	3.665	1.93
0.801	161.60	323.10	161.49	323.33	0.801	0.905	0.001	0.228	1.140	3.087	2.38
0.750	160.02	323.11	159.95	323.26	0.749	0.901	0.001	0.153	1.204	2.557	3.03
0.700	158.29	323.10	158.25	323.18	0.699	0.897	0.000	0.074	1.275	2.200	3.74
0.645	156.25	323.11	156.26	323.09	0.644	0.893	0.000	0.015	1.371	1.899	4.61
0.602	154.75	323.11	154.77	323.07	0.602	0.890	0.000	0.037	1.455	1.723	5.34
0.545	151.78	323.11	151.84	322.98	0.540	0.885	0.001	0.128	1.611	1.513	6.46
0.501	149.38	323.11	149.45	322.95	0.495	0.881	0.001	0.157	1.727	1.410	7.43
0.456	146.52	323.11	146.60	322.94	0.450	0.876	0.001	0.165	1.855	1.327	8.52
0.403	142.92	323.11	142.97	322.99	0.399	0.870	0.001	0.115	2.005	1.256	9.94
0.357	138.08	323.11	138.14	322.98	0.350	0.862	0.001	0.130	2.190	1.193	11.41
0.308	132.28	323.11	132.32	323.02	0.302	0.852	0.000	0.083	2.396	1.143	13.18
0.258	124.75	323.11	124.77	323.07	0.253	0.839	0.000	0.040	2.644	1.101	15.24
0.205	114.06	323.11	114.06	323.12	0.201	0.818	0.000	0.009	2.972	1.064	17.84
0.155	100.66	323.11	100.64	323.17	0.152	0.786	0.000	0.061	3.365	1.036	20.76
0.111	84.99	323.11	84.97	323.18	0.108	0.739	0.000	0.069	3.781	1.018	23.70
0.046	53.53	323.11	53.52	323.19	0.044	0.566	0.000	0.084	4.556	1.003	28.83
0.000	23.40	323.11	23.42	322.77	0.000	0.000	0.000	0.333	-	-	-

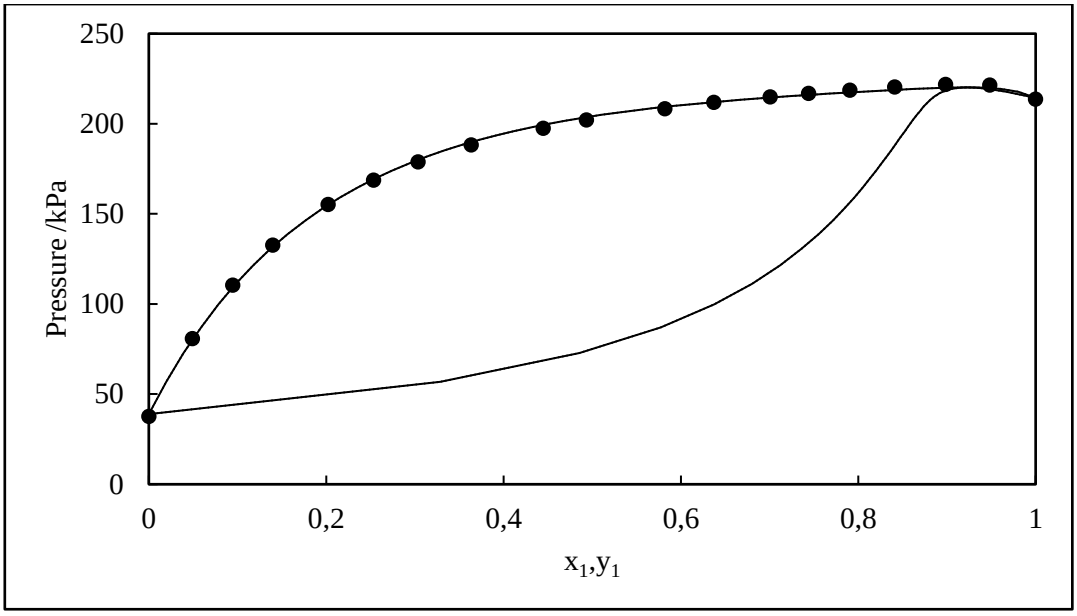

Figure 5-40: P-x plot for the n-pentane (1) + 2-propanol (2) system at 333.12 K. ●, P-x Experimental; ──, Wilson + HOC model; ·····, Wilson + Ideal Gas model.

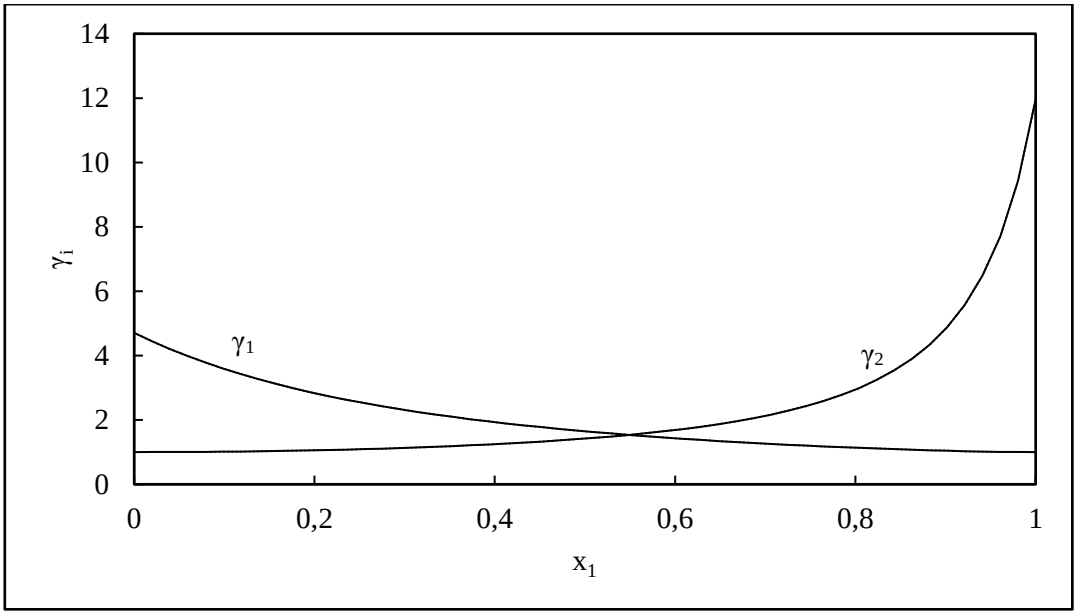

Figure 5-41: γ_i-x plot for the n-pentane (1) + 2-propanol (2) system at 333.12 K. ──, Wilson + Ideal Gas model; ·····, Wilson + HOC model.

Table 5-25: Regressed data for the n-pentane (1) + 2-propanol (2) system at 333.12 K using the Wilson + Ideal Gas models.

Experimental			Wilson + Ideal Gas								
z_1	P/kPa	T/K	P_{calc}/kPa	T_{calc}/K	x_1	y_1	ΔP	ΔT	γ_1	γ_2	α
1.000	213.70	333.12	213.76	333.03	1.000	1.000	0.001	0.088	-	-	-
0.948	221.51	333.12	221.34	333.35	0.948	0.937	0.002	0.222	1.014	6.894	0.81
0.899	221.77	333.12	221.59	333.36	0.899	0.914	0.002	0.240	1.044	4.780	1.20
0.842	220.40	333.12	220.24	333.34	0.841	0.901	0.002	0.219	1.094	3.505	1.71
0.791	218.72	333.13	218.60	333.30	0.791	0.893	0.001	0.170	1.147	2.838	2.22
0.745	216.92	333.13	216.84	333.25	0.745	0.888	0.001	0.120	1.203	2.419	2.74
0.702	214.97	333.12	214.93	333.18	0.701	0.884	0.000	0.057	1.264	2.131	3.27
0.638	211.96	333.13	211.97	333.11	0.637	0.879	0.000	0.019	1.365	1.822	4.12
0.582	208.36	333.12	208.44	333.00	0.578	0.873	0.001	0.123	1.502	1.578	4.96
0.494	202.12	333.13	202.24	332.95	0.488	0.864	0.001	0.171	1.711	1.370	6.50
0.447	197.43	333.12	197.56	332.92	0.438	0.857	0.001	0.208	1.851	1.284	7.49
0.367	188.19	333.12	188.28	332.97	0.359	0.843	0.001	0.158	2.098	1.186	9.40
0.308	178.87	333.12	178.93	333.02	0.301	0.829	0.001	0.097	2.320	1.130	11.09
0.258	168.74	333.13	168.76	333.09	0.252	0.812	0.000	0.038	2.542	1.091	12.74
0.207	155.21	333.12	155.20	333.13	0.203	0.788	0.000	0.013	2.820	1.058	14.69
0.145	132.65	333.12	132.62	333.18	0.141	0.740	0.000	0.062	3.249	1.028	17.52
0.099	110.46	333.12	110.43	333.21	0.096	0.676	0.000	0.086	3.630	1.013	19.93
0.052	80.79	333.12	80.78	333.18	0.050	0.539	0.000	0.058	4.092	1.004	22.61
0.000	37.73	333.13	37.78	332.50	0.000	0.000	0.001	0.623	-	-	-

Table 5-26: Regressed data for the n-pentane (1) + 2-propanol (2) system at 333.12 K using the Wilson + HOC models.

Experimental			Wilson + HOC								
z_1	P/kPa	T/K	P_{calc}/kPa	T_{calc}/K	x_1	y_1	ΔP	ΔT	γ_1	γ_2	α
1.000	213.70	333.12	213.76	333.03	1.000	1.000	0.001	0.088	-	-	-
0.948	221.51	333.12	221.34	333.35	0.948	0.937	0.002	0.222	1.014	6.894	0.80
0.899	221.77	333.12	221.59	333.36	0.899	0.914	0.002	0.240	1.044	4.780	1.16
0.842	220.40	333.12	220.24	333.34	0.841	0.901	0.002	0.219	1.094	3.505	1.63
0.791	218.72	333.13	218.60	333.30	0.791	0.893	0.001	0.170	1.147	2.838	2.10
0.745	216.92	333.13	216.84	333.25	0.745	0.888	0.001	0.120	1.203	2.419	2.57
0.702	214.97	333.12	214.93	333.18	0.701	0.884	0.000	0.057	1.264	2.131	3.06
0.638	211.96	333.13	211.97	333.11	0.637	0.879	0.000	0.019	1.365	1.822	3.86
0.582	208.36	333.12	208.44	333.00	0.578	0.873	0.001	0.123	1.502	1.578	4.65
0.494	202.12	333.13	202.24	332.95	0.488	0.864	0.001	0.171	1.711	1.370	6.11
0.447	197.43	333.12	197.56	332.92	0.438	0.857	0.001	0.208	1.851	1.284	7.06
0.367	188.19	333.12	188.28	332.97	0.359	0.843	0.001	0.158	2.098	1.186	8.90
0.308	178.87	333.12	178.93	333.02	0.301	0.829	0.001	0.097	2.320	1.130	10.54
0.258	168.74	333.13	168.76	333.09	0.252	0.812	0.000	0.038	2.542	1.091	12.15
0.207	155.21	333.12	155.20	333.13	0.203	0.788	0.000	0.013	2.820	1.058	14.07
0.145	132.65	333.12	132.62	333.18	0.141	0.740	0.000	0.062	3.249	1.028	16.87
0.099	110.46	333.12	110.43	333.21	0.096	0.676	0.000	0.086	3.630	1.013	19.29
0.052	80.79	333.12	80.78	333.18	0.050	0.539	0.000	0.058	4.092	1.004	21.99
0.000	37.73	333.13	37.78	332.50	0.000	0.000	0.001	0.623	-	-	-

For the new alkane + alcohol systems measured i.e. n-pentane (1) + 2-propanol (2) at 313.11 K, 323.11 K and 333.21 K, the Wilson – Ideal Gas and Wilson – HOC combinations were employed. As mentioned earlier the Wilson model was chosen as it provides a superior fit to the alcohol + hydrocarbon mixtures compared to algebraic expressions (Palmer, 1987). Similar results were observed for all three isotherms measured. Both model combinations yielded similar results for each isotherm and provided a good fit to the experimental data as seen in Figures 5-36, 5-38 and 5-40. Azeotropes were observed at x = 0.95 for all three isotherms, indicating poor separation between n-pentane + 2-propanol in this region due to both components having a similar boiling point at these conditions. In terms of activity coefficients, the models produced a similar result and did not deviate from one another, as depicted in Figures 5-37, 5-39 and 5-41. In the equimolar region, the activity coefficients were close to 1, indicating ideality at these mole fractions. However, in the concentrated region of each component, γ values ranged from 4.5 to 15 indicating a divergence from ideality. The ΔP_{AVG} and ΔT_{AVG} values for each isotherm were similar, as displayed in Table 5-20. All three isotherms behaved similarly whereby azeotropic behaviour was observed between the region of x = 0.92 to x = 1, in all three cases. The ΔP_{AVG} values were found to be well within the pressure uncertainty of 0.36 kPa, whilst the ΔT_{AVG} was slightly above the temperature uncertainty of 0.06 K.

5.7.4 Sensitivity analyses

In order to determine exactly how much of an impact an error in certain factors will have on the experimental data, sensitivity analyses were conducted using the test system n-pentane (1) + 2-butanol (2) at 303.17 K. An error was induced on the following factors:

- Disregarding the volume calibration
- Inducing a 5% error on the y value
- Inducing a 10 ml error on the total cell working volume

The system was modelled using the Wilson activity coefficient model in all three cases and the resulting parameters along with the temperature and pressure residuals are presented in Table 5-27. Figures 5-42 to 5-47 present the experimental data compared to the error-induced experimental results as well as the literature data and model. The activity coefficient plots are also displayed in these figures. Table 5-31 presents the residuals calculated between the liquid mole fraction and overall composition for the sensitivity analyses, and a discussion is presented thereof.

Table 5-27: Model parameters and pressure and temperature residuals for error analyses using the system n-pentane (1) + 2-butanol (2) at 303.17 K.

Model and Model Parameters	A 303.17 K	B 303.17 K	C 303.17 K	D 303.17 K
Wilson – Ideal Gas				
$(\lambda_{12} - \lambda_{11})/K$	-174.14	-174.63	-174.14	-175.70
$(\lambda_{12} - \lambda_{22})/K$	-646.67	-646.54	-646.67	-645.22
$\Delta P_{AVG}/kPa$	0.03	0.03	0.03	0.03
$\Delta T_{AVG}/K$	0.23	0.23	0.23	0.23

A = original experimental data, B = disregarding volume calibration, C = 5 % error on y value, D = 10 ml error on cell volume.

Disregarding the volume calibration

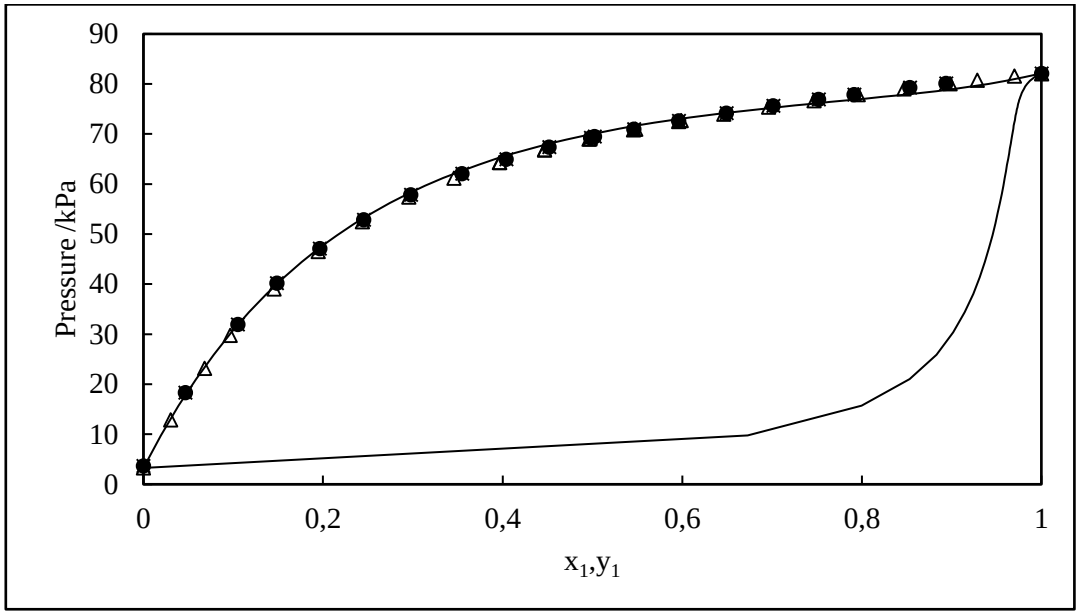

Figure 5-42: P-x plot for the n-pentane (1) + 2-butanol (2) system at 303.17 K. ●, P-x Experimental (correct); *, P-x Experimental (error); —, Wilson + Ideal Gas model; Δ, Thomas et al. (1991).

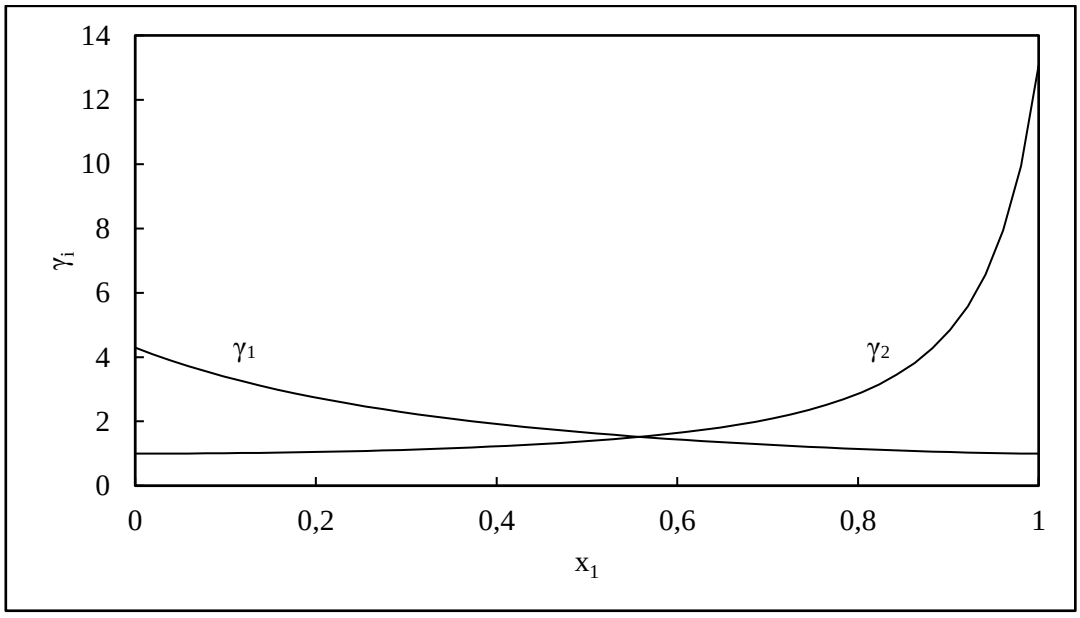

Figure 5-43: γ_i-x plot for the n-pentane (1) + 2-butanol (2) system at 303.17 K (error). —, Wilson + Ideal Gas model.

Table 5-28: Regressed data for the n-pentane (1) + 2-butanol (2) system at 303.17 K using the Wilson + Ideal Gas models (error induced).

Experimental			Wilson + Ideal Gas								
z_1	P/kPa	T/K	P_{calc}/kPa	T_{calc}/K	x_1	y_1	ΔP*	ΔT†	γ_1	γ_2	α
1.000	82.15	303.17	82.15	303.18	1.000	1.000	0.000	0.010	-	-	-
0.894	80.15	303.17	80.05	303.60	0.894	0.980	0.001	0.430	1.052	4.583	5.72
0.854	79.31	303.17	79.21	303.61	0.854	0.977	0.001	0.432	1.088	3.634	7.45
0.792	77.89	303.17	77.82	303.51	0.792	0.975	0.001	0.336	1.154	2.764	10.41
0.753	76.91	303.17	76.86	303.41	0.753	0.974	0.001	0.241	1.202	2.403	12.52
0.702	75.66	303.17	75.63	303.30	0.702	0.973	0.000	0.129	1.272	2.068	15.43
0.650	74.22	303.17	74.22	303.17	0.649	0.972	0.000	0.002	1.354	1.818	18.73
0.597	72.63	303.17	72.65	303.08	0.592	0.971	0.000	0.093	1.472	1.588	22.38
0.547	71.01	303.17	71.04	303.03	0.541	0.969	0.000	0.148	1.585	1.448	26.10
0.503	69.54	303.16	69.57	303.03	0.497	0.968	0.000	0.132	1.681	1.363	29.69
0.499	69.25	303.17	69.28	303.00	0.491	0.968	0.000	0.171	1.699	1.349	30.06
0.452	67.39	303.17	67.42	303.02	0.446	0.966	0.000	0.152	1.811	1.278	34.19
0.405	65.01	303.16	65.04	303.02	0.398	0.963	0.000	0.140	1.945	1.215	38.89
0.356	62.11	303.16	62.13	303.05	0.350	0.960	0.000	0.110	2.097	1.163	44.25
0.299	57.86	303.16	57.87	303.08	0.295	0.956	0.000	0.079	2.303	1.112	51.20
0.247	52.87	303.16	52.88	303.11	0.243	0.950	0.000	0.056	2.527	1.076	58.43
0.198	47.10	303.16	47.10	303.14	0.196	0.942	0.000	0.020	2.767	1.048	66.16
0.150	40.24	303.16	40.23	303.21	0.150	0.929	0.000	0.045	3.046	1.028	74.96
0.107	31.93	303.16	31.93	303.18	0.105	0.907	0.000	0.023	3.346	1.014	83.33
0.048	18.35	303.16	18.34	303.35	0.048	0.828	0.000	0.191	3.830	1.003	98.69
0.000	3.71	303.16	3.70	305.11	0.000	0.000	0.000	1.946	-	-	-

Inducing a 5 % error in the y value

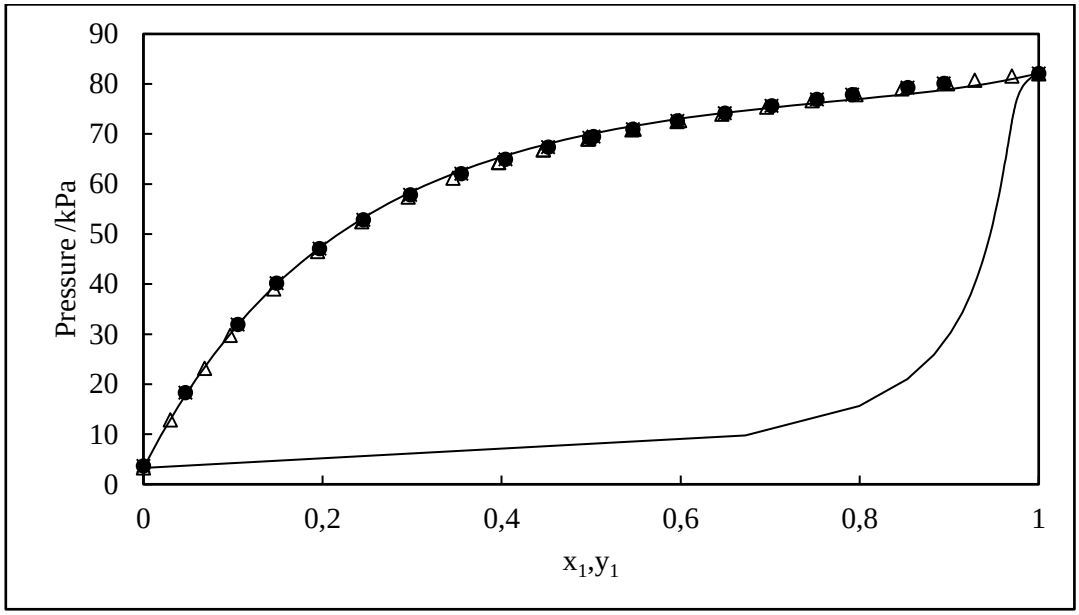

Figure 5-44: P-x plot for the n-pentane (1) + 2-butanol (2) system at 303.17 K. ●, P-x Experimental (correct); *, P-x Experimental (error); —, Wilson + Ideal Gas model; Δ, Thomas et al. (1991).

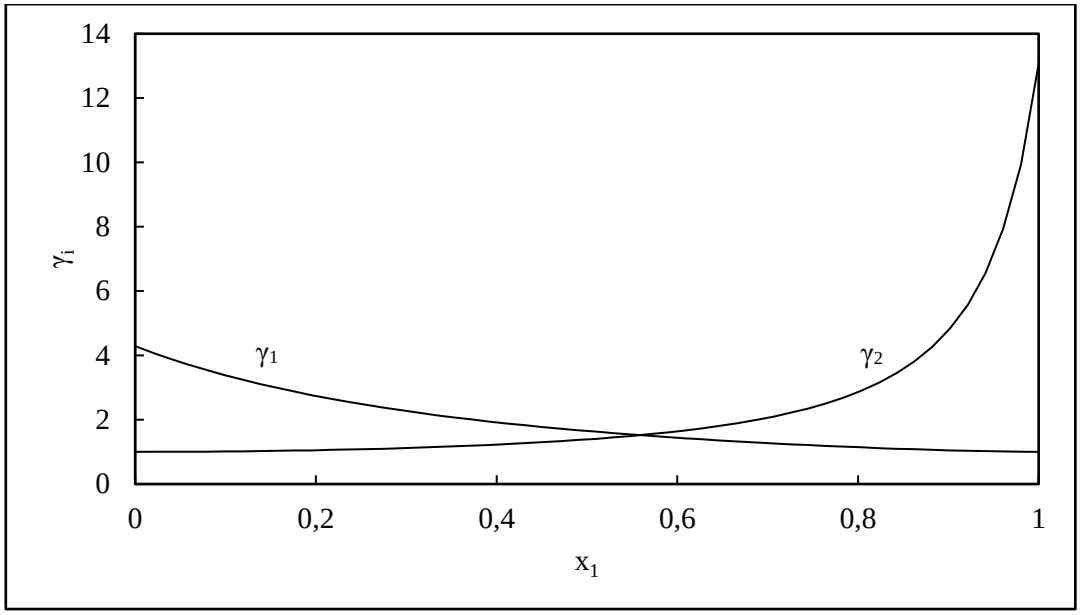

Figure 5-45: γ_i-x plot for the n-pentane (1) + 2-butanol (2) system at 303.17 K (error). —, Wilson + Ideal Gas model.

Table 5-29: Regressed data for the n-pentane (1) + 2-butanol (2) system at 303.17 K using the Wilson + Ideal Gas models (error induced).

Experimental			Wilson + Ideal Gas								
z_1	P/kPa	T/K	P_{calc}/kPa	T_{calc}/K	x_1	y_1	ΔP*	ΔT†	γ_1	γ_2	α
1.000	82.15	303.17	82.15	303.18	1.000	1.000	0.000	0.010	-	-	-
0.894	80.15	303.17	80.05	303.60	0.894	0.980	0.001	0.427	1.052	4.590	1.59
0.854	79.31	303.17	79.21	303.60	0.854	0.977	0.001	0.429	1.088	3.638	2.23
0.793	77.89	303.17	77.82	303.51	0.793	0.975	0.001	0.333	1.153	2.766	3.32
0.753	76.91	303.17	76.86	303.41	0.753	0.974	0.001	0.238	1.202	2.404	4.10
0.703	75.66	303.17	75.63	303.30	0.702	0.973	0.000	0.126	1.272	2.068	5.21
0.650	74.22	303.17	74.22	303.17	0.649	0.972	0.000	0.004	1.353	1.817	6.50
0.597	72.63	303.17	72.65	303.08	0.593	0.971	0.000	0.094	1.471	1.588	8.01
0.547	71.01	303.17	71.04	303.03	0.541	0.969	0.000	0.148	1.584	1.448	9.64
0.503	69.54	303.16	69.57	303.03	0.498	0.968	0.000	0.131	1.679	1.363	11.28
0.499	69.25	303.17	69.28	303.00	0.492	0.968	0.000	0.170	1.697	1.349	11.46
0.453	67.39	303.17	67.42	303.02	0.446	0.966	0.000	0.151	1.809	1.278	13.47
0.405	65.01	303.16	65.03	303.02	0.399	0.963	0.000	0.138	1.942	1.215	15.92
0.356	62.11	303.16	62.13	303.05	0.351	0.960	0.000	0.107	2.094	1.163	18.95
0.299	57.86	303.16	57.87	303.08	0.295	0.956	0.000	0.077	2.299	1.113	23.30
0.247	52.87	303.16	52.88	303.11	0.244	0.950	0.000	0.054	2.522	1.076	28.43
0.198	47.10	303.16	47.10	303.14	0.196	0.942	0.000	0.018	2.762	1.048	34.71
0.151	40.24	303.16	40.23	303.21	0.150	0.929	0.000	0.045	3.040	1.028	42.98
0.107	31.93	303.16	31.93	303.19	0.106	0.907	0.000	0.025	3.339	1.014	53.05
0.048	18.35	303.16	18.34	303.35	0.048	0.828	0.000	0.184	3.819	1.003	75.40
0.000	3.71	303.16	3.70	305.11	0.000	0.000	0.000	1.946	-	-	-

Inducing a 10 ml error in the total working volume of the cell

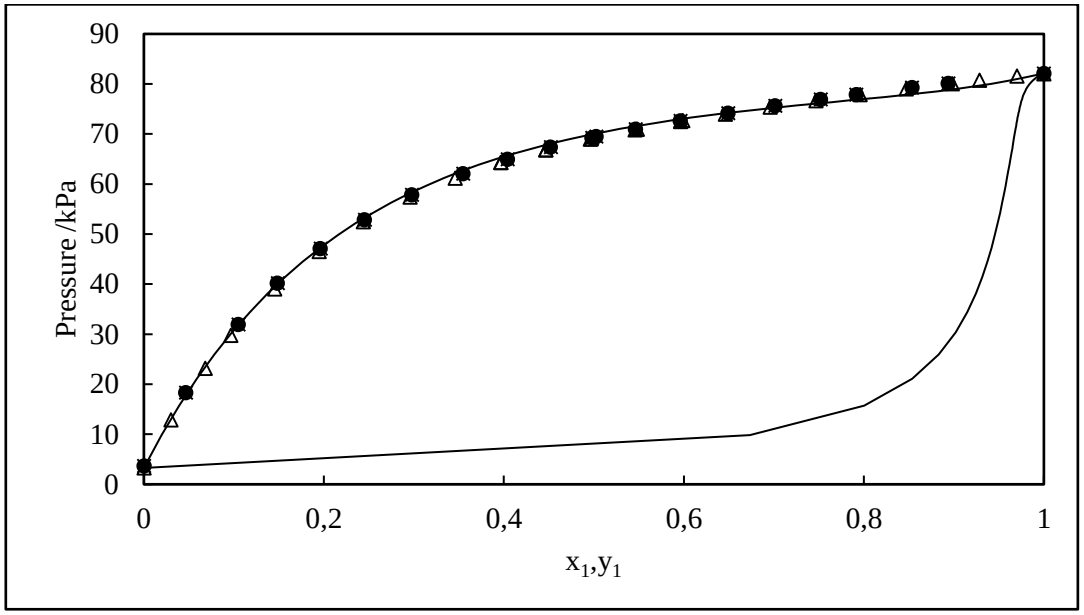

Figure 5-46: P-x plot for the n-pentane (1) + 2-butanol (2) system at 303.17 K. ●, P-x Experimental (correct); *, P-x Experimental (error); —, Wilson + Ideal Gas model; Δ, Thomas et al. (1991).

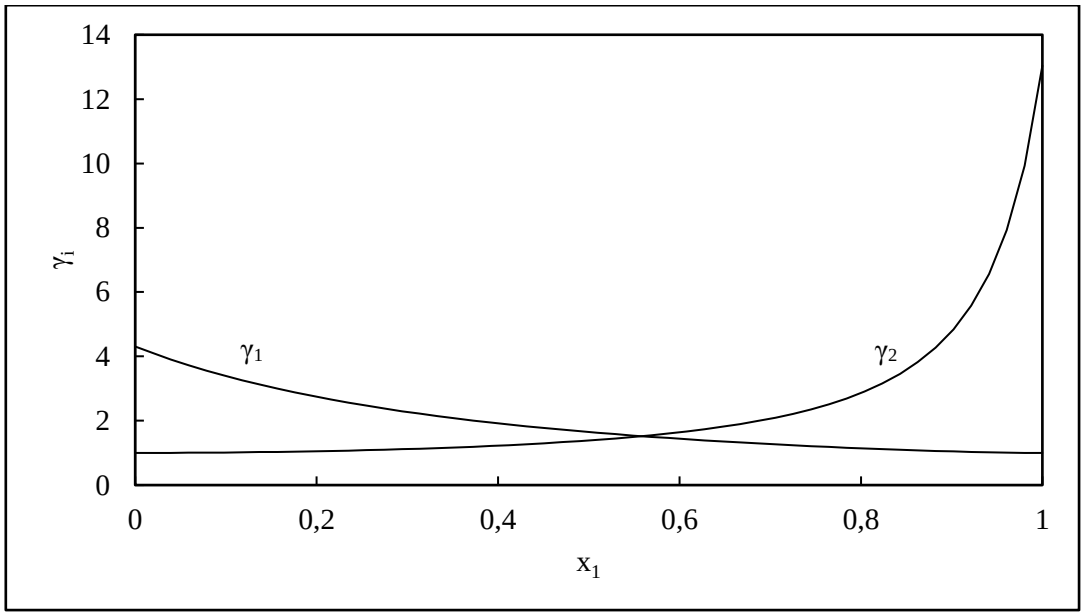

Figure 5-47: γ_i-x plot for the n-pentane (1) + 2-butanol (2) system at 303.17 K (error). —, Wilson + Ideal Gas model.

Table 5-30: Regressed data for the n-pentane (1) + 2-butanol (2) system at 303.17 K using the Wilson + Ideal Gas models (error induced).

Experimental			Wilson + Ideal Gas								
z_1	P/kPa	T/K	P_{calc}/kPa	T_{calc}/K	x_1	y_1	ΔP*	ΔT†	γ_1	γ_2	α
1.000	82.15	303.17	82.15	303.18	1.000	1.000	0.000	0.010	-	-	-
0.894	80.15	303.17	80.05	303.61	0.894	0.980	0.001	0.433	1.052	4.583	5.72
0.854	79.31	303.17	79.21	303.61	0.854	0.977	0.001	0.435	1.088	3.638	7.45
0.793	77.89	303.17	77.82	303.51	0.792	0.975	0.001	0.341	1.154	2.766	10.40
0.753	76.91	303.17	76.86	303.42	0.753	0.974	0.001	0.245	1.202	2.405	12.50
0.703	75.66	303.17	75.63	303.30	0.702	0.973	0.000	0.132	1.272	2.070	15.42
0.650	74.22	303.17	74.22	303.17	0.649	0.972	0.000	0.002	1.354	1.819	18.72
0.597	72.63	303.17	72.65	303.08	0.592	0.971	0.000	0.091	1.472	1.590	22.36
0.547	71.01	303.17	71.04	303.03	0.541	0.969	0.000	0.147	1.585	1.449	26.09
0.503	69.54	303.16	69.57	303.03	0.497	0.968	0.000	0.133	1.681	1.363	29.67
0.499	69.25	303.17	69.28	303.00	0.491	0.967	0.000	0.172	1.700	1.350	30.04
0.453	67.39	303.17	67.42	303.02	0.446	0.966	0.000	0.155	1.812	1.278	34.18
0.405	65.01	303.16	65.04	303.02	0.398	0.963	0.000	0.143	1.947	1.215	38.89
0.356	62.11	303.16	62.13	303.05	0.350	0.960	0.000	0.113	2.099	1.163	44.27
0.299	57.86	303.16	57.87	303.08	0.294	0.956	0.000	0.083	2.306	1.113	51.25
0.247	52.87	303.16	52.88	303.10	0.243	0.950	0.000	0.058	2.531	1.075	58.51
0.198	47.10	303.16	47.10	303.14	0.195	0.942	0.000	0.023	2.773	1.048	66.28
0.151	40.24	303.16	40.23	303.21	0.149	0.929	0.000	0.043	3.053	1.028	75.14
0.107	31.93	303.16	31.93	303.19	0.105	0.907	0.000	0.024	3.355	1.014	83.58
0.048	18.35	303.16	18.34	303.36	0.048	0.828	0.000	0.197	3.841	1.003	99.08
0.000	3.71	303.16	3.70	305.11	0.000	0.000	0.000	1.946	-	-	-

Table 5-31: Sensitivity analyses of the mole fraction and overall composition.

Experimental		**Disregarding the volume calibration**				**Inducing a 5% error on the y_1 value**				**Inducing a 10 ml error on the cell volume**			
x_1	z_1	x_1	Δx	z_1	Δz	x_1	Δx	z_1	Δz	x_1	Δx	z_1	Δz
1.00	1.00	1.00	0.0000	1.00	0.0000	1.00	0.0000	1.00	0.0000	1.00	0.0000	1.00	0.0000
0.89	0.89	0.89	0.0001	0.89	0.0001	0.89	0.0003	0.89	0.0000	0.89	0.0001	0.89	0.0000
0.85	0.85	0.85	0.0002	0.85	0.0001	0.85	0.0003	0.85	0.0000	0.85	0.0002	0.85	0.0000
0.79	0.79	0.79	0.0002	0.79	0.0002	0.79	0.0003	0.79	0.0000	0.79	0.0003	0.79	0.0000
0.75	0.75	0.75	0.0002	0.75	0.0002	0.75	0.0002	0.75	0.0000	0.75	0.0003	0.75	0.0000
0.70	0.70	0.70	0.0003	0.70	0.0002	0.70	0.0002	0.70	0.0000	0.70	0.0003	0.70	0.0000
0.65	0.65	0.65	0.0003	0.65	0.0003	0.65	0.0002	0.65	0.0000	0.65	0.0004	0.65	0.0000
0.60	0.60	0.60	0.0003	0.60	0.0003	0.60	0.0001	0.60	0.0000	0.60	0.0004	0.60	0.0000
0.55	0.55	0.55	0.0003	0.55	0.0003	0.55	0.0001	0.55	0.0000	0.55	0.0004	0.55	0.0000
0.50	0.50	0.50	0.0003	0.50	0.0003	0.50	0.0001	0.50	0.0000	0.50	0.0003	0.50	0.0000
0.50	0.50	0.50	0.0003	0.50	0.0003	0.50	0.0001	0.50	0.0000	0.50	0.0004	0.50	0.0000
0.45	0.45	0.45	0.0003	0.45	0.0003	0.45	0.0001	0.45	0.0000	0.45	0.0004	0.45	0.0000
0.40	0.41	0.40	0.0003	0.40	0.0003	0.40	0.0001	0.41	0.0000	0.40	0.0004	0.41	0.0000
0.35	0.36	0.35	0.0003	0.36	0.0003	0.35	0.0001	0.36	0.0000	0.35	0.0005	0.36	0.0000
0.30	0.30	0.30	0.0003	0.30	0.0003	0.30	0.0001	0.30	0.0000	0.30	0.0005	0.30	0.0000
0.25	0.25	0.25	0.0002	0.25	0.0002	0.25	0.0001	0.25	0.0000	0.24	0.0006	0.25	0.0000
0.20	0.20	0.20	0.0002	0.20	0.0002	0.20	0.0001	0.20	0.0000	0.20	0.0006	0.20	0.0000
0.15	0.15	0.15	0.0002	0.15	0.0002	0.15	0.0001	0.15	0.0000	0.15	0.0005	0.15	0.0000
0.11	0.11	0.10	0.0001	0.11	0.0001	0.11	0.0001	0.11	0.0000	0.10	0.0005	0.11	0.0000
0.05	0.05	0.05	0.0001	0.05	0.0001	0.05	0.0001	0.05	0.0000	0.05	0.0003	0.05	0.0000
0.00	0.00	0.00	0.0000	0.00	0.0000	0.00	0.0000	0.00	0.0000	0.00	0.0000	0.00	0.0000

From Figures 5-42 to 5-47, it can be seen that the data with the errors induced, produce an excellent fit with the experimental data, as well as the literature data of Thomas (1991) and the Wilson activity coefficient model. From Table 5-27 it can be observed that the model parameters obtained in each of the three cases are almost identical to the parameters obtained for the original experimental data. The ΔT_{AVG} and ΔP_{AVG} were found to be 0.23 K and 0.03 kPa respectively in all three cases, the same as that of the original experimental data. The ΔP_{AVG} was found to be within the overall pressure uncertainty of 0.36 kPa whilst the ΔT_{AVG} was slightly above the overall temperature uncertainty of 0.06 K. As indicated earlier, this is due to the "*maximum likelihood*" objective function being utilised in Aspen Plus® whereby the error in experimental variables are placed onto one variable, whereas the second (in this case pressure) is kept to a minimum.

Table 5-31 displays a comparison of the mole fraction and overall composition between the original experimental data and sensitivity cases. From the table it can be observed that any change to the mole fraction or overall composition in the above mentioned cases is only effective to the fourth decimal place. This indicates that an error in any of the variables discussed above does not a make a significant impact to the experimental data, provided it is of an equal or smaller magnitude than the errors utilised in this sensitivity analysis.

CHAPTER 6 : Conclusions

- The main objective of this project was to set up and commission a new static synthetic apparatus for phase equilibrium measurements in the moderate pressure region. The equilibrium cell utilised in this project constitutes of a total working volume of 60 cm^3. One of the key features of this experimental setup is the high-accuracy Teledyne Isco pumps, employed to dispense the feed into the cell.

- The overall uncertainties yielded from the calibrations were found to be 0.06 K, 0.36 kPa and 0.1 ml for temperature, pressure and volume respectively.

- Binary P-x measurements were conducted for the test systems:
    - water (1) + 2-butanol (2) at 323.16 K
    - n-hexane (1) + 2-butanol (2) at 329.21 K
    - n-pentane (1) + 1-propanol (2) at 317.18 K
    - n-pentane (1) + 2-butanol (2) at 303.17 K
    - n-pentane (1) + ethanol (2) at 303.11 K

- It was observed that the vapour pressures measured, produced a good fit with literature, indicating that the degassing procedure utilised in this study works successfully.

- For the test systems, the system water (1) + 2-butanol (2) at 323.16 K produced a good fit with literature, however a deviation from the Wilson activity coefficient model was observed. Thereafter, the system n-hexane (1) + 2-butanol (2) at 329.21 K was measured. This system produced a satisfactory fit with both the literature data and regression models. The third test system was thereafter measured i.e. n-pentane (1) + 1-propanol (2) at 317.18 K. Although this system produced and excellent fit to the Wilson activity coefficient model, there was a slight negative deviation from the literature data. The remaining two test systems were measured and both systems produced an excellent fit to both the model as well as the literature data.

- All measurements conducted in this project were done so isothermally and the systems measured were successfully modelled on Aspen Plus®. The method of Barker (1953) was utilized to convert the overall composition (z_i) to the liquid mole fraction (x_i) using a suitable algorithm. All systems measured were modelled using the Wilson activity coefficient model with the Ideal Gas law or Hayden O'Connell second virial coefficient. The fluorinated systems were also modelled using the NRTL activity coefficient model.

- After the measurement of the test systems, it could be concluded that the apparatus was successfully set up and commissioned, and the experimental technique developed was verified and approved.

- The measurement of new systems thereafter commenced. These systems were:
    - n-hexane (1) + perfluoro-n-heptane (2) at 313.21 and 333.12 K.
    - n-pentane (1) + 2-propanol (2) at 313.11, 323.11 and 333.12 K

- For both the fluorinated and alkane + alcohol systems, the experimental data produced an excellent fit with the activity coefficient models. For the system n-hexane (1) + perfluoro-n-heptane (2) at 313.21 and 333.12 K, azeotropes were observed at approximately x = 0.7, and the Wilson activity coefficient model yielded a slightly better fit than the NRTL model. For the system n-pentane (1) + 2-propanol (2) at 313.11, 323.11 and 333.12 K azeotropes were observed between x = 0.92 to x = 1. This is an indication of poor separation of these binary combinations at the above mentioned mole fractions.

- The sensitivity analyses were conducted for the following cases
    - Disregarding the volume calibration
    - Inducing a 5% error on the y_1 value
    - Inducing a 10 ml error on the total cell working volume

- The results obtained indicate that the error induced on the experimental data due to the above mentioned cases is negligible. It can therefore be concluded that accurate determination of the cell volume, calibration of the Isco pumps and accurate calculation of the y_1 value during the data regression procedure, is not a pivotal step in yielding accurate P-x data when utilising this apparatus.

- During experimentation it was also observed that equilibrium can be achieved as early as 5 minutes into the run, depending on the system being measured. In this study, such observations were made for most of the test systems and new systems, excluding the system water (1) + 2-butanol (2) at 323.16 K.

CHAPTER 7 : Recommendations

Modifications to Auxiliary Equipment

When measuring the density of the liquid in the pumps, the densitometer utilised only takes into consideration the pump temperature. In order to achieve better accuracy in the data, it is recommended that the density of the components under investigation be measured using a densitometer that can account for temperature and pressure. The pure liquids in the feed pumps are stored at 313.15 K and 2 000 kPa (gauge).

Although the current degassing procedure yields accurate results, adjustments to the procedure can improve the efficiency of the degassing apparatus. It is recommended that a more powerful chiller be employed in order to decrease the temperature of the coolant in the degassing bath to about 253.15 K. This low temperature should result in a smaller amount of sample being lost during the degassing procedure. It is also recommended that a Vigreux® fractionating column be employed. The current degassing setup only uses a condenser, which is equivalent to a batch distillation procedure. The Vigreux® column will allow for a longer degassing time whilst avoiding the loss of a significant amount of chemical.

Experimental Measurements

It is recommended that measurements be conducted at higher temperatures and pressures, 343.15-393.15 K and 300-500 kPa respectively, in order to further confirm the accuracy of the apparatus at these conditions. The water in the cell bath will need to be replaced with an alternative heating medium such as silicone oil to operate at high temperatures.

It is further recommended that measurements for the system 1-pentene + 2-propanol at 313.15, 323.15 and 333.15 K be conducted in order to understand the phase separation behaviour of the selected solvent with 1-pentene. This is to ultimately aid in the separation of 1-pentene from n-pentane.

References

Abbott, M. M., 1986. Low pressure phase equilibria: Measurement of VLE. *Fluid Phase Equilibria*, 29, p.193-207.

Abrams, D. S. and Prausnitz, J. M., 1975. Statistical thermodynamics of liquid mixtures: A new expression for the excess Gibbs energy of partly or completely miscible systems. *AIChE Journal*, 21, p.116-127.

Aspen Tech, 2014. ASPEN Plus® Simulation Package (V8.6).

Barker, J.A., 1953. Determination of activity coefficients from total pressure measurements. *Australian Journal of Chemistry*, 6, p.207–210.

Black, C., 1958. Vapor phase imperfections in vapor-liquid equilibria. Semi-empirical equation. *Industrial & Engineering Chemistry*, 50, p.391–402.

Bosch, A. B. and de Haan, H., 2013. *Industrial separation processes: Fundamentals*. Berlin: De Gruyter.

Brown, R. C. and Brown, T. R., 2014. *Biorenewable resources: Engineering new products from agriculture.* United States of America: John Wiley and Sons, Inc.

Clifford, S.L., 2004, *Low-pressure vapour-liquid equilibrium and molecular simulation of carboxylic acids.* M.Sc. University of Kwa Zulu Natal.

Coquelet, C., Chareton, A., Valtz, A., Baba-Ahmed, A. and Richon, D., 2003. Vapor-liquid equilibrium data for the azeotropic difluoromethane + propane system at temperatures form 294.83 to 343.26K and pressures up to 5.4MPa. *Journal of Chemical and Engineering Data*, 48 p.317–323.

Dean, J. A., 1998. *Lange's handbook of chemistry.* United States of America: McGraw-Hill.

Dohrn, R., Peper, S. and Fonseca, J. M. S., 2010. High-pressure fluid-phase equilibria: Experimental methods and systems investigated. *Fluid Phase Equilibria*, 288, p.1-54.

Fischer, K. and Gmehling J., 1994. P-x and y^{∞} data for the different binary butanol-water systems at 50 ^{0}C. *Journal of Chemical and Engineering Data*, 39, p.309-315.

Fonseca, J. M. S., Dohrn, R. and Peper, S., 2011. High-pressure fluid-phase equilibria: Experimental methods and systems investigated (2005–2008). *Fluid Phase Equilibria*, 300, p.1-69.

Fredenslund, A., Gmehling, J., and Rasmussen, P., 1977. Vapour liquid equilibrium using UNIFAC. *Elsevier Scientific Publishing Company*.

Gibbs, R. E. and Van Ness, H. C., 1972. Vapour-liquid equilibria from total pressure measurements. A new apparatus. *Industrial & Engineering Chemistry Fundamentals*, 11, p.410-413.

Gladysz, J. A., Curran, D. P. and Horváth, I. T., 2005. *Handbook of fluorous chemistry.* Germany: John Wiley and Sons, Inc.

Grant, n.d. *TXF200 - Heating Circulator.* [online] Available at: <http://www.grantinstruments.com/txf200-heating-circulator/> [Accessed 22 March 2016].

References

Guillevic, J. L., Richon, D. and Renon, H., 1983. Vapor-liquid equilibrium measurements up to 558 K and 7 MPa: A new apparatus. *Industrial & Engineering Chemistry Fundamentals*, 22, p.495-499.

Hayden, J. G. and O'Connell, J. P., 1975. A generalized method for predicting second virial coefficients. *Industrial & Engineering Chemistry Process Design and Development*, 14, p.209–216.

Joseph, M. A., Raal, J. D. and Ramjugernath, D., 2001. Phase equilibrium properties of binary systems with diacetyl from a computer controlled vapour-liquid equilibrium still. *Fluid Phase Equilibria*, 182, p.157-176.

Karrer, L. and Gaube, J., 1988. Determination of ternary VLLE by p(x1, x2) measurements. *Fluid Phase Equilibria*, 42, p.195-207.

Kolbe, B. and Gmehling, J., 1985. Thermodynamic properties of ethanol water. I. Vapour-liquid equilibria measurements 90 to 150°C by the static method. *Fluid Phase Equilibria*, 23, p.213.

Koretsky, M. D., 2004. *Engineering and chemical thermodynamics.* Oregon: John Wiley and Sons, Inc.

Kreglewski, A., 1968. Semi-empirical treatment of properties of fluid mixtures. ii. Estimation of the effects of molecular sizes in fluids and fluid mixtures. *Journal of Physical Chemistry*, 72, p.1897-1905.

Laursen, T., Rasmussen, P. and Andersen, S. I., 2002. VLE and VLLE measurements of dimethyl ether containing systems. *Journal of Chemical and Engineering Data*, 47, p.198-202.

Lee, K. R. and Tan, C.S., 1998. Vapor-liquid equilibria for the systems propane + m-cresol, propane + p-cresol, and propane + m-cresol + p-cresol at high pressures. *Fluid Phase Equilibria*, 143, p.125-141.

Lilwanth, H., 2014. *Vapour-liquid equilibrium measurements at moderate pressures using a semi-automatic glass recirculating still.* M.Sc. University of Kwa-Zulu Natal.

Ljunglin, J. J. and Van Ness, H. C., 1962. Calculation of vapour liquid equilibria from vapour pressure data. *Chemical Engineering Science*, 17, p.531–539.

Maher, P. J. and Smith, B. D., 1979. A new total pressure vapor-liquid equilibrium apparatus. The ethanol aniline system at 313.15, 350.81, and 386.67 K. *Journal of Chemical and Engineering Data*, 24 p.16-22.

Moodley, K., 2012. *Automation of a static-synthetic apparatus for vapour-liquid equilibrium measurement*. M.Sc. University of KwaZulu-Natal.

Morgado, P., McCabe, C. and Filipe, E. J. M., 2005. Modelling the phase behaviour and excess properties of alkane + perfluoroalkane binary mixtures with the SAFT–VR approach. *Fluid Phase Equilibria*, 228–229, p. 389–393.

Motchelaho, A. M. M., 2006. *Vapour-liquid equilibrium measurements using a static total pressure apparatus*. M.Sc. University of KwaZulu-Natal.

Mühlbauer, A. L. and Raal, J. D., 1991. Measurements and thermodynamic interpretation of high-pressure vapor-liquid equilibria in the toluene-carbon dioxide system. *Fluid Phase Equilibria*, 64, p.213-236.

Mühlbauer, A. L. and Raal, J. D., 1995, Computation and thermodynamic interpretation of high pressure vapour-liquid equilibria – A review. *Journal of Chemical and Engineering Data*, 60, p.1-29.

Naidoo, P., Ramjugernath, D. and Raal, J.D., 2008. A new versatile high pressure vapor-liquid apparatus. *Fluid Phase Equilibria*, 269, p.104–112.

References

Nala, M. E., 2012. *Measurements of phase equilibrium for systems containing oxygenated compounds*. M.Sc. University of KwaZulu-Natal.

Narasigadu, C., Naidoo, P., Coquelet, C., Richon, D. and Ramjugernath, D., 2013. A novel static analytical apparatus for phase equilibrium measurements. *Fluid Phase Equilibria*, 338, p.188-196.

Ndlovu, M., 2005. *Development of dynamic still for measuring low pressure vapour-liquid-liquid equilibria (systems of partial liquid miscibility).* M.Sc. University of Kwa-Zulu Natal.

Nelson, W. 2016. [Personal Communication, 04 April 2016].

Ng, H. J. and Robinson, D. B., 1978. Equilibrium phase properties of the toluene-carbon dioxide system. *Journal of Chemical and Engineering Data,* 23, p.325-327.

O'Connell, J. P. and Prausnitz, J. M., 1967. Empirical correlation of second virial coefficients for vapor-liquid equilibrium calculations. *Industrial & Engineering Chemistry Process Design and Development*, 6, p.245–306.

Palmer, D. A., 1987. *Handbook of Applied Thermodynamics*. Boca Raton: CRC Press.

Patnaik, P., 2007. *A comprehensive guide to the hazardous properties of chemical substances.* New Jersey: John Wiley and Sons, Inc.

Peng, D., and Robinson, D. B., 1976. A new two constant equation of state. *Industrial & Engineering Chemistry Fundamentals*, 15, p.59-64.

Physical Measurement Laboratory, 2016. *The NIST Reference on Constants, Units and Uncertainty*. [online] Available at: <http://physics.nist.gov/cgi-bin/cuu/Info/Uncertainty/index.html> [Accessed 03 May 2016].

Pitzer, K. S. and Curl, R. F., 1957. The volumetric and thermodynamic properties of fluids. iii. Empirical equation for the second virial coefficient. *Journal of the American Chemical Society*, 79, p.2369-2370.

Poling, B. E., Prausnitz, J. M. and O' Connell, J. P., 2001. *The properties of gases and liquids*. New York: McGraw-Hill.

Prausnitz, J. M., Anderson, T. F., Grens, E. A., Eckert, C. A. and O'Connell, J. P., 1967. *Computer calculations for multicomponent vapour liquid equilibria*. Englewood Cliffs, NJ: Prentice- Hall.

Prausnitz, J., M., Anderson, T., Grens, E., Eckert, C., Hsieh, R. and O'Connell, J. P., 1980. *Computer calculations for multicomponent vapour-liquid and liquid-liquid equilibria*. Englewood Cliffs, NJ: Prentice- Hall.

Raabe, G., Janisch, J. and Koehler, J., 2001. Experimental studies of phase equilibria in mixtures relevant for the description of natural gases. *Fluid Phase Equilibria,* 185, p.199-208.

Raal, J. D., Motchelaho, A. M., Perumal, Y., Courtial, X. and Ramjugernath, D., 2011. P-x data for binary systems using a novel static total pressure apparatus. *Fluid Phase Equilibria*., 310, p.156-165.

Raal, J.D. and Mühlbauer, A.L., 1998. *Phase equilibria: measurement and computation*. Bristol: Taylor and Francis.

Rarey, J. R. and Gmehling, J., 1993. Computer-operated differential static apparatus for the measurement of vapor-liquid equilibrium data. *Fluid Phase Equilibria*, 83, p.279-287.

Reddy, P., 2006. *Development of a novel apparatus for the measurement of vapour-liquid equilibria at elevated temperatures and moderate pressures*. Ph.D. University of KwaZulu-Natal.

Redlich, O., and Kwong, J. N. S., 1949. On thermodynamics of solutions: an equation of state. Fugacities of gaseous solutions. *Chemical Reviews*, 44, p.233 – 244.

Reimers, J. L., Bhethanabotla, V. R. and Campbell, S. W., 1992. Total pressure measurements for pentane + methanol + ethanol at 303.15 K. *Journal of Chemical and Engineering Data*, 37, p.127-130.

Renon, H. and Prausnitz, J. M., 1968. Local compositions in thermodynamic excess functions for liquid mixtures. *AIChE Journal*, 14, p.135-144.

Rice, P. and El-Nikheli, A., 1995. Isothermal vapour-liquid equilibrium data for the systems n-pentane with n-hexane, n-octane and n-decane. *Fluid Phase Equilibria*, 107, p.257-267.

Seker, E. and Somer T. G., 1993. Vapour-liquid equilibrium still – a new design. *Measurement Science and Technology*, 4, p.776–779

Sinnott, R. K., 2005. *Coulson & Richardson's chemical engineering – Chemical engineering design*. Oxford: Elsevier Butterworth Heinemann.

Smith, J. M., Van Ness, H. C. and Abbott, M. M., 2005. *Introduction to chemical engineering thermodynamics*. New York: McGraw-Hill.

Soo, C. B., 2011. *Experimental thermodynamic measurements of biofuel-related associating compounds and modelling using the PC-SAFT equation of state.* Ph.D. l'École Nationale Supérieure des Mines de Paris.

Statemaster, 2005. *Isopropanol*. [online] Available at: <http://www.statemaster.com/encyclopedia/Isopropanol> [Accessed 17 July 2015].

Sue, K., Mizutani, T., Usami, T., Arai, K., Kasai, H. and Nakanishi, H., 2004. Titanyl phthalocyanine solubility in supercritical acetone. *Journal of Supercritical Fluids*, 30, p.281–285.

Taylor, B. N. and Kuyatt, C. E., 1994. *Guidelines for evaluating and expressing the uncertainty of NIST measurement results*. [technical report], National Institute of Standards and Technology, Gaithersburg.

Teledyne Isco, 2003. *100 DM Syringe Pump*. [online] Available at: <http://www.isco.com/products/products3.asp?PL=1051050> [Accessed 20 March 2016].

Thomas, S., Bhethanabotla, V. R. and Campbell, S. W., 1991. Total pressure measurements for n-pentane – methanol – 2-butanol at 303.15 K. *Journal of Chemical and Engineering Data*, 36, p.374-378.

Tsonopoulos, C., 1974. An empirical correlation of second virial coefficients. *AIChE Journal*, 20, p.263-272.

Tsuboka, T. and Katayama, T., 1975. Modified Wilson equation for vapour-liquid and liquid-liquid equilibria. *Journal of Chemical Engineering Data*, 8, p.181-187.

Twu, C. H. and Coon, J. E., 1996. CEOS/AE Mixing rules constrained by vdW mixing rule and second virial coefficient. *American Institute of Chemical Engineering Journals*, 42, p.3212-3222.

Uusi-Kyyny P., Pokki, J. P., Laakkonen, M., Aittamaa, J. and Liukkonen, S., 2002. Vapor liquid equilibrium for the binary systems 2-methylpentane + 2-butanol at 329.2 K and n-hexane + 2-butanol at 329.2 and 363.2 K with a static apparatus. *Fluid Phase Equilibria*, 201, p.343–358.

Valco Instruments Co. Inc., 2016. *Reducing Ferrules – Internal.* [online] Available at: <http://www.vici.com/vfit/rf_int.php> [Accessed 22 March 2016].

Valtz, A., Coquelet, C., Baba-Ahmed, A. and Richon, D., 2002. Vapor-liquid equilibrium data for the propane + 1,1,1,2,3,3,3-heptafluoropropane (R227ea) system at temperatures from 293.16 to 353.18K and pressures up to 3.4 Mpa. *Fluid Phase Equilibrium*, 202, p.29-47.

Van der Waals, J. D., 1873. *Over de continuitet van den gas - en vloeistoftoestand*, Ph.D, Leiden, as given by Anderko, 1990.

Van Laar, J. J., 1910. The vapour pressure of binary mixtures. *Zeitschrift feur Physik Chemie*, 72, p.723-751.

Van Ness, H. C. and Abbott, M. M., 1978. A procedure for rapid degassing of liquids. *Industrial & Engineering Chemistry Fundamentals*, 17, p.66–67.

Van Ness, H. C., Byer, S. M. and Gibbs, R. E., 1973. Vapor-liquid equilibrium: Part I. An appraisal of data reduction methods. *AIChE Journal*, 19, p.238-244.

Van Ness, H. C., Soczek, C. A., Kochar, N. K., 1967a. Thermodynamic excess properties for ethanol-n-heptane. *Journal of Chemical and Engineering Data*, 12, 346-351.

Van Ness, H. C., Soczek, C.A., Peloquin G. L., and Machado R. L., 1967b. Thermodynamic excess properties of three alcohol-hydrocarbon systems. *Journal of Chemical and Engineering Data*, 12, p.217.

Walas, S. M., 1985. *Phase Equilibrium in Chemical Engineering*. Boston: Butterworth.

Wikimedia, 2014. *Hexane displayed*. [online] Available at: <https://commons.wikimedia.org/wiki/File:Hexane_displayed.svg> [Accessed 17 July 2015].

Wilson, G. M., 1964. Vapour-liquid equilibrium, a new expression for the excess free energy of mixing. *Journal of the American Chemical Society*, 86, p.127–130.

Wong, D. S. H. and Sandler, S. I., 1992. A theoretically correct mixing rule for cubic equation of state vapour-liquid equilibrium, a new expression for the excess free energy of mixing. *American Institute of Chemical Engineers Journals*, 10, p.660-665.

Zimmermann, A. and Keller, J. U., 1989. Vapor-liquid equilibrium in the system water-ammonia-lithium bromide. *Fluid Phase Equilibria*, 53, p.229-234.

APPENDIX A : Thermodynamic Principles

Criterion for Thermodynamic Equilibrium

Consider a closed system at equilibrium, consisting of two phases, α and β. Each of the individual phases within the closed system can freely transfer mass from one phase to the other. Assuming that the temperature and pressure are constant throughout the system at equilibrium, each of the phases can be described as follows

$$d(nG)^{\alpha} = (nV)^{\alpha} dP - (nS)^{\alpha} dT + \sum \mu_i{}^{\alpha} \, dn_i{}^{\alpha} \tag{A-1}$$

$$d(nG)^{\beta} = (nV)^{\beta} dP - (nS)^{\beta} dT + \sum \mu_i{}^{\beta} \, dn_i{}^{\beta} \tag{A-2}$$

Where μ_i is the chemical potential energy for species *i* and is defined in terms of Gibbs energy as

$$\mu_i = \left[\frac{\partial(nG)}{\partial n_i}\right]_{T.P.n_j} \tag{A-3}$$

Combining equations (A-1) and (A-2) result in the following total changes within the system

$$d(nG) = (nV)dP - (nS)dT + \sum \mu_i{}^{\alpha} \, dn_i{}^{\alpha} + \sum \mu_i{}^{\beta} \, dn_i{}^{\beta} \tag{A-4}$$

The total system properties are yielded using the following relationship

$$nM = (nM)^{\alpha} + (nM)^{\beta} \tag{A-5}$$

Considering that the system is closed. The following is true

$$d(nG) = (nV)dP - (nS)dT \tag{A-6}$$

By comparing equations (A-4) and (A-6) it can be seen that

$$\sum \mu_i{}^{\alpha} \, dn_i{}^{\alpha} + \sum \mu_i{}^{\beta} \, dn_i{}^{\beta} = 0 \tag{A-7}$$

For systems in which chemical reactions do not occur. Conservation of mass requires that $dn_i{}^{\alpha} = -dn_i{}^{\beta}$ and equation (A-7) therefore reduces to

$$\sum(\mu_i{}^{\alpha} - \mu_i{}^{\beta})\, dn_i{}^{\alpha} = 0 \qquad \text{(A-8)}$$

Only if the term in the parenthesis is zero, can equation (A-8) be satisfied as quantities dn_i are independent. Therefore

$$\mu_i{}^{\alpha} = \mu_i{}^{\beta} \qquad \text{(A-9)}$$

The resulting equation may be used as a generalization for more than two phases, by grouping the phases by pairs. The general result for π phases with N chemical species is

$$\mu_i{}^{\alpha} = \mu_i{}^{\beta} = \ldots\ldots \mu_i{}^{\pi} \qquad (i = 1.2.\ldots.N) \qquad \text{(A-10)}$$

Pure Species Fugacity and Fugacity Coefficient

A general equation that describes phase equilibrium which incorporates the fugacity of a species *i* can be described as

$$d\bar{G}_i = RTdln(f_i) \qquad at\ constant\ T \qquad \text{(A-11)}$$

$\bar{G}_i$ is the partial molar Gibbs energy and is described as

$$\bar{G}_i = \left[\frac{\partial(nG)}{\partial n_i}\right]_{T.P.n_j} \qquad \text{(A-12)}$$

The comparison of equations (A-3) and (A-12) imply that $\mu_i = \bar{G}_i$. Thus equation (A-11) now becomes

$$d\,\mu_i = RTdln(f_i) \qquad at\ constant\ T \qquad \text{(A-13)}$$

Integrating equation (A-13) at constant temperature yields

$$\mu_i = RTln(f_i) + \theta_i(T) \qquad \text{(A-14)}$$

Because θ_i is dependent on temperature only and since all phases are at constant temperature. Substituting equation (A-14) in (A-10) gives

$$f_i{}^{\alpha} = f_i{}^{\beta} = \ldots\ldots f_i{}^{\pi} \qquad (i = 1.2.\ldots.N) \qquad \text{(A.15)}$$

Equation (A-15) indicates that the conditions for phase equilibrium between a vapour and liquid phase at the same temperature and pressure yields

$$\hat{f}_i{}^{L} = \hat{f}_i{}^{V} \qquad \text{(A-16)}$$

In the case of ideal systems, the compositions of the vapour and liquid phases can be related as follows

$$y_i P = x_i P_i^{sat} \tag{A-17}$$

Equation (A-17) is more commonly known as Raoult's Law.

APPENDIX B : Additional Temperature Calibrations

The calibration curves for the additional Pt-100 sensors calibrated are presented below.

Temperature sensor of feed pump heating fluid

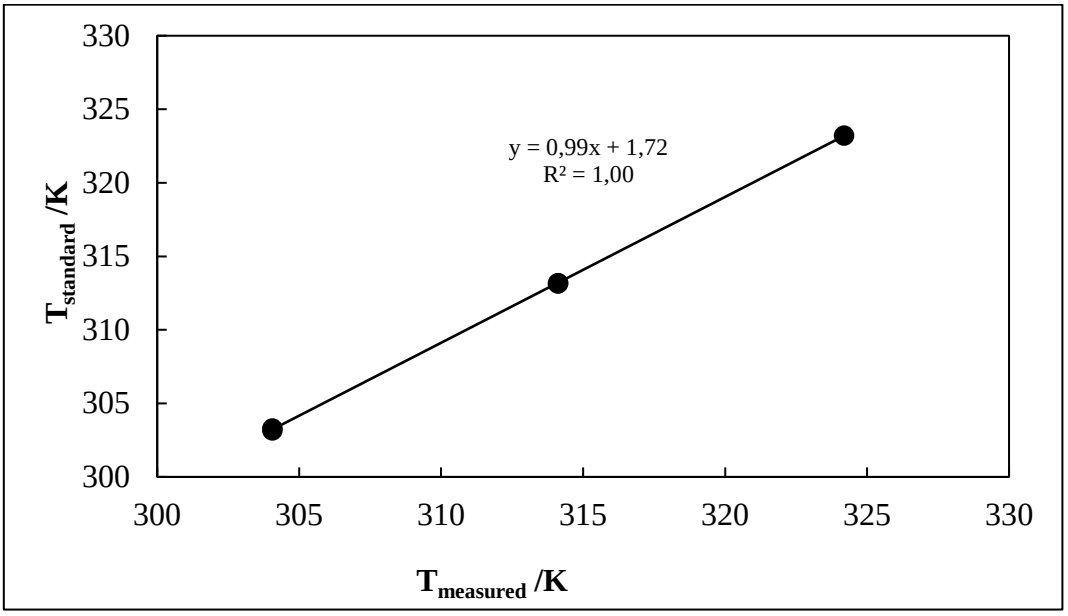

Figure B-1: Calibration curve for the temperature sensor of feed pump heating fluid. First order relation between standard and temperature sensor.

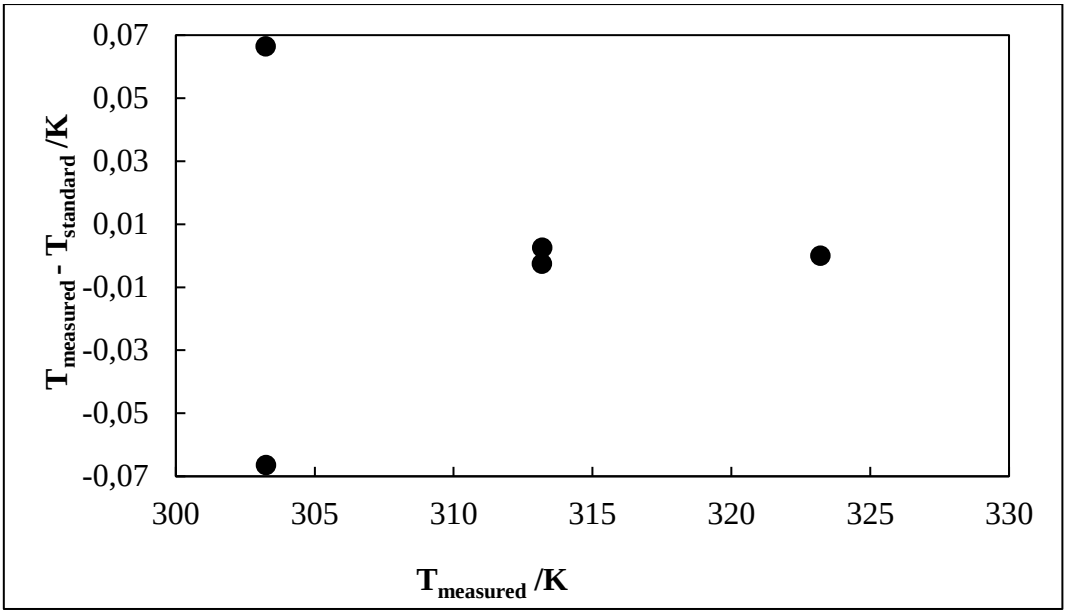

Figure B-2: Deviations of the standard temperature from the temperature sensor of feed pump heating fluid.

Temperature of pump lines

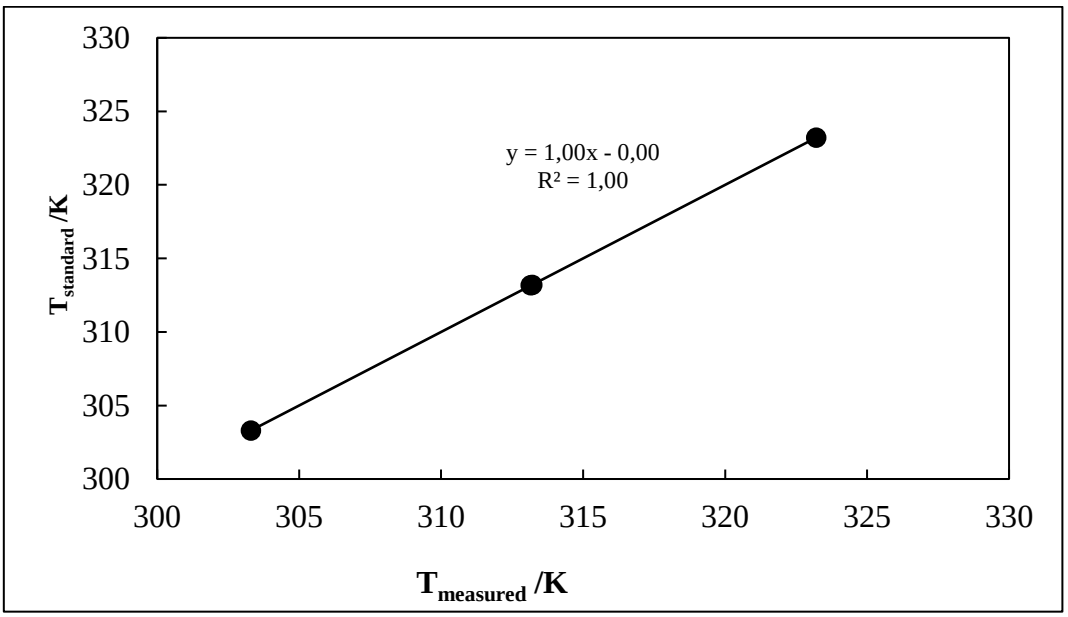

Figure B-3: Calibration curve for the temperature sensor of the pump lines. First order relation between standard and temperature sensor.

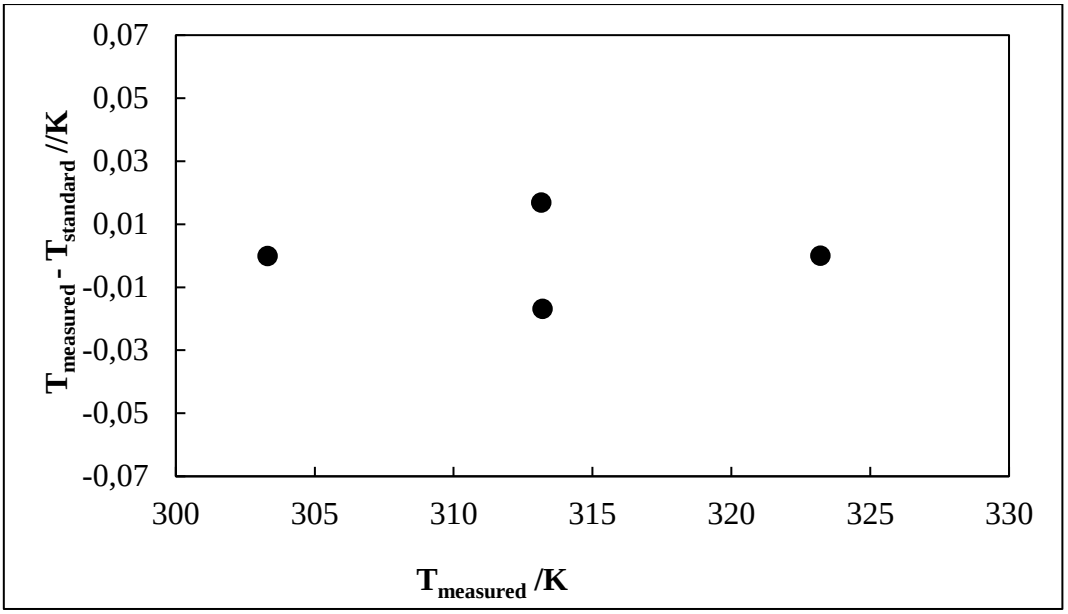

Figure B-4: Deviations of the standard temperature from the temperature sensor of the pump lines.

APPENDIX C : Experimental Raw Data

The tables and figures presented below display the raw data obtained from experimental measurements for both the test systems and new systems measured. The variables reported include temperature, pressure, overall composition and the number of moles.

Test Systems

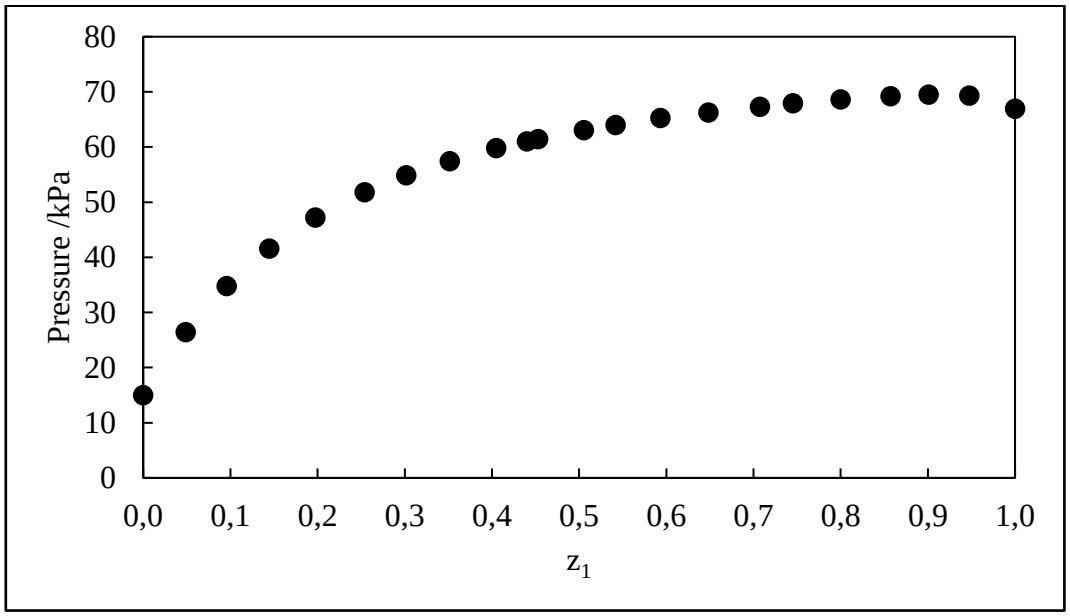

Figure C-1: P-z plot for the system n-hexane (1) + 2-butanol (2) at 329.21 K.

Table C-1: Experimental T-P-z data for the n-hexane (1) + 2-butanol (2) system at 329.21 K.

n_1/moles	n_2/moles	z_1	T/K	P/kPa
0.1500 ± 0.0010	0.0000 ± 0.0000	1.0000 ± 0.0000	329.21	66.93
0.1500 ± 0.0010	0.0083 ± 0.0001	0.9476 ± 0.0005	329.21	69.33
0.1500 ± 0.0010	0.0165 ± 0.0001	0.9009 ± 0.0008	329.21	69.46
0.1500 ± 0.0010	0.0250 ± 0.0002	0.8572 ± 0.0012	329.21	69.20
0.1500 ± 0.0010	0.0376 ± 0.0003	0.7997 ± 0.0015	329.21	68.62
0.1500 ± 0.0010	0.0513 ± 0.0003	0.7452 ± 0.0018	329.21	67.90
0.1500 ± 0.0010	0.0621 ± 0.0004	0.7073 ± 0.0020	329.20	67.29
0.1500 ± 0.0010	0.0814 ± 0.0005	0.6483 ± 0.0022	329.20	66.22
0.2227 ± 0.0015	0.1528 ± 0.0010	0.5931 ± 0.0023	329.20	65.23
0.1500 ± 0.0010	0.1269 ± 0.0008	0.5417 ± 0.0023	329.21	63.95
0.1562 ± 0.0010	0.1528 ± 0.0010	0.5055 ± 0.0024	329.20	63.03
0.1264 ± 0.0008	0.1528 ± 0.0010	0.4528 ± 0.0023	329.20	61.41
0.1500 ± 0.0010	0.1910 ± 0.0013	0.4399 ± 0.0023	329.21	61.03
0.1500 ± 0.0010	0.2204 ± 0.0015	0.4049 ± 0.0023	329.20	59.76
0.0828 ± 0.0006	0.1528 ± 0.0010	0.3516 ± 0.0022	329.20	57.44
0.0660 ± 0.0004	0.1528 ± 0.0010	0.3016 ± 0.0020	329.20	54.83
0.0519 ± 0.0003	0.1528 ± 0.0010	0.2537 ± 0.0018	329.20	51.76
0.0376 ± 0.0003	0.1528 ± 0.0010	0.1973 ± 0.0015	329.20	47.17
0.0258 ± 0.0002	0.1528 ± 0.0010	0.1447 ± 0.0012	329.20	41.56
0.0161 ± 0.0001	0.1528 ± 0.0010	0.0956 ± 0.0008	329.20	34.77
0.0078 ± 0.0001	0.1528 ± 0.0010	0.0488 ± 0.0004	329.20	26.43
0.0000 ± 0.0000	0.1528 ± 0.0010	0.0000 ± 0.0000	329.20	15.00

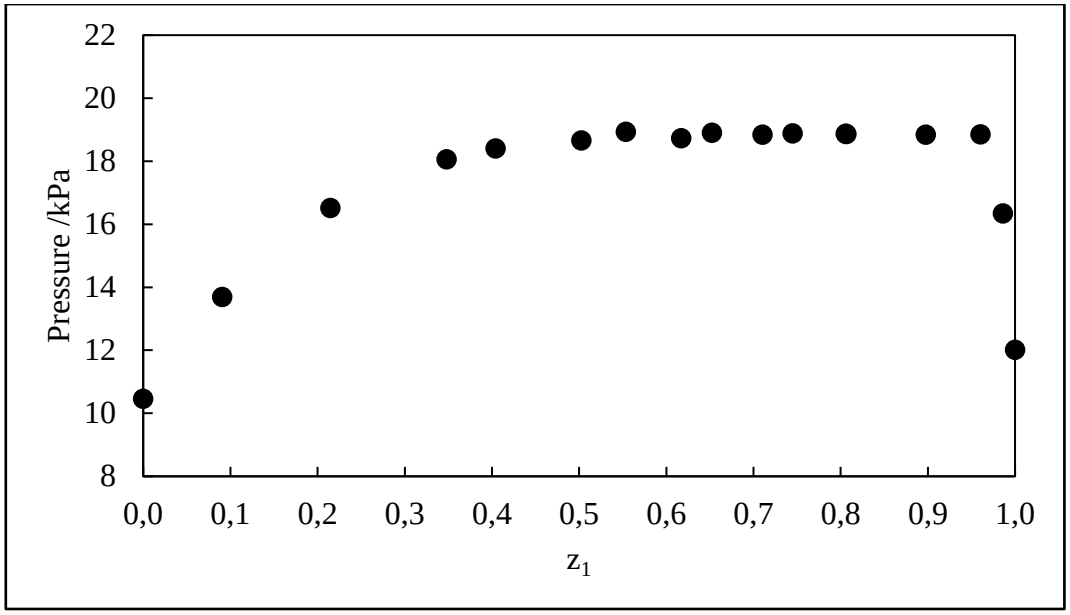

Figure C-2: P-z plot for the system water (1) + 2-butanol (2) at 323.16 K.

Table C-2: Experimental T-P-z data for the water (1) + 2-butanol (2) system at 323.16 K.

n_1/moles	n_2/moles	z_1	T/K	P/kPa
0.4370 ± 0.0029	0.0000 ± 0.0000	1.0000 ± 0.0000	323.16	12.02
0.4370 ± 0.0029	0.0060 ± 0.0000	0.9859 ± 0.0001	323.16	16.34
0.4370 ± 0.0029	0.0180 ± 0.0001	0.9605 ± 0.0004	323.16	18.85
0.4370 ± 0.0029	0.0500 ± 0.0003	0.8977 ± 0.0009	323.16	18.84
0.8870 ± 0.0059	0.2130 ± 0.0014	0.8066 ± 0.0015	323.17	18.86
0.4370 ± 0.0029	0.1050 ± 0.0007	0.8058 ± 0.0015	323.16	18.87
0.4370 ± 0.0029	0.1500 ± 0.0010	0.7449 ± 0.0018	323.17	18.88
0.5210 ± 0.0035	0.2130 ± 0.0014	0.7102 ± 0.0019	323.16	18.84
0.4370 ± 0.0029	0.2330 ± 0.0016	0.6524 ± 0.0021	323.16	18.90
0.3420 ± 0.0023	0.2130 ± 0.0014	0.6169 ± 0.0022	323.16	18.73
0.4370 ± 0.0029	0.3530 ± 0.0024	0.5534 ± 0.0023	323.16	18.93
0.2150 ± 0.0014	0.2130 ± 0.0014	0.5023 ± 0.0024	323.17	18.66
0.1440 ± 0.0010	0.2130 ± 0.0014	0.4042 ± 0.0023	323.17	18.40
0.1130 ± 0.0008	0.2130 ± 0.0014	0.3479 ± 0.0021	323.16	18.06
0.0580 ± 0.0004	0.2130 ± 0.0014	0.2146 ± 0.0016	323.16	16.51
0.0210 ± 0.0001	0.2130 ± 0.0014	0.0907 ± 0.0008	323.16	13.69
0.0000 ± 0.0000	0.2130 ± 0.0014	0.0000 ± 0.0000	323.16	10.46

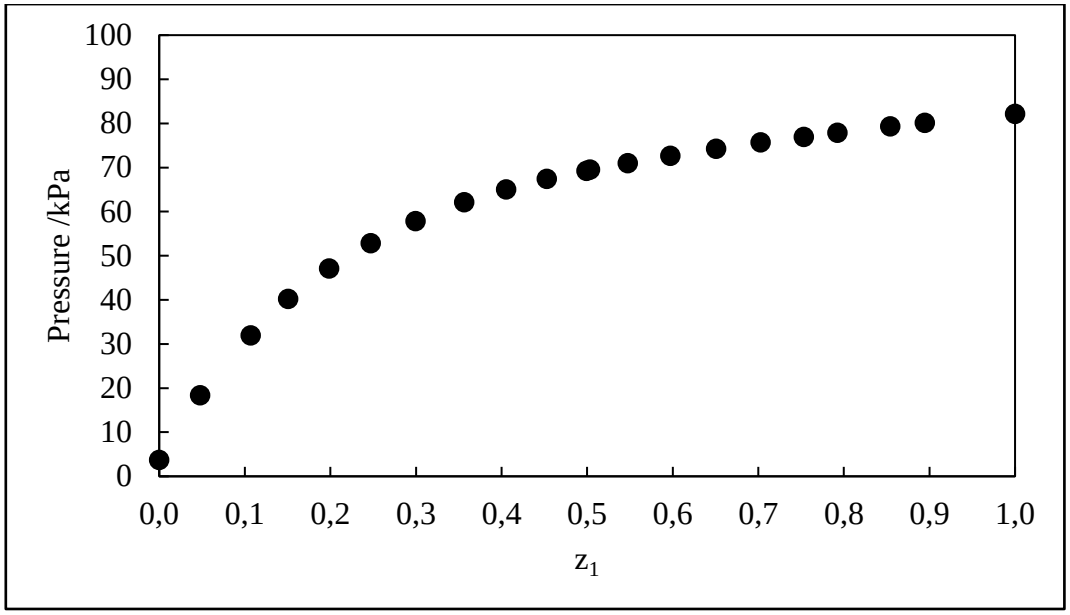

Figure C-3: P-z plot for the system n-pentane (1) + 2-butanol (2) at 303.17 K.

Table C-3: Experimental T-P-z data for the n-pentane (1) + 2-butanol (2) system at 303.17 K.

n_1/moles	n_2/moles	z_1	T/K	P/kPa
0.1689 ± 0.0011	0.0000 ± 0.0000	1.0000 ± 0.0000	303.17	82.15
0.1689 ± 0.0011	0.0200 ± 0.0001	0.8943 ± 0.0009	303.17	80.15
0.1689 ± 0.0011	0.0288 ± 0.0002	0.8542 ± 0.0012	303.17	79.31
0.1689 ± 0.0011	0.0442 ± 0.0003	0.7926 ± 0.0016	303.17	77.89
0.1689 ± 0.0011	0.0554 ± 0.0004	0.7530 ± 0.0018	303.17	76.91
0.1689 ± 0.0011	0.0715 ± 0.0005	0.7025 ± 0.0020	303.17	75.66
0.1689 ± 0.0011	0.0907 ± 0.0006	0.6505 ± 0.0021	303.17	74.22
0.1689 ± 0.0011	0.1139 ± 0.0008	0.5972 ± 0.0023	303.17	72.63
0.1689 ± 0.0011	0.1396 ± 0.0009	0.5474 ± 0.0023	303.17	71.01
0.2050 ± 0.0014	0.2024 ± 0.0014	0.5031 ± 0.0024	303.16	69.54
0.1689 ± 0.0011	0.1695 ± 0.0011	0.4990 ± 0.0024	303.17	69.25
0.1689 ± 0.0011	0.2041 ± 0.0014	0.4527 ± 0.0023	303.17	67.39
0.1379 ± 0.0009	0.2024 ± 0.0014	0.4052 ± 0.0023	303.16	65.01
0.1120 ± 0.0007	0.2024 ± 0.0014	0.3562 ± 0.0022	303.16	62.11
0.0865 ± 0.0006	0.2024 ± 0.0014	0.2994 ± 0.0020	303.16	57.86
0.0665 ± 0.0004	0.2024 ± 0.0014	0.2472 ± 0.0018	303.16	52.87
0.0501 ± 0.0003	0.2024 ± 0.0014	0.1983 ± 0.0015	303.16	47.10
0.0359 ± 0.0002	0.2024 ± 0.0014	0.1505 ± 0.0012	303.16	40.24
0.0242 ± 0.0002	0.2024 ± 0.0014	0.1068 ± 0.0009	303.16	31.93
0.0101 ± 0.0001	0.2024 ± 0.0014	0.0477 ± 0.0004	303.16	18.35
0.0000 ± 0.0000	0.2024 ± 0.0014	0.0000 ± 0.0000	303.16	3.71

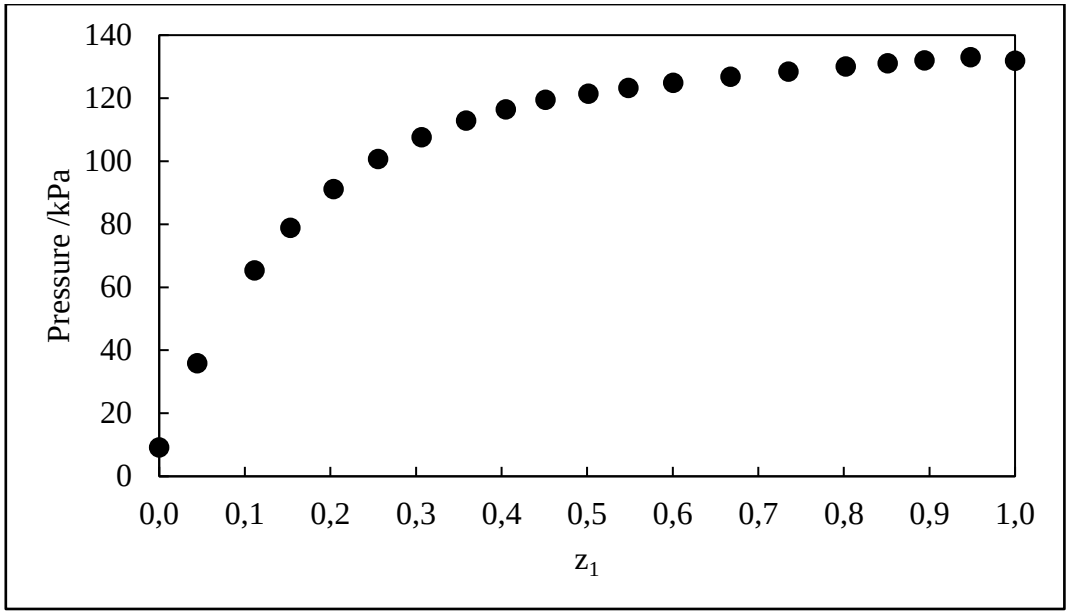

Figure C-4: P-z plot for the system n-pentane (1) + 1-propanol (2) at 317.18 K.

Table C-4: Experimental T-P-z data for the n-pentane (1) + 1-propanol (2) system at 317.18 K.

n_1/moles	n_2/moles	z_1	T/K	P/kPa
0.1669 ± 0.0011	0.0000 ± 0.0000	1.0000 ± 0.0000	317.18	131.85
0.1669 ± 0.0011	0.0091 ± 0.0001	0.9481 ± 0.0005	317.18	133.00
0.1669 ± 0.0011	0.0198 ± 0.0001	0.8940 ± 0.0009	317.18	131.97
0.1669 ± 0.0011	0.0292 ± 0.0002	0.8511 ± 0.0012	317.18	131.10
0.1669 ± 0.0011	0.0411 ± 0.0003	0.8023 ± 0.0015	317.17	130.06
0.1669 ± 0.0011	0.0601 ± 0.0004	0.7353 ± 0.0018	317.17	128.38
0.1669 ± 0.0011	0.0831 ± 0.0006	0.6676 ± 0.0021	317.17	126.77
0.1669 ± 0.0011	0.1110 ± 0.0007	0.6006 ± 0.0023	317.17	124.91
0.1669 ± 0.0011	0.1376 ± 0.0009	0.5482 ± 0.0023	317.18	123.24
0.1669 ± 0.0011	0.1660 ± 0.0011	0.5014 ± 0.0024	317.18	121.46
0.1829 ± 0.0012	0.2225 ± 0.0015	0.4511 ± 0.0023	317.17	119.46
0.1669 ± 0.0011	0.2454 ± 0.0016	0.4048 ± 0.0023	317.18	116.48
0.1243 ± 0.0008	0.2225 ± 0.0015	0.3585 ± 0.0022	317.17	112.90
0.0984 ± 0.0007	0.2225 ± 0.0015	0.3066 ± 0.0020	317.17	107.64
0.0765 ± 0.0005	0.2225 ± 0.0015	0.2558 ± 0.0018	317.17	100.68
0.0569 ± 0.0004	0.2225 ± 0.0015	0.2037 ± 0.0015	317.18	91.17
0.0403 ± 0.0003	0.2225 ± 0.0015	0.1533 ± 0.0012	317.17	78.86
0.0278 ± 0.0002	0.2225 ± 0.0015	0.1112 ± 0.0009	317.17	65.34
0.0103 ± 0.0001	0.2225 ± 0.0015	0.0442 ± 0.0004	317.18	35.87
0.0000 ± 0.0000	0.2225 ± 0.0015	0.0000 ± 0.0000	317.18	9.14

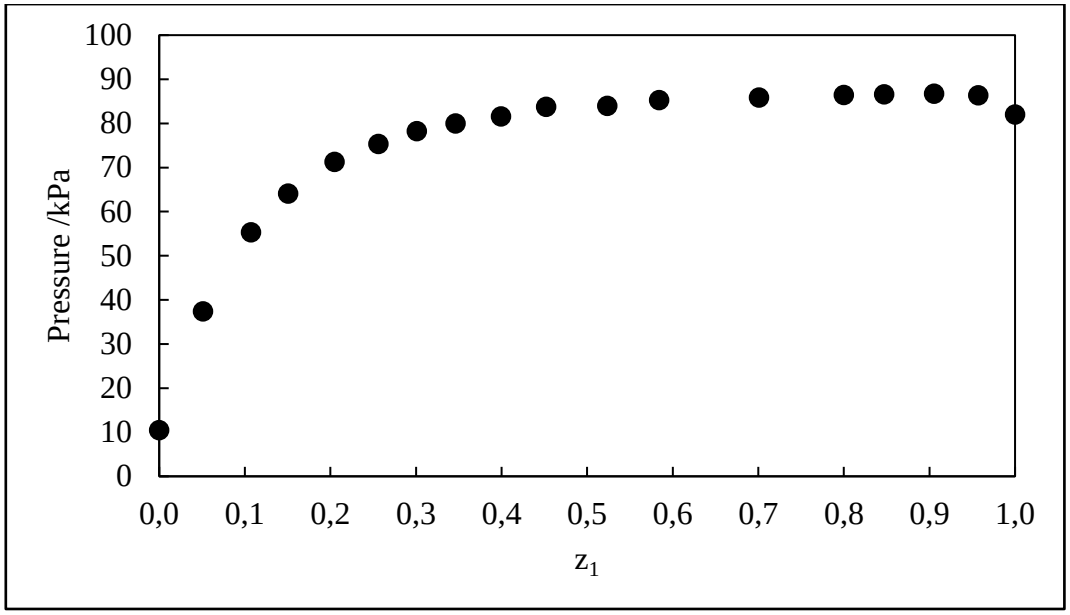

Figure C-5: P-z plot for the system n-pentane (1) + ethanol (2) at 303.11 K.

Table C-5: Experimental T-P-z data for the n-pentane (1) + ethanol (2) system at 303.11 K.

n_1/moles	n_2/moles	z_1	T/K	P/kPa
0.2960 ± 0.0020	0.0000 ± 0.0000	1.0000 ± 0.0000	303.11	82.02
0.2960 ± 0.0020	0.0133 ± 0.0001	0.9569 ± 0.0004	303.11	86.39
0.2960 ± 0.0020	0.0309 ± 0.0002	0.9055 ± 0.0008	303.11	86.74
0.2960 ± 0.0020	0.0535 ± 0.0004	0.8468 ± 0.0012	303.12	86.55
0.2960 ± 0.0020	0.0741 ± 0.0005	0.7998 ± 0.0015	303.11	86.40
0.2960 ± 0.0020	0.1263 ± 0.0008	0.7009 ± 0.0020	303.11	85.88
0.2960 ± 0.0020	0.2107 ± 0.0014	0.5841 ± 0.0023	303.11	85.28
0.2888 ± 0.0019	0.2629 ± 0.0018	0.5235 ± 0.0024	303.11	83.95
0.2960 ± 0.0020	0.359 ± 0.0024	0.4519 ± 0.0023	303.11	83.77
0.1747 ± 0.0012	0.2629 ± 0.0018	0.3993 ± 0.0023	303.11	81.59
0.1392 ± 0.0009	0.2629 ± 0.0018	0.3463 ± 0.0021	303.11	79.96
0.1132 ± 0.0008	0.2629 ± 0.0018	0.3010 ± 0.0020	303.11	78.21
0.0904 ± 0.0006	0.2629 ± 0.0018	0.2560 ± 0.0018	303.11	75.36
0.0677 ± 0.0005	0.2629 ± 0.0018	0.2049 ± 0.0015	303.11	71.30
0.0465 ± 0.0003	0.2629 ± 0.0018	0.1504 ± 0.0012	303.11	64.07
0.0316 ± 0.0002	0.2629 ± 0.0018	0.1073 ± 0.0009	303.12	55.31
0.0141 ± 0.0001	0.2629 ± 0.0018	0.0510 ± 0.0005	303.11	37.36
0.0000 ± 0.0000	0.2629 ± 0.0018	0.0000 ± 0.0000	303.12	10.45

Fluorinated Systems

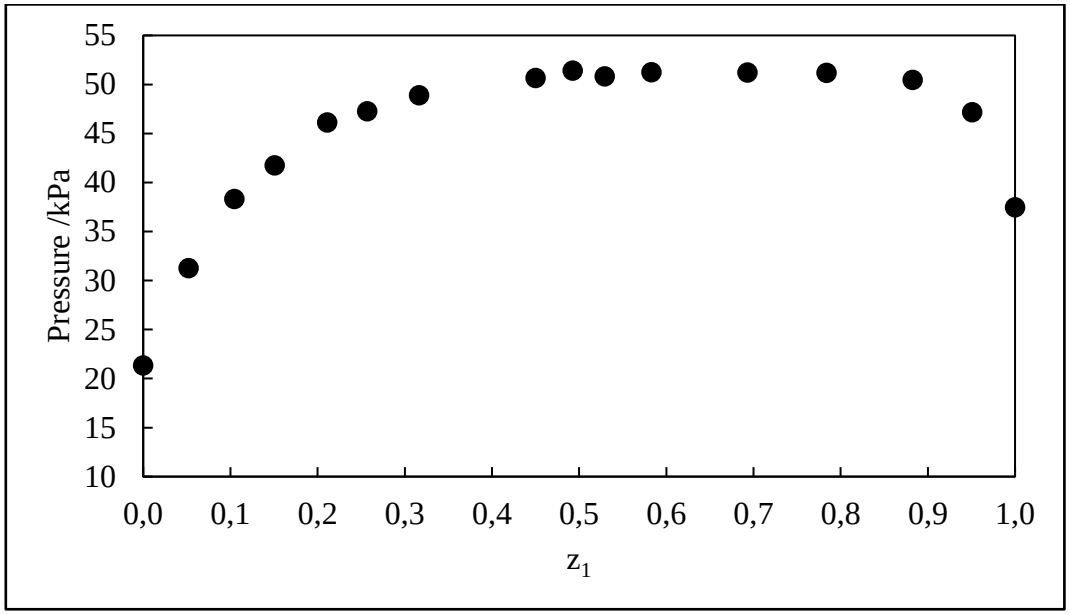

Figure C-6: P-z plot for the system n-hexane (1) + perfluoro-n-heptane (2) at 313.21 K.

Table C-6: Experimental T-P-z data for the n-hexane (1) + perfluoro-n-heptane (2) system at 313.21 K.

n_1/moles	n_2/moles	z_1	T/K	P/kPa
0.1345 ± 0.0009	0.0000 ± 0.0000	1.0000 ± 0.0000	313.21	37.48
0.1345 ± 0.0009	0.0069 ± 0.0000	0.9509 ± 0.0004	313.21	47.17
0.1345 ± 0.0009	0.0179 ± 0.0001	0.8826 ± 0.0010	313.21	50.48
0.1345 ± 0.0009	0.0371 ± 0.0002	0.7839 ± 0.0016	313.20	51.21
0.1345 ± 0.0009	0.0595 ± 0.0004	0.6932 ± 0.0020	313.21	51.24
0.1879 ± 0.0013	0.1345 ± 0.0009	0.5828 ± 0.0023	313.21	51.27
0.1513 ± 0.0010	0.1345 ± 0.0009	0.5293 ± 0.0024	313.21	50.83
0.1345 ± 0.0009	0.1384 ± 0.0009	0.4927 ± 0.0024	313.20	51.42
0.1101 ± 0.0007	0.1345 ± 0.0009	0.4500 ± 0.0023	313.21	50.68
0.0622 ± 0.0004	0.1345 ± 0.0009	0.3163 ± 0.0020	313.21	48.92
0.0465 ± 0.0003	0.1345 ± 0.0009	0.2570 ± 0.0018	313.21	47.28
0.0360 ± 0.0002	0.1345 ± 0.0009	0.2110 ± 0.0016	313.21	46.14
0.0239 ± 0.0002	0.1345 ± 0.0009	0.1508 ± 0.0012	313.21	41.77
0.0157 ± 0.0001	0.1345 ± 0.0009	0.1044 ± 0.0009	313.21	38.33
0.0074 ± 0.0000	0.1345 ± 0.0009	0.0519 ± 0.0005	313.21	31.28
0.0000 ± 0.0000	0.1345 ± 0.0009	0.0000 ± 0.0000	313.20	21.36

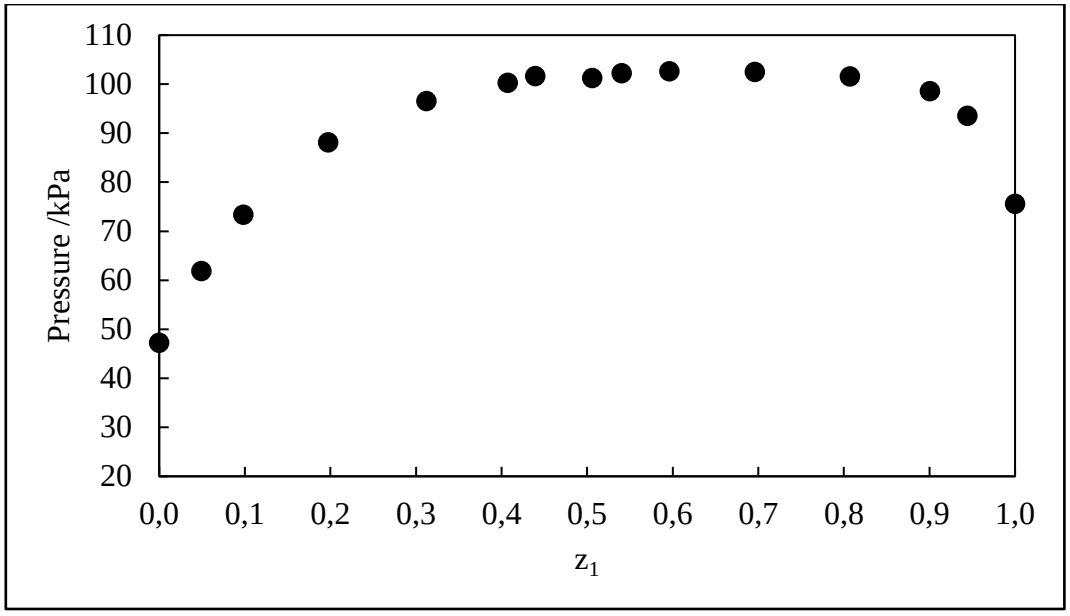

Figure C-7: P-z plot for the system n-hexane (1) + perfluoro-n-heptane (2) at 333.12 K.

Table C-7: Experimental T-P-z data for the n-hexane (1) + perfluoro-n-heptane (2) system at 333.12 K.

n_1/moles	n_2/moles	z_1	T/K	P/kPa
0.1136 ± 0.0008	0.0000 ± 0.0000	1.0000 ± 0.0000	333.12	75.56
0.1136 ± 0.0008	0.0067 ± 0.0000	0.9442 ± 0.0005	333.12	93.52
0.1136 ± 0.0008	0.0125 ± 0.0001	0.9006 ± 0.0008	333.11	98.56
0.1136 ± 0.0008	0.0272 ± 0.0002	0.8070 ± 0.0015	333.12	101.58
0.1136 ± 0.0008	0.0496 ± 0.0003	0.6960 ± 0.0020	333.11	102.51
0.1625 ± 0.0011	0.1102 ± 0.0007	0.5959 ± 0.0023	333.12	102.60
0.1136 ± 0.0008	0.0967 ± 0.0006	0.5402 ± 0.0023	333.12	102.26
0.1129 ± 0.0008	0.1102 ± 0.0007	0.5059 ± 0.0024	333.12	101.27
0.1136 ± 0.0008	0.1450 ± 0.0010	0.4394 ± 0.0023	333.12	101.63
0.0757 ± 0.0005	0.1102 ± 0.0007	0.4072 ± 0.0023	333.12	100.28
0.0500 ± 0.0003	0.1102 ± 0.0007	0.3122 ± 0.0020	333.12	96.58
0.0271 ± 0.0002	0.1102 ± 0.0007	0.1972 ± 0.0015	333.13	88.14
0.0120 ± 0.0001	0.1102 ± 0.0007	0.0982 ± 0.0008	333.13	73.34
0.0057 ± 0.0000	0.1102 ± 0.0007	0.0493 ± 0.0004	333.13	61.89
0.0000 ± 0.0000	0.1102 ± 0.0007	0.0000 ± 0.0000	333.13	47.27

Alkane + Alcohol Systems

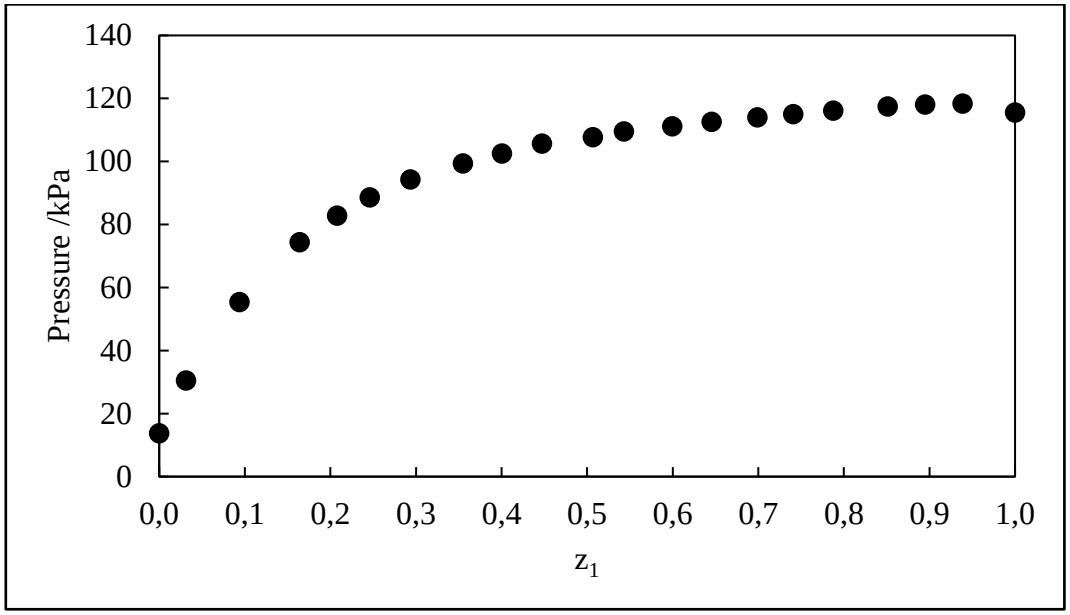

Figure C-8: P-z plot for the system n-pentane (1) + 2-propanol (2) at 313.11 K.

Table C-8: Experimental T-P-z data for the n-pentane (1) + 2-propanol (2) system at 313.11 K.

n_1/moles	n_2/moles	z_1	T/K	P/kPa
0.2279 ± 0.0015	0.0000 ± 0.0000	1.0000 ± 0.0000	313.12	115.57
0.2279 ± 0.0015	0.0149 ± 0.0001	0.9385 ± 0.0005	313.11	118.46
0.2279 ± 0.0015	0.0268 ± 0.0002	0.8947 ± 0.0009	313.11	118.15
0.2279 ± 0.0015	0.0399 ± 0.0003	0.8511 ± 0.0012	313.11	117.47
0.2279 ± 0.0015	0.0615 ± 0.0004	0.7875 ± 0.0016	313.11	116.16
0.2279 ± 0.0015	0.0798 ± 0.0005	0.7406 ± 0.0018	313.11	115.08
0.2279 ± 0.0015	0.0981 ± 0.0007	0.6991 ± 0.0020	313.11	114.06
0.2279 ± 0.0015	0.1252 ± 0.0008	0.6454 ± 0.0022	313.11	112.66
0.2911 ± 0.0019	0.1947 ± 0.0013	0.5993 ± 0.0023	313.11	111.19
0.2279 ± 0.0015	0.1919 ± 0.0013	0.5428 ± 0.0023	313.11	109.54
0.1999 ± 0.0013	0.1947 ± 0.0013	0.5066 ± 0.0024	313.11	107.76
0.2279 ± 0.0015	0.2816 ± 0.0019	0.4473 ± 0.0023	313.11	105.73
0.1300 ± 0.0009	0.1947 ± 0.0013	0.4004 ± 0.0023	313.11	102.55
0.1071 ± 0.0007	0.1947 ± 0.0013	0.3549 ± 0.0022	313.11	99.38
0.0809 ± 0.0005	0.1947 ± 0.0013	0.2935 ± 0.0020	313.11	94.29
0.0635 ± 0.0004	0.1947 ± 0.0013	0.2461 ± 0.0018	313.12	88.67
0.0511 ± 0.0003	0.1947 ± 0.0013	0.2078 ± 0.0016	313.11	82.87
0.0382 ± 0.0003	0.1947 ± 0.0013	0.1639 ± 0.0013	313.11	74.42
0.0201 ± 0.0001	0.1947 ± 0.0013	0.0936 ± 0.0008	313.11	55.42
0.0063 ± 0.0000	0.1947 ± 0.0013	0.0314 ± 0.0003	313.11	30.59
0.0000 ± 0.0000	0.1947 ± 0.0013	0.0000 ± 0.0000	313.11	13.83

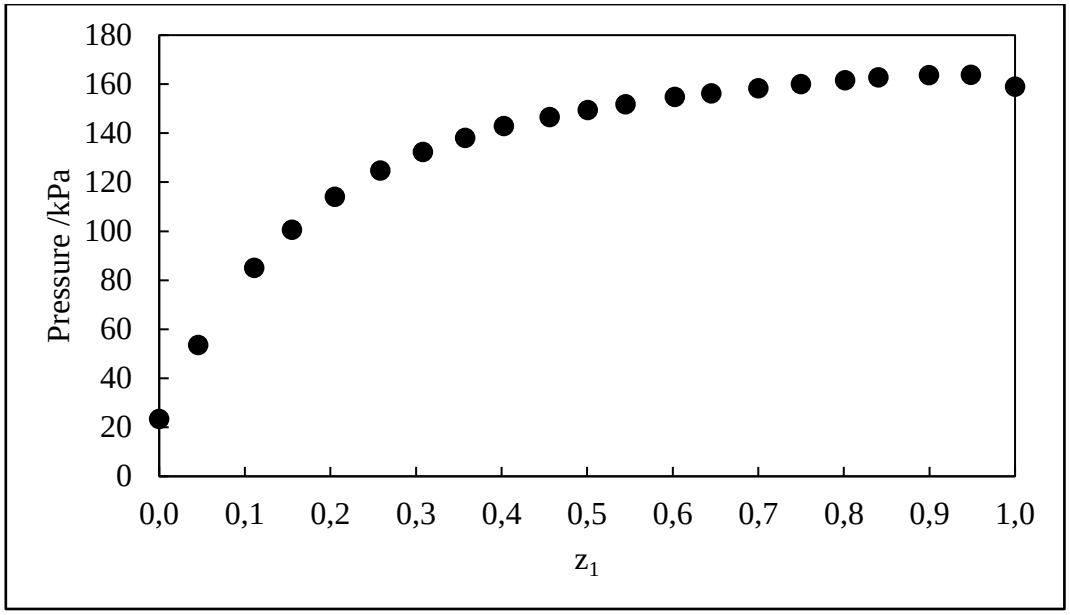

Figure C-9: P-z plot for the system n-pentane (1) + 2-propanol (2) at 323.11 K.

Table C-9: Experimental T-P-z data for the n-pentane (1) + 2-propanol (2) system at 323.11 K.

n_1/moles	n_2/moles	z_1	T/K	P/kPa
0.2378 ± 0.0016	0.0000 ± 0.0000	1.0000 ± 0.0000	323.10	158.94
0.2378 ± 0.0016	0.0130 ± 0.0001	0.9483 ± 0.0005	323.10	163.80
0.2378 ± 0.0016	0.0266 ± 0.0002	0.8994 ± 0.0009	323.11	163.68
0.2378 ± 0.0016	0.0451 ± 0.0003	0.8404 ± 0.0013	323.11	162.73
0.2378 ± 0.0016	0.0589 ± 0.0004	0.8014 ± 0.0015	323.10	161.60
0.2378 ± 0.0016	0.0794 ± 0.0005	0.7497 ± 0.0018	323.11	160.02
0.2378 ± 0.0016	0.1019 ± 0.0007	0.7000 ± 0.0020	323.10	158.29
0.2378 ± 0.0016	0.1309 ± 0.0009	0.6450 ± 0.0022	323.11	156.25
0.2974 ± 0.0020	0.1963 ± 0.0013	0.6024 ± 0.0023	323.11	154.75
0.2378 ± 0.0016	0.1988 ± 0.0013	0.5447 ± 0.0023	323.11	151.78
0.1968 ± 0.0013	0.1963 ± 0.0013	0.5006 ± 0.0024	323.11	149.38
0.1647 ± 0.0011	0.1963 ± 0.0013	0.4562 ± 0.0023	323.11	146.52
0.2378 ± 0.0016	0.3527 ± 0.0024	0.4027 ± 0.0023	323.11	142.92
0.1091 ± 0.0007	0.1963 ± 0.0013	0.3573 ± 0.0022	323.11	138.08
0.0874 ± 0.0006	0.1963 ± 0.0013	0.3080 ± 0.0020	323.11	132.28
0.0684 ± 0.0005	0.1963 ± 0.0013	0.2585 ± 0.0018	323.11	124.75
0.0507 ± 0.0003	0.1963 ± 0.0013	0.2053 ± 0.0015	323.11	114.06
0.0360 ± 0.0002	0.1963 ± 0.0013	0.1550 ± 0.0012	323.11	100.66
0.0245 ± 0.0002	0.1963 ± 0.0013	0.1108 ± 0.0009	323.11	84.99
0.0094 ± 0.0001	0.1963 ± 0.0013	0.0456 ± 0.0004	323.11	53.53
0.0000 ± 0.0000	0.1963 ± 0.0013	0.0000 ± 0.0000	323.11	23.40

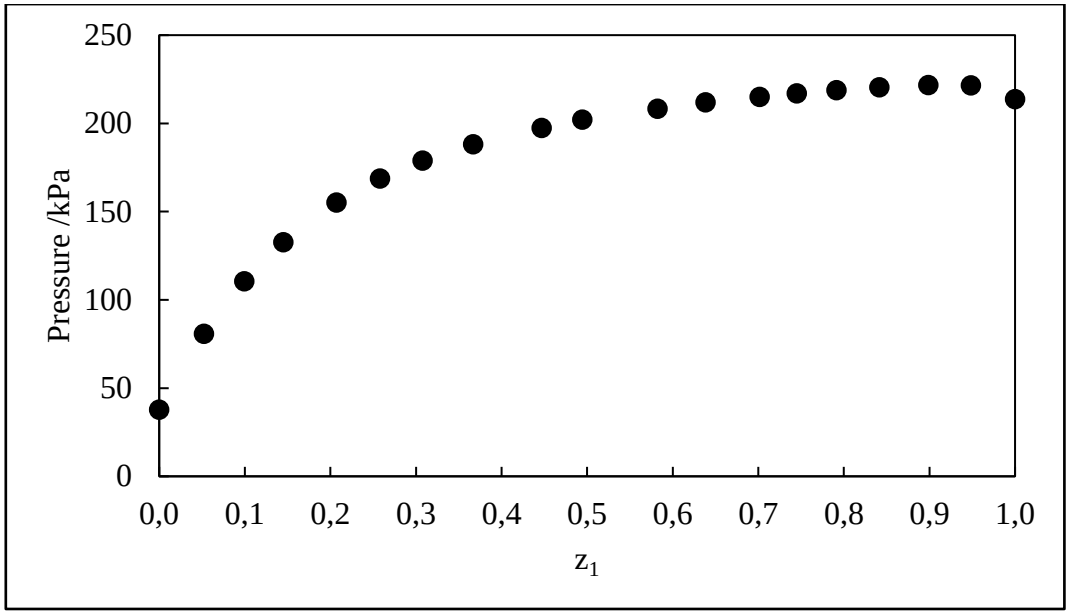

Figure C-10: P-z plot for the system n-pentane (1) + 2-propanol (2) at 333.12 K.

Table C-10: Experimental T-P-z data for the n-pentane (1) + 2-propanol (2) system at 333.12 K.

n_1/moles	n_2/moles	z_1	T/K	P/kPa
0.2452 ± 0.0016	0.0000 ± 0.0000	1.0000 ± 0.0000	333.12	213.70
0.2452 ± 0.0016	0.0134 ± 0.0001	0.9483 ± 0.0005	333.12	221.51
0.2452 ± 0.0016	0.0277 ± 0.0002	0.8986 ± 0.0009	333.12	221.77
0.2452 ± 0.0016	0.0462 ± 0.0003	0.8416 ± 0.0013	333.12	220.40
0.2452 ± 0.0016	0.0647 ± 0.0004	0.7913 ± 0.0016	333.13	218.72
0.2452 ± 0.0016	0.0839 ± 0.0006	0.7450 ± 0.0018	333.13	216.92
0.2452 ± 0.0016	0.1043 ± 0.0007	0.7015 ± 0.0020	333.12	214.97
0.2452 ± 0.0016	0.1390 ± 0.0009	0.6381 ± 0.0022	333.13	211.96
0.2762 ± 0.0018	0.1981 ± 0.0013	0.5823 ± 0.0023	333.12	208.36
0.2452 ± 0.0016	0.2509 ± 0.0017	0.4942 ± 0.0024	333.13	202.12
0.1600 ± 0.0011	0.1981 ± 0.0013	0.4468 ± 0.0023	333.12	197.43
0.1147 ± 0.0008	0.1981 ± 0.0013	0.3667 ± 0.0022	333.12	188.19
0.0880 ± 0.0006	0.1981 ± 0.0013	0.3076 ± 0.0020	333.12	178.87
0.0689 ± 0.0005	0.1981 ± 0.0013	0.2579 ± 0.0018	333.13	168.74
0.0518 ± 0.0003	0.1981 ± 0.0013	0.2072 ± 0.0016	333.12	155.21
0.0336 ± 0.0002	0.1981 ± 0.0013	0.1449 ± 0.0012	333.12	132.65
0.0218 ± 0.0001	0.1981 ± 0.0013	0.0992 ± 0.0008	333.12	110.46
0.0109 ± 0.0001	0.1981 ± 0.0013	0.0522 ± 0.0005	333.12	80.79
0.0000 ± 0.0000	0.1981 ± 0.0013	0.0000 ± 0.0000	333.13	37.73